THE UNIVERSITY OF HULL

ENCAPSULATION OF FLUIDS BY SOLID PARTICLES

being a Thesis submitted for the Degree of Doctor of Philosophy in
the University of Hull

by

Sophie Anne Darragh

MChem (University of Hull)

June 2015

ABSTRACT

This thesis aimed to investigate and understand the properties and behaviour of particles at fluid interfaces. The primary aim of this research was to develop a novel hand sanitiser based on the Fenton reaction, that is, the reduction of hydrogen peroxide into hydroxyl radicals by a metal ion catalyst (traditionally iron). The hydroxyl radicals produced can act as highly efficacious anti-bacterial agents, and thus have important application as a hand sanitiser. This thesis focused on the use of copper sulfate as a skin- friendly and water-soluble ion, suitable as a catalyst for the Fenton reaction due to its multiple valency states. For the reaction in question to be successfully utilised as a hand sanitiser, the two components must be kept apart until the point of use on the skin. Thus to achieve this, dry water technology has been explored, whereby the two aqueous components have been encapsulated separately so that by shearing on the skin surface at the point of use the contents can be released. Much of the research to date on dry water has only been carried out with pure water and no other components in the aqueous phase. In order to generate an understanding of the behaviour of particles at interfaces of varying surface tension, this thesis contains a systematic investigation of many types of silica particles at liquid-air interfaces.

The first study comprised an investigation into the foaming behaviour of two commercial nonionic surfactants. These surfactants are in use in a current formulation (InstantFOAM™) marketed by the industrial sponsor (Deb Group Ltd.). The foaming hand sanitiser contains a high proportion of ethanol, and thus there are difficulties in stabilising the foam produced. A systematic study of the foaming behaviour of the nonionic surfactants (Lamesoft PO65 and Silsurf DI-2510) was carried out in pure water and aqueous ethanol. A maximum in foamability of the surfactants was seen at 30 wt. % and 70 wt. % ethanol for Lamesoft PO65 and Silsurf DI-2510, respectively.

The ability of particles as foam stabilisers is well known. Irreversible attachment of particles to the air-water interface results in aqueous foams stable for many years. Therefore the potential for particles as stabilising agents of aqueous ethanol foams was explored. Extremely stable foams of hydrophobic (covered in 20% SiOH groups, so that 80% covered in hydrophobic dichlorodimethylsilane groups) fumed silica were generated in 20 wt. % ethanol, in pure water aeration of these particles generated particle-laden films that travelled up the walls of the vessels (termed 'climbing films').

Aeration of particles of intermediate hydrophobicity (47% SiOH) in pure water resulted in foams stable to collapse for over 1 year. Introduction of 20 wt. % ethanol to the aqueous phase resulted in a complete destabilisation of the foams, which all collapsed within 90 seconds.

The synergistic effect of particle and surfactant mixtures on foam stability is well known, a significant quantity of the literature covers the adsorption of ionic surfactants to charged solid particles. Much less is understood about the synergy between charged surfaces and nonionic surfactants. The foaming behaviour of mixtures of the nonionic surfactants with fumed silica particles was investigated. The effect of surfactant concentration, particle concentration and particle hydrophobicity was studied. It was found that the addition of particles to all foaming surfactant solutions, enhanced the foamability and stability (with the exception of 1 wt. % 100% SiOH and 1 wt. % Silsurf DI-2510 which formed a viscous gel). The effect of varying the particle hydrophobicity demonstrated that the two surfactants behaved completely differently. Addition of hydrophobic particles to Lamesoft PO65 solutions caused a reduction in the foamability, but an increase in the foamability of Silsurf DI-2510 solutions.

The second study in the thesis explored the fluorination of a series of monodisperse silica particles. A set of particles of varying hydrophobicity was generated by treating with different concentrations of a perfluorosilane. The particle contact angles at an air-water interface were measured directly with the film calliper method and found to range from 50.7° to >90°. As the two most hydrophobic particles broke the thin film, they were therefore assumed to have contact angles above 90°.

The particle contact angles were measured after introduction of 15 wt. % to the aqueous phase. Ethanol addition was seen to effect a reduction in the contact angle of all particles, demonstrating the effect of lowering the surface tension of the aqueous phase on the particle properties at the interface. Monolayers of the particles were then spread at air-water and aqueous ethanol-air interfaces and observed with optical microscopy. Aggregation was seen for all particles except the two most hydrophobic sets of particles, where ordered, repulsive arrays were observed. Introduction of 15 wt. % ethanol to the aqueous phase resulted in heavy aggregation, except for the two most hydrophobic particles which still demonstrated localised areas of the spread monolayers that formed repulsive arrays.

The foaming properties of these particles in pure water and 15 wt. % ethanol was then explored by aerating with a high shear method. In pure water, aqueous foams were formed for all particles but an inversion of the curvature of the interface was observed for particles treated with 3.4×10^{-4} M silane and above. The dry powders were stable for many months but the foams demonstrated poor stability of around 10 days. Introduction of 15 wt. % ethanol to the aqueous phase improved the foamability and stability significantly. An intermediate material between a foam and dry powder was observed for the most hydrophobic particles. The particles were wetted much better by the ethanol solutions which may have enhanced their transport to the interface, enhancing the foam properties.

Finally, the Fenton reaction was explored kinetically by studying the degradation of an azo-dye (with UV-Visible spectrophotometry) by the Fenton reagents. The initial rate of the reactions was determined by measurement of the reduction in concentration of the probe dye as a function of time. The intial rates passed through a maximum at 60 mM and 6 mM for hydrogen peroxide and copper sulfate, respectively. The effect of the pH was also investigated and seen to have a significant effect on the initial reaction rate, with the rate lowering with decrease in the pH. *In vitro* studies of the formulations demonstrated a 100% bacterial kill when exposed to E.Coli cultures for 60 seconds. A similar pH dependent effect was observed and the anti-bacterial efficacy was reduced at lower pH values. The high efficacy did not translate to *in vivo* studies on the skin surface, where there was no evidence of synergy when the Fenton components were applied to the skin surface. There was also a loss of efficacy when the formulations were applied as a powder, however no pH dependence was observed in *in vivo* studies.

PRESENTATIONS

This work has been presented by the author at the following events:

1. Oral presentation titled: "The effect of particle hydrophobicity on the behaviour of silica nanoparticles at an aqueous ethanol-air interface", Surfactant and Colloid Group Seminar, 1st November 2012, University of Hull, U.K.

2. Oral Presentation titled: "Particle-stabilised aqueous ethanol foams", 14th European Student Colloid Conference, 10-13th June 2013, Potsdam, Germany.

3. Poster presentation (1st Prize): "Particle-stabilised aqueous ethanol foams", Departmental Research Colloquium, 8-9th July 2013, University of Hull, U.K.

4. Oral presentation titled: "Behaviour of hydrophobised silica particles in mixtures of air, water and ethanol", Surfactant and Colloid Group Seminar, 14th May 2014, University of Hull, U.K.

5. Oral presentation titled: "Behaviour of surface-modified silica particles in mixtures of air, water and ethanol", Departmental Research Colloquium, 18-19th June 2014, University of Hull, U.K.

6. Poster presentation: "Particle-stabilised aqueous ethanol foams", U.K. Colloids Conference, 6-9th July 2014, London, U.K.

CONTENTS

CHAPTER 1

INTRODUCTION

1.1   Industrial relevance of current research

The research presented in this thesis concerns the encapsulation of fluids by particles for application in anti-bacterial skin care formulations. The industrial sponsor, Deb group Ltd., is a skincare company that produce anti-bacterial soaps, hand sanitiser gels/foams and skin care creams. Deb Silkware Protection Ltd. was established in 1941 by A.B. Williamson, selling a rinse-aid designed to enhance the lifespan of ladies' silk stockings. The product was called "Deb" originating from the term "debutante". Depletion of silk due to the Second World War, in combination with the introduction of Nylon stockings in the early 1940's, threatened the company's livelihood. The company changed their name to Deb Chemical Proprietaries Ltd. and launched Swarfega in 1947, which is still a household name today. Since then Deb have gone on to develop the world's first pump-based dispensers, and the world's first foaming soap and ethanol sanitiser.

Generating an understanding of the role of particles in stabilising aqueous-ethanolic foams is important to the industrial sponsor, as current formulations are surfactant-based, posing issues with their foamability and stability. Obtaining an understanding of these systems can enable the sponsor to reformulate current products to enhance their properties. Furthermore, the sponsor wishes to explore the role of particles in generating encapsulated sanitiser systems. This would have the end application of a novel aqueous hand sanitiser in powdered form (or so-called "dry water"). The requirement for the hand sanitiser to be encapsulated results from the need to keep two reactive components apart until the point of use. The reaction to be explored is the Fenton reaction, which is traditionally the iron-catalysed reduction of hydrogen peroxide into hydroxyl radicals. The industrial sponsor wishes to explore this reaction as a more efficacious and skin-friendly alternative to current alcohol sanitisers. It is proposed that dry water could be used as a delivery mechanism to keep the two reactive components of the Fenton reaction apart until the powder is sheared on the skin surface. Upon shearing on the skin surface, the aqueous core of the dry water would be released onto the skin surface, killing bacteria.

1.2 Aqueous foams

A foam is a thermodynamically unstable dispersion of gas bubbles in a liquid or solid continuous phase. Foams (and emulsions) are thermodynamically unstable colloidal systems because the generation of foam results in a significant increase in the interfacial area. This increase in interfacial area causes a subsequent increase in the surface free energy. Figure 1.1 illustrates the structure of foam, whereby gas (e.g. air) bubbles are separated by a thin liquid film, or *lamella*. Multiple lamellae join together at junctions called Plateau borders.[1] The Plateau borders signify the joining together of three thin liquid films. Since film tensions are equal, the forces acting in one plane can balance one another only if the angles between them are equal, in this case, 120°. This is known as the first law of Plateau.[2]

Figure 1.1. Schematic diagram depicting a foam comprising gas bubbles separated by thin liquid films (lamellae) which join at Plateau borders.
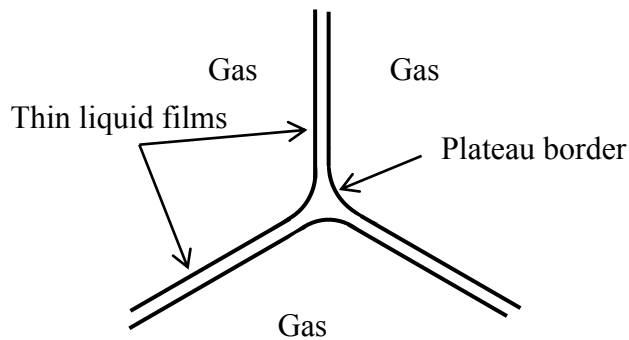
Foams can be generated by a number of methods. Often, hand shaking a foaming solution is sufficient to generate foam, but in other cases higher shear methods are required. In some cases, foam can be generated by nucleation of bubbles by depressurisation.[3] An important feature of foams to note is that pure liquids do not generate meta-stable foams; the liquid must comprise a mixture of two different components. Foam structure immediately comprises initially spherical bubbles separated by thick liquid films. As liquid drains from the foam lamellae, polyhedral shapes with thin liquid films are formed at the top of the foam; this dry portion of the foam is described as *"Polyederschaum"*.The initial spherical shape of bubbles is due to the interface adopting a configuration that minimises the interfacial free energy.[4] The bubbles at the bottom of the foam remain wet and spherical, and this portion of the foam is described as *"Kugelschaum"*.[5]

The destruction of foam structure can occur via three different mechanisms, namely, liquid drainage, coalescence and disproportionation (or Ostwald ripening). Liquid drainage occurs due to gravitational drainage of liquid from the lamellae and capillary pressure from Plateau borders between air bubbles. It is therefore possible to hinder liquid drainage by increasing the viscosity of the continuous phase. Coalescence occurs when two bubbles collide together and the thin liquid film between the bubbles breaks, forming one large bubble.

The Laplace pressure describes the pressure difference between the inside and outside of a curved interface and is responsible for disproportionation. Laplace pressure (Δp) is related to the surface tension of the interface and the radii of curvature of the bubbles as shown in equations 1.1 and 1.2.

$$p_1 - p_2 = \gamma \left(\frac{1}{R_1} + \frac{1}{R_2} \right)$$

(1.1)

where R_1 and R_2 are the radii of curvature of the bubble (for a general curved surface where it can be said that there are two local radii of curvature orthogonal to each other at a defined point) and γ is the surface tension of the air-water interface. In the case of spherical bubbles or droplets, the radii of curvature are equal ($R_1 = R_2$) and the equation can be written as:

$$\Delta p = \frac{2\gamma}{r}$$

(1.2)

where r is the radius of the bubble.[6] Disproportionation (or Ostwald ripening) is due to the internal Laplace pressure in a small bubble being higher than that of a large bubble. This causes diffusion of gas from the area of high pressure to the area of low pressure through the foam lamella, causing small bubbles to shrink and large bubbles to increase in size. Eventually the small bubbles effectively disappear leaving only very large bubbles. Due to Laplace's law, the pressure in the Plateau border is lower than the pressure in the flat films, causing a flow of liquid out of the film, hence thinning it. Foam can also be destroyed by evaporation of liquid from the top of the foam layer.[1] Figure 1.2 summarises all three collapse mechanisms. In most cases, complete foam destruction is due to a combination of all three mechanisms.

Figure 1.2. Schematic diagram depicting the three main collapse mechanisms of an aqueous foam. (a) Liquid drainage, (b) coalescence and (c) disproportionation. "a" indicates air bubble, "w" indicates water.

(a)

(b)

(c)
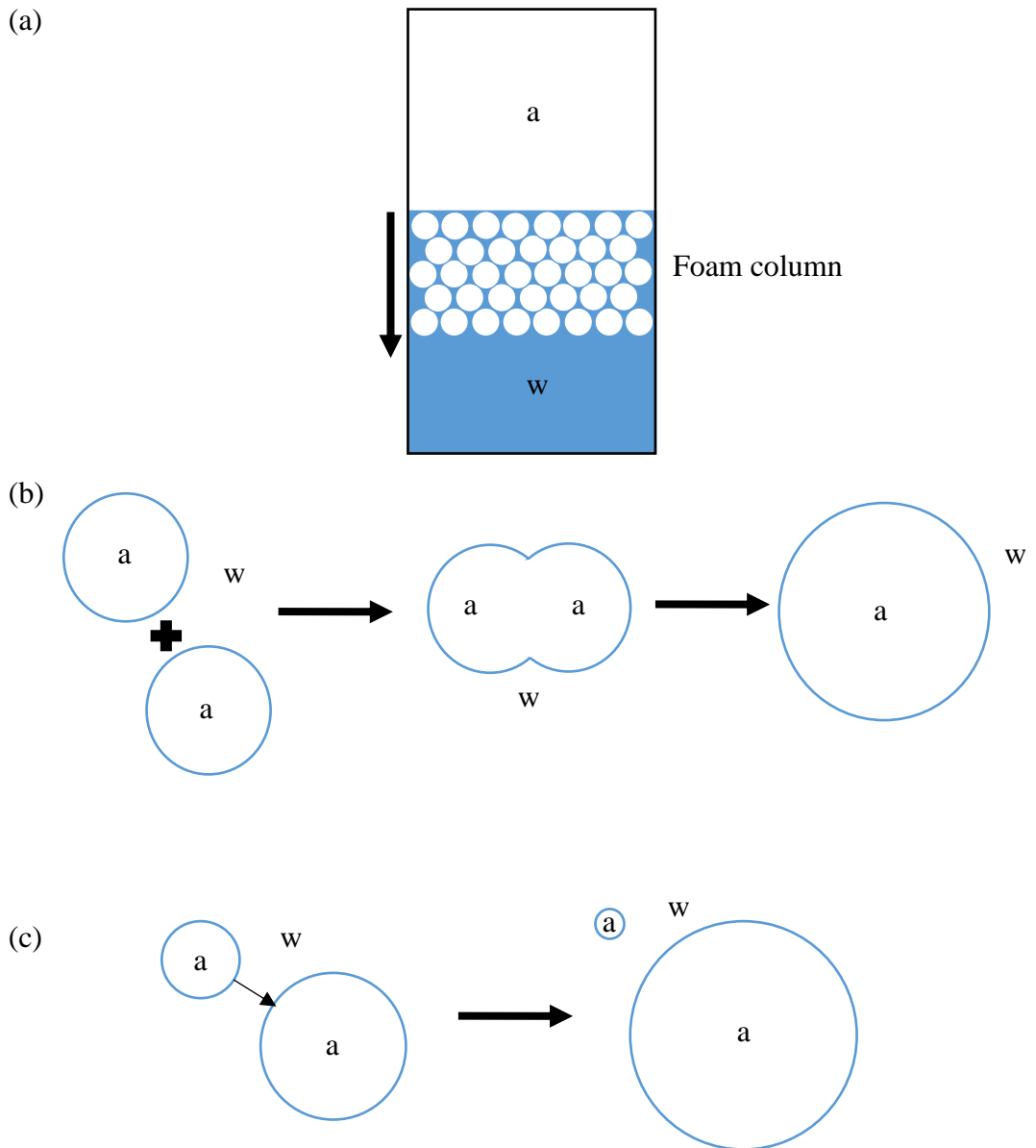
1.3 Surfactants

Surfactants (surface-active agents) are molecules that aid in the generation of stable foams and emulsions by adsorbing at the interface between the two phases of the system (dispersed and continuous phase). Surfactants are responsible for the foaming ability of many foaming formulations used in a multitude of industries. A surfactant molecule comprises a hydrophilic head and a hydrophobic tail, making it *amphiphilic* in nature. The hydrophobic portion of the molecule often comprises a straight or branched hydrocarbon or fluorocarbon chain of between 8-18 carbon atoms. A number of tail groups can be bound to one or more head groups, as shown in Figure 1.3.

Figure 1.3.   Schematic diagram of general surfactant structure and possible permutations of surfactant structures.
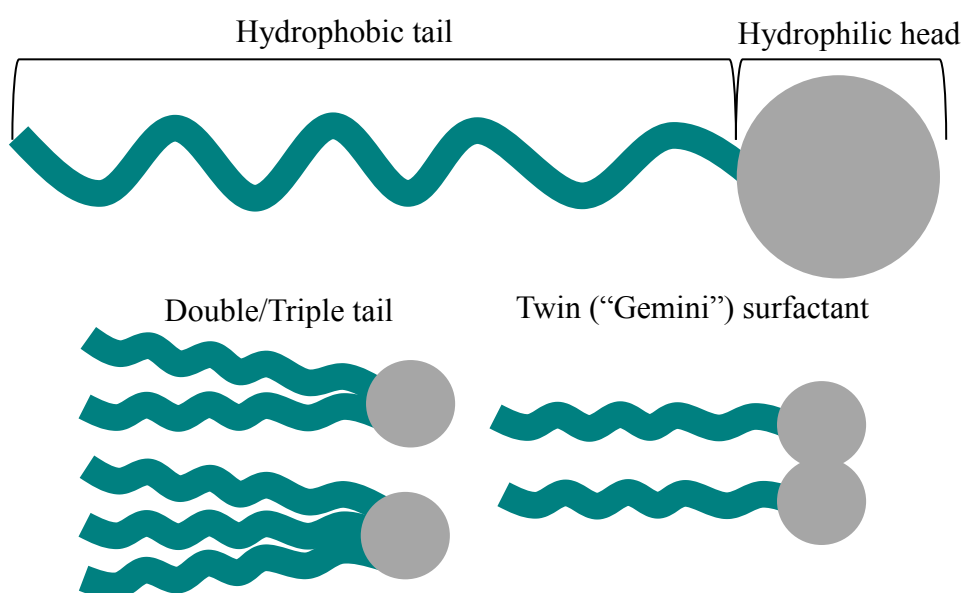
The surface activity of surfactant molecules (in water) is primarily due to the presence of the hydrophobic tail; this drives the surfactant molecules to the interface, where adsorption with the tail group protruding into the air or oil phase, and the hydrophilic head group in the aqueous phase occurs. The adsorption of surfactant molecules to the interface reduces the interfacial tension. Surface tension is defined as the force per unit length acting on an imaginary line drawn in the air-water surface and arises from a difference in the intermolecular interactions experienced by molecules at the surface and in the bulk.

Consider the attractive forces experienced by a molecule in the bulk (Figure 1.4). There is no net force pulling a molecule in any given direction, the attractive force in the bulk can therefore be defined as isotropic. Conversely, a molecule at the surface will experience an unbalanced force due to the relative scarcity of neighbouring molecules in the gas phase. This results in a tendency for molecules at the surface to be pulled into the bulk, explaining the tendency for a minimisation of the surface area.

Figure 1.4. Schematic diagram to demonstrate differences in interactions experienced by molecules at an air-water interface. Redrawn from ref. 7.
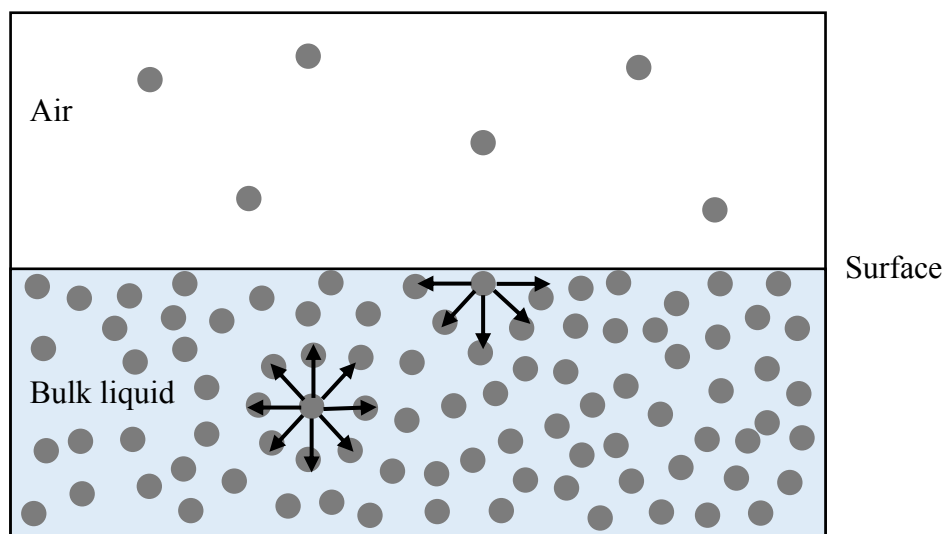
1.3.1 Behaviour in bulk solution

The surfactant structure can have implications in many aspects of the behaviour of the surfactant, in particular, the critical micelle concentration or CMC. The CMC is the concentration at which micelles begin to form. At low concentrations, surfactant exists in solution as monomers. At concentrations above the critical micelle concentration, excess surfactant forms water-soluble aggregates called micelles. Micelles comprise a hydrophobic, disordered core of surfactant tails, and a water-soluble exterior due to hydrophilic surfactant head groups. The structure of a micelle is shown in Figure 1.5

Figure 1.5. Schematic diagram of a spherical aqueous surfactant micelle.

Oily Core   Hydrophilic exterior
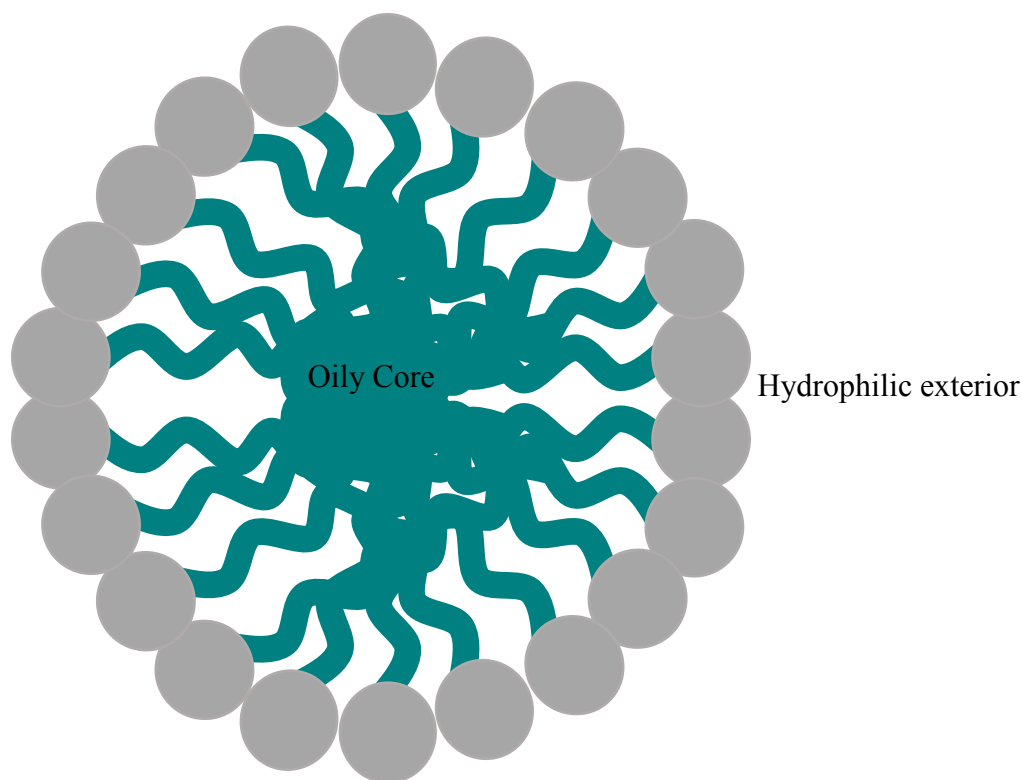
The critical micelle concentration results from the tendency of surfactants to self-assemble in solution. There are various driving forces for micelle formation. Micellisation is entropically favourable as the oily core of a micelle is more disordered than free surfactant in solution. The free monomers in solution are highly ordered with respect to the ordering of water molecules around the monomer molecules in the solution, thus the entropic driving force for micellisation can be seen. Secondly, the hydrophobic effect results from the unfavourable contact of hydrophobic tails with the aqueous phase. By forming micelles, the tails can be removed from contact with the water.

It is possible to measure the critical micelle concentration of a surfactant solution with a variety of methods, namely, by the measurement of the surface tension, osmotic pressure, molar conductivity or light scattering intensity as a function of surfactant concentration. Figure 1.6 shows a graph of the expected trends for determination of the CMC via these methods. The surfactant tail group affects the CMC significantly, in that the longer the tail group, the lower the CMC as the molecules aggregate at lower concentrations to minimise contact of their hydrophobic tails with the aqueous solution.

Figure 1.6. Graph to demonstrate expected trends for determination of CMC of sodium dodecyl sulfate by measurement of surface tension, osmotic pressure, conductivity and molar conductivity as a function of surfactant concentration. Redrawn from ref. 7.
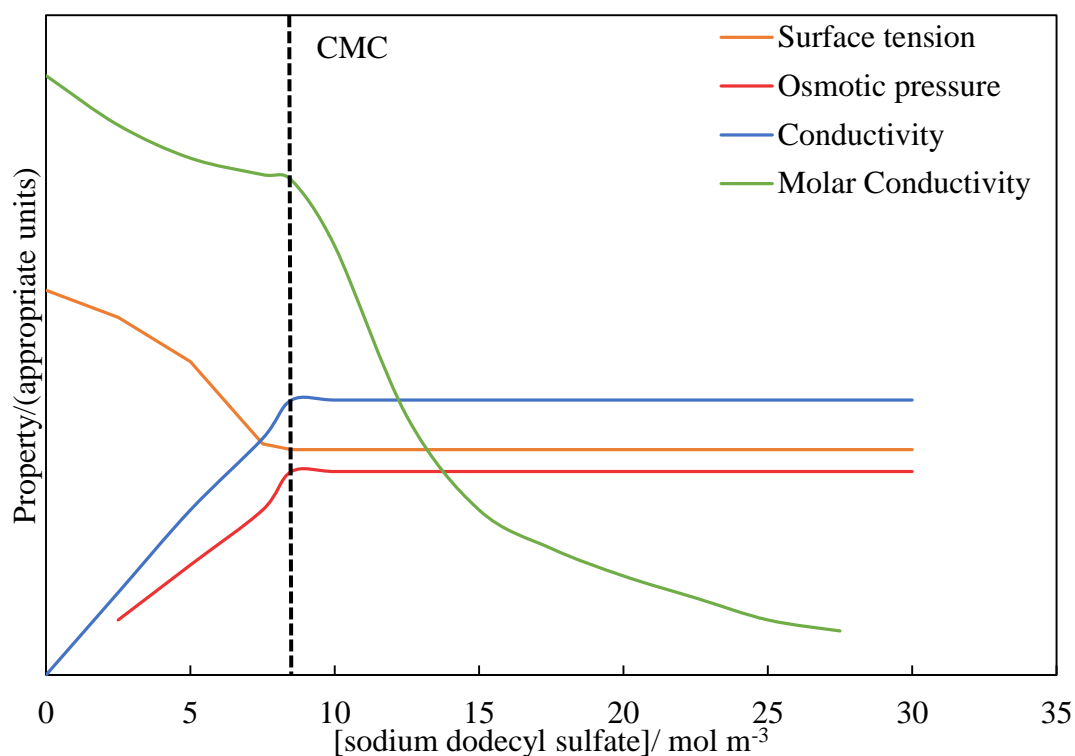
1.3.2 Aqueous foams stabilised by surfactants

The ability of surfactant molecules to generate and stabilise foam has been attributed to various reasons, but primarily due to their adsorption at the gas-liquid interface. As previously mentioned, foams are thermodynamically unstable due to the surface free energy created from generating new surfaces. The adsorption of surfactant at the gas-water interface causes a reduction in the surface tension, lowering the energy of the system, and temporarily stabilising it.[5]

The Gibbs-Marangoni stabilisation of foams depends upon an increase in surface tension at the stressed and thin areas of the foam lamella.[8] The expanded portions of the film have a lower degree of surfactant adsorption because the surface area has increased; this causes a localised increase in surface tension, providing a resistance to further thinning. Consequently, the increase in surface tension in the thin region causes an immediate contraction of the surface. This induces flow of liquid from the low tension region to the high tension region, re-thickening the film and restoring it. This is known as the Gibbs-Marangoni effect and only exists until the surfactant adsorption equilibrium has been restored in the film. Further to this, time may be required to restore the equilibrium surface concentration of surfactant, so any disturbance in the original adsorbed surfactant layer cause Gibbs-Marangoni forces to act in opposition to the disturbance. At equilibrium, the surface elasticity (E_G) is defined as:

$$E_G = \frac{d\gamma}{d \ln A}$$

(1.3)

where γ is the surface tension and A is the geometric area of the surface. For a foam lamella, there are two such surfaces and the elasticity becomes:

$$E_G = \frac{2d\gamma}{d \ln A}$$

(1.4)

The Gibbs surface elasticity occurs in very thin films where the number of molecules is significantly low that the surfactant alone cannot restore the equilibrium surface concentration after the film deformation. Surface elasticity measures the resistance against creation of surface tension gradients.

Most stable foams can be produced at surfactant concentrations around or above the CMC. If the surfactant concentration is high enough it can increase the viscosity of the continuous phase and reduce liquid drainage. Other factors such as the solubility of the aeration gas in water can slow down the disproportionation process. For example, a gas that is insoluble in the continuous phase will show reduced solubility into the lamellae and consequently into bubbles of lower Laplace pressure.

The behaviour of various "Tween" surfactants was investigated by Samanta and Ghosh.[9] The Tween-series of surfactants are non-ionic, polyoxyethylene sorbitan esters of aliphatic fatty acids. The surfactant type was varied by changing the tail length, with polyoxyethylene sorbitan monolaurate, monopalmitate, monostearate and monooleate, known commercially as Tween 20, 40, 60 and 80, respectively. The researchers measured surface tension as a function of surfactant concentration using the Wilhelmy plate method. The time for bubbles injected into surfactant solution to coalesce was measured, with an average of 100 bubbles measured in each experiment. The "Ross-Miles" foam test was carried out by allowing 200 ml surfactant solution to fall 90 cm into 50 cm^3 of the same solution in a container. The initial foam height and decay in foam height with time were measured using a digital camera.

The surface tension of all surfactant solutions was seen to initially decrease rapidly with increasing concentration, until a plateau was reached. The point at which the surface tension ceased to reduce further was taken as the CMC, which were taken as 0.06, 0.03, 0.022 and 0.012 mol/m^3 for Tween 20, 40, 60 and 80, respectively. The experimental CMC's followed a trend whereby increasing tail length reduced the CMC. With increasing concentration of all surfactants, the coalescence time and foam height were both seen to increase. The researchers attributed the increase in stability to an increased number of adsorbed surfactant molecules to the bubble surface and flat air-water interface.

The adsorbed layer of surfactant experiences a reduction in entropy as the bubble approaches the planar air-water surface, as this reduction in entropy is thermodynamically unfavourable; the approach of bubbles and their consequent coalescence is inhibited. Tween 20 showed the highest foam height and this was attributed to a higher rate of adsorption to the interface resulting from the highest CMC.

A vast amount of research in the area of surfactant-stabilised foams exists, as the significance of surfactants in many industries is extremely important. Tamura *et al.* investigated the foaming properties of aqueous polyoxyethylene dodecyl ether surfactants (nonionic) with a range of ethylene oxide (EO) units.[10] The surface tension of aqueous solutions was seen to increase as the number of EO units increased, indicating that as the number of EO units increased, the concentration of surfactant at the air-water surface decreased. Foaming experiments on 1 mM surfactant solution were carried out by the Ross-Miles test. The initial foam height was seen to increase with increasing number of EO units up to 11 EO units, after which the initial foam volume decreased. The researchers concluded that foam stability of nonionic surfactants is dependent on the surface viscosity and the surface-tension gradient, also referred to as the Marangoni effect. A later study by Tamura *et al.* gave further support for the role of the Marangoni effect in foam film stabilisation with nonionic surfactants.[11]

Dutta *et al.* have investigated the synergistic effect of nonionic surfactants (propylene glycol stearate, triglycerol stearate and sucrose stearate) on aqueous foam properties.[12] Either propylene glycol stearate or triglycerol stearate was mixed with sucrose stearate for 15 minutes so that the total surfactant concentration was 6 wt. %. The solutions were then whipped for 3 minutes and the foam overrun measured. The overrun is defined by the percentage of incorporated air with respect to the initial solution volume. The blend of propylene glycol stearate and sucrose stearate was found to have a higher overrun than that of triglycerol stearate, however it had a lower long-term stability. Even though both systems had a similar mean bubble size the propylene stearate system was seen to lose 78% of its initial overrun when compared to the triglycerol stearate, which lost 67% of the initial overrun after a week. The foams were seen to be more stable when refrigerated, this was attributed to the lower diffusivity of air in liquid at lower temperatures. It was observed that sucrose stearate could not be aerated alone. Furthermore, dynamic surface tension measurements were measured and it was found that as the dynamic surface tension decreased, the mean bubble size decreased.

It has been demonstrated that the rate of adsorption to freshly generated interfaces is an important consideration for foam stability. These parameters do not tend to increase further once the surfactant CMC has been reached. Furthermore, the adsorption of a monolayer of surfactant to bubble surfaces with hydrophilic headgroups in the aqueous phase means that as liquid films begin to thin, the surfaces of both films approach each other and can repel each other (repulsion between surfactant headgroups), enhancing the repulsive disjoining pressure and counterbalancing the capillary pressure (which forces thinning of the film). At equilibrium the disjoining pressure and capillary pressure of the Plateau border walls are exactly balanced.

1.4   Particles

Solid particles of size in the colloidal size domain (micron to nanometre size) can be surface-active and irreversibly attach to fluid-fluid interfaces imparting long-term stability on these systems. Various shapes and sizes of particles exist, from spherical to cubic, or even rod-like. Particle adsorption to liquid-liquid interfaces can enable formation and stabilisation of emulsions, often referred to as Pickering emulsions named after the works of Pickering.[13] However, it should be noted that historically Ramsden played an intrinsic role in the observation of particle-stabilised bubbles and emulsions.[14] This work will focus solely on behaviour of particles in fluid systems of aqueous-ethanol and air.

1.4.1 Behaviour in bulk solution

Consider a dispersion of hydrophilic, spherical particles in water; the dispersion is thermodynamically unstable as the particles gathering into a bulk phase (i.e. formation of particle clusters or sedimentation) results in a decrease in the free energy of the system. However, apparent stability of dispersions is due to the presence of an energy barrier for flocculation or coagulation of the particles. The origin of this meta-stability can be explained by the balance of repulsive (electrostatic) and attractive (dispersive) interaction forces, known as DLVO theory. The DLVO theory is named after Derjaguin, Landau, Verwey and Overbeek after their publications in 1941 and 1948[15-17] on the stability of lyophobic sols/colloids. The DLVO theory states that the overall interaction energy (V_T) is the sum of the electrostatic (V_R) and van der Waals (V_A) energies, and can be expressed as:

$$V_T = V_R + V_A \tag{1.5}$$

As two particles approach each other, the change in overall potential energy determines whether they will experience an attractive (decrease in energy) or repulsive (increase in energy) force. The repulsive electrostatic force is only experienced when two particles approach each other close enough so that their electrical double layers overlap each other. This is due to the fact that the overall charge on a single particle is neutralised by its electrical double layer. Solid surfaces can acquire a surface electrical charge when brought into contact with a polar medium (such as water) by dissociation and solvation of surface groups. Lattice imperfections on the solid surface can also result in a surface charge.

Alternatively, adsorption of ions of impurities at the interface between solid and liquid can result in surface charge. The acquired surface charge influences the distribution of ions in the surrounding solution. The Gouy-Chapman model accounts for the distribution of counter ions and the thermal motion of these counter-ions near the charged surface by basing the structure of the electrical double layer on a Boltzmann distribution of ions near the charged surface.[7] The electrical double layer structure and charge distribution around a spherical particle are shown in Figures 1.7 and 1.8, respectively.

Figure 1.7.   Schematic representation of the electrical double layer at the solid-liquid interface. Redrawn from ref. 18.
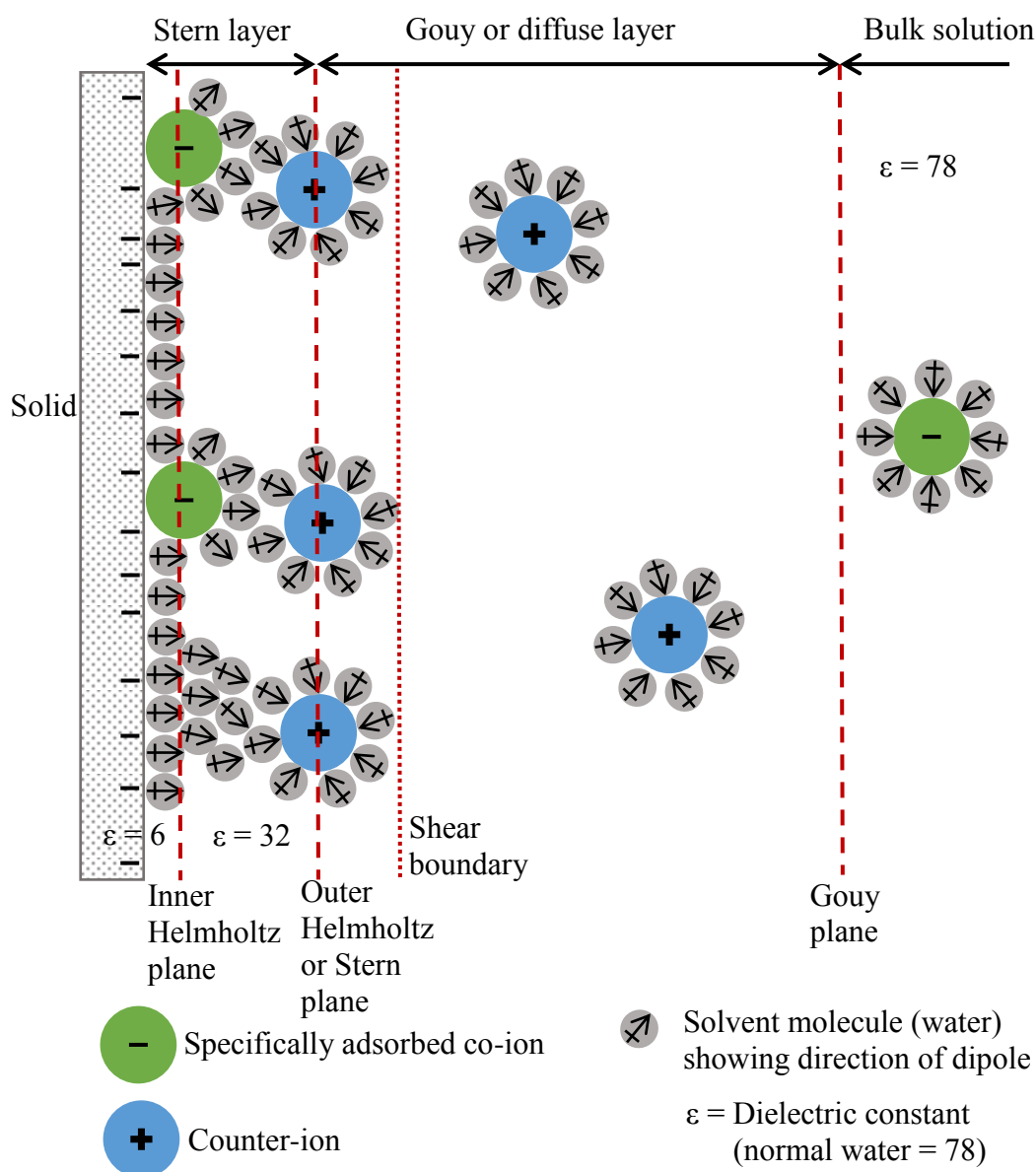
Figure 1.8.   Schematic representation of distribution of electrical potential in the double layer region around a charge particle. The zeta potential (potential between stern and shear planes) and reciprocal Debye length are also shown. Redrawn from ref. 19.

Gouy plane
Diffuse layer
Shear plane
Stern plane
Particle surface

ψ_o = Surface potential
ψ_δ = Stern potential
ζ = Zeta potential
$1/\kappa$ = Double-layer thickness
(reciprocal Debye length)

Potential, ψ_o

ψ_δ

ζ

$1/\kappa$

Distance from particle surface
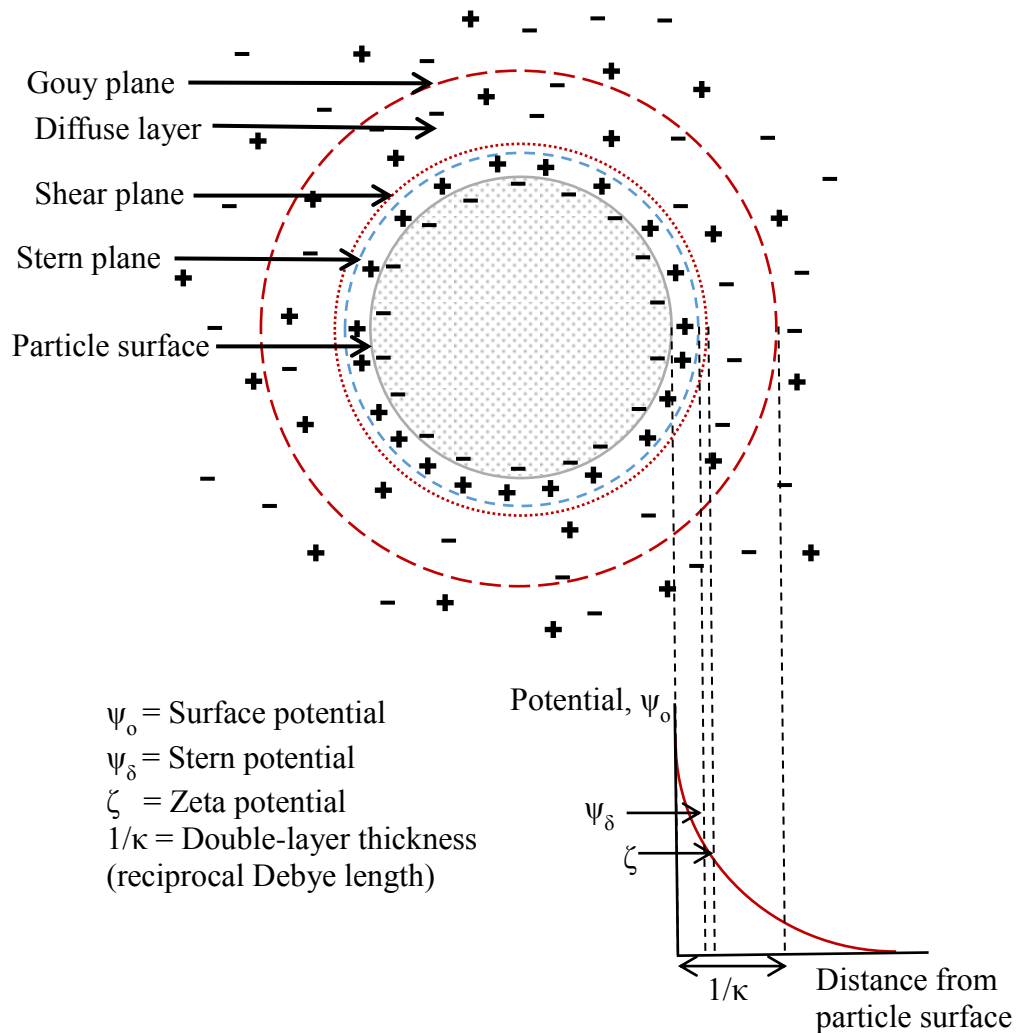
As previously stated, the overall interaction energy is calculated from the sum of the attractive and repulsive potentials. The attractive force between particles is often referred to as van der Waals attraction, and results from dipole-dipole, dipole-induced dipole and instantaneous dipole-induced dipole (London dispersion forces) interactions. The potential energy of attraction for spherical particles of radius r in a vacuum separated by a distance of (s= 2r) is given by:

$$V_a = \frac{-H_r}{12_s}$$

(1.6)

where *H* is the Hamaker constant and s is the interparticle separation. In liquid medium, *H* is replaced by an effective Hamaker constant:

$$H = \left(\sqrt{H_p} - \sqrt{H_m}\right)^2$$

(1.7)

where H_p and H_m are the Hamaker constants for the particle and liquid medium, respectively. If the two interacting particles are of the same material, the Hamaker constant will always be positive, and therefore V_a will always be attractive (negative value).

As mentioned previously, repulsive interactions results from overlap of the electrical double layers surrounding two particles. The DLVO theory assumes the surface potential remains constant and that the two particle surfaces are identical. The equilibrium repulsion is dependent on the particle size, shape, ionic strength, inter-particle distance and permittivity of the dispersion medium. Approximate solutions for the repulsive potential between two particles are given by Hunter:[20]

$$V_r = 2\pi\varepsilon r \psi_O^2 \exp(-\kappa s) \qquad \text{for } \kappa r \ll 1 \qquad (1.8)$$

$$V_r = 2\pi\varepsilon r \psi_O^2 \ln\left(1 + \exp(-\kappa s)\right) \qquad \text{for } \kappa r \gg 1 \qquad (1.9)$$

where ψ_o is the potential at the surface of the particles, ε is the vacuum permittivity, s is the distance of the closest approach and κ is the reciprocal of the Debye length (as shown in Figure 1.7, therefore κs is the relative separation between two particles). Additionally, the term κr is the ratio of the particle size to the double layer thickness. By summing the van der Waals-Hamaker attraction and double-layer repulsion, the overall potential energy of interaction as a function of inter-particle distance can be plotted, and is shown in Figure 1.9.

For a stable dispersion, an energy barrier of ~15 kT or greater is needed. It is understood that the shape of the potential curve shown in Figure 1.9 is dependent on the particle radius, electrolyte concentration and surface potential.

Figure 1.9. Overall potential energy of interaction between two particles as a function of relative inter-particle separation. The potentials of the repulsive (double-layer/electrostatic) and attractive (van der Waals interactions) are also shown.
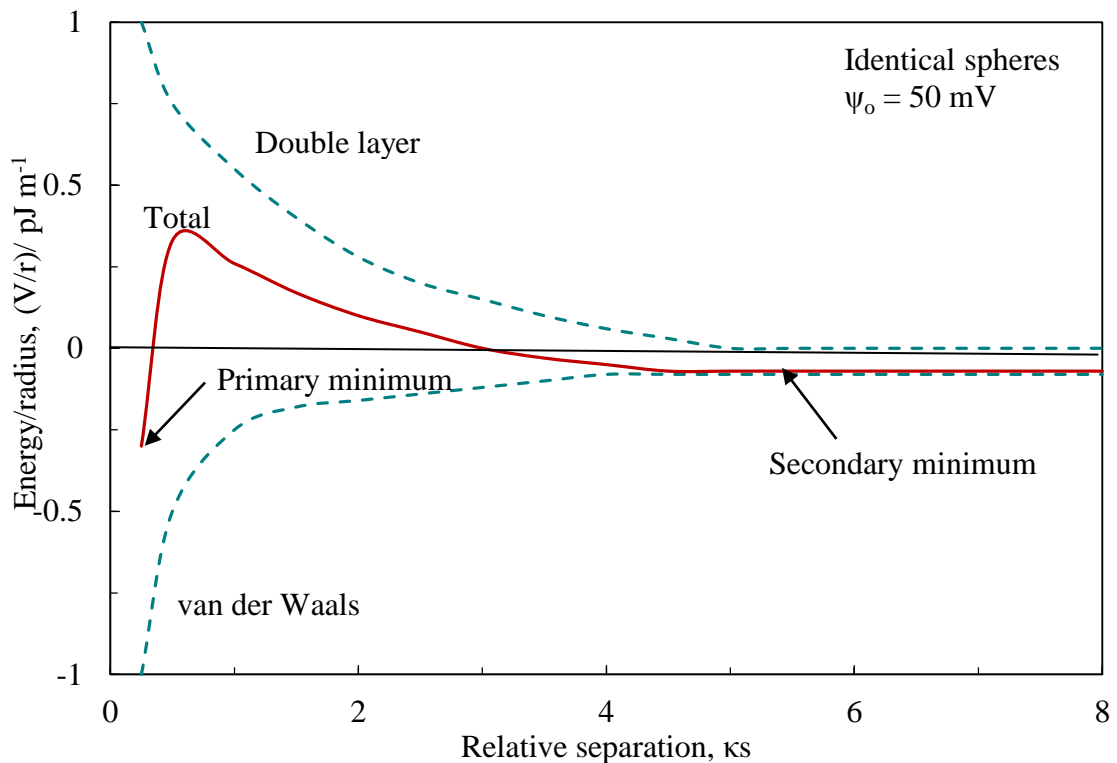
As shown in Figure 1.9, the red curve shows the overall potential energy as a function of the distance between two particles. The maximum in the curve is the energy barrier that the particles must overcome to coagulate. The height of this energy barrier can be reduced by addition of electrolyte, which reduces ψ_o and the size of the double layer. The secondary minimum shown is due to the van der Waals attraction being greater than double layer repulsion at long distances, and so particles may aggregate with long distances between them. This is known as flocculation.

1.4.2 Behaviour at air-liquid interface

It is clear that particles can demonstrate surface activity and adsorb at fluid interfaces, however unlike adsorbed surfactant molecules which exist in dynamic equilibrium with monomers in the bulk phase, particles can become irreversibly attached to the interface. An important parameter when considering solid particles at a liquid interface is the three-phase contact angle, θ, given by Young's equation:[21]

$$\cos \theta = \frac{\gamma_{pa} - \gamma_{pw}}{\gamma_{aw}}$$

(1.10)

where γ_{pa}, γ_{pw} and γ_{aw} are the interfacial tensions of the particle-air, particle-water and air-water interfaces, respectively. This is the angle between tangents to the solid surface and the liquid-liquid or liquid-air interface, measured through one of the liquids at each point of the three-phase contact line where the solid particle, liquid and gas interfaces meet (shown in Figure 1.10).

Figure 1.10.   Schematic diagram of a particle attached to an air-water interface. The three-phase contact angle is shown as θ. Redrawn from ref 21.

18
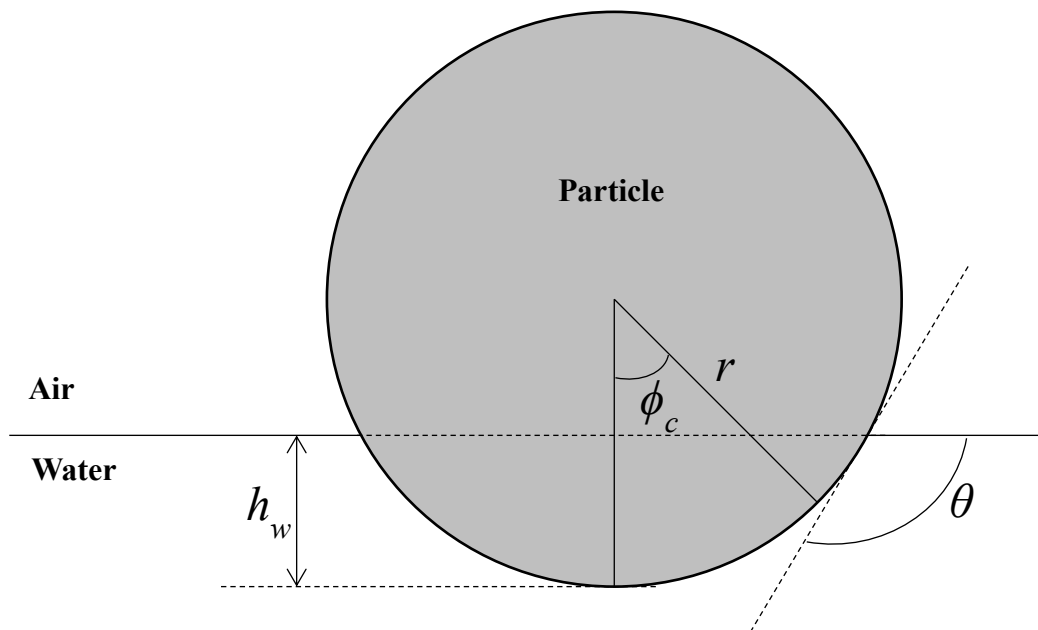
The contact angle of a particle can dictate the particle behaviour at an interface. Particle-stabilised colloidal systems often demonstrate exceptional stability when compared to their surfactant-stabilised equivalents; this characteristic can be attributed to the ability of particles to irreversibly attach to an interface. Equations 1.11 and 1.12 show the free energy of detachment of a spherical particle from an air/water interface into both the air phase (1.11) and the water phase (1.12).

$$\Delta G_{da} = \pi r^2 \gamma_{aw} (1 + \cos\theta)^2 \qquad (1.11)$$

$$\Delta G_{da} = \pi r^2 \gamma_{aw} (1 - \cos\theta)^2 \qquad (1.12)$$

where r is the particle radius, γ_{aw} is the surface tension of the air-water interface and θ is the three-phase contact angle of the particle. Apart from very large and very small contact angles, the minimum energy of particle detachment from the interface is much greater than kT and reaches its maximum at a contact angle of 90°. This high energy of detachment makes particle adsorption irreversible and allows for the high stability of particle-stabilised colloidal systems, such as foams and emulsions. The energy of particle attachment to the fluid interface, $\Delta G_a = -\Delta G_d$, is negative and hence particle attachment to the interface is thermodynamically favourable. The minimum energy of particle detachment as a function of particle contact angle can be seen in Figure 1.11.

Figure 1.11. Energy of particle detachment (E_{min}) of a 10 nm particle from the air-water interface as a function of the three-phase contact angle. Redrawn from ref 21.
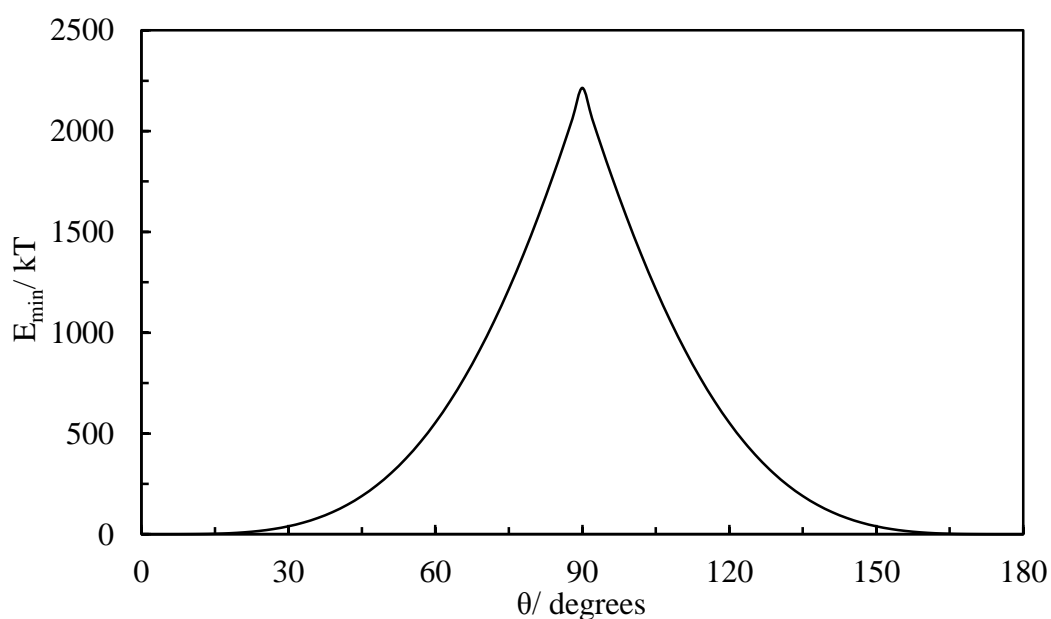
The contact angle that a solid makes with a liquid in air (three-phase contact angle) can be measured using goniometry. When a liquid drop is placed on a solid surface, the triple interface formed between solid, liquid and gas will move in accordance with the forces that arise from the three interfacial tensions until a position of equilibrium is reached. Figure 1.12 shows a sessile drop of liquid on a solid surface to demonstrate this. Differences in wettability of a surface arise from variations in the adhesive forces between the liquid drop and the surface and cohesive forces between liquid molecules within the liquid drop. A solid surface that has many polar groups on the surface (e.g. hydroxyl groups) will have a good affinity for water and thus strong adhesive forces between the water droplet and the surface. This will result in a spreading of the liquid drop and the surface is termed hydrophilic. A surface covered with non-polar groups will repel a water droplet, and such surfaces are termed hydrophobic. Hydrophilic and hydrophobic surfaces are characterised by low (<90°) and high (>90°) contact angles, respectively. The effect of surface roughness has been presented in detail by Wenzel[22] where it is understood that a surface with a higher roughness can demonstrate a greater hydrophobicity and higher contact angles for water drops in air. The work of Cassie[23] has further examined the effects of porosity and surface roughness on apparent contact angle, with reference to waterproof feathers observed in nature. It has been noted that this waterproofness is not due to any chemical agent on the feather surface but due to microstructure and roughness instead. Further to this, it is also known that chemical heterogeneity can have a significant effect on the advancing and receding contact angles, as studied by Decker and Garoff.[24] By chemically treating surfaces with a homogeneous monolayer of a perfluorinated surfactact (Aquapel) and then altering these surfaces by exposure to UV/ozone the surfaces became more heterogeneous. It was seen that with continual exposure to the UV/ozone treatment, both the advancing and receding contact angles of water droplets on the solid surfaces in air were seen to continually decrease.

Figure 1.12. Schematic diagram to demonstrate the three-phase contact angle of a sessile drop of liquid on a solid surface in air.
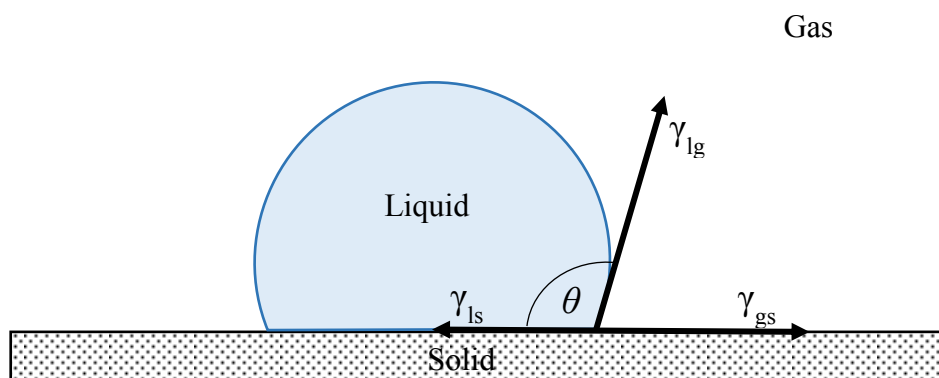
The contact angle of particles at an immiscible interface can be measured by a range of techniques. The film calliper method is an optical method that can be used to measure the contact angle of micron sized particles at an air-water interface.[25] Particles are trapped in a thick liquid film in air, the film is then forced to thin by withdrawing liquid from the meniscus, forcing the particles to bridge both interfaces of the newly formed thin liquid film. The particles attain their equilibrium position in the film according to their contact angle, which is measured by observing the bridged particles in reflected monochromatic light. The gel-trapping technique allows for the measurement of smaller particles (to nanometer size) by trapping the particles in a gelled agar phase and imaging the particles using scanning electron microscopy.[26,27] Other techniques such as optical imaging[28], film trapping technique[29] and atomic force microscopy[30] have been developed but all pose various challenges either in measurement or interpretation of the data collected. Additionally, some methods are unsuitable for measurement at the oil-water interface, or are limited in the size of particles that can be measured.

The behaviour of particles at an interface can be controlled by variation of the chemical structure on the particle surface. Grafting hydrophobic reagents to the particle can render the particle hydrophobic. Chemically modifying the surface of a particle can be carried out by chemically grafting a hydrophobic molecule (for example, dichlorodimethylsilane) to the surface. Alternatively, surface modification can occur by physical adsorption of a hydrophobic molecule to the surface (for example, the adsorption of surfactants to solid surfaces by electrostatic interaction or hydrogen bonds[31,32]).

1.4.3 Particle-stabilised foams

As mentioned briefly in Section 1.4, Ramsden was one of the first to observe the potential for particles in the application of stabilising aqueous foams. Their irreversible attachment to the air-water interface can greatly enhance foam stability in comparison to surfactant-stabilised foams.

1.4.3.1   Aqueous foams stabilised by particles alone

In a review by Horozov, various particle types and shapes and their role in foam stabilisation were explored. Spherical polystyrene latex particles, rod-like polymer particles, non-spherical silica particles and plate-like particles were all shown to be effective foam stabilisers.[33] Binks and Murakami observed aqueous systems generated with fumed silica particles hydrophobised to varying extents.[34] The fumed silica particles were coated with different amounts of dichlorodimethylsilane so the remaining untreated surface groups on the particles were silanol groups (denoted as "SiOH"). Therefore the particle hydrophobicity was defined by the percentage of residual silanol groups on the particle surface; with 100% SiOH being the least hydrophobic and 14% SiOH being the most. Quantification of the concentration of surface silanol groups[35] can be carried out by measuring the conductivity of particle suspensions with increasing concentration of sodium hydroxide. The number of deprotonated silanol groups increases with increasing concentration of hydroxide ions in solution (from NaOH) until a plateau is reached, at which all surface silanol groups are deprotonated. By measuring the conductivity and the surface area of the particles, the percentage of surface silanol groups can be quantified. In the work of Binks and Murakami,[34] aqueous suspensions of 2 wt. % particles were aerated, stable foams were generated with particles of hydrophobicity 32-62% SiOH. As the particle hydrophobicity increased, the initial foam volume also increased. Furthermore, the turbidity of the liquid phase beneath the foam became clearer with increasing particle hydrophobicity, implying that more particles were attached to the bubble surfaces. With particles of 14-20% SiOH dry powders of water drops in air (dry water) were formed. The most hydrophilic particles (above 62% SiOH) formed stable particle dispersions. A photo of the aerated suspensions is shown in Figure 1.13 where the inversion from water-in-air to air-in-water systems can be seen clearly. Figure 1.14 shows the effect of contact angle on the position of a spherical particle at an air-water interface. With increasing contact angle, there is an inversion of the interface curvature, from an air-in-water system (foam) to a water-in-air system (dry water/liquid marble).

22

Figure 1.13. Photo of aqueous systems generated with 2 wt. % fumed silica particles in water after aeration (by blending for 30 s). Particle hydrophobicity decreases from left to right (numbers indicate % SiOH groups). Dashed lines indicate point of phase inversion. Picture republished with permission from reference 34.
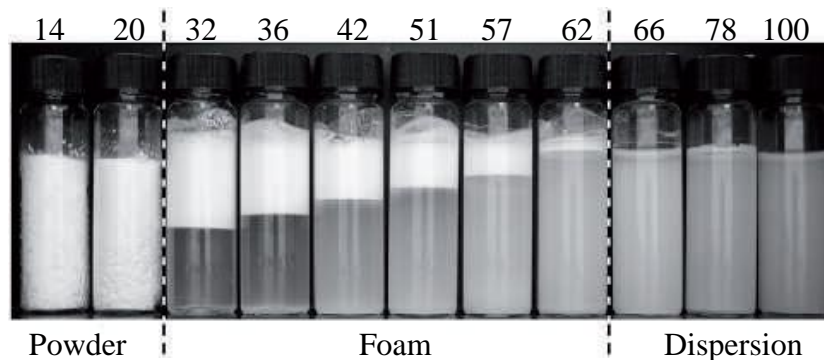
Figure 1.14. Schematic representation on the effect of the three-phase contact angle of particles on the curvature of an air-water interface.
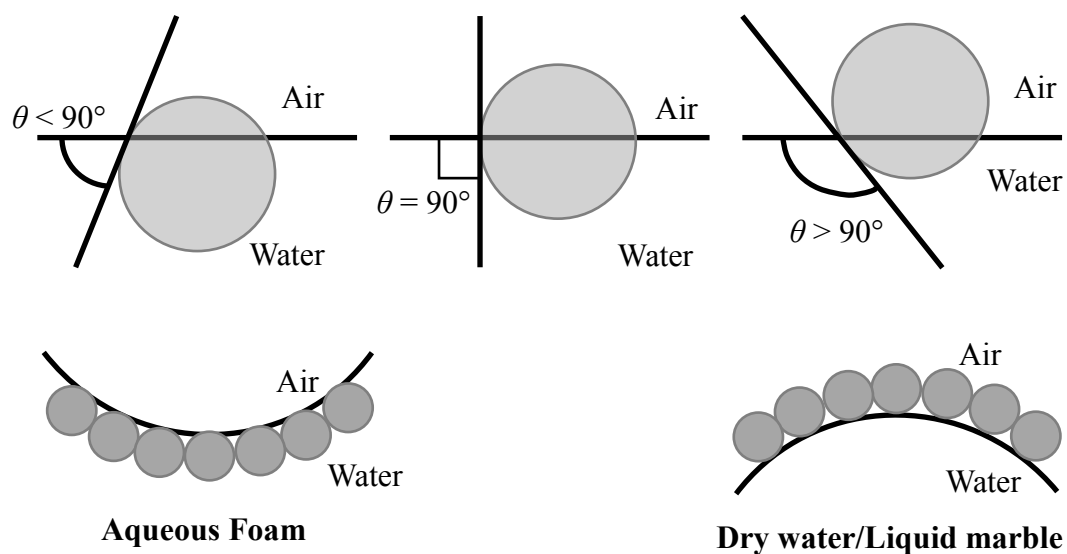
Binks and Horozov[36] demonstrated that fumed silica particles with varying surface hydrophobicity generated highly stable aqueous foams. Foams were generated by hand shaking or homogenising a 3 wt./v. % silica particle dispersion in 7 cm^3 purified water (with the aid of ethanol which was removed after particles dispersed).

Similar to that observed by Binks and Murakami, foams were not observed with the most hydrophobic and most hydrophilic particles. In these regions, the particle contact angle at the air-water interface is significantly high (hydrophobic) or low (hydrophilic) and the particles sit too far into either of the interfaces to stabilise foam effectively. It is known from Figure 1.11, that the minimum energy of particle detachment is lowest at extremely high/low contact angles; so, it is likely that the particles will detach from the interface, making foam generation and stabilisation difficult. Extremely stable foams were observed in regions of intermediate particle hydrophobicity, with 32% and 20% SiOH particles, the foams retained 60% of their water content after a considerable time period, foam collapse was attributed to liquid drainage and not bubble coalescence. Optical microscopy of the particle foams showed a rippled surface characteristic of a dense particle layer.

Stocco *et al.* investigated the foamability and stability of 1 wt. % fumed silica particles with 35% surface SiOH content dispersed in water.[37] The samples were then hand shaken and foamability and stability were observed as a function of time. Similarly to the findings by Binks and Horozov,[36] particles of intermediate hydrophobicity (32% and 42% SiOH) were shown to produce the most stable foams. In the more hydrophobic and hydrophilic particle systems, powders and dispersions were observed, respectively.

When discussing the instability of particle foams with respect to the surface hydrophobicity of the particles, there are a multitude of factors that can be responsible for the foam instability. In a short communication paper by Vivaldini *et al.*, silica-containing foam systems were investigated, specifically their behaviour at the air-water interface.[38] The researchers commented on the well-known fact that adsorption of a particle to the interface causes a reduction in the Gibbs free energy of the system. If the thermal energy is high enough so that it equals the adsorption energy, the system will become unstable as the thermal energy is high enough to remove particles from the interface. This was confirmed by observing data taken from multiple other research papers, which demonstrated that the adsorption energy must be many orders of magnitude larger than the thermal energy to enable foam stabilisation.

A study by Jin *et al.* investigated the use of edible ethyl cellulose particles for stabilisation of food-grade foams.[39] Ethyl cellulose powder was dissolved in acetone at a concentration of 1 wt. %. To this, the same volume of deionised water was added rapidly, leading to a system supersaturated with ethyl cellulose. This led to a formation of ethyl cellulose colloidal particles via a nucleation and growth mechanism. Foams were generated by aerating a 2 wt. % dispersion of ethyl cellulose in water by hand shaking or shear mixing for two minutes. Measurements on the foamability, foam stability and disproportion rate of the foams were made. Zeta potential measurements on the particles gave a value of -50 mV, indicating a strong negative charge on the particle surfaces. Foams in water at a neutral pH showed fair stability and foamability (collapse within a few hours) this was attributed to some residual water soluble surface-active component from the particles. Particle adsorption to the bubble surfaces was seen to be poor at neutral pH.

Foam volumes and stability of 2 wt. % ethyl cellulose foams were shown to be significantly increased by acidification of the solution. The subnatant liquid that drained from the foams was clear and micrscopy of the bubbles demonstrated multilayers of particles at the bubble surfaces. The foam bubbles also had wrinkled surfaces, indicative of particle adsorption. Cryo-SEM observations supported this. The increase in foaming properties at acidic pH was attributed to the reduction of the energy barrier for particle attachement to the interface by addition of salt/acidification. For extremely high pH values, the surface charge of the particles is still expected to be very negative, but the overall ionic strength may induce a screening of the surface charge, resulting in a reduced repulsion barrier between particles and the air-water interface.

Foaming methods with higher shear generated foams with an overrun of around 1000% with much smaller and more monodisperse bubbles. The higher amount of mechanical energy input into the systems using high shear methods enables incorporation of a much higher volume fraction of gas, generating bubbles with a much higher surface area. This in turn requires more particles to stabilise and so the maximum overrun in these systems is limited by the number of particles available.

Most of the literature discussed has covered the use of particles in the stabilisation of aqueous foams. This project however, aims to investigate the behaviour of particles in alcohol-containing systems, for which the literature is a little sparser.

Fletcher and Holt investigated the behaviour of fumed silica particles coated to varying extents with DCDMS in aqueous methanol-air systems.[35] Immersion times of 5 mg of hydrophobised powders in 5 ml liquid were measured and used to characterise the surface hydrophobicity of the powders, along with an acid-base conductivity titration to calculate the surface percentage of silanol groups. It was observed that with increasing DCDMS volume, both the immersion time and volume of methanol required to wet the particles increased. Vessels containing mixtures of the powders and liquids were hand-shaken and the colloidal systems produced were observed. With increasing methanol concentration a transition through liquid marbles (macroscopic drops of liquid in air coated with particles), climbing films (particle laden films that travel up the vessel walls), foams and then dispersions was observed. The systems generated were a result of the particle affinity for either the air phase or the aqueous methanol phase; the hydrophobic particles demonstrated an affinity for the surface in order to minimise contact with the liquid. With increasing concentration of methanol, the particles became progressively more wet and formed particle dispersions.

The particle affinity for a particular phase is determined by the particle contact angle and surface tension at the aqueous methanol-air interface. Contact angles of aqueous methanol sessile drops (in air) on glass slides hydrophobised with DCDMS were seen to decrease with increasing methanol concentration. From the contact angle values it was deduced that foams were generated in a region of contact angles of $30°> \theta <60°$, climbing films in a region of $60°> \theta <90°$ and liquid marbles at contact angles approaching 90°. It is important to note however, that the researchers made no direct measurement of particle contact angle, as no method for measurement of non-spherical, polydisperse particles currently exists. It is therefore not appropriate to assume that the contact angle of planar glass slides is identical to that of fractal fumed silica. Variation in the contact angle of smooth and rough surfaces can be observed in the contact angle hysteresis, that is the difference between the advancing and receding contact angle made at the three-phase contact line.

1.4.3.2   Particle-surfactant mixtures in foam stabilisation

Foams stabilised by particles alone have been shown to impart extreme stability to a foam structure. Much research has additionally investigated the effect of mixing surfactants and particles together,[40-49] with the intention of adsorbing surfactant molecules to the particle surfaces. Binks *et al.* discussed the generation of aqueous foams generated by a mixture of silica nanoparticles and pure cationic surfactant.[40] Aqueous dispersions (2 wt. %) of Ludox HS-30 silica nanoparticles (diameter = 13 nm) in the presence of di-decyldimethylammonium bromide (di-C_{10}DMAB) over a range of surfactant concentrations (0-47 mM) at a pH of 9.8 were observed. Adsorption isotherms of the dispersions were made by an Epton titration of supernatant liquid after centrifugation. Contact angles through water of aqueous surfactant solution sessile drops on silica coated planar silicon wafers were measured. Foams were generated by hand shaking 20 cm^3 liquid in a 140 cm^3 graduated volumetric cylinder.

It was observed that at a constant concentration of particles, varying surfactant concentration can have a significant effect on the foam stability. At high pH the silica surface is negatively charged, enabling adsorption of the cationic surfactant to the surface. A monolayer of adsorbed surfactant causes the particle surface to become hydrophobic, and can enhance foam stability. With further increasing concentration of surfactant, it was suggested that the surfactant adsorbs to the surfactant covered particle surface with tails down, forming a bilayer with a hydrophilic surface. At this point, it was theorised that foams would destabilise due to the increased hydrophilicity in the particle surface. Surfactant adsorption isotherms on particles demonstrated a gentle increase in the amount of adsorbed surfactant, with a more significant increase seen at higher concentrations. Measurements of ζ potential showed the addition of surfactant to the silica dispersions caused a reduction in the magnitude of the ζ potential (from an initial -48 mV) and at a surfactant concentration of 10 mM, a reversal in the sign was seen, indicating that the particle surface had become positively charged.

These measurements supported the theory that with increasing concentration of surfactant, the particle surface is initially hydrophobic and with increasing surfactant concentration, a bilayer forms and the surface becomes hydrophilic. Further support was seen in contact angle measurements, where contact angle was initially low, an increase in the contact angle was seen with increasing surfactant concentration, indicating the surface had become hydrophobic.

With further increase in surfactant concentration, the contact angle was seen to decrease. Generation of foams with particles alone showed them to be poor foaming agents. Surfactant alone however, was shown to be a much more effective foaming agent. Nonetheless, all surfactant foams had fully drained liquid within 10 minutes with full foam collapse occurring shortly after. Foams of particle-surfactant mixtures had a lower initial foam volume, however at high surfactant concentrations, the mixtures were seen to have much higher stability than surfactant alone system. This was most likely due to irreversible particle attachment (supported by microscopy) to the bubble surfaces, hindering disproportionation and coalescence. Disproportionation is reduced as the bubble size will shrink until the particles form a close-packed jammed layer at the interface, further bubble shrinkage would require ejection of the particles from the interface, which is energetically unfavourable. Coalescence is also reduced for this reason.

Similar observations have been made in systems of particles with charged surfaces and ionic surfactants in many other studies.[41-48] As a result of this, the synergistic relationship between particles and surfactants in foam and emulsion stabilisation is fairly well understood thanks to a considerable amount of research existing in this area. The stabilisation of foams using surfactants adsorbed to the surface of particles can utilise both stabilising aspects of these materials to generate foams with much higher stability than surfactant alone, and much higher foamability than particles alone. For example, the addition of surfactants to particle surfaces can reduce the air-water surface tension, aiding in foam formation.

1.5   Encapsulation of liquids by solid particles

In Figure 1.14, systems of liquid marbles and dry water were shown, both systems comprise liquid drops surrounded by a coating of hydrophobic (or oleophobic) particles at the liquid-air interface. Dry water is known to comprise significantly smaller liquid drops coated with a layer of particles in air, resulting in a fluffy free-flowing powder, which releases the encapsulated liquid upon shearing. Liquid marbles comprise larger liquid droplets coated in a particle layer in air. Much is understood about these systems and they have been demonstrated to have great potential for cosmetic, healthcare and gas sensing applications, amongst many other things.

1.5.1 Liquid marbles

Liquid marbles can be defined as macro-sized non-stick droplets encapsulated with micron or nanometre sized solid particles,[54] the first pioneering research into the area of liquid marbles was carried out by Aussilous and Quere.[50,51] Significant research in the area of aqueous liquid marbles has additionally been carried out by Bormashenko et al.[52-56] In one study, an investigation into the surface tensions of liquid marbles using three independent techniques was carried out.[55] Marbles were prepared by depositing drops of a fixed volume onto a superhydrophobic surface covered with a layer of powder. Four different powders were used; polyvinylidene fluoride (PVDF), polytetrafluoroethylene (PTFE), lycopodium and polyethylene (PE). The drops were rolled around in the powder gently, allowing them to become coated with powder and form a liquid marble. Three techniques were used to measure the surface tension of the liquid marbles, namely, the puddle height method, analysis of marble shape and vibration of marbles. The puddle height method briefly comprised increasing the volume of the liquid marble so that the shape changed from spherical to "puddle shaped" and measuring the height difference of the marbles with increasing liquid volume.

Using equation 1.13, the surface tension could be determined from knowing the density of the liquid (ρ) and the height of the marble (H).

$$\gamma = \frac{\rho g H^2}{4}$$

(1.13)

Analysis of marble shape was carried out by observation of contact diameter and height of the droplet using a goniometer, then comparing to analogous quantities calculated using the "oblate spheroid model". Marble vibration was carried out by producing horizontal vibrations and illumination using a horizontal laser beam which projected an enlarged image of the marble onto a screen via multiple lenses.

According to the puddle height method the surface tension values were as follows: 70, 66, 60 and 50 mJ/m^2 for PVDF, PE, PTFE and lycopodium powder-coated water marbles, respectively. Using marble shape analysis, surface tensions were determined to be 79, 63, 53 and 62 mJ/m^2 for PVDF, PE, PTFE and lycopodium powders, respectively. Finally, using the vibration method, surface tensions were determined to be 75, 60, 53 and 43 mJ/m^2 for PVDF, PE, PTFE and lycopodium powders, respectively. It was concluded therefore that all methods could accurately and consistently determine the surface tensions of liquid marbles. The researchers noted that attractive capillary forces between particles result in an increase in the effective surface tension of a liquid marble, while repulsive capillary forces can decrease the effective surface tension.

Some further work by Bormashenko *et al.* discussed the formation of liquid marbles comprising an aqueous ethanol core.[53] Three different types of powder were used; PTFE, PVDF and PE particles were used to coat 10 μl drops of water/ethanol solutions. The apparent contact angle of the marbles were carried out using goniometry. The apparent contact angles of the marbles were seen to decrease as the ethanol concentration inside the drop increased. The researchers found that for every liquid marble generated, there existed a limiting ethanol concentration and corresponding surface tension for generation of the marble. It was also seen that the surface tension decreases with increasing ethanol concentration. The maximum concentration which allowed liquid marble formation was using 21% ethanol, corresponding to a critical surface tension of 46.52 mN/m (using PE powder). Study of wetting transitions by increasing the ethanol concentration of a marble adhered to sticky tape was carried out.

With increasing ethanol concentration, the apparent contact angle decreased gradually until a point where an abrupt change was observed, indicating the onset of the wetting transition. The onset of the wetting transition defined the critical concentration of ethanol, or in other words, the point at which the particle surface becomes wet by the liquid comprising the marble core.

The concept of encapsulating liquids is very relevant to the current piece of work, and the study of marbles enables us to obtain information about potential core components on a macroscopic scale, as opposed to studying dry water directly. It is also possible for liquid marbles to perhaps themselves be used as a delivery system for antimicrobial agents, as much current research has demonstrated their use for sensing applications.[57,58]

Some other research has utilised titanate nanobelts to form liquid marbles which were mechanically and physically stable to manipulation, such as picking up and dropping from a height.[59] Evaporation through the particle shell is also another possible issue to consider when using liquid marbles for encapsulation. A review by McHale and Newton highlighted some properties of liquid marbles and some potential applications.[60] Liquid marbles have been demonstrated to be responsive to external stimuli such as a magnetic field[61] or exposure to gas.[62] This can demonstrate the potential of liquid marbles for applications such as sensing and miniature reactors for biological reactions (such as blood typing) or catalysis. There are many advantages of miniaturising chemical and biological reactions; smaller amounts of samples and reagents result in a reduced cost, reduced hazard and potentially faster reaction times.

1.5.2 Dry water

Dry water is a material similar in structure to liquid marbles, whereby drops of liquid (water in this case) are coated with a layer of hydrophobic particles. However, the encapsulated liquid drops in dry water are much smaller, resulting in a free-flowing powder (shown in Figure 1.15.). Upon shear, the dry water can release the encapsulated liquid, giving many potential applications in cosmetic and healthcare industries. Dry water was initially discovered and patented in 1968 by Degussa[63] and after initial attention the discovery became relatively dormant, until it was rediscovered in 2006 at the University of Hull.[34] Further work by Binks *et al.* investigated the properties of dry water on addition of different components to the aqueous phase, such as surfactants, acid or salt or by varying the particle composition itself.[34,45,64] Additionally, it has been noted that the inversion of an air-in-water foam to a water-in-air system is similar to that of catastrophic phase inversion of oil-water emulsions.[65]

Research has been carried out on the capability of dry water to act as means of uptaking and storing gas due to the significantly increased surface area of the encapsulated liquid. Studies carried out by Wang *et al.* have demonstrated dry water to be a successful means of storing methane,[66] and the work of Carter *et al.* utilised dry water as a means of storing carbon dioxide and krypton.[67] Furthermore, this work investigated the potential of encapsulating an aqueous gel in fumed silica, named "dry gel" by the researchers. A separate study explored the potential of dry water to act as a heterogeneous catalyst by encapsulating maleic acid and exposing to hydrogen gas.[68]

The conversion to succinic acid of maleic acid in dry water was compared to aqueous maleic acid being stirred at 1200 r.p.m. for two hours. The dry water was shown to have similar quantity of maleic acid converted to succinic acid when compared to the sample being stirred for two hours, but was expected to be a lot more energetically favourable than stirring for two hours. The work of Yang *et al.* has also reported the use of "dry" alkanolamine, that is, alkanolamine encapsulated by fluorinated silica, for capture of carbon dioxide gas.[69]

Figure 1.15. Photo of dry water (95g water and 5g fumed silica particles of 32% SiOH) passing through a funnel. Scale bar = 1 cm. Image republished with permission from reference 34.

It has been found that the addition of salt to aqueous dispersions of relatively hydrophilic (66% SiOH) silica particles increased the ability to generate aqueous foams. In the absence of salt, no foams could be formed. The addition of salt was shown to reduce the particle zeta potential, making the particles more hydrophobic. It was also seen in the same study, that increasing the pH of the aqueous phase of dry water systems caused an inversion to aqueous foams. With further increase in the pH the systems inverted completely to dispersions.[64] This inversion was attributed to a decrease in the receding contact angle of the particles upon increasing the pH, caused by the varying ionisation of the surface silanol groups with varying pH. The addition of surfactant to the aqueous phase of dry water systems has also shown to induce phase inversion to aqueous foams.[45]

The effect of varying the surface tension of the liquid phase on the colloidal systems generated has been explored by Binks and Rocher.[70] Polytetrafluoroethylene (PTFE) particles were spread on the surfaces of various liquids (short and long alkanes, toluene, alcohols, esters. glycerol and water) and their wetting behaviour observed. The particles were seen to be completely wet by liquids of low surface tension (short alkanes, perfluorohexane) or partially wet by liquids of slightly higher surface tension, such as long alkanes or toluene.

The PTFE particles were completely non-wetted by liquids of higher surface tension, such as alcohols, glycerol and water. The mixtures of particles, liquid and air were then agitated by homogenisation, blending and hand shaking. For particles that were completely wet by the liquid, unstable dispersions were formed upon aeration. For liquids of higher surface tension, air in liquid foams were formed that were stable to coalescence and disproportionation for many days. For liquids of significantly higher surface tension, such as water and glycerol, an inversion of the material was seen, so that a water in air material (termed "soufflé") was formed. The material was termed soufflé as it was not free-flowing like dry water but upon shearing, released the encapsulated liquid, much like dry water. Systems of encapsulated liquids other than water have been reported in the literature, with examples of materials such as "dry oil" (oil droplets encapsulated by particles) being reported.[71] It is clear that for the successful encapsulation of liquids of much lower surface tension, particles of very low surface energy are required.

1.6   The Fenton reaction

The primary aim of this research is to generate a novel hand sanitiser based on the Fenton reaction. This novel sanitiser should demonstrate an enhanced antibacterial efficacy in comparison to current alcohol-based sanitisers. Additionally, the novel hand sanitiser should be kinder to the skin surface in comparision to current sanitisers. The traditional Fenton reaction comprises the iron-catalysed reduction of hydrogen peroxide into hydroxyl radicals and was discovered in 1894 by Fenton[72,73] after observing that hydrogen peroxide in the presence of iron salts could rapidly oxidise tartaric acid. It was Haber and Weiss in 1934[74] who first suggested the formation of hydroxyl radicals as an intermediate in the decomposition of hydrogen peroxide by iron salt:[81]

$$Fe^{2+} + H_2O_2 + H^+ \rightarrow Fe^{3+} + H_2O + {}^{\bullet}OH \tag{1.14}$$
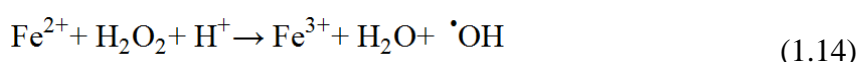
The formation of the hydroxyl radical ($\cdot$OH) has been confirmed by Baxendale *et al.* by initiating a polymeric reaction with hydroxyl radicals produced from the Fenton reaction.[75] Additionally Fenton reagent has been shown to be an effective hydroxylating agent in many other systems, giving support for the formation of hydroxyl radical intermediates.[76] In 1950, Barb *et al.* suggested a mechanism for the Fenton reaction in which the Fe^{2+} is regenerated, thus acting as a true catalyst:[77]

$$Fe^{2+} + H_2O_2 \rightarrow Fe^{3+} + HO^{\bullet} + HO^{-} \tag{1.15}$$

$$Fe^{2+} + {}^{\bullet}OH \rightarrow Fe^{3+} + HO^{-} \tag{1.16}$$

$$HO^{\bullet} + H_2O_2 \rightarrow HO_2^{\bullet} + H_2O \tag{1.17}$$

$$HO_2^{\bullet} + Fe^{2+} \rightarrow Fe^{3+} + HO_2^{-} \tag{1.18}$$

$$HO_2^{\bullet} + Fe^{3+} \rightarrow Fe^{2+} + O_2 + H^+ \tag{1.19}$$

However, despite the work carried out to date, much controversy still surrounds the exact mechanism of the reaction. Many other researchers have suggested other mechanisms for the reaction in which high valent metal species are formed as intermediates.[78-81] The work of Goldstein *et al.* has proposed the formation of a transient metal complex (L_mM-$H_2O_2^{n+}$) which may degrade to hydroxyl radicals or a higher oxidation state of the metal ion ($L_mM^{(n+2)+}$).[81]

There are many contradicting opinions (with supporting evidence) on the true mechanism of the Fenton reaction, all of which are viable. It can therefore be said that the exact mechanism of the Fenton reactions remains unknown to this day, over 100 years since the reaction was first discovered.

1.6.1 Copper-catalysed Fenton reaction

The catalytic behaviour of iron salts with hydrogen peroxide is clear. However, the potential of other multi-valent metal ions as catalysts for the degradation of hydrogen peroxide has been illuminated recently in the literature. Multiple other metal ions, such as chromium, cerium, cobalt, manganese and copper have been shown to demonstrate catalytic behaviour in the degradation of hydrogen peroxide, in what has been called the "Fenton-like reaction".[82] Specifically the role of copper in the Fenton-like redox chemistry of hydrogen peroxide is of particular interest in this research. The high solubility of copper (II) sulfate makes it an ideal copper salt for use in the current project.

The Fenton-like activity of copper (II) salts has been widely investigated and a proposed mechanism has been put forward by Bokare and Choi:[82]

$$Cu^{2+} + H_2O_2 \rightarrow Cu^+ + HO_2^\bullet + OH^- \tag{1.20}$$

$$Cu^+ + H_2O_2 \rightarrow Cu^{2+} + HO^\bullet + HO^- \tag{1.21}$$
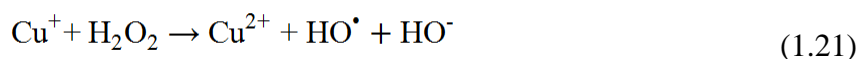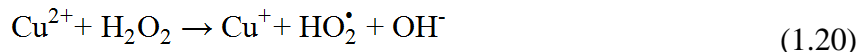
It can be seen that the copper is initially reduced to copper (I) and again further oxidised back to copper (II) forming hydroxyl and hydroperoxyl radicals in the process. Similarly to the iron-catalysed Fenton reaction, there are many different potential reaction pathways proposed throughout the literature. Support for the formation of hyroxyl radicals has been demonstrated by Ozawa and Hanaki and Kim and Metcalfe by measurement using electron spin resonance-spin trapping.[83,84] Additional support has come from research carried out by measuring the degradation of dye molecules by hydroxyl radicals.[85,86] Gabriel *et al.* confirmed the production of hydroxyl radicals by measuring the degradation of polycyclic aromatic hydrocarbons by copper (II) and hydrogen peroxide.[87]

Conversely, Lee *et al.* proposed the formation of high valent metal complexes of copper (cupryl ions) to be responsible for the oxidation of organic probe compounds.[88]Additionally, a study by Pham *et al.* suggested that Cu (III) is formed as a result of the oxidation of Cu(I) with hydrogen peroxide,[89] although it was noted by these researchers the complexities in elucidating the intermediates in the reaction of Cu(II) and H_2O_2.

1.6.2 Anti-bacterial activity of Fenton reaction

The anti-bacterial activity of Fentons reagent is well known and well-understood, and is suspected to be a reason for the high susceptibility of bacterial cells to hydrogen peroxide, as the components of the microbial cells contain high concentrations of iron.[90] This has been supported by the work of Repine *et al.* who found that cells of *Staphylococcus aureus* grown overnight in an overnight broth containing iron, had higher intracellular content of iron.[91] The cells with higher intracellular iron content were found to be more susceptible to cell death by exposure to hydrogen peroxide.

The behaviour of copper as a biocidal agent in conjunction with hydrogen peroxide has also been extensively studied. Research by Cross *et al.* demonstrated the killing of *Bacillus globigii* spores by a modified Fenton reagent of Cu^{2+}, ascorbic acid and sodium chloride.[92] It was proposed that hydrogen peroxide was produced by the reaction of Cu^{2+} with dissolved oxygen and that the production of hydroxyl radicals occurred within the bacterial spores, deactivating them. The work of Dittmar *et al.* showed that the addition of Cu^{2+} salts to cultures of *Escherichia coli* and *Staphylococcus aureus* in the presence of hydrogen peroxide resulted in a significant reduction in bacterial growth.[93] Further to this, a study by Bayliss and Waites demonstrated the addition of Cu^{2+} salts to *Clostridium bifermentans* colonies with hydrogen peroxide, increased the lethal effect of the hydrogen peroxide by a factor of around 3000.[94] In a separate study, analysis of calf thymus DNA samples after exposure to Cu^{2+} and Fe^{2+} salts in the presence of H_2O_2 for 1 hour showed the degradation of the DNA into DNA bases.[95] It was found that for the copper system, a much higher amount of DNA bases were produced, indicating the system attacked the DNA structure to a greater extent than the iron system. Additional support for the production of radicals in many of the studies shown comes from the study of addition of radical scavengers to the systems. The addition of hydroxyl scavengers in the systems explained above results in a reduction in the bacterial kill.

The anti-bacterial effects of the Fenton-like system of copper (II) salts and hydrogen peroxide is clear from the portion of literature presented above. As a result of the clear anti-microbial efficacy, it is intended in this research to utilise the Cu^{2+}/H_2O_2 Fenton-like system as a novel hand sanitiser.

1.7   Aims of research

The overall aim of the research presented in this thesis is to develop a novel encapsulated hand sanitiser. This sanitiser will be based on the Fenton reaction, and thus should comprise two separate components, namely copper (II) sulfate and hydrogen peroxide. As shown throughout the literature, the rapid generation of hydroxyl radicals upon combining the two Fenton reagents is suggested to be a very effective mechanism for killing bacteria, therefore the two components of the reaction will need to be kept apart until the point of use on the skin. To achieve this, we intend to utilise dry water technology and encapsulate aqueous copper sulfate, and aqueous hydrogen peroxide as two separate dry powders (shown in Figure 1.16). It is intended that upon application and shearing of the two separate powders to the skin surface, the aqueous Fenton components will be released onto the surface on the skin where they can mix, react and consequently kill bacteria residing on the skin surface.

Figure 1.16.   Schematic representation of aqueous copper (II) sulfate and aqueous hydrogen peroxide, encapsulated with hydrophobic fumed silica powder, to form dry water containing the aqueous Fenton reagents.
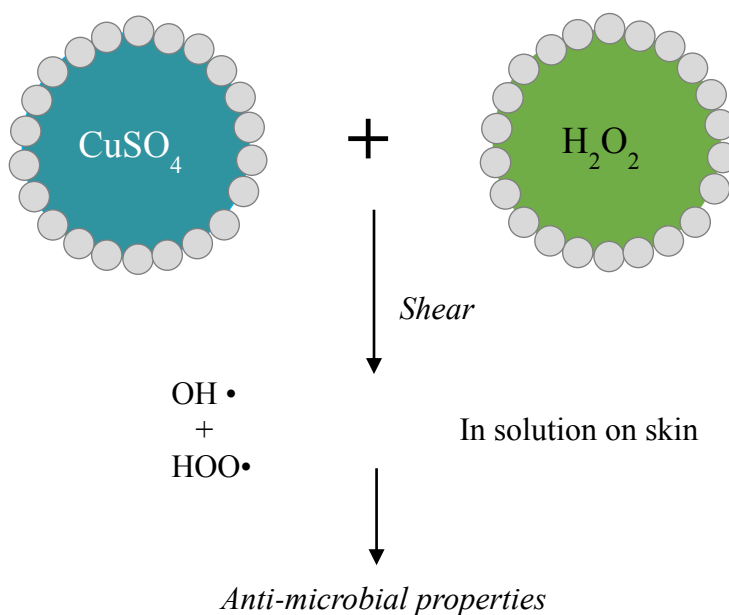
As a review of the literature has shown, encapsulation of liquids of varying surface tension may require particles with a lower surface energy. To explore this, the surface modification of monodisperse silica particles with fluorine groups will be carried out. The behaviour of these hydrophibic particles at air-water interfaces will be explored. Furthermore, the effect of addition of a liquid of lower surface tension (ethanol) will be investigated. The contact angles of the particles at the air-liquid interface will be measured directly with the film calliper method. The behaviour of these particles when spread at horizontal air-liquid interfaces and when aerated will also be investigated. This will give insight into the behaviour of these fluorinated particles at aqueous ethanol-air interfaces for application of encapsulation of liquids of lower surface tension.

Additionally, a separate study will be carried out where it is intended to gain an understanding of the behaviour of fumed silica particles as foaming agents in the presence of aqueous ethanol and surfactant. It is well understood from the literature that a synergistic relationship exists between particles and surfactants with respect to stability and foamability of aqueous solutions. For potential application in current foaming aqueous ethanol sanitiser products (Deb ''InstantFOAM$^{®}$''), an understanding of the foaming properties of particles alone, in the presence of surfactants and in the presence of aqueous ethanol is necessary. Thus, a systematic investigation into the foaming behaviour of fumed silica in solutions of two different commercial nonionic surfactants, and in the presence of aqueous ethanol will be carried out.

1.8   Presentation of thesis

The thesis is divided into six chapters, three of which present experimental results. Chapter 2 details all of the materials and experimental techniques used throughout the project. Chapter 3 concerns the stabilisation of aqueous foams using fumed silica particles; the chapter is broken down into 3 main investigations, namely the behaviour of aqueous-ethanolic foams in the presence of surfactant alone and in the presence of particles alone. The surfactants investigated are two commercial grade, nonionic surfactants obtained from the industrial sponsor (currently used in a foaming alcohol sanitiser on the market). Finally, an investigation into the behaviour of aqueous foams of the two surfactants in the presence of fumed silica particles is presented. Parameters such as the surfactant concentration, particle concentration and particle hydrophobicity have been explored.

Chapter 4 presents a protocol for the fluorination of hydrophilic, silica particles of 2 μm diameter. A study in which various experimental conditions in the surface modification of glass slides with 1H, 1H, 2H, 2H-perfluorooctyldimethylchlorosilane and 1H, 1H, 2H, 2H-perfluorooctylmethyldichlorosilane is presented. From this, the protocol for the controlled fluorination of the surface of monodisperse silica particles of 2 μm diameter was developed. The contact angle of these surface modified particles at air-water and aqueous ethanol-air interfaces has been measured directly using the film calliper method. In addition to this, the effect of particle hydrophobicity on the lateral interactions at air-water and aqueous ethanol-air interfaces, as well as their colloidal behaviour upon aeration is presented.

The kinetic behaviour of the copper-catalysed Fenton-like reaction as a function of the concentration of both Fenton reagents is presented in Chapter 5. Additional parameters such as the effect of pH on the rate of the Fenton reaction are also explored in this chapter. The potential for encapsulation of various formulation components including the Fenton reagents in the format of dry water is investigated. Finally, the application of the Fenton reaction for anti-bacterial efficacy is studied by means of *in vitro* and *in vivo* experiments on *Escherichia coli* bacteria. Due to the nature of the testing methods for *in vitro* testing, only solutions of the Fenton reagents are studied. However, for *in vivo* studies, where the hands can be used to shear dry water, a comparison between the efficacy of the Fenton solution and encapsulated Fenton solutions is carried out. Finally, a summary of conclusions and proposals for future work are presented in Chapter 6.

1.9   References

1. R.K. Prud'homme and S.A. Khan, *Foams Theory, Measurements, and Applications*, Marcel Dekker Inc., New York, 1996.

2. D. Exerowa and P.M. Kruglyakov, *Foams and Foam Films: Theory, Experiment, Application*, Elvesier, Amsterdam, 1998.

3. J. Haedelt, D.L. Pyle, S.T. Beckett and K. Niranjan, *J. Food Sci.*, 2005, **70**, 159.

4. I.B. Ivanov, *Thin Liquid Films Fundamentals and Applications, Marcel Dekker Inc.*, New York, 1988.

5. L.L. Schramm, *Emulsions, Foams and Suspensions*, Wiley-VCH, Weinhein, 2005.

6. P. Atkins and J. De Paula, *Atkins' Physical Chemistry*, 8th Edition, Oxford University Press, Oxford, 2006.

7. G.T. Barnes and I.R. Gentle, *Interfacial Science: an introduction*, 2nd Ed., Oxford University Press, New York, 2011.

8. P.J. Wilde, *Curr. Opin. Colloid Interface Sci.*, 2000, **5**, 176.

9. S. Samanta and P. Ghosh, *Chem. Eng. Res. Des.*, 2011, **89**, 2344.

10. T. Tamura, Y. Kaneko and M. Ohyama, *J. Colloid. Int. Sci.*, 1995, **173**, 493.

11. T. Tamura, Y. Takeuchi and Y. Kaneko, *J. Colloid. Int. Sci.*, 1998, **206**, 112.

12. A. Dutta, A. Chengara, A. Nikolov, D.T. Wasan, K. Chen and B. Campbell, *J. Food Sci.*, 2002, **67,** 3080.

13. S.U. Pickering, *J. Chem. Soc., Trans.*, 1907, **91**, 2001.

14. W. Ramsden, *Proc. Roy. Soc.*, 1903, **72**, 156.

15. B. Derjanguin and L. Landau, *Acta Physico Chemica URSS*, 1941, **14**, 633.

16. E.J.W. Verwey and J.Th.G. Overbeek, *Theory of the Stability of Lyophobic Colloids*, Elsevier Publishing Company Inc., New York, 1948.

17. J.Th.G. Overbeek, *J. Colloid Interface Sci.*, 1977, **58**, 408.

18. R.A. Williams, *Colloid and Surface Engineering: Applications in the Process Industries*, Butterworth-Heinemann, Oxford, 1992.

19. K.S. Birdi, *Handbook of Surface and Colloid Chemistry*, 2nd Ed., CRC Press, Florida, 2003.

20. R.J. Hunter, *Introduction to Modern Colloid Science*, Oxford University Press, Oxford, 1993.

21. B.P. Binks and T.S. Horozov, *Colloidal Particles at Liquid Interfaces*, Cambridge University Press, Cambridge, 2006.

22. R.N.Wenzel, *Ind. Eng. Chem.*, 1936, **28**, 988.

23. A.B.D. Cassie and S. Baxter, *Trans. Faraday Soc.*, 1944, **40**, 546.

24. E.L. Decker and S. Garoff, *Langmuir*, 1997, **13**, 6321.

25. T.S. Horozov, D.A. Braz, P.D.I. Fletcher, B.P. Binks and J.H. Clint, *Langmuir*, 2008, **24**, 1678.

26. V.N. Paunov, *Langmuir*, 2003, **19**, 7970.

27. O.J. Cayre and V.N. Paunov, *Langmuir*, 2004, **20**, 9594.

28. Z. Hórvölgyi, M. Máté, A. Dániel and J. Szalma, *Colloids Surf. A*, 1999, **156**, 501.

29. A. Hadjiiski, R. Dimova, R. Denkov, N.D. Ivanov and R. Borwankar, *Langmuir*, 1996, **12**, 6665.

30. M. Preuss and H.J. Butt, *J. Colloid Interface Sci.*, 1998, **208**, 468.

31. Z.-G. Cui, Y.-Z. Cui, Z. Chen and B.P. Binks, *Langmuir*, 2010, **26**, 12567.

32. L. Zhang, P. Somasundaran and C. Maltesh, *J. Colloid Interface Sci.*, 1997, **191**, 202.

33. T.S. Horozov, *Curr. Opin. Colloid Interface Sci.*, 2008, **13**, 134.

34. B.P. Binks and R. Murakami, *Nat. Mater.*, 2006, **5**, 865.

35. P.D.I. Fletcher and B.L. Holt, *Langmuir*, 2011, **27**, 12869.

36. B.P. Binks and T. S. Horozov, *Angew. Chem. Int. Ed.*, 2005, **44**, 3722.

37. A. Stocco, E. Rio, B.P. Binks and D. Langevin, *Soft Matter*, 2011, **7**, 1260.

38. D.O. Vivaldini, A.P. Luz, V.R. Salvini and V.C. Pandolfelli, *Ceram. Int.*, 2013, **39**, 6005.

39. H. Jin, W. Zhou, J. Cao, S.D. Stoyanov, T.B.J. Blijdenstein, P.W.N. de Groot, L.N. Arnaudov and E.G. Pelan, *Soft Matter*, 2012, **8**, 2194.

40. B.P. Binks, M. Kirkland and J.A. Rodrigues, *Soft Matter*, 2008, **4**, 2373.

41. B.S. Murray, K. Durga, A. Yusoff and S.D. Stoyanov, *Food Hydrocoll.*, 2011, **25**, 627.

42. Z.-G. Cui, Y.-Z. Cui, C.-F. Cui, Z. Chen and B.P. Binks, *Langmuir*, 2010, **26**, 12567.

43. B. Tigges, T. Dederichs, M. Möller, T. Liu, W. Richtering and O. Weichold, *Langmuir*, 2010, **26**, 17913.

44. F. Carn, A. Colin, O. Pitois, M. Vignes-Adler and R. Backov, *Langmuir*, 2009, **25**, 7847.

45. B.P. Binks, A.J. Johnson, J.A. Rodrigues, *Soft Matter*, 2009, **6**, 126.

46. T.N. Hunter, E.J. Wanless, G.J. Jameson and R.J. Pugh, *Colloids Surf. A*, 2009, **347**, 81.

47. L.R. Arriaga, W. Drenckhan, A. Salonen, J.A. Rodrigues, R. Íniguez-Palomares, E. Rio and D. Langevin, *Soft Matter*, 2012, **8**, 11085.

48. S. Zhang, Q. Lan, Q. Liu, J. Xu and D. Sun, *Colloids Surf. A*, 2008, **317**, 406.

49. S. Zhang, D. Sun, X. Dong, C. Li and J. Xu, *Colloids Surf. A*, 2008, **324**, 1.

50. P. Aussillous and D. Quere, *Nature*, 2001, **411**, 924.

51. P. Aussillous and D. Quere, *Proc. Roy. Soc. Lond. A. Mat.*, 2006, **462**, 973.

52. E. Bormashenko, *Curr. Opin. Colloid Interface Sci.*, 2011, **16**, 266.

53. E. Bormashenko, R. Balter and D. Aurbach, *J. Colloid Interface Sci.*, 2012, **384**, 157.

54. E. Bormashenko, *Soft Matter*, 2012, **8**, 11018.

55. E. Bormashenko, R. Pogreb, G. Whyman and A. Musin, *Colloid. Surface. A*, 2009, **351**, 78.

56. E. Bormashenko, Y. Bormashenko and A. Musin, *J. Colloid Interface Sci.*, 2009, **333**, 419.

57. J. Tian, T. Arbatan, X. Li and W. Shen, *Chem. Eng. J.*, 2010, **165**, 347.

58. J. Tian, T. Arbatan, X. Li and W. Shen, *Chem. Commun.*, 2010, **46**, 4734.

59. Y. Lai, Y. Tang, J. Huang, H. Wang, H. Li, D. Gong, X. Ji, J. Gong, C. Lin, L. Sun and Z. Chen, *Soft Matter*, 2011, **7**, 6313.

60. G. McHale and M.I. Newton, *Soft Matter*, 2015, **11**, 2530.

61. S. Zhang, Y. Zhang, Y. Wang, S. Liu and Y. Deng, *Phys. Chem. Chem. Phys.*, 2012, **14**, 5137.

62. T. Iharaf and Y. Iriyama, *J. Photopolm. Sci. Technol.*, 2011, **24**, 435.

63. D. Schutte, F.-T. Schmitz and H. Brünner, *Predominantly aqueous compositions in a fluffy powder form approximating powdered solids behaviour and process for forming same*, 1968, US 3393155 A.

64. B.P. Binks, B. Duncumb and R. Murakami, *Langmuir*, 2007, **23**, 9143.

65. B.P. Binks and S.O. Lumsdon, *Langmuir*, 2000, **16**, 8622.

66. W. Wang, C.L. Bray, D.J. Adams and A.I. Cooper, *J. Am. Chem. Soc.*, 2008, **130**, 11608.

67. B.O. Carter, W. Wang, D.J. Adams and A.I. Cooper, *Langmuir*, 2010, **26**, 3186.

68. B.O. Carter, D.J. Adams and A.I. Cooper, *Green Chem.*, 2010, **12**, 783.

69. J. Yang, H.Y. Tan, Q.X. Low, B.P. Binks and J.M. Chin, *J. Mater. Chem. A*, 2015, **3**, 6440.

70. B.P. Binks and A. Rocher, *Phys. Chem. Chem. Phys.*, 2010, **12,** 9169.

71. B.P. Binks, T. Sekine and A.T. Tyowua, *Soft Matter*, 2014, **10**, 578.

72. H.J.H. Fenton, *J. Chem. Soc. Trans.*, 1894, **65**, 899.

73. K. Barbusiński, *Chemia Dydaktyka Ekologica Metrologica*, 2009, **14**, 101.

74. F. Haber and J. Weiss, *Proc. Roy. Soc. A*, 1934, **147**, 332.

75. J.H. Baxendale, M.G. Evans and G.S. Park, *Trans.Faraday Soc.*, 1946, **42**, 155.

76. J.H. Merz and W.A. Waters, *Discuss. Faraday Soc.*, 1947, **2**, 179.

77. W.G. Barb, J.H. Baxendale, P. George and K.R. Hargrave, *Trans. Faraday Soc.*, 1957, **47**, 462.

78. W.C. Bray and M.H. Gorin, *J. Am. Chem. Soc.*, 1932, **54**, 2124.

79. D.T. Sawyer, A. Sobkowiak and T. Matsushita, *Acc. Chem. Res.*, 1996, **29**, 409.

80. S. Goldstein and D. Meyerstein, *Acc. Chem. Res.*, 1999, **32**, 547.

81. S. Goldstein, D. Meyerstein and G. Czapski, *Free Radical Bio. Med.*, 1993, **15**, 435.

82. A.D. Bokare and W. Choi, *J. Hazard. Mater.*, 2014, **275**, 121.

83. T. Ozawa and A. Hanaki, *J. Chem. Soc., Chem. Commun.*, 1991, **5**, 330.

84. J.K. Kim and I.S. Metcalfe, *Chemosphere*, 2007, **69**, 689.

85. I.A. Salem, *App. Catal. B: Environ.*, 2000, **28**, 153.

86. V. Shah, P. Verma, P. Stopka, J. Gabriel, P. Baldrian and F. Nerud, *App. Catal. B: Environ.*, 2003, **46**, 287.

87. J. Gabriel, V. Shah, P. Baldrian and F. Nerud, *Folia. Microbiol.*, 2000, **45**, 573.

88. H. Lee, H.-J. Lee, D.L. Sedak and C. Lee, *Chemosphere*, 2013, **92**, 652.

89. A.N. Pham, G. Xing, C.J. Miller and T.D. Waite, *J. Catal.*, 2013, **301**, 54.

90. E. Linley, S.P. Denyer, G. McDonnell, C. Simons and J.-Y. Maillard, *J. Antimicrob. Chemother.*, 2012, **67**, 1589.

91. J.E. Repine, R.B. Fox and E.M. Berger, *J. Biol. Chem.*, 1981, **256**, 7094.

92. J.B. Cross, R.P. Currier, D.J. Torraco, L.A. Vanderberg, G.L. Wagner and P.D. Gladen, *App. Environ. Microbiol.*, 2003, **69**, 2245.

93. H.R. Dittmar, I.L.Baldwin and S.B. Miller, *J. Bacteriol.*, 1930, **19**, 203.

94. C.E. Bayliss and W.M. Waites, *J. Gen. Microbiol.*, 1976, **96**, 401.

95. O.I. Aruoma, B. Halliwell, E. Gajewski and M. Dizdaroglu, *Biochem. J.*, 1991, **273**, 601.
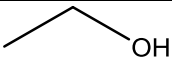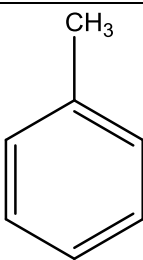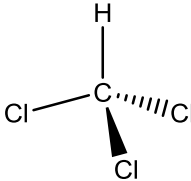
CHAPTER 2

EXPERIMENTAL
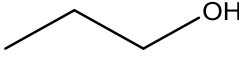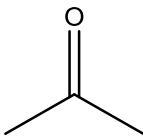
This chapter provides a detailed description of the materials used along with a comprehensive review of all experimental methods.

2.1 Materials

2.1.1 Solvents

Water was purified by passing through an Elgastat Prima reverse osmosis unit followed by a Millipore Milli-Q reagent water system. The resistivity of the water was always approximately 18 mΩ cm. The surface tension of the water was measured (Krüss K12 tensiometer, Wilhelmy plate method) at regular intervals. The tension was found to be 71.9 $\pm$ 0.2 mN m^{-1} at 25°C which is in good agreement with the literature value[1] and indicates the water was free of any surface-active impurities. Table 2.1 shows the solvents used in all experiments discussed throughout the thesis.
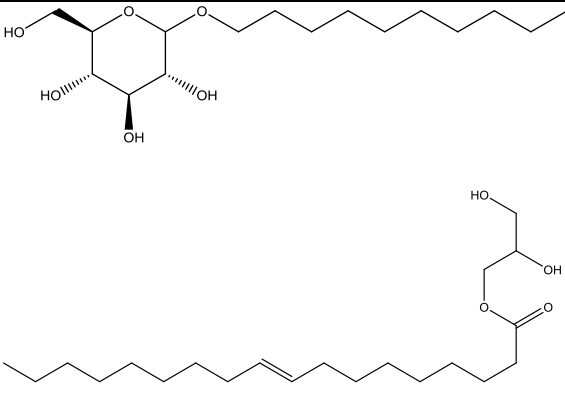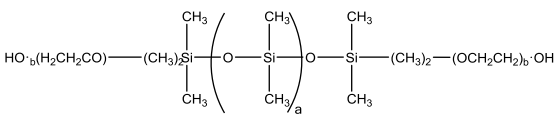
Table 2.1.   Structure, suppliers and purity of solvents used.

Solvent	Structure	Supplier	Purity/ %
Ethanol (absolute)		VWR	99.8
Methanol	H_3C——OH	Fisher Scientific	99.99
Toluene (anhydrous)		Acros Organics	99.8
Chloroform		Fisher Scientific	99.0
Propan-2-ol		VWR	99.7
Acetone		VWR	99.8

Two commercial nonionic surfactants were used to generate surfactant-stabilised foams. The surfactants were used as received and dissolved in water to prepare surfactant solutions. The surfactant structures are given in Table 2.2. It can be seen that Lamesoft PO65 is a mixture of coco glucoside and glyceryl oleate, the relative quantities of these two components was unknown and unavailable from the supplier. Analysis methods such as Nucelar Magnetic Resonance Spectroscopy (NMR) could be used to quantify the relative amounts of each surfactant in the mixtures. Silsurf DI-2510 is a silicone polymer with between 20-28 di-functional silicone groups ("a" units) and the silicone backbone is end capped with 12 oxyethylene units ("b" units). Gel Permeation Chromatography (GPC) could be used to identify the molecular weight distribution of this polymeric surfactant.

Table 2.2.   Structure and supplier of two commercial nonionic surfactants used.

Surfactant	Structure	Supplier	Batch Number
Lamesoft PO65 (Coco glucoside + Glycerol oleate)		BASF	0008704 820
Silsurf DI-2510 (bis-PEG-12 dimethicone)		Siltech	1207054

2.1.3   Particles

2.1.3.1 Fumed silica

Fumed silica is a fractal, non-spherical silicon dioxide. Fumed silica is prepared by passing silicon tetrachloride through an oxyhydrogen flame at around 1500°C. The primary particle size of fumed silica particles is 10-20 nm. These particles then irreversibly fuse together forming larger aggregates, which can entangle to form large agglomerates in the micron size range.[2] Figure 2.1 shows a transmission electron microscopy image of fumed silica particles. Fumed silica particles are initially hydrophilic due to a surface coating of hydroxyl groups bound to silicon atoms. However, the particles can be hydrophobised to varying extents with dichlorodimethylsilane (DCDMS). The particle hydrophobicity is characterised by the percentage of silanol groups remaining on the particle surface. Relative surface silanol content of 100% corresponds to the original hydrophilic fumed silica. All fumed silica particles provided and hydrophobised by Wacker-Chemie and the details are given in Table 2.3.

Figure 2.1.   TEM images of dry fumed 20% SiOH silica powder. TEM carried out by Ann Lowry at The University of Hull.
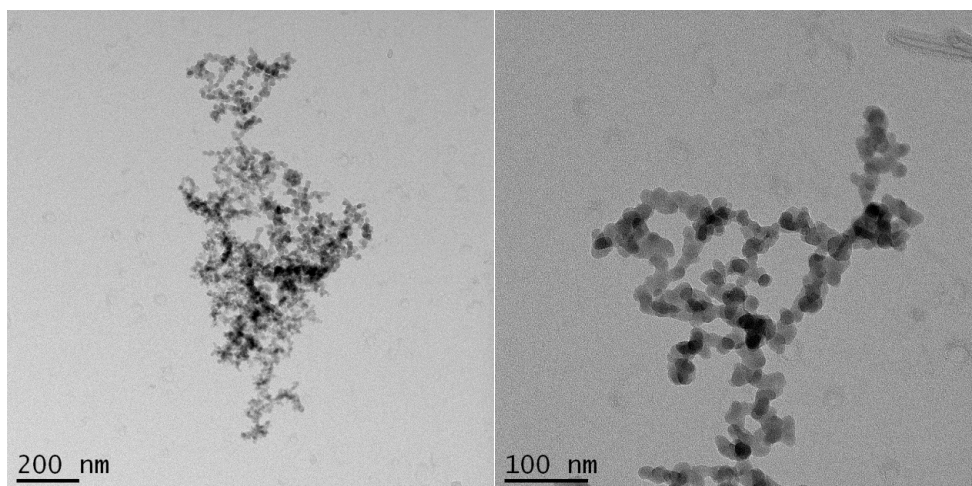
Table 2.3.   Fumed silica particles used in all experiments.

Relative surface silanol content/ %	Batch number
20	HDK H18 SK31350
47	HDK H30 ZK34676
100	HDK N20

2.1.3.2 Monodisperse silica

Monodisperse silica particles were obtained from Fibre Optic Centre Ltd. (Massachusetts). All monodisperse silica particles were untreated and so were initially hydrophilic. The powders were prepared by the manufacturer using the Stöber process as detailed by Stöber *et al.*[3] The process consists of addition of a tetraester of silicic acid (such as tetraethylorthosilicate, TEOS) to a dilute solution of alcohol and ammonia as a catalyst.[4,5] Hydrolysis of the TEOS forms an intermediate hydrolysed TEOS species – $(OC_2H_5)_3Si(OH)$. Further condensation of this species results in monodisperse solid silica particles. Details of the particles are given in Table 2.4 including the measured average particle diameter (average of 130 particles) carried out using scanning electron microscopy. The laser diffraction values (Malvern Mastersizer 2000 SM on 5 wt. % particle dispersion in water) reported are an average of 3 separate measurements, and the volume weighted mean, [4, 3] is shown. Images obtained of the silica particles can be seen in Figure 2.2.

Table 2.4. Hydrophilic monodisperse silica powder used (Fibre Optic Centre Ltd.) including particle diameters obtained by SEM and laser diffraction measurements.

Grade	Nominal particle diameter/ μm	SEM particle diameter/ μm	Laser diffraction particle diameter/ μm	Refractive index	Batch number
SIO2P200-01-100g	2	1.8 ± 0.1	1.79 ± 0.01	1.425 ± 0.003	120617-01

Figure 2.2. SEM images of monodisperse silica particles of 2 μm diameter. Particles were sputter coated with Au/Pd to enhance resolution.


```
TM-1000_2487        2012/11/22  17:24        x3.0k    30 um
```
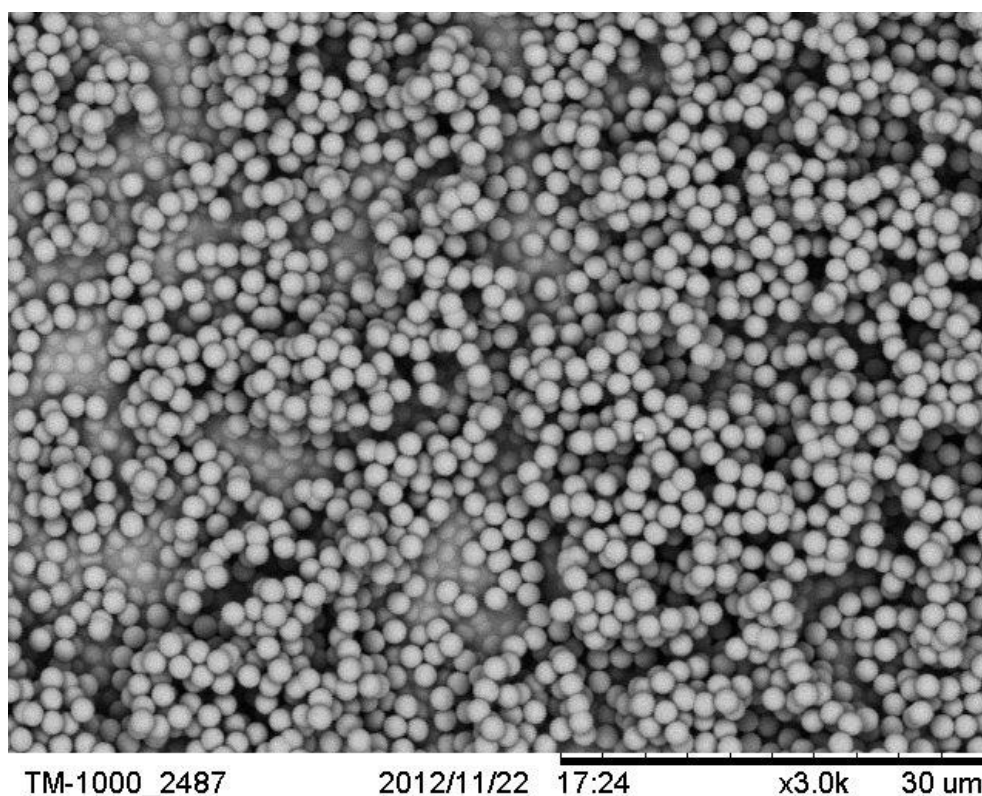
2.1.3.3 Polystyrene latex

Polystyrene latex particles were used for film calliper measurements. A non-cross-linked polystyrene latex with sulfate groups on the surface (sulfate latex) with a particle diameter was obtained from Invitrogen as a suspension in liquid (4 wt. % particles in water). The particles were used as received. Details of these particles are given in Table 2.5.
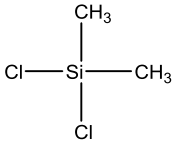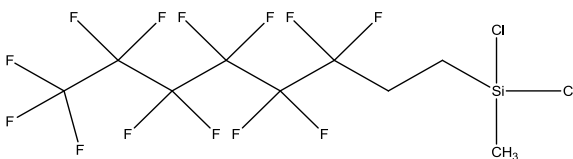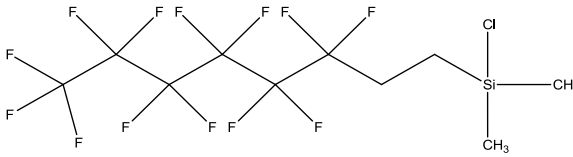
Table 2.5. Details of latex particles used.

Particle	Particle diameter/ μm	Supplier	Batch Number
Sulfate Latex	2.9	Invitrogen	962,1

2.1.4 Silanising agents

Two fluoroalkylchlorosilanes (Fluorochem) were used for hydrophobisation of silica particles and glass slides. Dichlorodimethylsilane (DCDMS) was also used in hydrophobising glass slides and was obtained from Sigma Aldrich. Details for these reagents can be found in Table 2.6. Reagents were used as received either in the vapour phase or dissolved in toluene.

Table 2.6. Details of all silanes used in hydrophobisation reactions.

Name	Structure	RMM/ g mol^{-1}	Batch No.
Dichlorodimethylsilane (DCDMS)		129.0712	SHBD0544V
1H,1H,2H,2H-perfluorooctylmethyldichlorosilane		461.13	S13100
1H,1H,2H,2H-perfluorooctyldimethylchlorosilane		440.71	S13075

49

2.1.5 Fenton reagents

This section details all reagents used for study and monitoring of the Fenton reaction (discussed in Section 2.2.7). The Fenton reaction traditionally comprises the iron-catalysed reduction of hydrogen peroxide into hydroxyl radicals (equations 2.1 and 2.2). Furthermore, other literature has utilised copper (II) as a reducing agent.[6-9] It is of particular interest in this work to investigate the reaction using copper (II) sulfate as the catalyst.

$$Fe^{2+} + H_2O_2 \rightarrow Fe^{3+} + HO^{\bullet} + HO^{-} \tag{2.1}$$

$$Fe^{3+} + H_2O_2 \rightarrow Fe^{2+} + HOO^{\bullet} + H^{+} \tag{2.2}$$
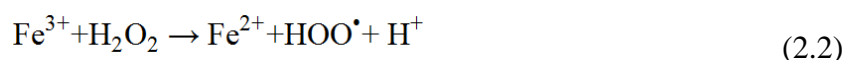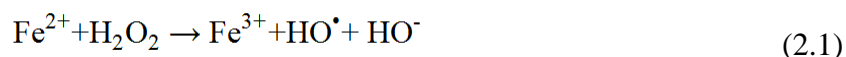
Table 2.7 details the materials used in all of the experiments concerning the Fenton reaction. Copper sulfate and hydrogen peroxide were used as the primary Fenton reagents by dissolving the appropriate amounts in water. It was necessary to acidify the solutions to stabilise the hydrogen peroxide and to denature bacterial catalase[10] which would consume any hydrogen peroxide present if active. Additionally, it is necessary to acidify solutions of hydrogen peroxide to stabilise the degradation of hydrogen peroxide. Thus phosphoric, maleic, citric and lactic acids were used as acidifying agents to stabilise the solutions of Fenton reagent. Sodium thiosulfate, sulfuric acid, starch and potassium iodide were used in a titration to determine hydrogen peroxide content. (section 2.2.7.2). In order to study the kinetics of the reaction, a UV-Visible spectrophotometry method comprising monitoring the degradation of an azo-dye molecule was carried out (section 2.2.7.3). The dye selected was naphthol blue black (NBB). The water-soluble azo-dye was used to measure the progression of the Fenton reaction with time.

Table 2.7.   Fenton reagents used.

Reagent	Supplier	Batch number
Copper (II) sulfate pentahydrate	Merck	F1576388
50% Hydrogen peroxide	Univar	11105549T
Potassium iodide	Fisher Scientific	1346288
Sodium thiosulfate	VWR	14B190530
Sulfuric acid	Fisher Scientific	1480980
Ammonium molybdate	BDH	A419986422
Starch, soluble	Fisher Scientific	1346547
Phosphoric acid	Univar	11105634T
Maleic acid	Merck	K43774158235
Citric acid	MKR	1311212327
Lactic acid	Kemcare	G-1101-009
Hydrochloric acid	Fisher Scientific	1410433
Naphthol Blue Black	Sigma Aldrich	MKBL7517V

2.1.6   Cleaning agents

For cleaning glassware and equipment, sulfochromic acid and alcoholic potassium hydroxide were used. Sulfochromic acid was prepared by dissolution of 40 g sodium dichromate in the minimum amount of water. To this solution, 1 L of sulfuric acid was added slowly and carefully with stirring. The solution was allowed to cool to room temperature then stored in a vented bottle for cleaning glassware. Alcoholic potassium hydroxide was prepared by dissolving 120 g potassium hydroxide pellets in 120 g water. A total of 2 L of ethanol was then added with stirring and the solution was used for cleaning glassware. Solutions were used until spent (sulfochromic acid turns dark green, alcoholic potassium hydroxide turns deep orange). Table 2.8 details the reagents used for these cleaning solutions. All reagents used were obtained from Fisher Scientific.

2.2   Methods

2.2.1   Foam preparation

2.2.1.1 Surfactant-stabilised foams

Surfactant-stabilised foams were prepared by adding 20 ml of surfactant solution into a 100 ml glass jointed graduated cylinder and sealed. The solution was then aerated by hand shaking for a period of 30 s. It is worth noting that the energy input obtained from hand shaking as a method of aeration may be difficult to reproduce. The foam height was recorded as a function of time, along with the volume of liquid drained from the foam. The solvent concentration was varied between water and neat ethanol. The experiments were carried out for both Silsurf DI-2510 and Lamesoft PO65 surfactants.

2.2.1.2 Particle-stabilised foams

Particle-stabilised foams of fumed silica particles were prepared by dispersing the required amount of particles into water or mixtures of ethanol and water (total mass of 20 g). Samples were then sonicated using a Branson model 450 digital sonifier (maximum power = 400W) and Branson 102C ultrasound probe, fitted with tapered microtip (estimated surface area = 12.15 cm^3). Samples were sonicated for a 5 minute period, at 20 % amplitude, with a 5 second pulse on and 1 second pulse off phase. Samples were held in ice during sonication to avoid any heat damage. Foams were generated by homogenisation using an Ultra Turrax homogeniser (T25 D52 S2 IKA) fitted with a rotor-stator head (10 mm diameter) operating at 17000 r.p.m. Samples were aerated for a total time of 2 minutes. The foam height was then measured immediately after generation and 30 minutes after generation.

Particle-stabilised foams of monodisperse fluorinated silica particles were generated by dispersing 5 wt. % of particles in water or a mixture of water and ethanol (total mass of 5 g). Samples were sonicated for 5 minutes at room temperature in a Grant ultrasonic bath then aerated using an Ultra Turrax homogeniser (T25 D52 S2 IKA) fitted with a rotor-stator head (8 mm diameter) operating at 13000 r.p.m. Samples were aerated for a total time of 1 minute. Foam heights were measured immediately after generation, then at time intervals of 30 minutes, 2 hours, 24 hours and one month after generation. Foam heights were analysed using Image-J software (National Institute of Health) due to the relatively small volumes of foam produced.

2.2.1.3 Foams from surfactant-particle mixtures

Surfactant and particle mixtures were prepared by adding 1 wt. % of the required fumed silica particles to 20 ml of surfactant solution. The samples were then sonicated using a Branson model 450 digital sonifier (maximum power = 400W) and Branson 102C ultrasound probe, fitted with tapered microtip (estimated surface area = 12.15 cm^3). Samples were sonicated for a 5 minute period, at 20 % amplitude, with a 5 second pulse on and 1 second pulse off phase. The dispersed samples were then transferred to a glass jointed 100 cm^3 graduated cylinder and subjected to a 30 s hand shaking aeration period. The foam height and liquid drainage were then measured as a function of time.

2.2.2 *Critical micelle concentration determination by surface tensiometry*

Critical micelle concentrations of the two surfactants investigated were determined by measuring the surface tension (γ) as a function of surfactant concentration in aqueous solution. Surface tension was measured using a Krüss K12 tensiometer using the Wilhelmy plate method. The Wilhelmy plate was developed by Ludwig Wilhelmy in 1863[11] and comprises immersing a flat plate through the surface of a liquid and measuring the force acting on it. If the plate is perfectly wetted by the liquid a meniscus will form where the plate passes though the liquid, with a contact angle (θ) of 0° as shown in Figure 2.4. This meniscus will contact the plate along a line of wetted length, L.

$$L=2\ (x+y)$$

(2.3)

where x and y respectively, are the horizontal length and thickness of the plate. The surface tension (γ) can then be calculated by:

$$\gamma = \frac{F}{L\ cos\theta}$$

(2.4)

where F is the force acting on the plate (mN, measured using a force balance within the tensiometer) and $cos\theta$ is assumed to be zero. It has been shown by Lane and Jordan[12] that despite the complex geometry of the meniscus around the plate, equation 2.1 still holds. Therefore, the only correction required is that to account for the buoyancy of the plate. However if the plate is set level with the flat liquid surface then the buoyancy correction is zero. A platinum plate is used for these measurements on account of its high surface free energy resulting in optimal wetting, alongside it being chemically inert and easy to clean.

Figure 2.4. Schematic diagram of a Wilhelmy plate (viewed side on) in air with liquid meniscus attached to plate.
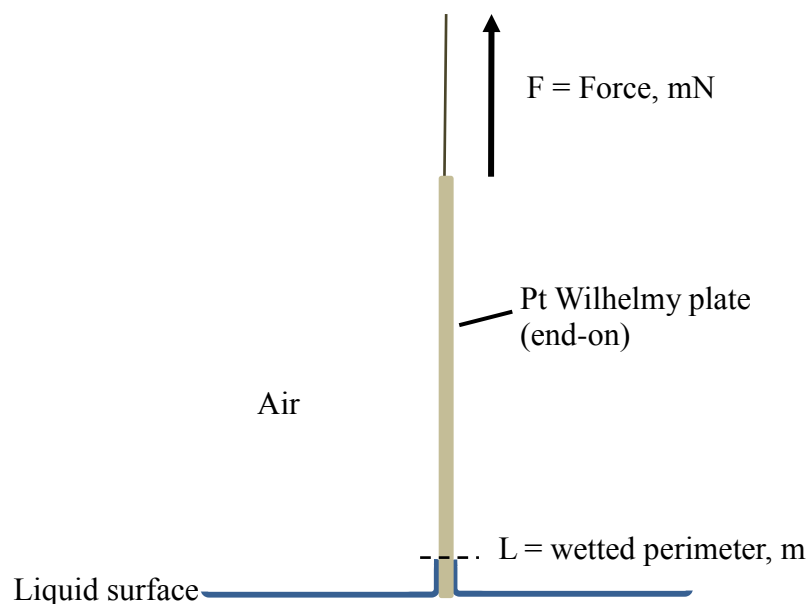
Measurements were made at 25 °C and the plate was cleaned by washing with ethanol and water, then by heating in the blue flame of a Bunsen burner. Glass measurement vessels were cleaned in alcoholic potassium hydroxide then rinsed with water and wrapped in foil. They were then placed in a dry oven for at least 30 minutes at 100 °C prior to making a measurement. The test solutions were dispensed into the measurement vessels, covered with glass microscope slides and stirred (using a magnetic stirrer bar) for at least one hour prior to starting the measurement to ensure equilibrium. Surface tension measurements were then measured periodically until they remained constant. Each measurement reported is an average of 3 repeat measurements made by generating a fresh interface and allowing to reach equilibrium.

2.2.3   Microscopy

2.2.3.1 Optical microscopy

Optical microscopy was carried out to observe foam bubble structures, including the bubble size and polydispersity. Samples were viewed on either a planar or dimpled glass microscope slides of dimensions 26×76 mm, cleaned with ethanol and dried before use. The foam sample was obtained by carefully removing a sample of foam with a spatula from the middle of the foam column and transferring to the glass slide.

A Nikon Optiphot 2 microscope fitted with $10\times$, $20\times$ and $40\times$ magnification objectives was used to view samples using transmitted visible light. Images were taken using a Lumenera Inifinity 1 camera and processed using Image Pro Plus software. A graticule (Pyser-SGI, PS8, 1 mm/0.01 mm divisions) was used at all magnifications to calibrate the microscope.

2.2.3.2 Scanning electron microscopy (SEM)

A bench-top Hitachi TM-100 scanning electron microscope was used to image monodisperse silica particles. The microscope was calibrated using a silicon test specimen on a 15 mm Hitachi aluminium stub (S1932C, Agar Scientific). This test specimen is made of single crystal silicon of overall dimensions 5×5 mm and is marked with clearly visible squares of periodicity 10 μm. Samples of dry monodisperse silica powder were attached to a 20 mm aluminium stub. The 2 μm diameter particles required sputter coating with an Au/Pd source to enhance the resolution of the images.

The samples were sputter coated using a Polaron model SC7640 fitted with an annular alloy foil (82%Au/18%Pd) sputtering source. The sputtering conditions were 1.5 KV 20 mA at 2-3 Pa Argon pressure, producing a gold coating of about 2 nm thickness, automatically terminated. Samples were rotated during coating. All sputter coating was carried out by Tony Sinclair at The University of Hull, U.K. All images were analysed using the software supplied with the microscope.

2.2.3.3 Cryogenic SEM

To image particle-stabilised foams using SEM, it was necessary to use a cryogenic preparation chamber (Quorum) to freeze and fracture the foam samples prior to imaging. A sample of particle-stabilised foam was transferred to an aluminium stub and immersed in a nitrogen "slush" of an approximate temperature of -210 °C (nitrogen slush generated by applying vacuum to liquid nitrogen of temperature around -196 °C). By freezing in a slush rather than using liquid nitrogen, the sample integrity is preserved as the boiling liquid nitrogen can destroy the foam structure. Once frozen the sample was transferred to the preparation chamber under vacuum (5×10^{-6} mbar) to keep it frozen. It was then fractured using a blade to expose the internal bubble structure, then sputter coated with platinum (platinum disc source coated for 1 minute in argon atmosphere giving ~2 nm thick Pt coating) on a preparation stage held at -140 °C. The anti-contaminator in the preparation chamber was held at a temperature of -170 °C. The sample was then transferred to the SEM chamber (Zeiss EVO60) onto an SEM cryo-stage held at -140 °C with a vacuum of around 1×10^{-6} mbar and imaged with an accelerating voltage of 15 kV and probe current of 35 pA. All cryogenic SEM was carried out by Tony Sinclair at The University of Hull, U.K.

2.2.3.4 Transmission electron microscopy (TEM)

Sample preparation for TEM consisted of coating 3 mm copper 300 mesh grids with a layer of carbon. For aqueous samples the grids were glow discharged using an Agar Scientific carbon coater with a glow discharge accessory to render the carbon surface hydrophilic. A 5 μl drop of liquid sample was placed on the grid surface, the excess removed and the grid allowed to dry at room temperature. For powders, the grids were rolled in dry sample and the excess solid tapped off. The microscope used was a JEOL JEM-2010 transmission electron microscope operating at 200 kV and images were taken using a Gatan Ultrascan 4000 digital camera (64 megapixels). All TEM was carried out by Ann Lowry at The University of Hull, U.K.

2.2.4 Contact angle determination

2.2.4.1 Drop shape analysis

Contact angles of aqueous sessile drops in air on hydrophobised glass surfaces were measured using a Krüss DSA 10 goniometer (Figure 2.5). The measurement chamber comprised a sample platform surrounded by a thermostatted trough filled with water. The chamber was sealed and allowed to equilibrate to reduce evaporation of the sessile drop. Advancing contact angles were measured by injection of a 10 µl drop of liquid onto the surface and removal of the syringe needle, the angle was then measured using automated software, on the left and right hand side of the drop. The receding angles were measured by withdrawing 5 µl from the droplets and again measuring the contact angle. At least 9 individual measurements were made for each sample and the average value was reported.

Figure 2.5.   Images of (a) Kruss DSA 10 Mk. 2 goniometer used for measurements of contact angle and (b) demonstration of advancing 10 µl sessile drop of water in air on a solid PTFE surface.
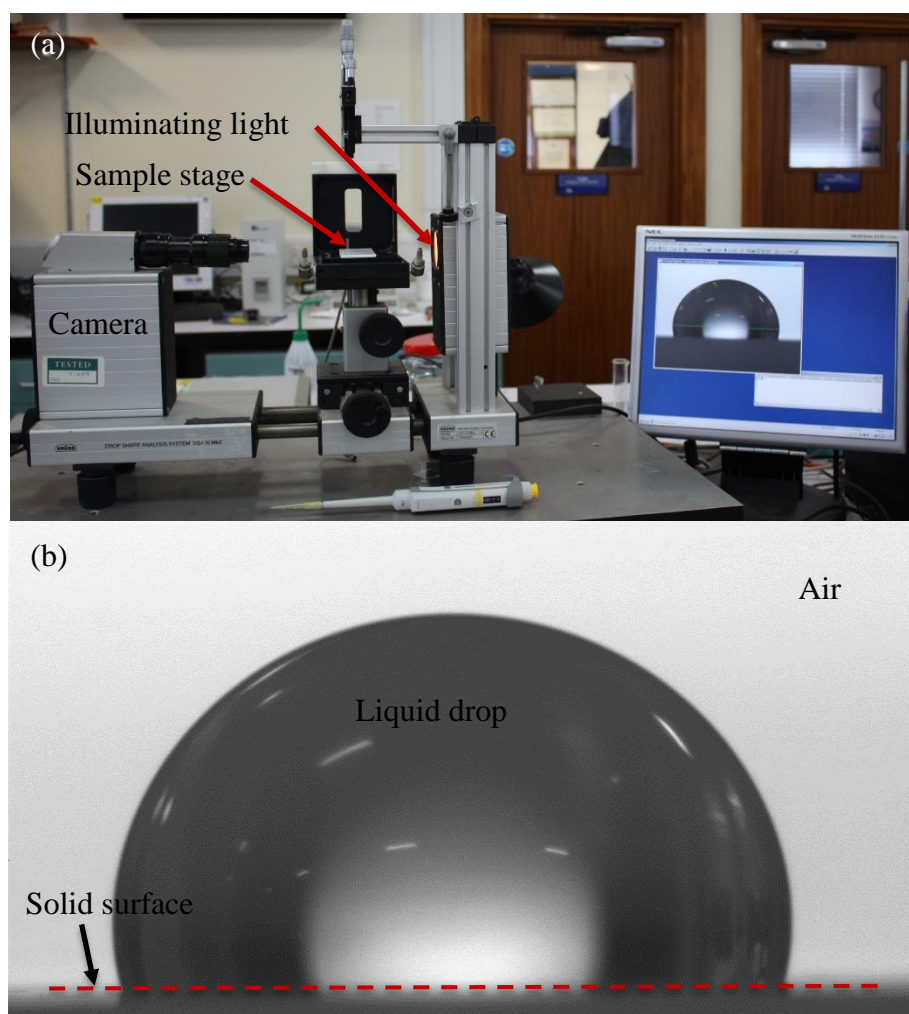
2.2.4.2 Film calliper method

Many techniques have been developed for measurement of the contact angle of micrometer and submicrometer particles at air-water and oil-water interfaces. Techniques such as using atomic force microscopy to make measurements on individual particles,[13] film trapping technique,[14] direct observation using optical microscopy,[15] and more recently, the gel trapping technique[16] have been developed. However, issues such as practicality, restrictions to micron-sized particles and complicated experimental preparation have hindered these methods. The film calliper method as described by Horozov *et al.*[17] was utilised to measure particle contact angles at the air-water interface up to 90°. The method is based on the principle that particles can bridge the surfaces of free standing thin liquid films and adjust their position with respect to the film thickness according to their contact angle at the air-water interface and to minimise deformation of the liquid interface. Figure 2.6 shows the experimental set up for the thin film calliper method. A glass ring is connected to a syringe filled with liquid (water) via Teflon tubing and a steel U-shaped needle.

Figure 2.6.   Schematic diagram of (a) the experimental set-up and close-up of the ring used in film calliper method, (b) front view of glass ring (c) cross-sectional side view of ring, re-drawn from ref. 18.
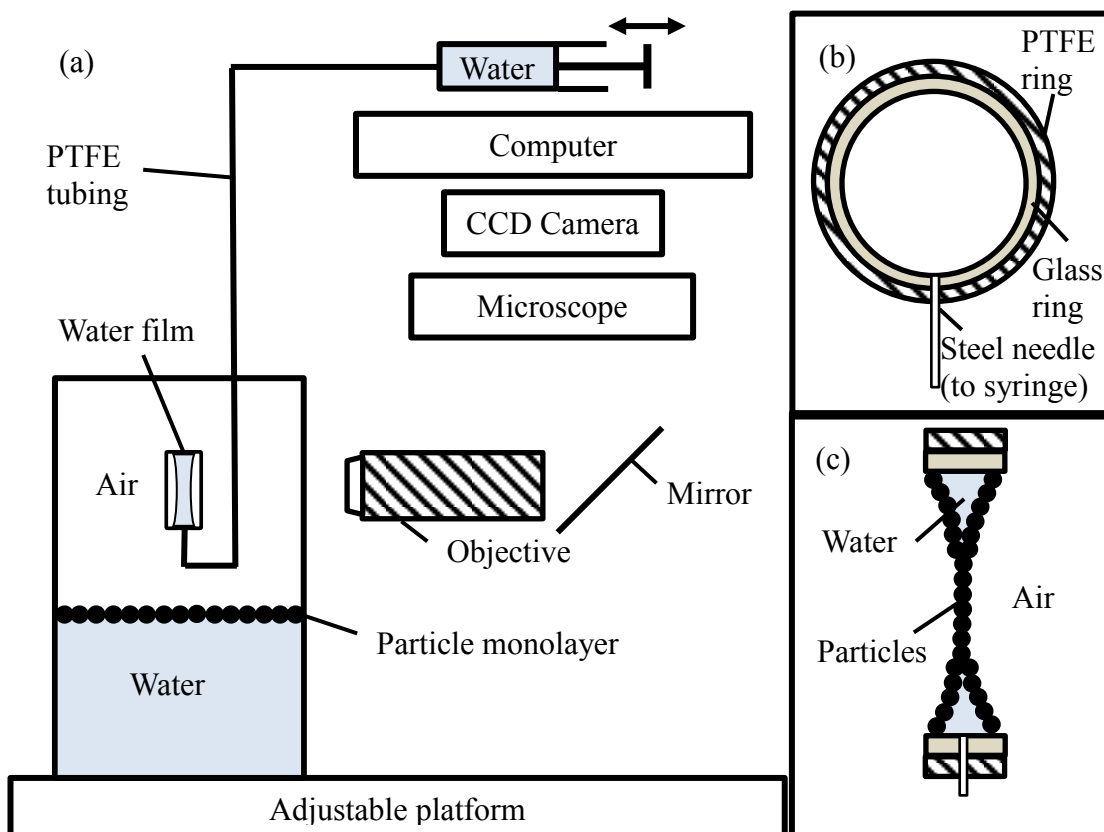
A glass cuvette of dimensions 53 × 55 × 25 mm (Helma 700.00-OG) was partially filled with water (or aqueous ethanol solution) and a dilute monolayer of particles spread on the surface (2 wt. % particle suspension of 50:50 methanol: water) using a 100 μl syringe (Hamilton). The ring is immersed in the test solution and withdrawn to form a thick liquid film with particles attached to both its surfaces. The film is then forced to thin by rapidly withdrawing liquid from the meniscus using a syringe. Consequently, some particles bridge both surfaces of the thin liquid film and move along the meniscus until they reach their equilibrium position. The film is observed horizontally in reflected monochromatic light (Mercury lamp of wavelength, λ= 546 nm) using a microscope (Nikon Optiphot 2) fitted with 10 × objective. A thin water film in air viewed in reflected monochromatic light is observed as a series of concentric rings with alternating light and dark fringes (Figure 2.7). This pattern occurs from interference of the light reflected from both surfaces of the film. The light fringes are due to constructive interference, and dark fringes due to destructive interference of the light source. The film thickness (h) corresponding to light intensity maxima or minima is calculated by:[18]

$$H = (m + \tfrac{1}{2})\, \lambda/2\, n$$

(2.5)

$$h = m\, \lambda/2\, n$$

(2.6)

where m = 0, 1, 2, 3, …and is named the order of interference and n is the refractive index of the thin liquid film. At the centre of the film the film thickness is approximately 100 nm and m = 0, therefore the first interference minima (dark fringe) has an order of interference = 1. Considering a particle diameter d, and a contact angle, θ, there is a unique film thickness h_e, at which the bridging particle will cause no deformation of the film surfaces (any movement out of this region will result in an increase in the surface free energy of the system). This position in the film is the equilibrium position of the particle and is related to the contact angle by:

$$h_e = d\, cos\, \theta$$

(2.7)

By knowing the order of interference of the particles at their equilibrium position, the particle diameter and the refractive index of the liquid, the equilibrium film thickness at which the particles are located can be calculated. From this, the particle contact angle can be calculated via equation 2.7. A macro has been written within the Image Pro Plus software to allow for determination of the contact angle.

Figure 2.7. Image of (a) a thin water film and (b) 2 µm silica particles (fluorinated with 6.8 x 10^{-6} M 1H, 1H, 2H, 2H-perfluorooctylmethyldichlorosilane, θ=51±3°) trapped in a thin water film. Images obtained using the film calliper method. Scale bar = 40 µm.
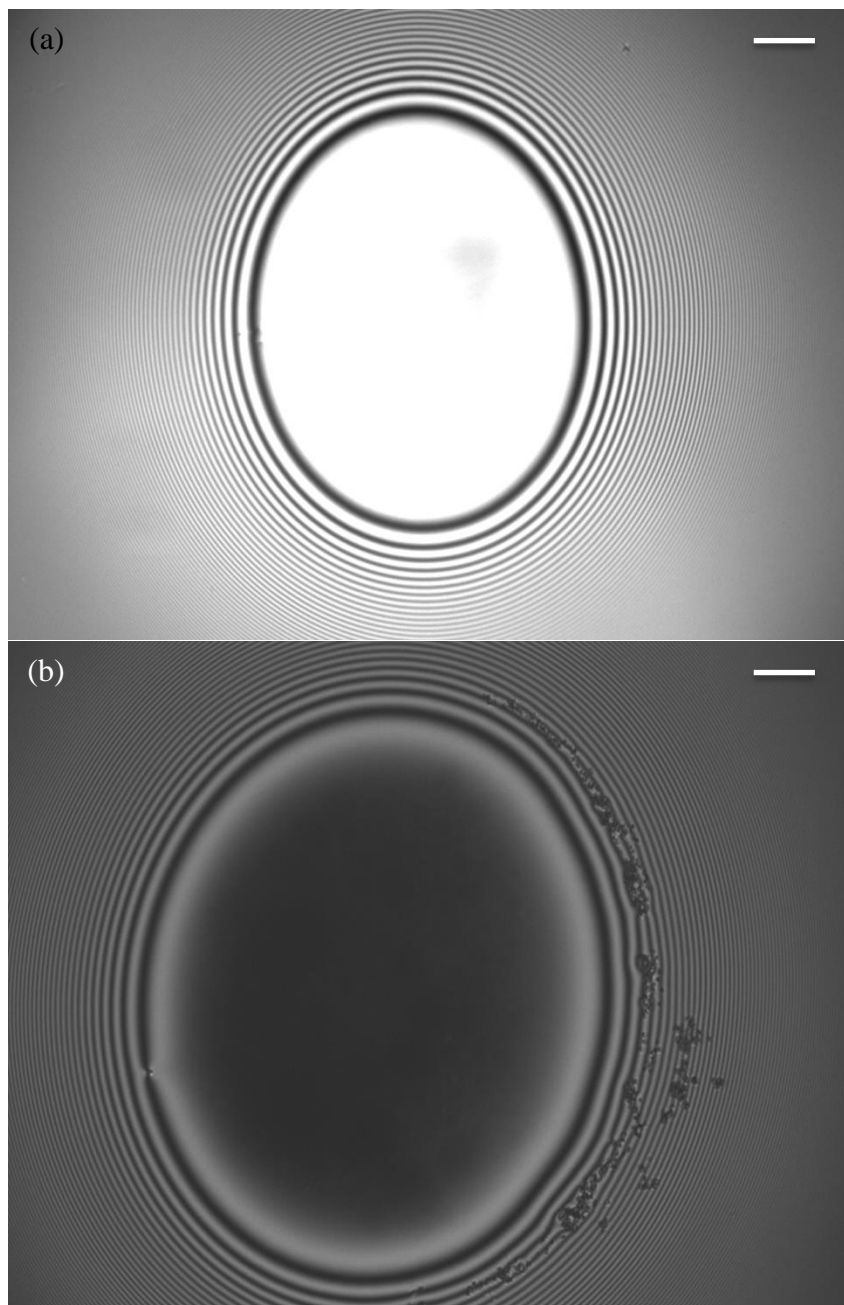
2.2.5 *Particle behaviour at planar interfaces*

The behaviour of particles spread at a horizontal aqueous ethanol-air interface was determined by optical microscopy using a Nikon Optiphot 2 optical microscope fitted with $10 \times$ objective. The experimental set-up comprised a small, circular glass dish (inner diameter = 23 mm) within a larger plastic petri dish, to contain any liquid overflow. The inner glass dish was completely filled with liquid until the surface was convex. The surface was then sucked with a syringe so that it was completely flat and clear of any dust. A plastic guard was placed around the dish to minimise draft across the liquid surface (causing disruption of the particle layer). Particles were spread at the interface by depositing 5-25 µl of a 2 wt. % suspension (50:50 methanol:water) then observed using the microscope.

2.2.6 *Surface hydrophobisation*
2.2.6.1 Glass slide hydrophobisation with DCDMS

Hydrophilic glass slides (38×26 mm, surface area = 98.8 mm^2) were cleaned in 30 wt. % aqueous sodium hydroxide at 60°C for 10 minutes. The slides were then thoroughly rinsed with water and dried with nitrogen. The slides were then placed in a glass slide holder and treated with DCDMS vapour (created by depositing 0.1 ml neat DCDMS into a glass jar flushed with nitrogen and sealed for 1 hour) to mimic the chemical structure of the hydrophobic (14% SiOH) particle surfaces. The slides were then rinsed in chloroform and ethanol to remove any unreacted DCDMS by sonicating in a Grant Ultrasonic bath for 10 minutes in each solvent then blow-dried with nitrogen.

2.2.6.2 Glass slide hydrophobisation with fluoroalkylchlorosilane

Glass microscope slides were cut so that the slide dimensions were approximately $18.5 \times 26 \times 1.058$ mm. Slides were then placed in a Teflon slide holder and immersed in 30 wt. % sodium hydroxide at 60 ºC for 10 minutes. The slides were then removed and rinsed thoroughly with deionised water then placed in an oven to dry for 1 hour at 120 ºC. The slides were then transferred to a 120 ml glass screw top jar (previously flushed with nitrogen for 30 seconds) containing 100 ml of reagent solution (fluoroalkylchlorosilane in anhydrous toluene), the vessel was then further flushed with nitrogen and sealed immediately. The concentration ranges of fluoroalkylchlorosilane reagent selected were calculated making assumptions that the glass microscope slide surface and particle surface had 5 SiOH groups per nm^2 (this assumption was based on literature values of the surface concentration of hydroxyl groups on glass surfaces[19]).

A further assumption is that the reaction between the fluoroalkylchlorosilane and silanol groups occurred in a 1:1 ratio.

Once the reaction has progressed for the desired amount of time, the glass slides were removed from the vessel and rinsed using an ultrasonic bath for 5 minutes, using consecutive washes of chloroform, ethanol, 50:50 ethanol:water. After washing, the slides were transferred to dry in an oven at 120 °C for 10 minutes then left to cool and used immediately after preparation.

2.2.6.3 Particle hydrophobisation with fluoroalkylchlorosilane

A mass of 2.5 g of 2 μm diameter monodisperse silica particles was weighed out and oven dried in a glass vial at 110 °C for one hour. The particles were then transferred to a vacuum oven at room temperature until cool. The dry particles were then transferred to a 100 cm^3 round bottom flask (previously flushed with a nitrogen gas stream for 1 minute) with 100 cm^3 of fluoroalkylchlorosilane solution in toluene. The flask was then immediately sealed with a suba-seal and the headspace was further flushed with nitrogen for 30 s. The flask and solution were then immediately transferred to a water bath held at 24 ± 0.1 °C with a Grant TC120 thermostat for two hours with stirring (Stuart hotplate stirrer SB162-3). The particles were transferred to a centrifuge tube and toluene was removed by centrifugation at 4000 rpm for 3 minutes (Thermo Scientific Sorvall Biofuge Primo Centrifuge). Particles were then cleaned by consecutive washes with chloroform (twice) and ethanol (thrice). The particles were dispersed in the wash solvent by sonication using a Grant Ultrasonic bath for 10 minutes at 20 °C, then centrifuged and the solvent was removed and replaced. After washing and removal of supernatant solvent, the particles were dried in an oven at 80 °C for one hour and transferred to a vacuum oven at ambient temperature overnight.

2.2.7 The Fenton reaction

2.2.7.1 Dry water preparation containing Fenton reagents

Samples of dry water were prepared by following a method described by Binks and Murakami.[20] The required liquid was added to a blender (Braun, Glass Jug PowerBlend MX2050, 1.7 l) with hydrophobic fumed silica (Degussa Aerosil R202) in a 95:5 ratio and sealed with the lid. In most cases, 95 g of liquid was added with 5 g silica particles. The samples were then blended at the highest speed setting for 30 seconds. The dry powder produced was then transferred to a plastic vessel for storage.

2.2.7.2 Stability testing

The stability of hydrogen peroxide in the presence of various different acids under accelerated conditions was investigated by a titration method. Four different acids were selected for investigation by the sponsor company (maleic, citric and phosphoric acids). Solutions of 2 wt. % H_2O_2 were prepared in water and acidified to a pH of 2-2.5 with the required acid. Details of the acid quantities are given in Table 2.8. These particular acids were selected by the sponsor company, as common acids utilised in cosmetic and skincare formulations for their relatively low skin irritancy. Lactic acid was also selected, but due to a higher acid dissociation constant ($pKa = 3.86$)[21] it was not possible to acidify to a pH of 2-2.5 and so this acid was not used for any further studies.

Table 2.8. Quantities of acids used and final pH of all solutions prepared.

Sample	Mass of acid used/ g	Total mass of $H_2O_2 + H_2O$/ g	pH
H_2O_2 control	n/a	100.2637	3.24
Maleic acid	0.1976	100.0000	2.28
Citric acid	1.9494	98.0506	2.29
Phosphoric acid	1.1678	98.8416	2.05

When the solutions were ready for testing, the following protocol was used to determine the concentration of hydrogen peroxide in the solution. A 4 g sample was added to a clean 1000 ml Erlenmeyer flask and 400 g of water was added, along with 10 ml 25 wt.% sulphuric acid solution, 25 ml of 10 wt.% potassium iodide solution and 6 drops of 5 wt.% ammonium molybdate. The solution turned a deep red at this point.

The solution was then titrated with 0.1M sodium thiosulphate solution until it turned a pale yellow colour, at this point 1 ml starch solution was added and the solution was further titrated until colourless. The peroxide content was then calculated by the following equation:

$$\textbf{\% H}_2\textbf{O}_2 = [(V_{STS}) \times (C_{STS}) \times 0.017 \times 100]/\text{weight of sample} \qquad (2.8)$$

where V_{STS} and C_{STS} were the volume and concentration of sodium thiosulfate, respectively. Samples were placed in an oven a 70 °C and samples withdrawn for analysis after 1 day, 5 days, 10 days and 25 days.

2.2.7.3 Measurement of Fenton reaction

A method[22,23] to observe the degradation of Naphthol Blue Black (NBB) by Fenton Oxidation was adapted for the current reagents required and equipment available. The method is based on the assumption that upon mixing of the two Fenton reagents, the production of hydroxyl radicals should degrade an azo-dye molecule, by attacking the azo-bond of the molecule. The structure of this can be seen in Figure 2.8.

Figure 2.8. Structure of azo dye (Napthol Blue Black, NBB) used in Fenton reaction measurements.
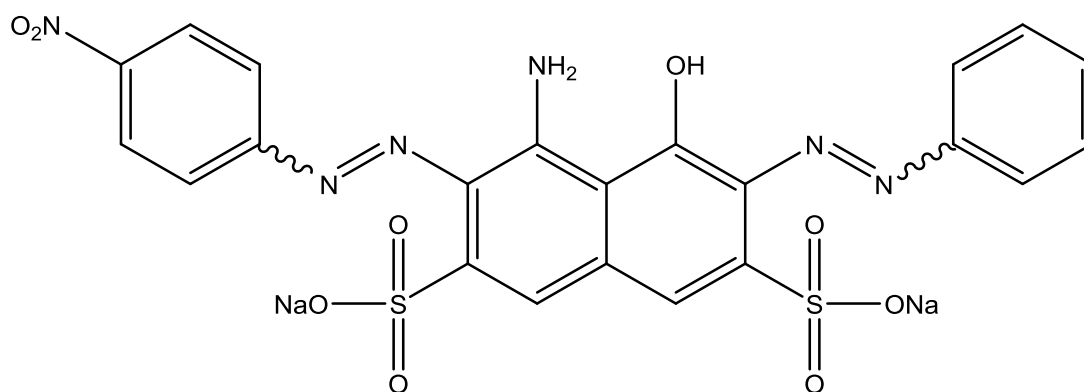
It was proposed that the reaction could therefore be tracked by measurement of the lambda max (λ_{max}) of the dye as a function of time after mixing of the Fenton reagents. Figure 2.9 shows a scan of the absorbance of a 16 µM solution of the dye in water using a UV-Visible spectrophotometer (Perkin-Elmer Lambda 25). The maximum absorbance (λ_{max}) of the dye can be seen at 618 nm. Therefore, a wavelength of 618 nm on a "timedrive" method, allowing for continual measurement of absorbance as a function of time was used. A quartz cuvette with a 10 mm path length was filled with 2 ml 16 µM NBB dye solution and 0.7 ml copper sulfate solution. The cuvette was then placed into the thermostatted cell holder within the spectrometer (held at 25.0 ± 0.3 °C) to equilibrate. Once the solutions were at the desired temperature, 0.7 ml hydrogen peroxide was added, the cuvette was quickly inverted twice to mix the solution and placed back in the spectrometer as quickly as possible. Spectra were collected and corrected by subtracting the measured absorbance for the concentration of copper sulfate (alone) used. The experiment was carried out under non-acidified and acidified conditions, and over a range of different concentrations of 0-10 mM $CuSO_4$ and 0-100 mM H_2O_2.

Figure 2.9. UV-Visible spectrum of 16 μM NBB dye in a Helma quartz cuvette of 10 mm path length.
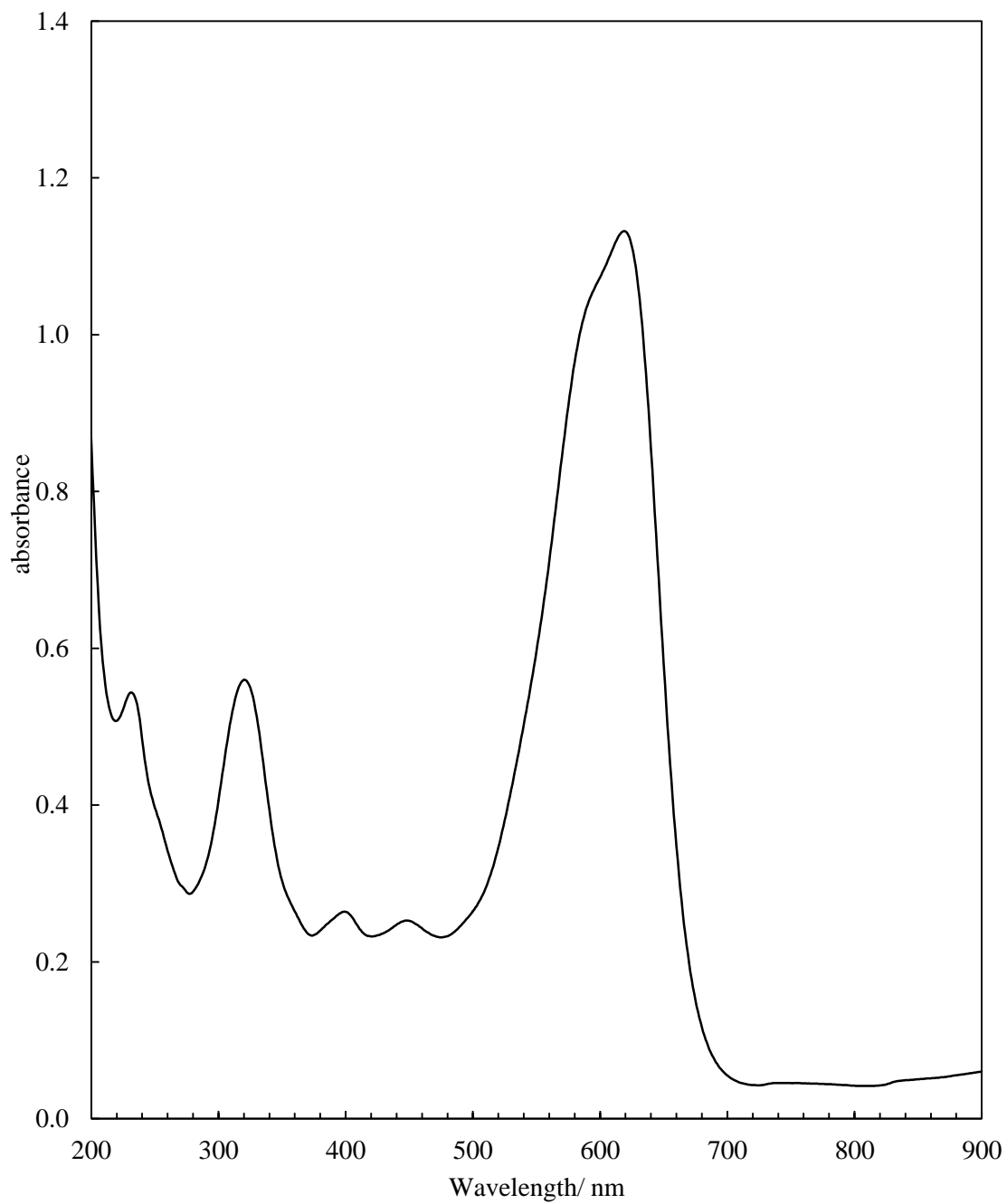
2.2.7.4 Anti-microbial efficacy testing of Fenton reagents

As the aim of this research is to generate a novel hand sanitiser utilising the Fenton reaction as an antibacterial agent, it was necessary to investigate the antimicrobial efficacy of the various Fenton solutions using a series of *in vitro* and *in vivo* tests. For the *in vitro* tests it was not possible to investigate the encapsulated formulation so only the aqueous solutions of Fenton reagents were studied. However, for the *in vivo* tests, the Fenton solutions in liquid and encapsulated form could be investigated, as the *in vivo* test comprised testing on participants.

2.2.7.4.1   In vitro efficacy

An adapted EN 1040 test was utilised to carry out the efficacy testing of aqueous solutions of Fenton reagents *in vitro*. A culture of 10^8 ml^{-1} bacterial cells of *Escherichia coli* (*E. coli*, strain number: ATCC 11229) was diluted using 7×10-fold serial dilutions in maximum recovery diluent (comprising aqueous sodium chloride and peptone). This is so that the bacterial cell concentration when plating and counting colonies is a manageable quantity to count manually, the number of cells is then multiplied by the dilution factor to give the log reduction in bacteria. The test method for testing the efficacy of the Fenton reaction then comprised adding 1 ml of the culture, 1 ml deionised water and 4 ml copper sulphate to a sterilised glass vessel. Finally, 4 ml of hydrogen peroxide was added to the solution and the reaction was allowed to proceed for either 30 or 60 seconds. The samples were then passed through a membrane filter under vacuum (Nalgene analytical test filter funnel with 0.45 μm pore diameter) rinsing with membrane rinse fluid (comprising aqueous Tween 80 surfactant and lecithin) to rinse away excess reagent and trap any remaining cells in the membrane. The membranes were then plated on tryptone soya agar plates and incubated at 32.5 ± 2.5 °C for 24-48 hours, after which they were removed and colonies counted manually. All samples were prepared in weight per cent (wt. %). All *in vitro* testing was carried out in microbiology labs at Deb Group Ltd. U.K., with Lisa Powell.

2.2.7.4.2   In vivo efficacy

An *in vivo* efficacy test was carried out to measure the efficacy of the formulations as solutions and encapsulated as a dry powder on the skin surface. The testing was carried out externally using an external CPA accredited clinical microbiology testing facility based at Queen Elizabeth Hospital, Birmingham, U.K. The testing was carried out by Tina Bradley and Martin Wilkinson at Queen Elizabeth Hospital. A European Standard EN1500[24] test was carried out using *Escherichia coli* as the bacteria. A culture of 2 L of 2×10^8-10^9 ml^{-1} *E. coli* (strain number: K12 NCTC 10538) was incubated overnight at 37 °C. All test subjects followed the standardised EN1500 procedure; a preparatory hand wash using 5 ml standard soft soap for 1 minute following a specified "five stroke technique".[25] The hands were then dried with paper towel and immediately immersed in the *E. coli* broth for 5 seconds, then withdrawn and the excess fluid allowed to drip back into the broth. The hands were then held horizontally and allowed to air dry for 3 minutes. The tips of the fingers on each hand were then immersed in two separate petri dishes containing 10 ml each of tryptone soya broth (TSB) and rubbed in the petri dishes for 1 minute. These samples gave the pre-bacterial count (by serial dilution and plating on tryptone soya agar plates). The test solution (3 ml total volume) was then applied to the contaminated hands and rubbed in following the same five stroke technique as previously, for 1 minute. The fingertips of each hand were then immersed in two petri dishes containing 10 ml of neutraliser and TSB each, then diluted in 0.25% Ringer's solution and plated on tryptone soya agar plates. Ringer's solution is an isotonic solution containing sodium chloride, potassium chloride, calcium chloride and sodium bicarbonate.[26] The neutraliser was necessary to ensure that any antibacterial activity of the test sample is neutralised so that the exposure time of the bacteria to the agent is restricted to that specified within the test method. Table 2.9 specifies the ingredients of the neutraliser broth used. The efficacy of this neutraliser for the Fenton reagents used was validated by the lab prior to testing. The samples were then incubated for 18-24 hours at 37 °C and the colonies counted.

Table 2.9. Ingredients for neutraliser used in *in vivo* bacterial testing. Quantities specified are per litre of TSB (TSB concentration 30 g/l).

Component	Concentration/ L^{-1}
Polysorbate (Tween) 80	30 ml
Lecithin	3g
Saponin	5g
Sodium thiosulphate	5g
L-histidine	1g

The log reduction was reported as the difference in the quantity of bacteria counted before and after application of the test product and was calculated by:

$$\text{Log reduction} = \log_{10}\left(\frac{A}{B}\right)$$

(2.9)

where A is the number of viable microorganisms before treatment and B is the number of viable microorganisms after treatment. For dry powders, the equivalent mass of liquid was used (accounting for the 95:5 liquid:powder ratio). Therefore for the equivalent of 3 ml liquid, 3.1575 g powder was used.

2.3   References

1. N.B. Vargaftik, B.N. Volkov and L.D. Voljak, *J. Phys. Chem. Ref. Data*, 1983, **12**, 817.

2. HDK - pyrogenic silica, Wacker-Chemie. (Accessed 18/06/2015) Available from: http://www.wacker.com/cms/media/publications/downloads/6180_EN.pdf

3. W. Stöber, A. Fink and E. Bohn, *J. Colloid Interface Sci.*, 1968, **26**, 62.

4. D.L. Green, J.S. Lin, Y-F. Lam, M.Z.-C. Hu, D.W. Schaefer and M. T. Harris, *J. Colloid Interface Sci.*, 2003, 266, 346.

5. X-D. Wang, Z-X. Shen, T. Sang, X-B. Cheng, M-F. Li, L-Y. Chen and Z-S. Wang, *J. Colloid Interface Sci.*, 2010, **341**, 23.

6. J.B. Cross, R.P. Currier, D.J. Torraco, L.A. Vanderberg, G.L. Wagner and P.D. Gladen, *Appl. Environ. Micro.*, 2003, **69**, 2245.

7. M. Masarwa, H. Cohen, D. Meyerstein, D.L. Hickman, A. Bakac and J.H. Espenson, *J. Am. Chem. Soc.*, 1988, **110**, 4293.

8. A.N. Pham, G. Xing, C.J. Miller and T.D. Waite, *J. Catal.*, 2013, **301**, 54.

9. A.D. Bokare and W. Choi, *J. Hazard. Mater.*, 2014, **275**, 121.

10. T. Samejima, T. Miyahara, A. Takeda, A. Hachimori and K. Hirano, *J. Biochem.*, 1981, **89**, 1325.

11. L. Wilhelmy, *Ann. Physik.*, 1863, **119**, 177.

12. D.O. Jordan and J.E. Lane, *Aust. J. Chem.*, 1964, **17**, 7.

13. M. Preuss and H-J. Butt, *J. Colloid Interface Sci.*, 1998, **208**, 468.

14. A. Hadjiiski, R. Dimova, N.D. Denkov, I.B Ivanov and R. Borwankar, *Langmuir*, 1996, **12**, 6665.

15. Z. Hórvölgyi, Z.S. Németh and J.H. Fendler, *Colloids Surf. A.*, 1993, **71**, 327.

16. V.N. Paunov, *Langmuir*, 2003, **19**, 7970.

17. T.S. Horozov, D.A. Braz, P.D.I. Fletcher, B.P. Binks and J.H. Clint, *Langmuir*, 2008, **24**, 1678.

18. D.A. Braz, *Ph.D. Thesis: Particle-stabilised foams and foam films*, 2009, University of Hull, U.K.

19. L.T. Zhuravlev, *Langmuir*, 1987, **3**, 316.

20. B.P. Binks and R. Murakami, *Nat. Mater.*, 2006, **5**, 865.

21. R.M.C. Dawson, *Data for biochemical research*, 3rd Edition, Clarendon Press, Oxford, 1986.

22. O.H. Bjorkedal and T. Bache, *Report: Kinetic studies using UV-Vis spectroscopy Fenton Oxidation*, 2013, Norwegian University of Science and Technology.

23. V.S. Shah, P. Verma, P. Stopka, J. Gabriel, P. Baldrian and F. Nerud, *Appl. Catal. B: Environ.*, 2003, **46**, 287.

24. M.A.C. Wilkinson, Standard operating prodedure, Determination of the efficacy of Hygienic Handrubs according to European Standard EN1500, University Hospital Birmingham, 2008.

25. G.A.J. Ayliffe, J.R. Babb and A.H. Quoraishi, *J. Clin. Path.*, 1978, **31**, 923.

26. W.M. Bayliss, *Principles of General Physiology*, 1st Ed., Longmans, Green and Co., New York, 1915.

CHAPTER 3

AQUEOUS ETHANOL-AIR FOAMS STABILISED BY SURFACTANTS AND PARTICLES

3.1   Introduction

Foams are thermodynamically unstable dispersions of air bubbles in a liquid or solid continuous phase. This instability is a result of the significant increase in the interfacial area on generation of the foam; an increase in the interfacial area causes an increase in the surface free energy. Foams collapse by three main mechanisms, namely coalescence, liquid drainage and disproportionation (or Ostwald ripening). It is known that stable foams cannot be generated with pure liquids, and for this reason foam bubbles are usually stabilised by addition of surfactants, particles or protein molecules that adsorb to and stabilise the interface by reducing the surface tension.[1] Increasing the surfactant concentration can additionally increase the viscosity of the continuous phase, aiding in slowing down liquid drainage from the liquid films of the foam. The means by which surfactants stabilise liquid-air interfaces is discussed in detail in Chapter 1.

Additionally discussed in detail in Chapter 1 is the ability of surface-active particles to stabilise aqueous foams. Unlike surfactant molecules at the interface which exist in dynamic equilibrium with molecules in the bulk, particles adsorb irreversibly to the air-liquid interface. The free energy of particle detachment from the interface is directly related to the particle contact angle and size. The irreversible attachment of particles to an interface reduces the highly energetic interfacial area and can significantly reduce disproportionation of foam bubbles.[2,3] Much research on aqueous particle-stabilised foams has demonstrated long-term stability of these foams, from months to years after their generation.[4-6] Recent work[7-11] has demonstrated that particles can be surface modified by adsorption of surfactant molecules to their surfaces. Many of these studies have demonstrated the adsorption of ionic surfactants to charged solid surfaces to enhance foam stability and have suggested the formation of a surfactant monolayer on the particle surface imparting hydrophobicity to be the reason for this. Upon increasing surfactant concentration it has been elucidated that foam systems destabilise, potentially due to the formation of a surfactant bilayer on the particle surfaces, rendering particle surfaces hydrophilic.

The long-term stability and foamability of a current foaming alcoholic sanitizer (InstantFOAM™) is poor, therefore it is of interest to the industrial sponsor to investigate potential means of enhancing the foaming properties of this product. Investigating the potential for synergistic behavior between particles and the surfactants currently used in the formulation may therefore provide a fruitful outcome. Some studies on the adsorption of nonionic surfactants to solid surfaces exists but much less is known on the impact of this on foaming properties.[12-16] The adsorption of cationic gemini surfactant and nonionic sugar surfactant on the surface of solid silica particles of 0.2 μm diameter was studied by Zhou and Somasundaran.[13] The cationic gemini surfactant, butane-1,4-bis(quaternary ammonium chloride) (represented as C_{12}-C_4-C_{12}) was shown to reach saturation adsorption on the silica surface around the CMC (as measured by an adsorption titration). Additionally the adsorption of C_{12}-C_4-C_{12} was greatly dependent on pH. Conversely, the adsorption of the sugar surfactant, n-dodecyl-β-D-maltoside (represented as DM) was shown to have poor adsorption to the silica surface, around 100 times lower than the C_{12}-C_4-C_{12} at neutral pH. However, when a mixture of the two surfactants was studied, a marked increase in the adsorption of DM to the surface was seen. It was suggested that the C_{12}-C_4-C_{12} molecules act as anchor sites for the DM molecules. The increased adsorption of DM was also shown to cause a decrease in the wettability of the particles by water, making them more hydrophobic. A separate study on the adsorption of DM to silica surfaces alone was shown to have a similarly poor adsorption.[14] The main mechanism for adsorption to hydrophilic surfaces in the absence of electrostatic interactions has been proposed to be hydrogen bonding at low surfactant concentrations.

A study on aqueous foams stabilised by silica particles and tetraethylene glycol monododecyl ether ($C_{12}E_4$) was carried out by Zhang *et al.*[15] It was seen that foamability was lower than that of the surfactant alone. As the surfactant concentration increased from 1-2 wt. % the foamability was close to that of the surfactant alone and particles were adsorbed onto the bubble surface. Above 2 wt. % a synergistic effect was observed although no particles were adsorbed on the bubble surface. It was suggested that the wettability of the particle changed with varying surfactant concentration.

Aqueous-alcohol based hand sanitisers exhibit significant bactericidal efficacy, additionally it has been shown that this efficacy can be enhanced when the sanitiser is applied as a foam.[17] The alcohols most commonly used are ethanol and propanol, with the formulations containing up to 70% alcohol. The low surface tension values of alcohol (21.82 mN m^{-1} and 21.22 mN m^{-1} for ethanol and isopropanol, respectively[18]) provide a challenge to produce good foaming properties.

3.2   Experimental

This chapter has systematically investigated the foaming properties of two commercial surfactants used as foaming agents in an aqueous-ethanol based hand sanitiser. The effect of addition of ethanol to the aqueous phase on the bulk surfactant properties (such as CMC) was investigated by means of surface tensiometry. The foaming behaviour of these surfactants in pure water and with addition of ethanol to the system was then investigated. Finally a study of the effect of addition of fumed silica particles to the aqueous surfactant solutions was carried out. The behavior of mixtures of particles and surfactants has been carried out in water only in order to elucidate the behavior of these multicomponent systems as clearly as possible. Adding another component (such as ethanol) to the system would make the behavior of the systems more difficult to study. Foams were generated by hand shaking 20 cm^3 of the solution to be investigated for 30 seconds, the foam height and liquid volume beneath the foam layer were recorded as a function of time. Foams containing surfactant and particles were prepared by dispersing the particles in the surfactant solution by sonication then aerating as above. All surfactant solutions have been prepared in wt. % as the precise relative molecular masses of the surfactants were unknown. Additionally, as mentioned in Chapter 2, the ratio of glyceryl oleate and coco glucoside within Lamesoft PO65 was unknown and unavailable from the supplier. The structure and relative quantities of Lamesoft PO65 could have been determined by NMR spectroscopy. It could have been possible to determine the weight distribution for the polymeric silicone surfactant by GPC, however time constraints and equipment availability did not allow for this.

3.3 Behaviour of surfactants alone

3.3.1 Critical micelle concentration

The CMC is an important parameter for explaining many different aspects of the behaviour of surfactant systems, such as detergency and foaming, and can be determined by a number of methods. Surface tensiometry, osmotic pressure and conductivity are all methods with which the CMC can be determined.[19] A common observation with all of these methods is that a break point and plateau is observed above the CMC after which the measured property will be unaffected by further increase in the surfactant concentration. In this work, surface tensiometry was used as a means for determining the CMC of two commercial nonionic surfactants used in a current aqueous-alcoholic foaming hand sanitiser. For a plot of surface tension as a function of the logarithm of surfactant concentration a trend of continually decreasing surface tension with increasing surfactant concentration is expected to be observed. The observed change in surface tension can be used to determine the extent of adsorption to the interface by the Gibbs adsorption isotherm equation[20]:

$$\Gamma_B = -\frac{1}{RT}\cdot\frac{d\gamma}{d\ln a_B} = -\frac{a_B}{RT}\cdot\frac{d\gamma}{da_B}$$

(3.1)

where Γ_B is the surface excess concentration of component B (solute), γ is the surface tension, R is the universal gas constant, T is the temperature and a_b is the activity of component B. The activity is essentially the concentration of monomers in solution. Above the CMC the concentration of monomers in bulk does not change, and so the surface excess concentration is unaffected. In dilute solutions, the activity term is replaced by concentration (C_B) so that:

$$\Gamma_B = -\frac{1}{RT}\cdot\frac{d\gamma}{d\ln C_B} = -\frac{C_B}{RT}\cdot\frac{d\gamma}{dC_B}$$

(3.2)

It can therefore be seen that measuring the surface tension as a function of surfactant concentration will yield a plot of gradient Γ_B. The CMC of both surfactants has been determined by surface tensiometry and plots of surface tension as a function of surfactant concentration for Lamesoft PO65 and Silsurf DI-2510 can be seen in Figures 3.1 and 3.2, respectively.

Both plots demonstrate the expected curves. By analysis of the intersect of two straight line portions of each graph, the CMC's for each surfactant were determined. For Lamesoft PO65, the CMC was calculated to be 2.3×10^{-3} wt. % and for Silsurf DI-2510 the CMC was calculated as 0.01 wt. %. These CMC values are somewhat higher than the range expected for typical nonionic surfactants at room temperature (10^{-5}-10^{-4}M, or 10^{-4}-10^{-3} wt. %)[1] but it should be noted that these are commercial surfactants and may contain some impurities. Additionally, it can be seen that the surface tension at the CMC for Silsurf DI-2510 is lower than that observed for Lamesoft PO65. The number of molecules per nm^2 was calculated using eq. 3.2 for both surfactants. For Lamesoft PO65 the number of molecules per nm^2 was calculated as 4 molecules nm^{-2}, meaning that each surfactant molecule occupied 0.25 nm^2 of the interface. Similarly for Silsurf DI-2510, the number of molecules per molecules per nm^2 was calculated as 2.5 molecules nm^{-2}, so that each surfactant molecule occupied 0.4 nm^2 of the interface. Therefore, it is clear that the Silsurf DI-2510 surfactant occupies a much larger interfacial area than Lamesoft PO65, this is likely due to its bulky siloxane structure sterically hindering other molecules from approaching the interface.

Figure 3.1. Equilibrium surface tension plot as a function of concentration of Lamesoft PO65 in water. Measurements made using a Pt Wilhelmy plate at 25 ± 0.3 °C with a Krüss K12 tensiometer. Values shown are the average of 3 measurements made on a fresh meniscus. Error bars show maximum and minimum measured values.
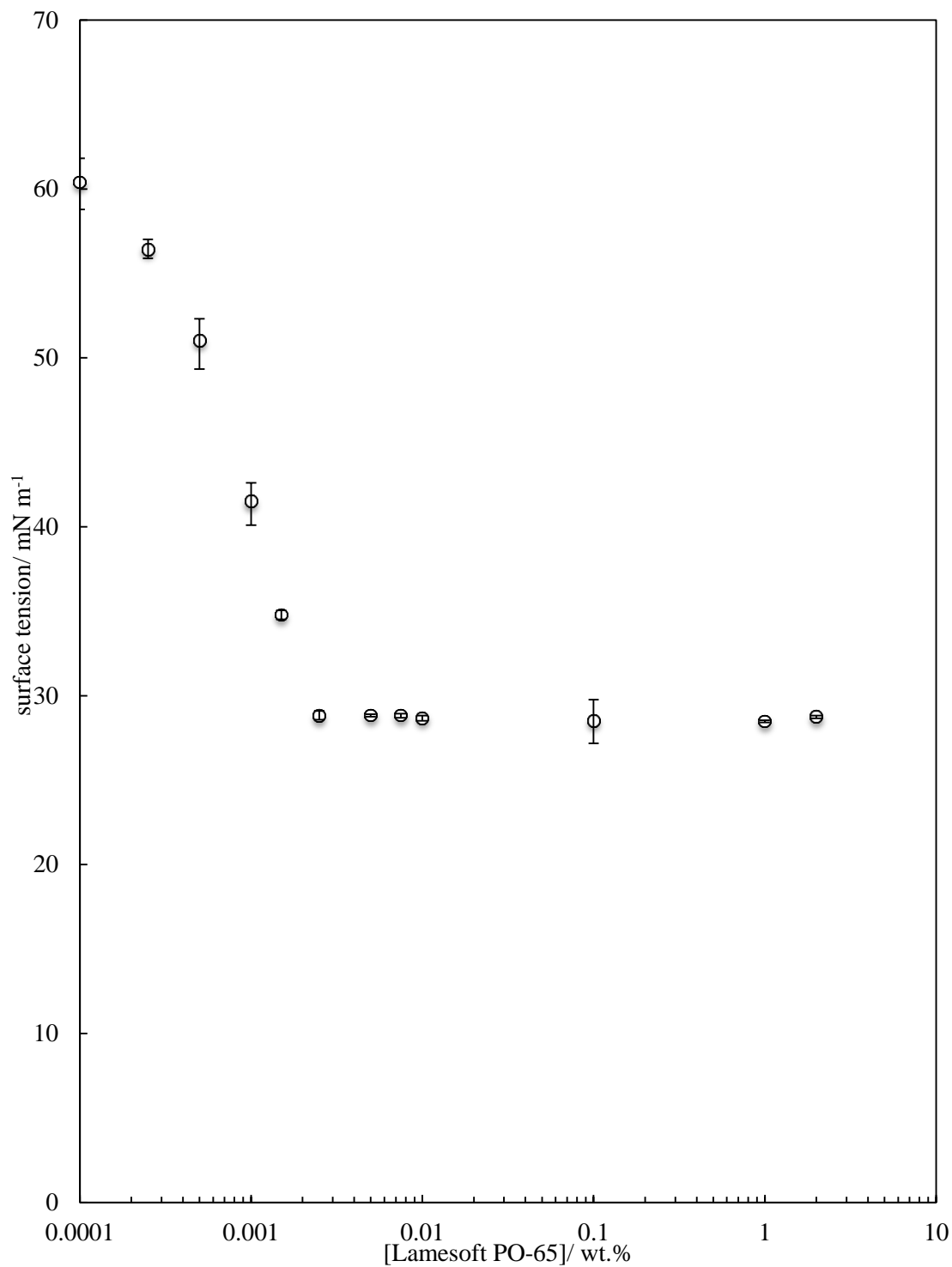
Figure 3.2. Equilibrium surface tension plot as a function of concentration of Silsurf DI-2510 in water. Measurements made using a Pt Wilhelmy plate at 25 ± 0.3 °C with a Krüss K12 tensiometer. Values shown are the average of 3 measurements made on a fresh meniscus. Error bars show maximum and minimum measured values.
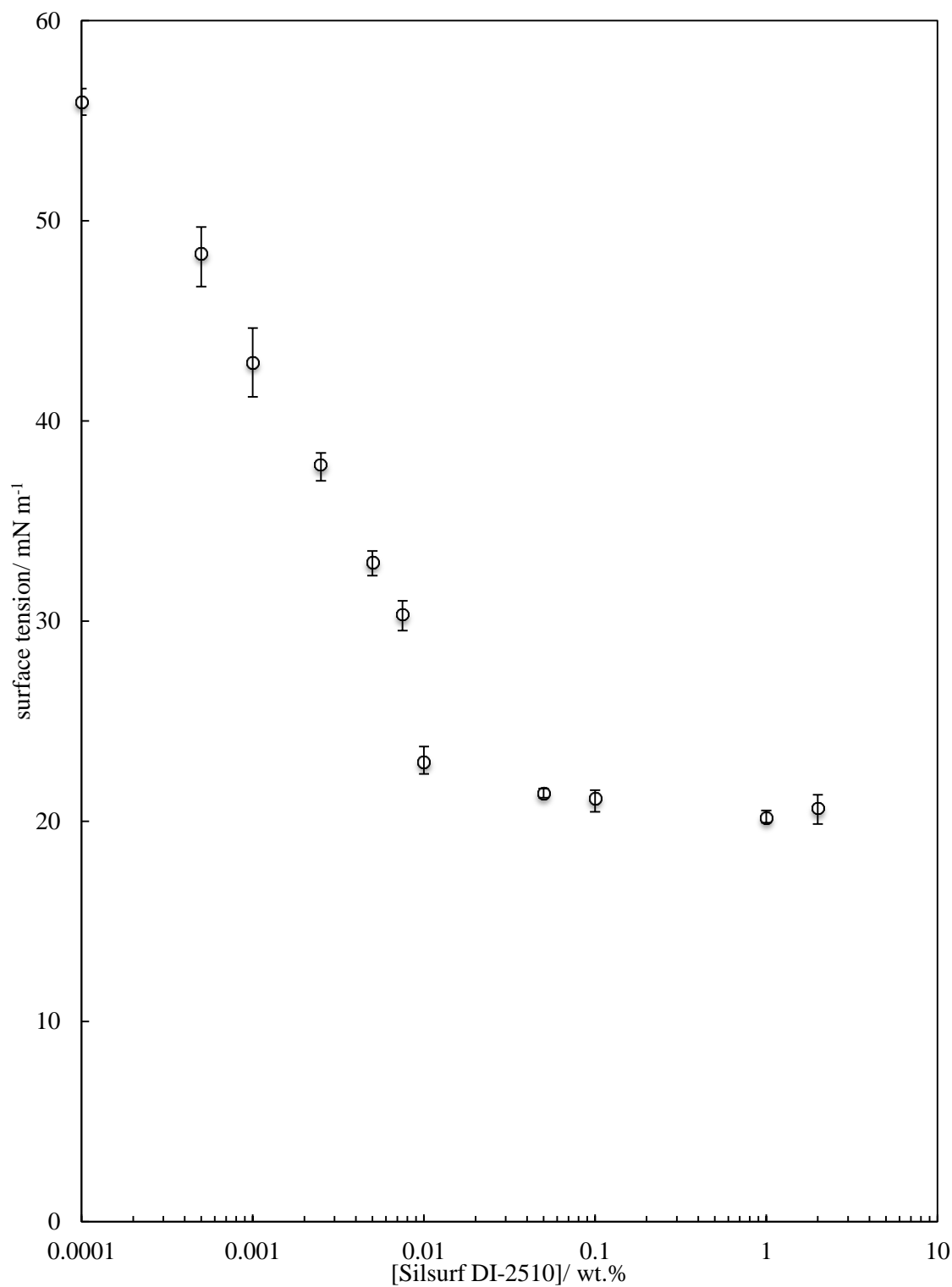
3.3.2 Aqueous surfactant foams

Aqueous foams of the surfactant solutions were prepared by dissolution of the neat surfactant into water. A batch of surfactant concentrations was prepared by serial 10-fold dilution of a concentrated 2 wt. % stock solution. The surfactant concentration range studied was 1×10^{-4}- 2 wt. %. The foams were prepared by dispensing 20 cm^3 solution into a volumetric cylinder, sealing and hand shaking vigorously for 30 seconds. The initial foam volumes and the half-life of the foam ($t_{1/2}$) are reported. The half-life ($t_{1/2}$) is defined as the time taken for half of the initial foam volume to collapse. Figures 3.3 (a) and (b) show images of the foams generated with Lamesoft PO65 and Silsurf DI-2510, respectively, with increasing surfactant concentration. The initial foam volume of these samples is shown as a function of surfactant concentration in Figure 3.4. The foam volume has been measured as the uppermost layer at which a complete layer of foam was observed. As all measurements of foam volume have been done by eye (checking foam layer on volumetric flask) some error may be introduced. It can be seen that no foam was generated at low surfactant concentrations. Lamesoft PO65 shows significantly better foamability than Silsurf DI-2510 in pure water and produces foams at lower surfactant concentration.

Figure 3.5 shows the average half-life, $t_{1/2}$ (calculated from foam volume vs. time curves of two separate foams) for each concentration of surfactant. Time constraints did not allow for further repeats, and it can be seen from the minimal spread of the data (error bars in Figure 3.4) that the foam volume is reproducible. However the data in Figure 3.5 may indicate that more repeats would be necessary to understand the errors associated with hand shaking the foams. It can be seen that with increasing surfactant concentration, the foam $t_{1/2}$ also increases and that overall, Lamesoft PO65 produced foams of a significantly higher stability than Silsurf DI-2510. It was also noted that in the case of both surfactants, foam was only generated above the CMC. To explain this, consider the generation of foam from a surfactant solution of concentration below the CMC. As the foam is generated, the interfacial area is significantly increased, it is plausible that there are simply not enough surfactant monomers present to stabilise the newly generated interface. Above the CMC, the micelles act as reservoirs to supply surfactant molecules to the interface, stabilising it.[21]

From microscopy images of the foams generated (shown in Figures 3.6 (a)-(g)) the bubble diameter and dispersity can be seen. The bubbles for both foams have smooth surfaces characteristic of surfactant-stabilised bubbles. The Lamesoft bubble diameter ranges from around 75-200 μm in comparison to the Silsurf bubble diameters, which are around 50-150 μm in diameter.

A plot of the mean bubble diameter as a function of surfactant concentration can be seen in Figure 3.7. The high standard deviation (as shown by the error bars) is indicative of a wide range of bubble diameters. This may be due to disproportionation and/or coalescence of the bubbles in the time taken to transfer the sample from the foam column to the microscope slide. However, the mean values show that there is a slight apparent increase in bubble diameter with increasing surfactant concentration. It is difficult to relate the bubble diameter to the stability of the foams as a significant proportion of the initial foam volume is lost through liquid drainage (in the first minute of foam generation) which is not reflected in the bubble diameter measurements.
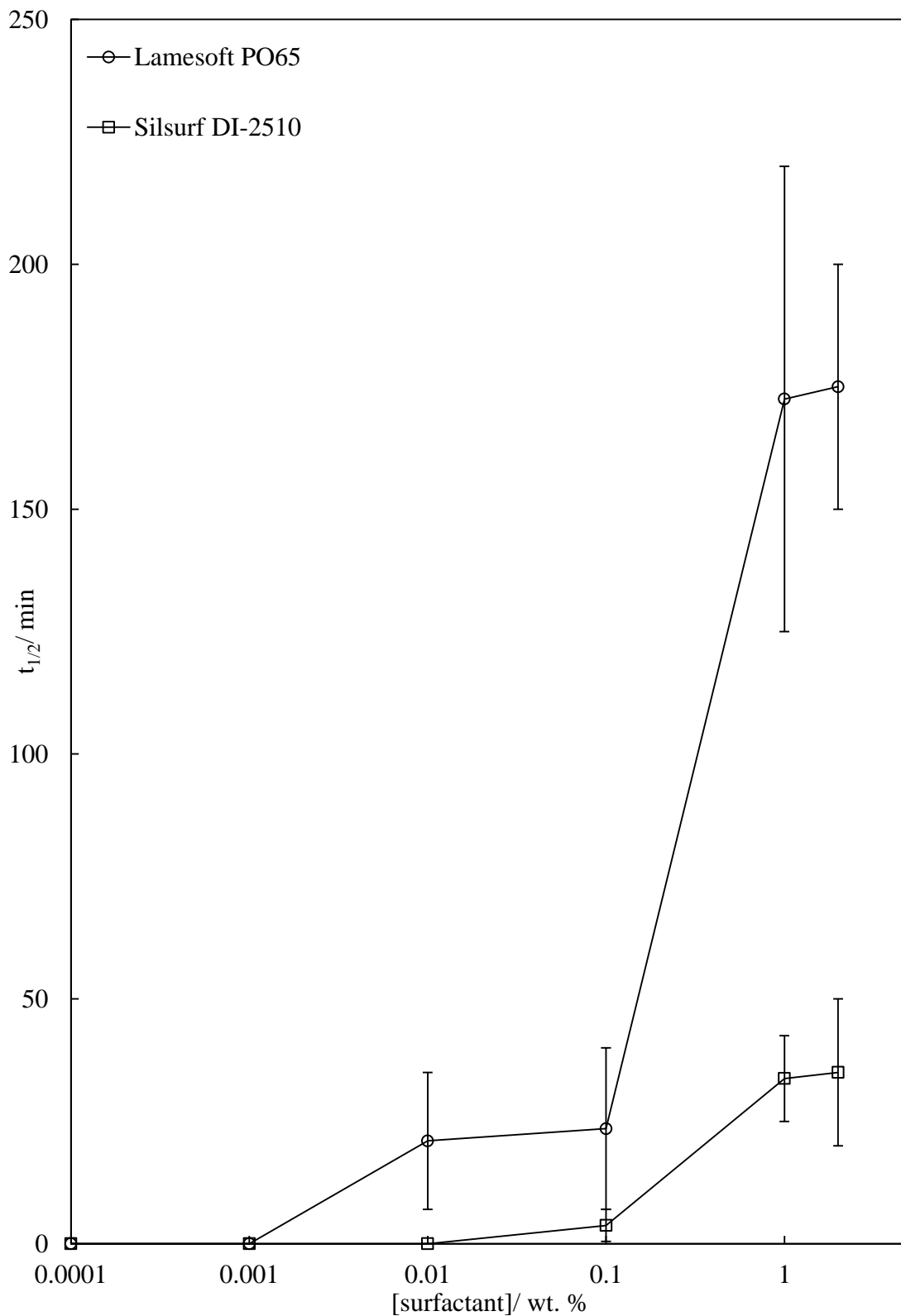
Figure 3.3. Foams generated by hand shaking (30 s) 20 ml surfactant solution (a) Lamesoft PO65 (b) Silsurf DI-2510 as a function of surfactant concentration (0.01-2 wt. %, left to right). Images taken with a Canon EOS450D camera immediately after generation.

Figure 3.4. Average initial foam volume of aqueous foams generated by hand shaking (30 s) 20 ml Lamesoft PO65 and Silsurf DI-2510 as a function of surfactant concentration. Error bars show maximum and minimum values of two separate measurements.
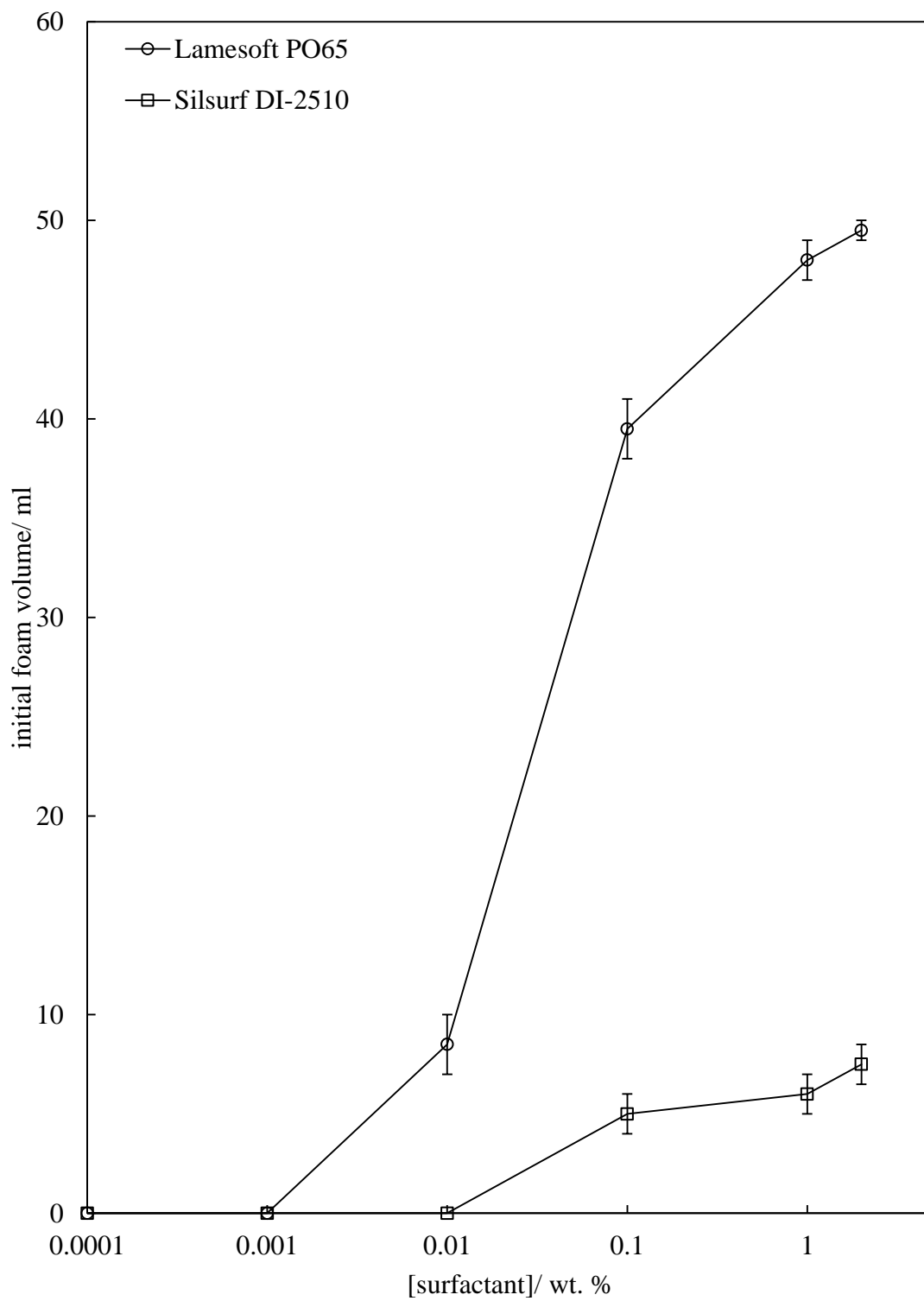
Figure 3.5. Average half-life ($t_{1/2}$) of aqueous foams generated by hand shaking (30 s) 20 ml Lamesoft PO65 and Silsurf DI-2510 solutions in water as a function of surfactant concentration. Error bars show maximum and minimum values of two separate measurements.

Figure 3.6. Microscopy of aqueous foams generated by hand shaking (30 s) 20 ml surfactant in water as a function of increasing surfactant concentration. (a) 0.01 wt. %, (b) 0.1 wt. %, (c), 1 wt. % and (d) 2 wt. %. Lamesoft PO65 (e) 0.1 wt. %, (f) 1 wt. % and (g) 2 wt. %. Silsurf DI-2510 Scale bar corresponds to 100 μm.
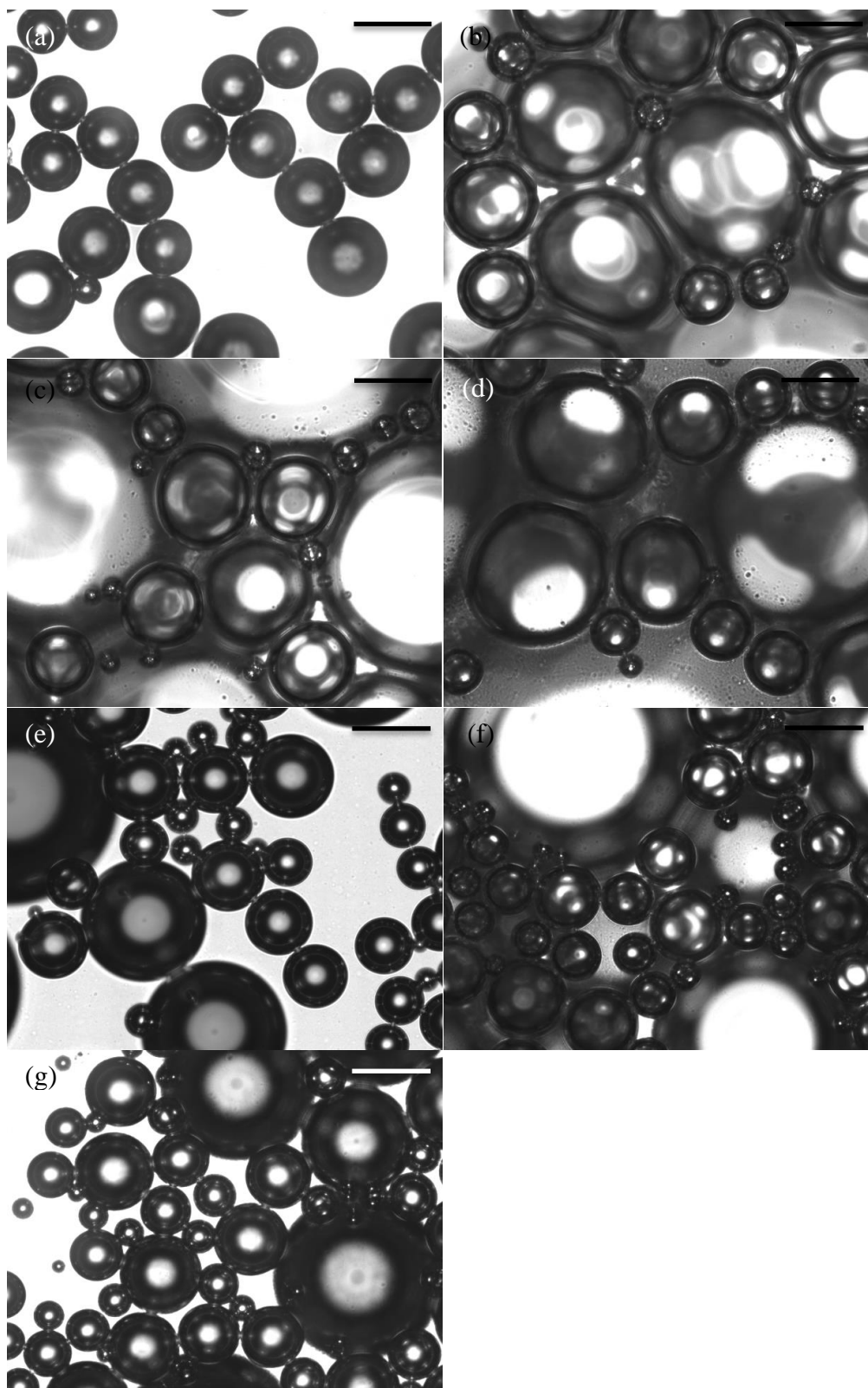
Figure 3.7. Measured average bubble diameter of Lamesoft PO65 and Silsurf DI2510 solutions in water after aeration by hand shaking 20ml solution for 30s. Mean bubble diameter calculated from at least 40 individual bubble measurements, taken within 5 minutes of foam generation. Error bars show standard deviation.
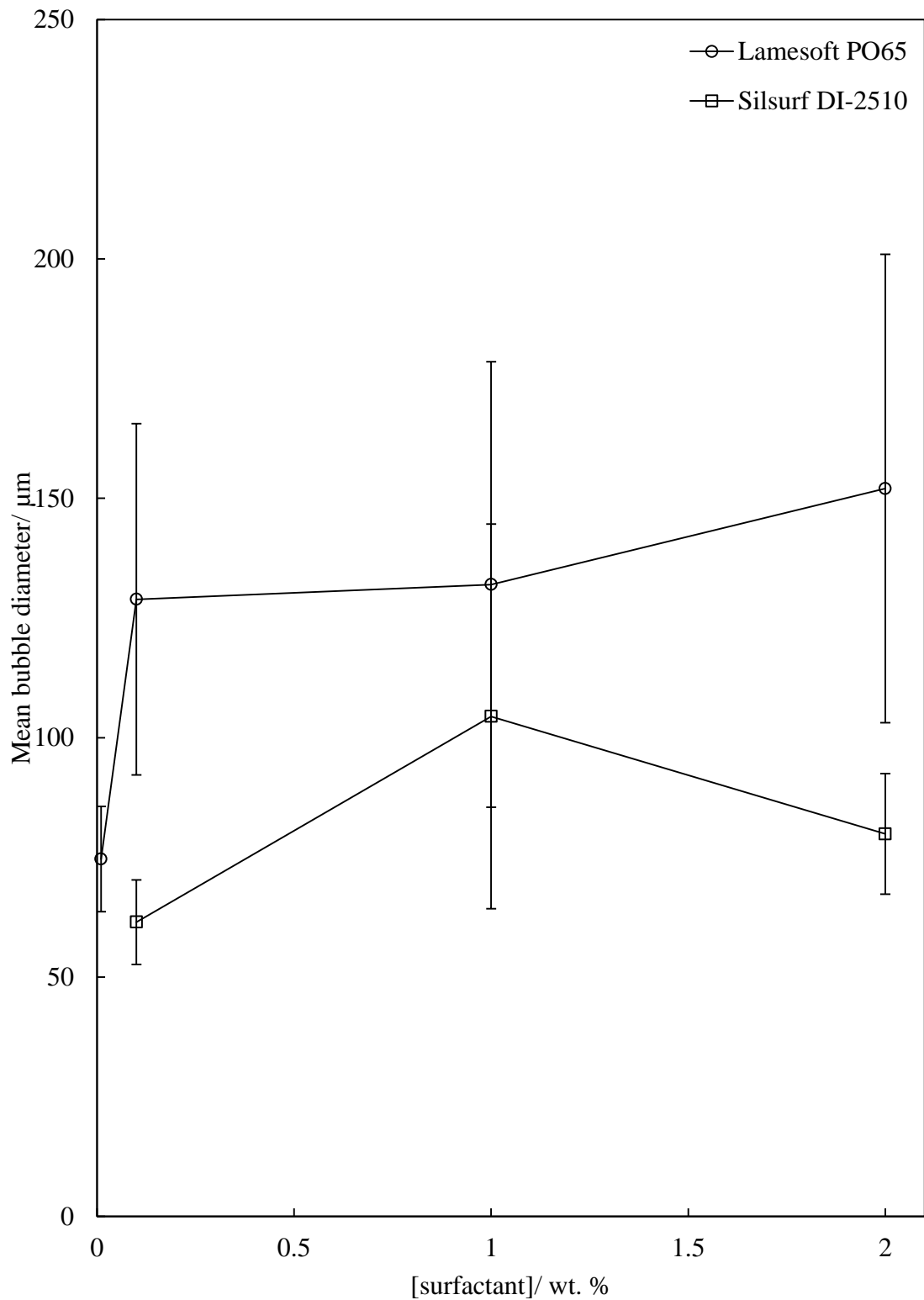
3.3.3   Aqueous-ethanolic surfactant solutions

As the formulation in which both of these surfactants are used comprises a high ethanol content (70 wt. %), the behaviour of these surfactants upon addition of ethanol to the aqueous phase was investigated. The effect of alcohol addition to the bulk properties of the surfactants was carried out by CMC measurements, then the effect of alcohol addition on the foam properties was explored.

3.3.3.1   Effect on CMC

As the micellisation behaviour of surfactants can have a significant influence on their foaming properties, the effect of ethanol addition to the CMC was studied. Figure 3.8 shows the effect of increasing ethanol concentration to the surface tension of pure water. A continual reduction in the surface tension with increasing ethanol concentration can be seen, and the results are in good agreement with literature results.[18] The surface tension of Lamesoft PO65 and Silsurf DI-2510 in 20 wt. % EtOH can be seen in Figures 3.9 and 3.10, respectively. The surface tension of the pure solution (20 wt. % EtOH) is 36.95 mN m^{-1} demonstrating that the reduction of surface tension of pure water with the addition of just 20 wt. % ethanol is significant.

The calculated CMCs for Lamesoft PO65 and Silsurf DI-2510 in 20 wt. % EtOH have been calculated from Figures 3.9 and 3.10 as 0.003 wt. % and 0.08 wt. %, respectively. Therefore the CMC is increased for both surfactants the addition of ethanol.

The increase in CMC is most likely due to the reduction of the hydrophobic effect due to better solubilisation of the hydrophobic tail groups in the presence of ethanol. The addition of ethanol to the system is suggested to destroy the water structure, and diminish the hydrophobic effect, leading to a continual increase in the CMC until a point is reached where no more micelles will form. These findings are supported by work carried out by Javadian *et al.*[22] whereby micelles of sodium dodecyl sulphate (SDS) were not observed to form above concentrations of 40% v/v ethanol due to disruption of the solvent such that the surfactant hydrocarbon tails could be accommodated without any unfavourable disruption. Further support for these findings is given by Becher[23] whereby micelles of polyoxyethylene lauryl alcohol were not observed to be formed above 25 wt. % ethanol.

It may be the case that the ethanol concentration at which micelles do not form in the current work is lower as there is less repulsion between the nonionic head groups of the commercial grade surfactants used. Further findings of Nishikido *et al.* demonstrated the effect of various alcohols on the micelle formation of polyoxyethylene lauryl ethers.[24] Ethanol addition was shown to increase the CMC of the surfactants due to a weakening of the hydrophobic effect. The surface concentrations of both surfactants in ethanol were also calculated and a summary of the values in pure water and ethanol is shown in Table 3.1. It can be seen that the surface concentration of molecules at the interface decreases for both surfactants in the presence of 20 wt. % ethanol. This is in keeping with the CMC measurements in ethanol. There are more surfactant molecules in solution, with reduced hydrophobic repulsion due to solubilisation by ethanol molecules. There were issues with evaporation of ethanol from the meniscus using surface tensiometry and therefore an alternative method may give more reliable data. It is suggested that the CMCs in ethanol be studied by a different method, such as the study of a hydrophobic dye/micelle solubilisation study (using UV-Visible spectrophotometry). Alternatively, methods such as the capillary rise method or dynamic light scattering for determination of surface tension, may provide more reliable data.

Table 3.1. Summary of CMC values and surface concentration of Lamesoft PO65 and Silsurf DI-2510 at CMC in pure water and 20 wt. % ethanol. Values calculated using equation 3.2

| Solvent	CMC/ wt. %		Surface concentration at CMC/ molecules nm^{-2}	
	Lamesoft PO65	Silsurf DI-2510	Lamesoft PO65	Silsurf DI-2510
Pure water	0.0023	0.01	4	2.5
20 wt. % EtOH	0.003	0.08	1.43	0.5

Figure 3.8. Measured and literature[18] surface tension as a function of ethanol concentration in pure water. Measurements made using a Pt Wilhelmy plate at 25 ± 0.3 °C with a Krüss K12 tensiometer. Values shown are the average of 3 measurements made on a fresh meniscus. Error bars show maximum and minimum measured values.
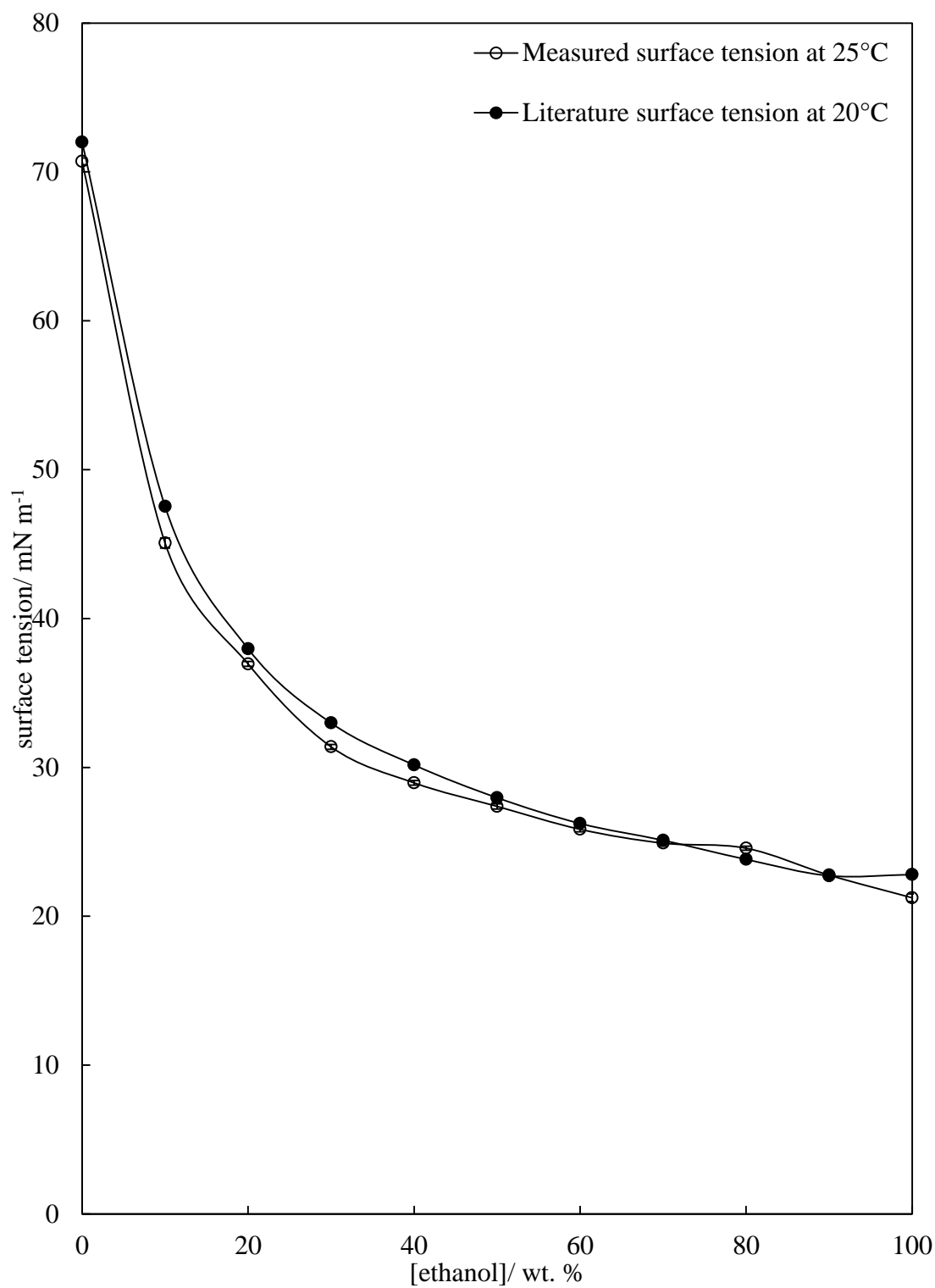
Figure 3.9.   Equilibrium surface tension as a function of concentration of Lamesoft PO65 in 20 wt. % EtOH. Measurements made using a Pt Wilhelmy plate at 25 ± 0.3 °C with a Krüss K12 tensiometer. Values shown are the average of 3 measurements made on a fresh meniscus. Error bars show maximum and minimum measured values.
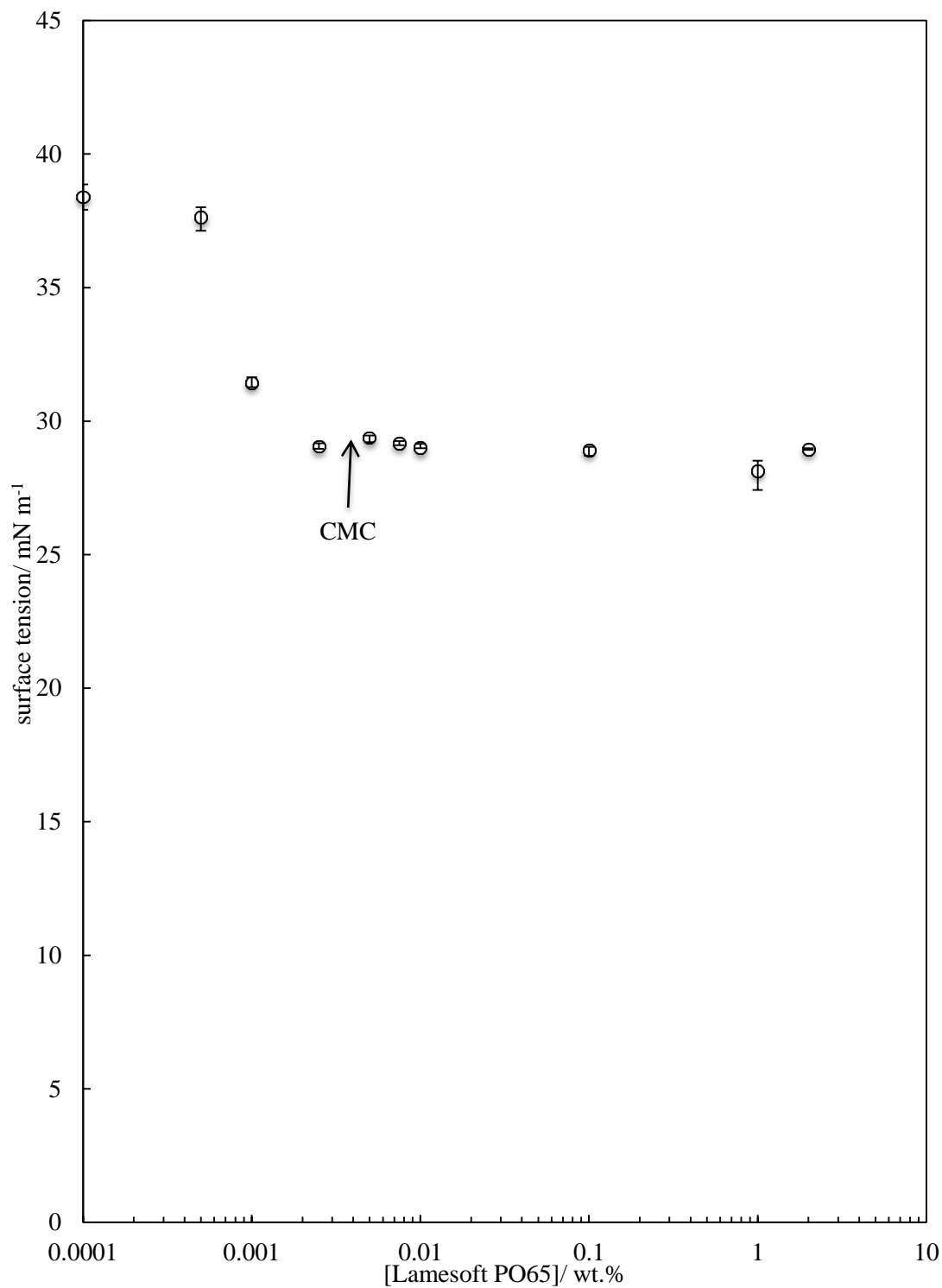
Figure 3.10. Equilibrium surface tension as a function of concentration of Silsurf DI-2510 in 20 wt. % EtOH. Measurements made using a Pt Wilhelmy plate at 25 ± 0.3 °C with a Krüss K12 tensiometer. Values shown are the average of 3 measurements made on a fresh meniscus. Error bars show maximum and minimum measured values.
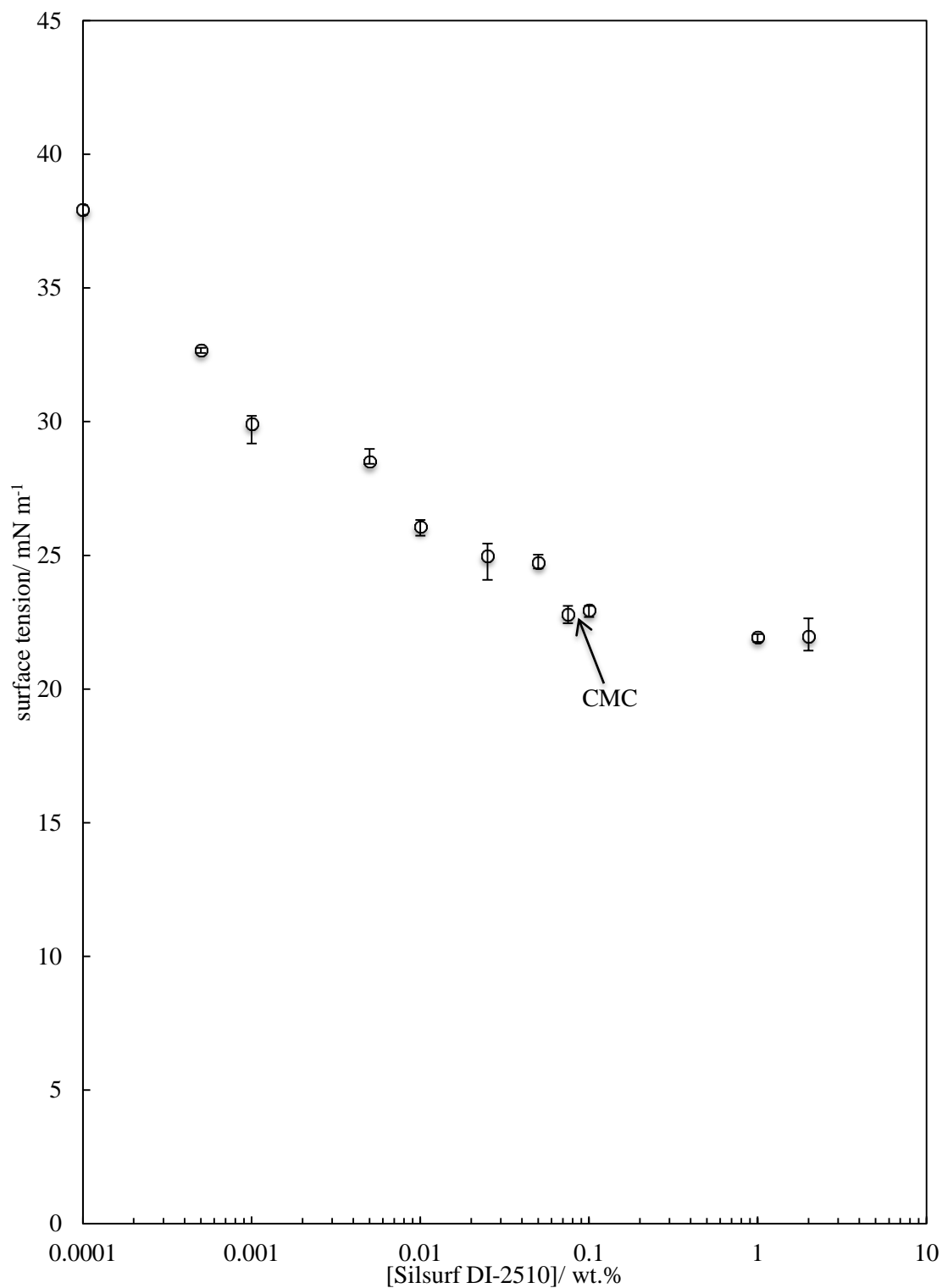
3.3.3.2 Effect on foam behaviour

The effect of ethanol addition to aqueous solutions of both surfactants on the foaming properties of these solutions was investigated by hand shaking 20 ml solutions in sealed volumetric cylinders for 30 s and monitoring the foam volume as a function of time. A plot of the initial foam volume as a function of ethanol concentration can be seen in Figures 3.11 and 3.12 for Lamesoft PO65 and Silsurf DI-2510, respectively. It can be seen that for both surfactants, a maximum in foamability is seen at an optimal ethanol concentration, this being 30 wt. % ethanol for Lamesoft PO65 and 70 wt. % ethanol for Silsurf DI-2510. Images of the foams generated at these optimal ethanol concentrations can be seen in Figures 3.15 (a) and (b).

The half-lives of the foams for both surfactants as a function of ethanol concentration are plotted in Figures 3.13 and 3.14 for Lamesoft PO65 and Silsurf DI-2510, respectively. It can be seen that with increasing ethanol concentration, the stability of the foams also passes through a maximum. For Lamesoft PO65 the maximum in stability is observed around 20 wt. % EtOH. However, for Silsurf DI-2510 the maximum in stability is observed over 20-60 wt. % EtOH. Additionally there is less of a clear surfactant concentration-dependent trend in the stability. As these surfactants are intentionally designed for performance in high ethanol concentrations, it is unsurprising that they demonstrate enhanced foam properties at high ethanol concentrations. Additionally, the use of PEG-8 to PEG-12 dimethicone surfactants (Silsurf DI-2510) in the use of stabilising alcohol foams has been documented in a patent by Wegner and Littau.[25]

Research in the area of surfactant-stabilised alcohol foams is relatively sparse. However, work by Samanta and Ghosh[26] has shown the addition of alcohols (butanol and hexanol) to aqueous Tween surfactant systems to enhance the stability of air bubbles formed with these solutions. Time for coalescence of single bubbles with the flat air-liquid surface was seen to increase with increasing alcohol concentration. The addition of sodium chloride to the system was shown to decrease the coalescence time and the researchers attributed this to two potential explanations. It was proposed that the addition of sodium chloride reduced the electrostatic double layer repulsion between the bubble surfaces. Alternatively, the hydration force is reduced with addition of sodium chloride as the salt disrupts the hydrogen bonding network of water.

Microscopy images of the foams generated are shown in Figures 3.16 and the measured mean bubble diameters obtained from these microscopy images are plotted in Figure 3.17. It can be seen that there is a slight trend of increasing bubble diameter with increasing surfactant concentration (this was also observed with foams in pure water).When comparing the mean bubble diameters for both surfactants in ethanol with those in pure water, there is an overall increase in the bubble size. This may be a result of the increased foamability of the surfactant solutions in ethanol. That is, the higher foam volume results in more bubbles with a reduced surface concentration of surfactant. This may result in higher disproportionation and hence larger bubbles in the systems of ethanol. However, it should be noted that the error on this data is large as the bubble distribution is so wide.

Figure 3.11. Average initial foam volume of foams generated by hand shaking (30 s) 20 ml Lamesoft PO65 as a function of ethanol concentration. Error bars show maximum and minimum values of two separate measurements.
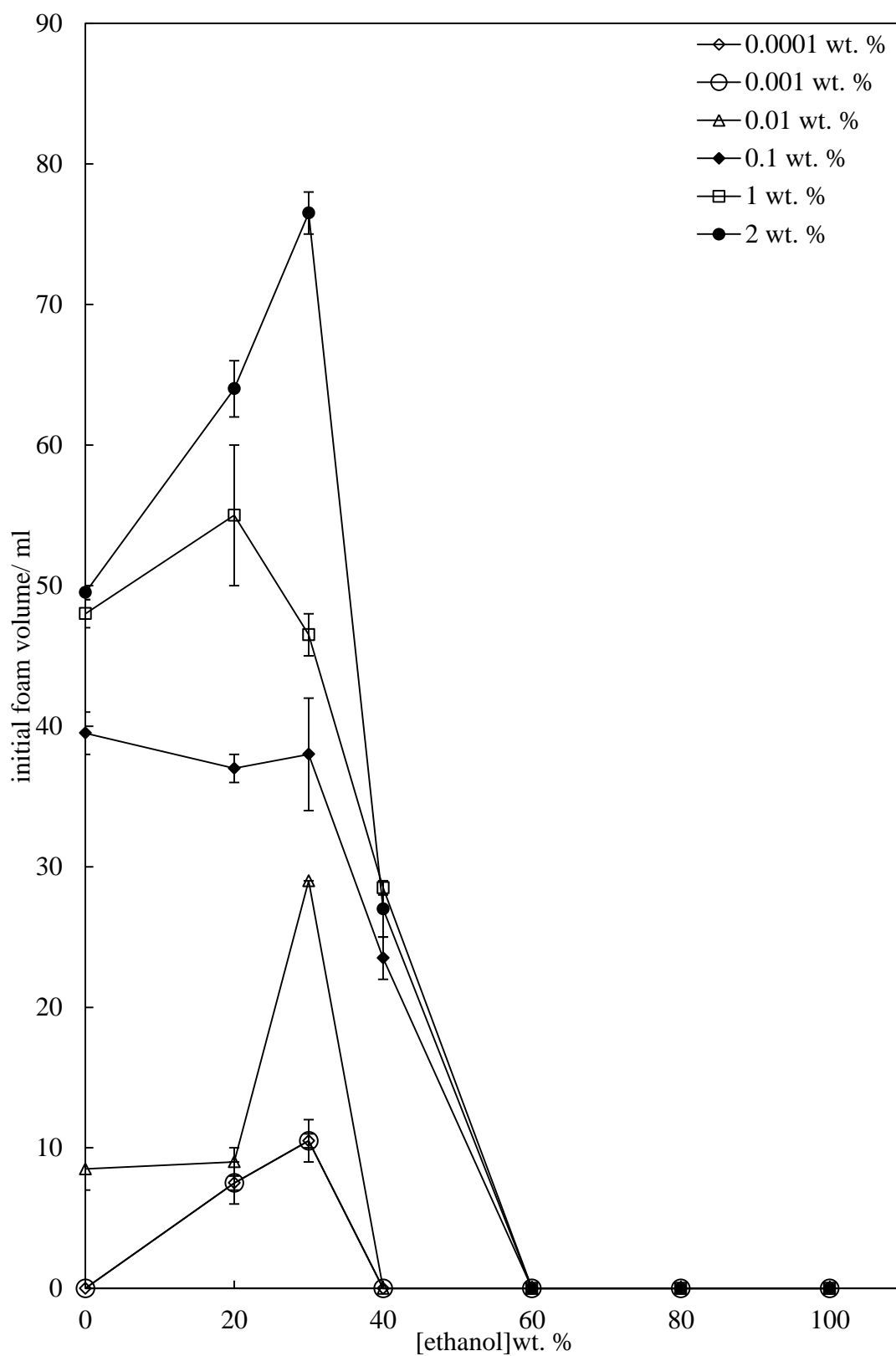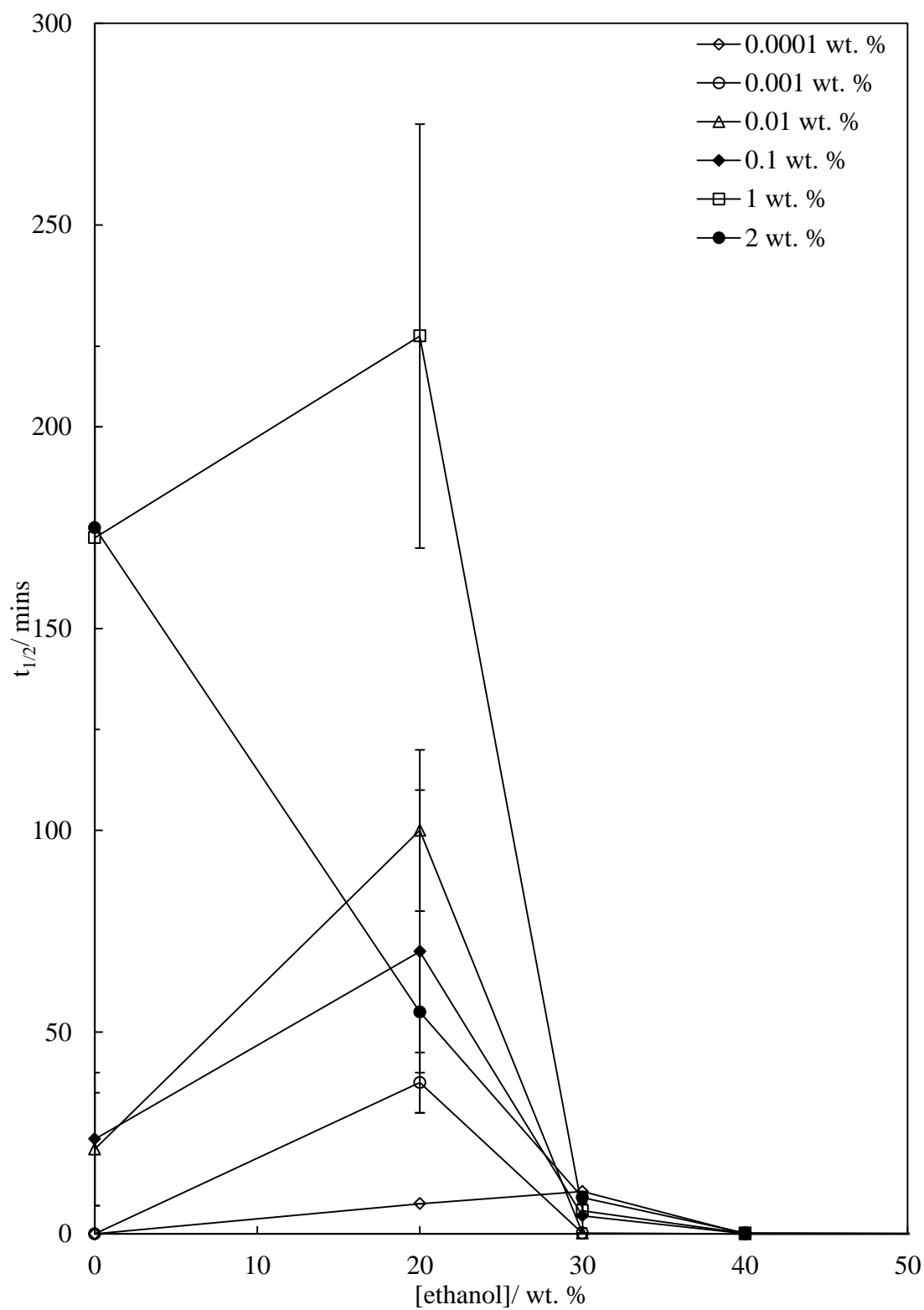
Figure 3.12. Average initial foam volume of foams generated by hand shaking (30 s) 20 ml Silsurf DI-2510 as a function of ethanol concentration. Error bars show maximum and minimum values of two separate measurements.
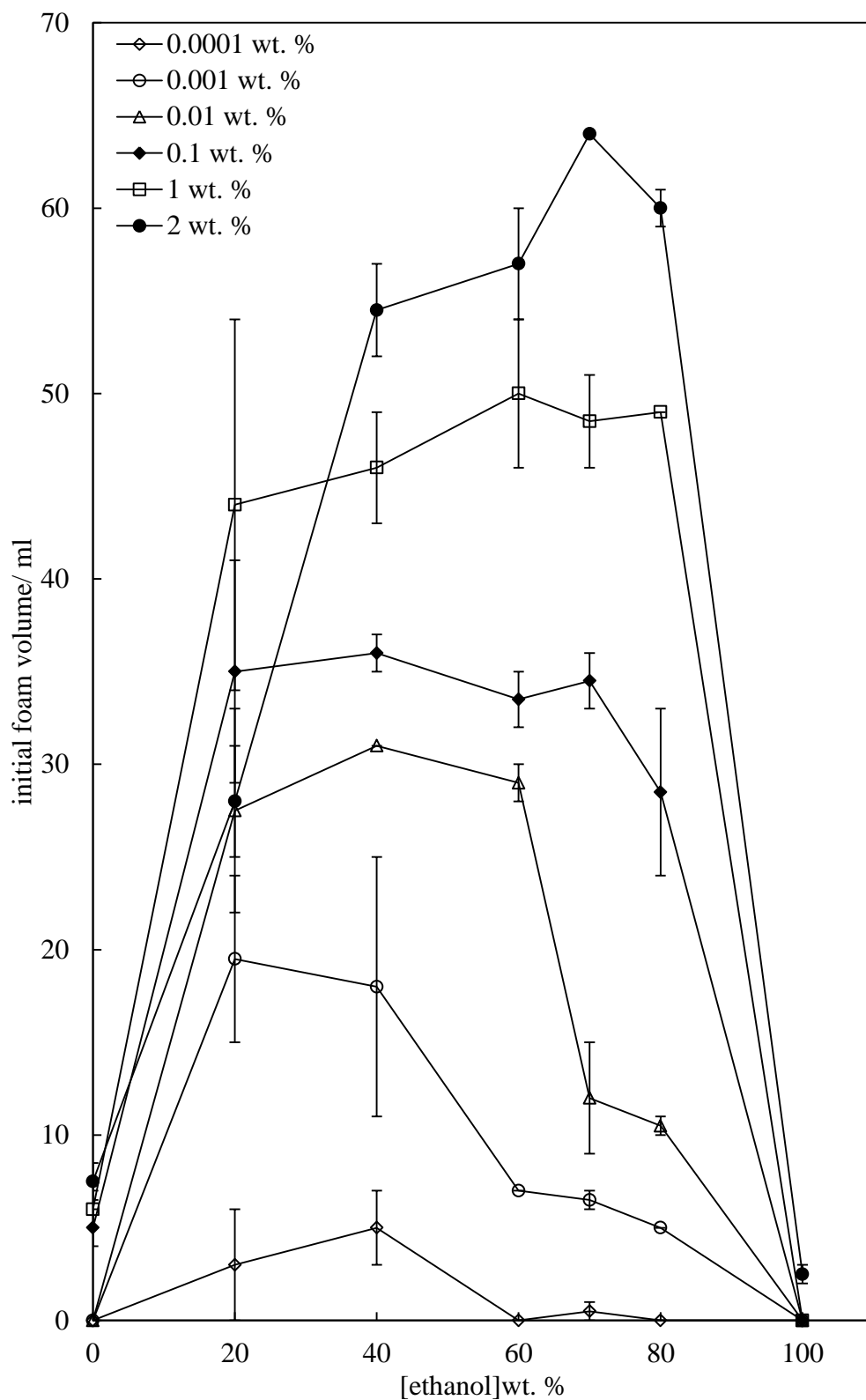
Figure 3.13. Average half-life ($t_{1/2}$) of foams generated by hand shaking (30 s) 20 ml Lamesoft PO65 as a function of ethanol concentration. Error bars show maximum and minimum values of two separate measurements.

Figure 3.14. Average half-life ($t_{1/2}$) of foams generated by hand shaking (30 s) 20 ml Silsurf DI-2510 as a function of ethanol concentration. Error bars show maximum and minimum values of two separate measurements.
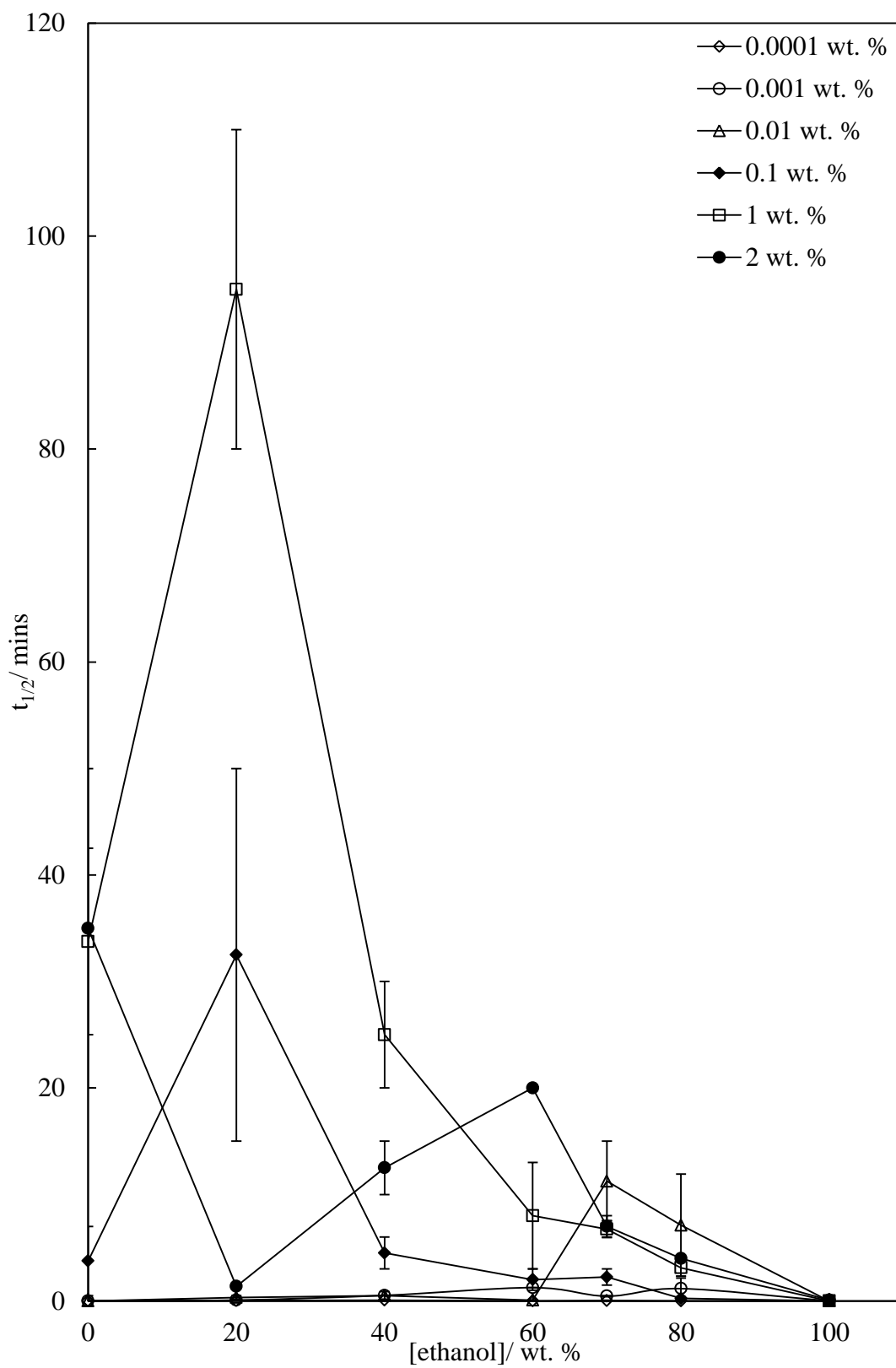
Figure 3.15. Photos of foams generated by hand shaking (30 s) 20 ml surfactant solution (a) Lamesoft PO65 in 30 wt. % ethanol (b) Silsurf DI-2510 in 70 wt. % ethanol. Surfactant concentration increases left to right. Images taken using a Canon EOS450D camera immediately after aeration.
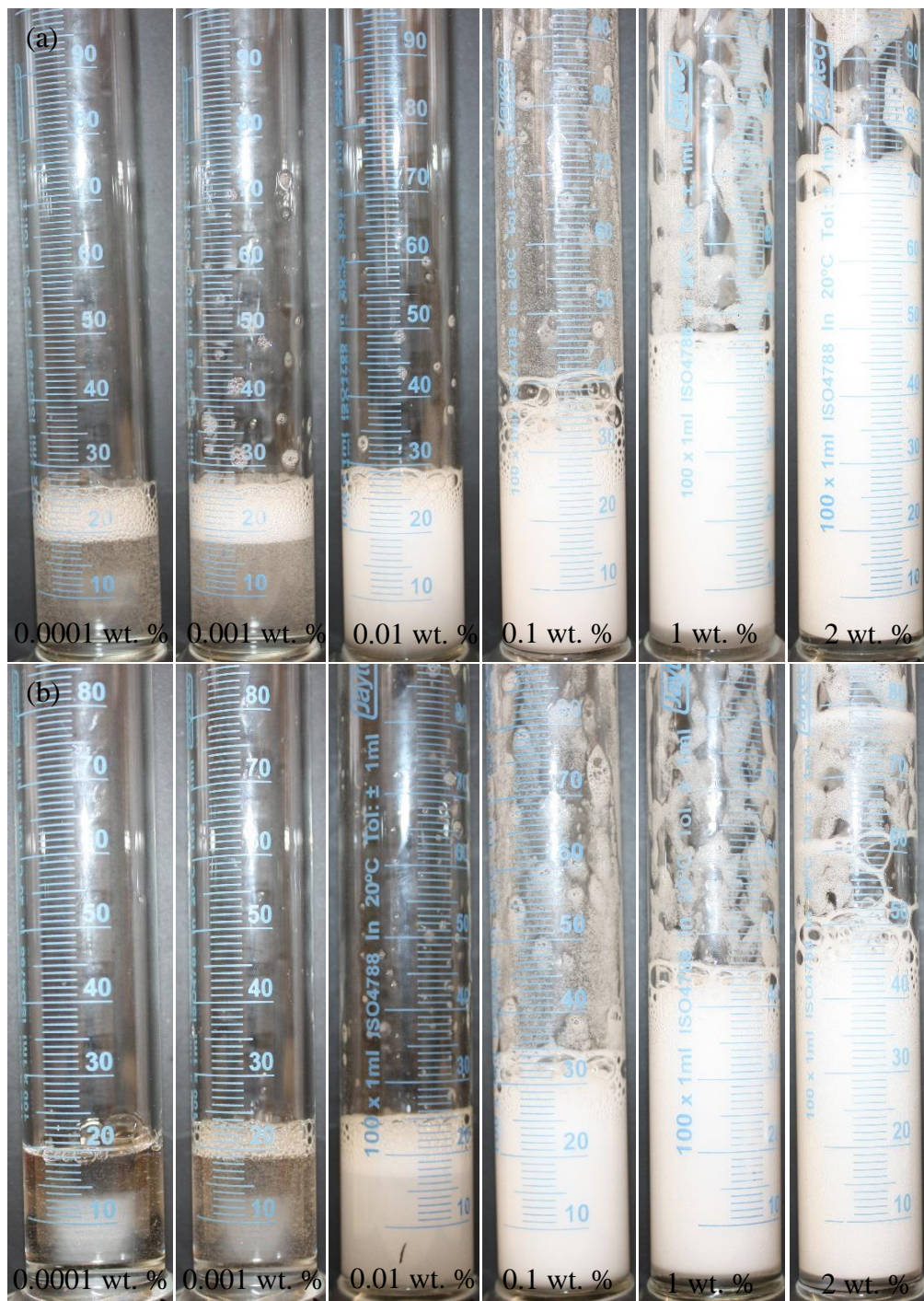
Figure 3.16. Microscopy of Lamesoft PO65 foams generated by hand shaking (30 s) 20 ml Lamesoft PO65 in 30 wt. % ethanol as a function of increasing surfactant concentration. (a) 0.01 wt. %, (b), 0.1 wt. % (c) 1 wt. % and (d) 2 wt. % Lamesoft PO65 in 30 wt. % ethanol. (e) 0.01 wt. %, (f) 0.1 wt. %, (g) 1 wt. % and (h) 2 wt. % Silsurf DI-2510 in 70 wt. % ethanol. Scale bar corresponds to 100 μm.
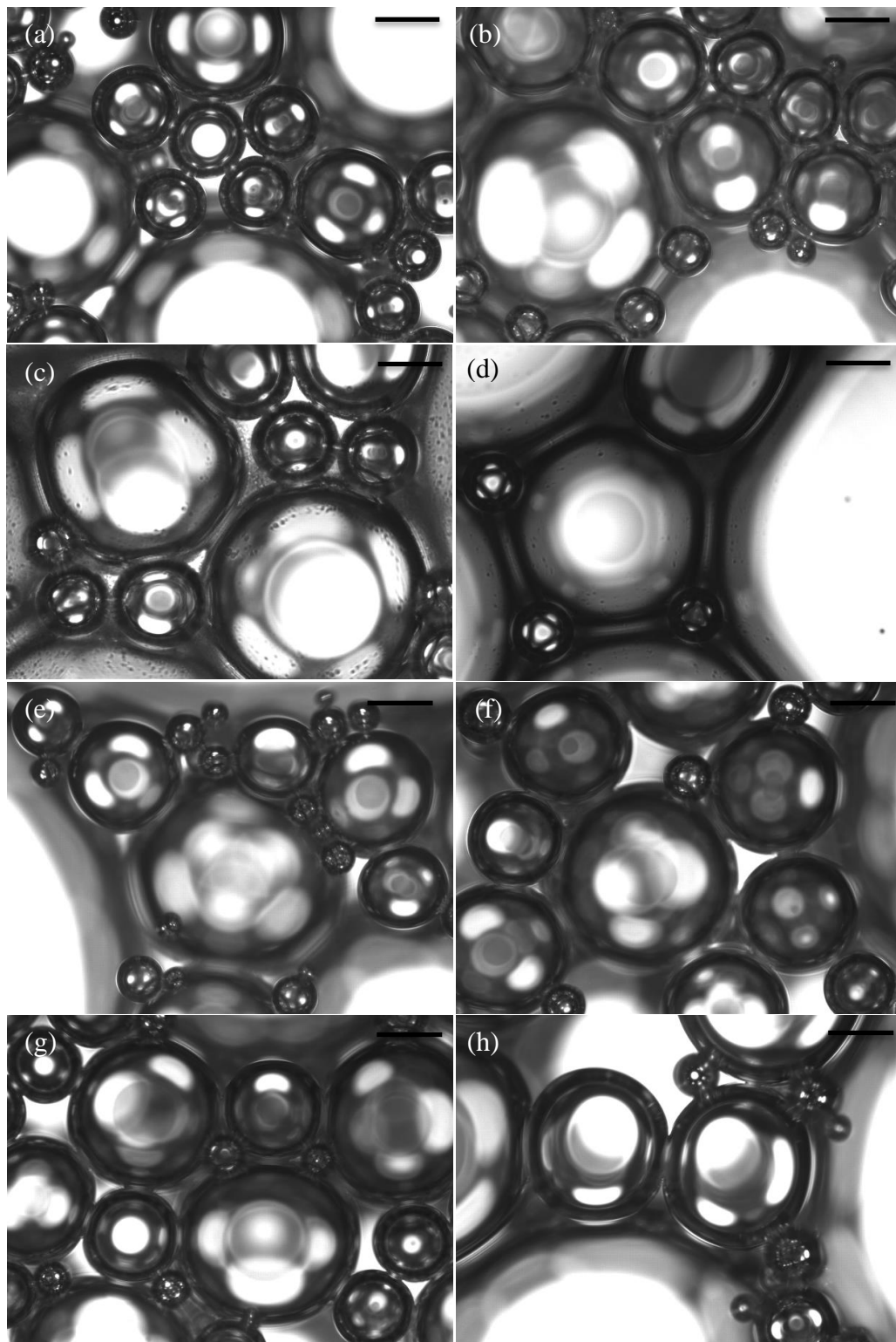
Figure 3.17. Measured average bubble diameter of Lamesoft PO65 and Silsurf DI2510 solutions in ethanol after aeration by hand shaking 20ml solution for 30s. Mean bubble diameter calculated from at least 40 individual bubble measurements, taken within 5 minutes of foam generation. Error bars show standard deviation.
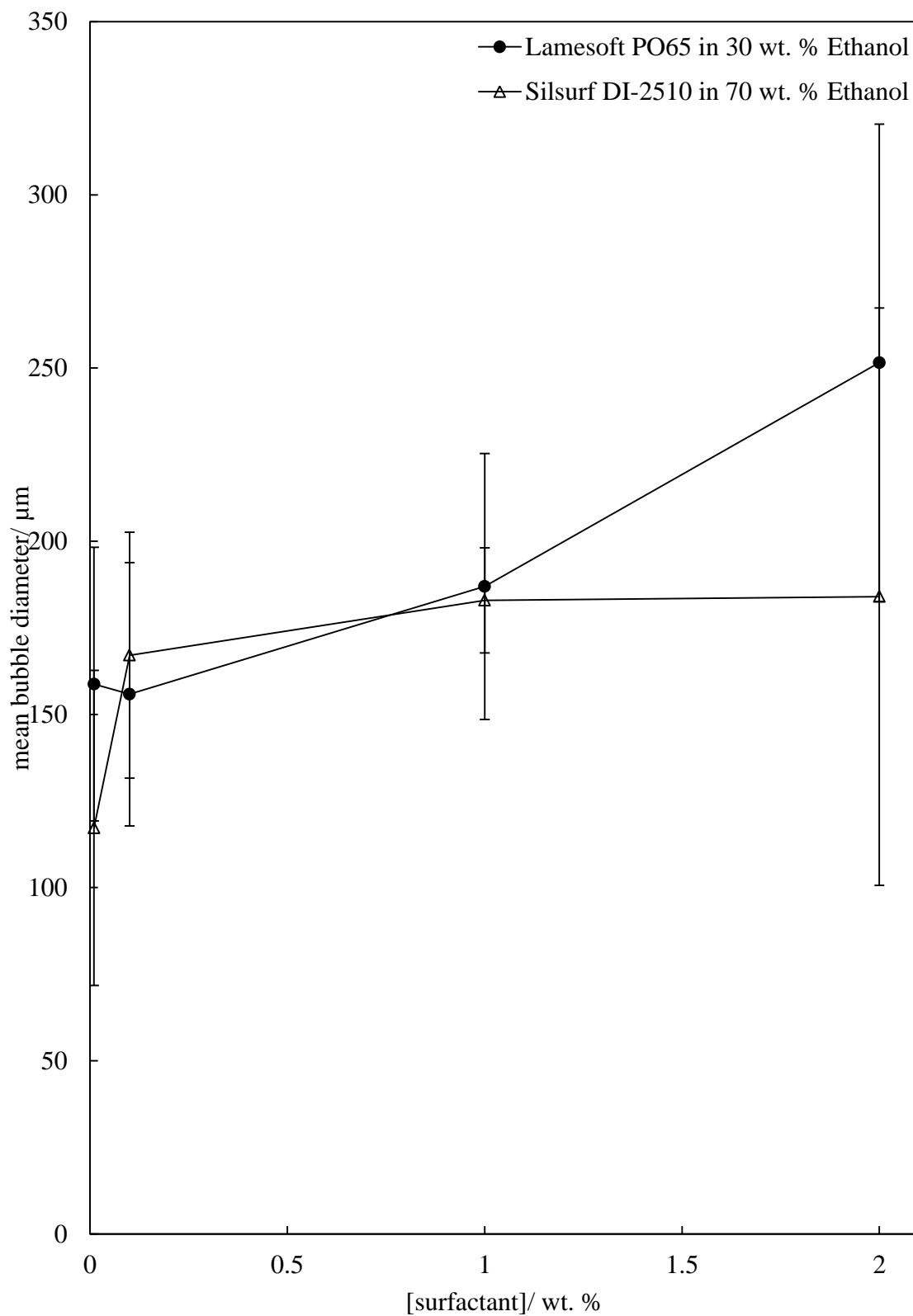
3.4   Foaming behaviour of particles

The stabilisation of aqueous foams by particles is well understood, and it is known that these foams often demonstrate long-term stability. As discussed in Section 3.1, this stability (compared to foams stabilised by surfactant alone) is assumed to arise from the irreversible adsorption of particles to the air-liquid interface. The aeration of dispersions of fumed silica particles of varying hydrophobicity in pure water and aqueous-ethanol has been explored.
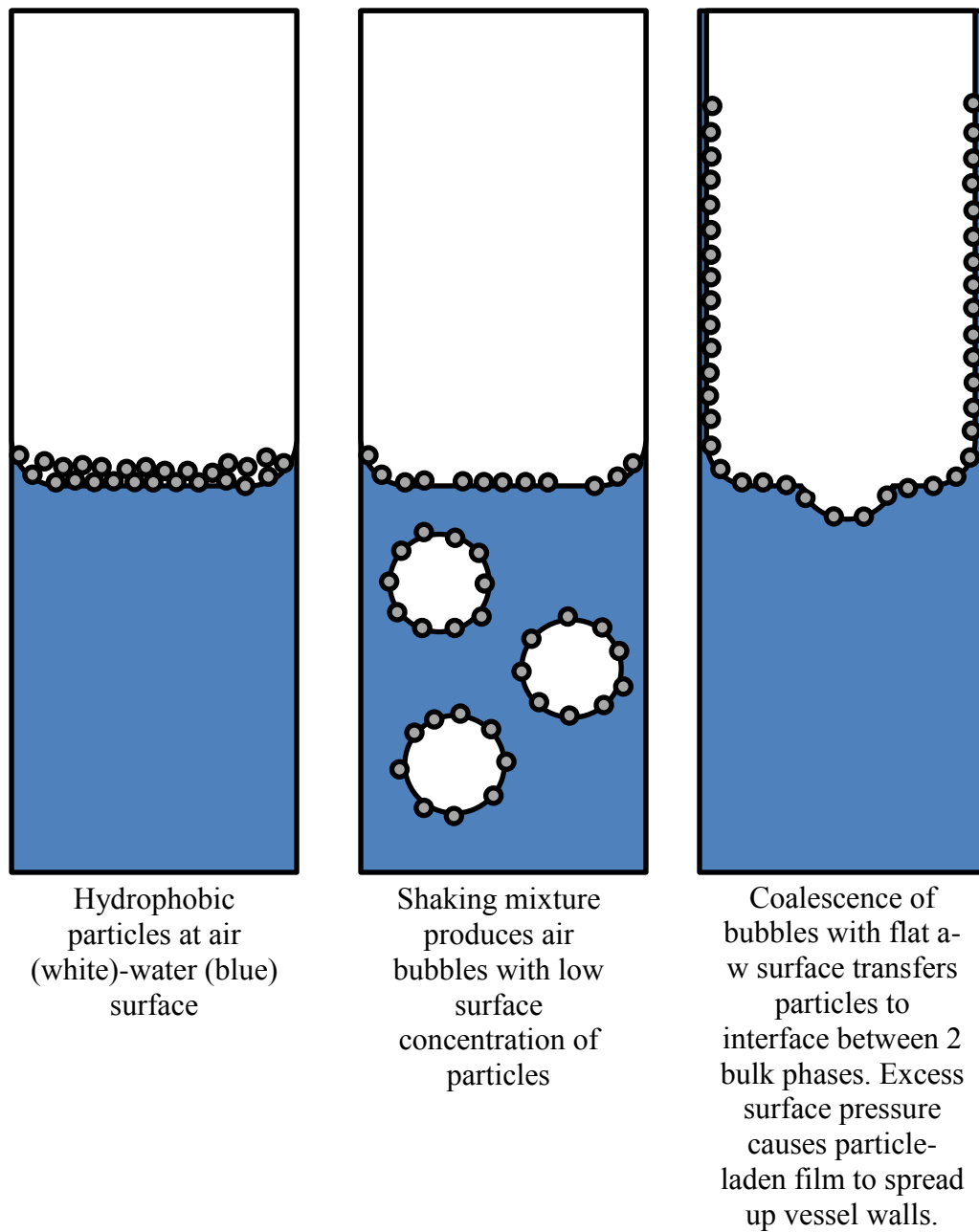
3.4.1   Aqueous foams of fumed silica

Figures 3.18 (a) and (b) show images of 0.1-2 wt. % dispersions of 20 and 47% SiOH fumed silica after a 30s hand shaking period of (20 ml liquid in 100 cm^3 volumetric cylinder). It can be seen that for 20% SiOH particles, climbing films were formed at all particle concentrations. Climbing films have been observed in the literature[27-29] and Binks *et al.* explained that climbing films arise from the formation of temporary bubbles coated with a dilute particle layer. When these sparsely coated air bubbles coalesce with the flat liquid-air surface, the excess surface pressure generated by particles adsorbed to the liquid surface in the vessel causes a particle-laden film to travel up the walls of the vessel (Figure 3.19).[29] As the hydrophobicity of the particles is reduced so that (47% SiOH), foams are observed after aeration, as seen in Figure 3.18(b). The volume of foam produced increased with increasing particle concentration, and the foams are stable to collapse for over 1 year. A graph of initial foam volume as a function of particle concentration is shown in Figure 3.20. Studies on the stability of foams stabilised solely by particles have shown foams of indefinite stability,[30-33] particularly by particles of intermediate hydrophobicity (around 90°).[4,5]

Optical microscopy images of the foams generated with 47% SiOH particles can be seen in Figure 3.21. It can be seen that the bubbles are non-spherical (making the bubble diameter difficult to measure accurately) with a rippled, textured surface; a distinct feature of particle-stabilised bubbles. This indicates the bubbles are coated with a dense layer of adsorbed particles compressed to high surface pressure. Binks and Horozov have suggested that this surface texture is a result of the interface corrugating to accommodate the increased surface concentration of particles as the particles cannot be ejected from the interface[4]. By increasing the hydrophilicity further (100% SiOH) no foams could be generated and stable dispersions were formed.

Figure 3.18. Images of aerated particle suspensions generated by hand shaking (30 s) 20 ml of (a) 20% SiOH fumed silica in water and (b) 47% SiOH fumed silica in water. Particle concentration increases from 0.1-2 wt. % (left to right). Images taken on a Canon EOS450D immediately after aeration.

Figure 3.19. Schematic diagram to demonstrate proposed mechanism for generation of particle-laden climbing films at air-water interface with hydrophobic particles. Redrawn from ref. 31.

| Hydrophobic particles at air (white)-water (blue) surface | Shaking mixture produces air bubbles with low surface concentration of particles | Coalescence of bubbles with flat a-w surface transfers particles to interface between 2 bulk phases. Excess surface pressure causes particle-laden film to spread up vessel walls. |

Figure 3.20. Average initial foam volume of aqueous foams generated by hand shaking (30 s) 20 ml of 47% SiOH fumed silica in water as a function of particle concentration. Error bars show maximum and minimum values taken from an average of two repeat measurements.
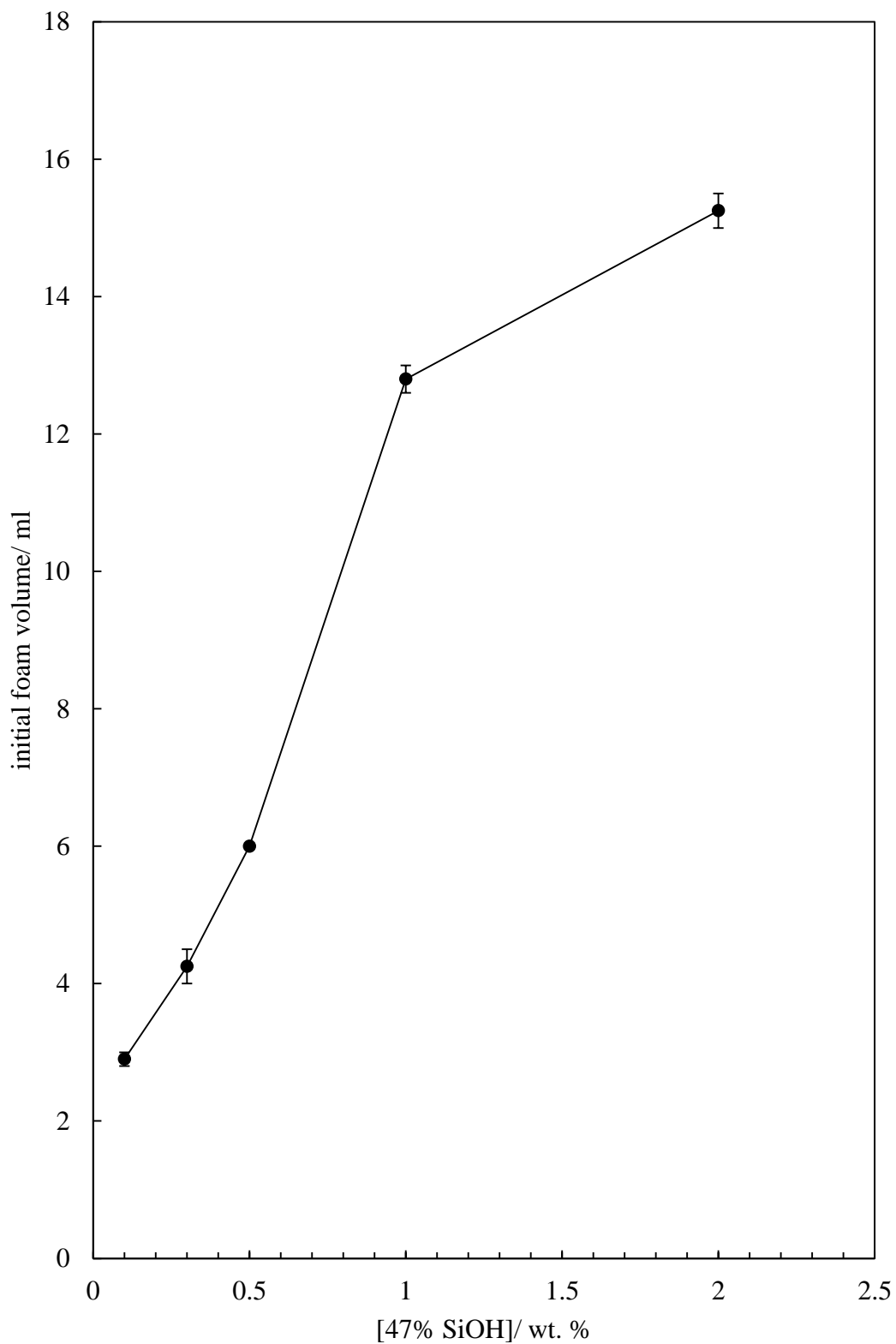
Figure 3.21. Optical microscopy of aqueous foams generated by hand shaking (30 s) 20 ml of 47% SiOH fumed silica in water with varying particle concentrations. (a) 0.1 wt. % (b) 0.3 wt. % (c) 0.5 wt. % (d) 1 wt. % (e) 2 wt. %. Scale bar corresponds to 100 μm.
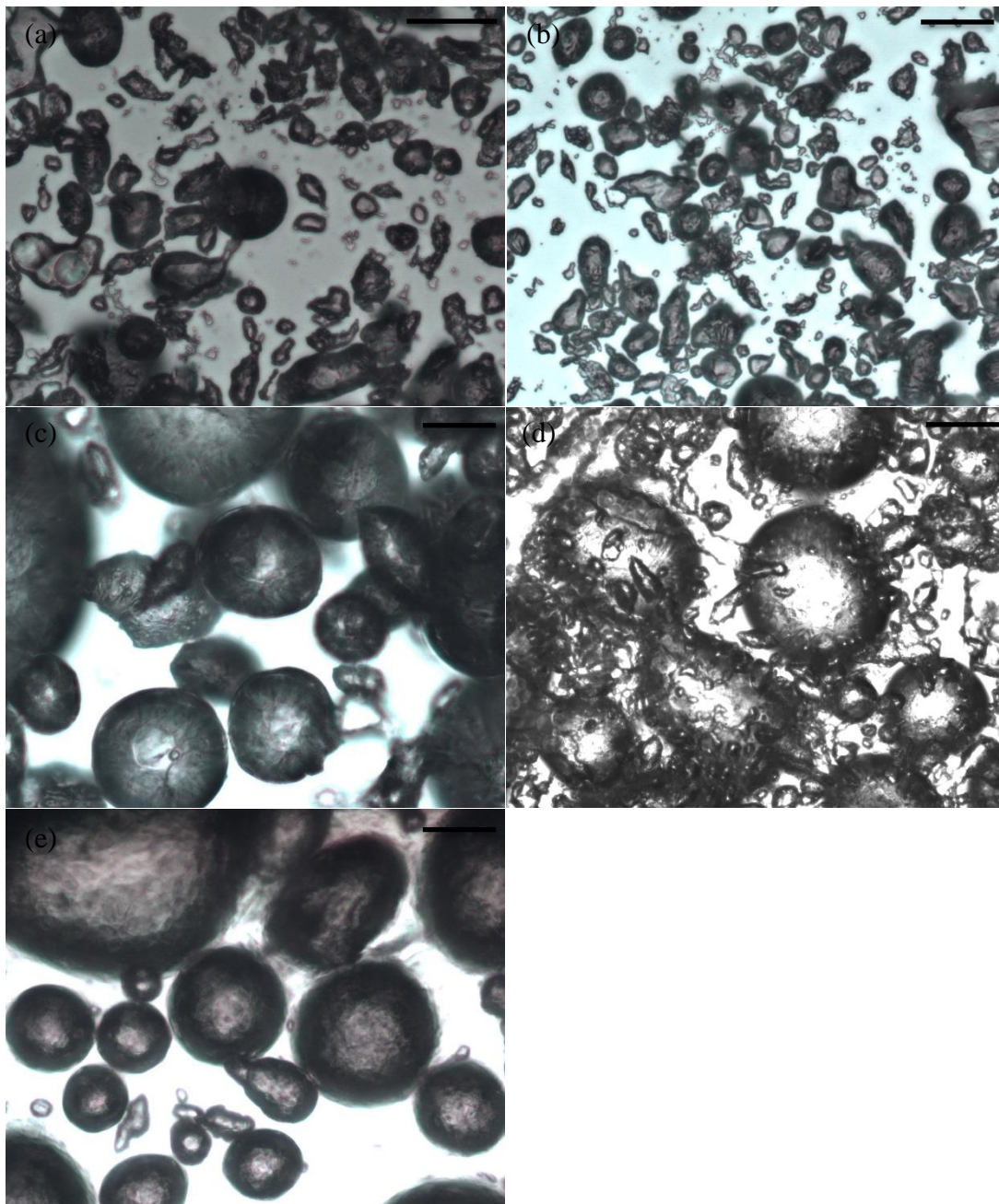
3.4.2   Aqueous-ethanolic foams of fumed silica

The effect of addition of ethanol to the aqueous phase of the particle dispersions and the subsequent effect on the foaming behaviour of these system was investigated. Varying the surface tension of the aqueous phase is of particular interest in this work as the behaviour of particles at interfaces of lower surface tension, particularly their foaming behavior, is less well understood. Specifically particle-stabilised foams of aqueous ethanol have been barely studied; only a handful of studies of these systems are known,[34,35] including the work of Sun and Gao.[32]

The maximum concentration of ethanol it was possible to generate foams with was 20 wt. %. Meta-stable foams could only be generated with 20% SiOH particles at this ethanol concentration. The 47% SiOH particles formed very unstable foam layers, all of which demonstrated complete collapse within 90 seconds. Photos of these foams can be seen in Figures 3.22 (a) and (b). A graph of the initial foam volume for both sets of particle foams is shown in Figure 3.23. There is an overall trend of increasing initial foam volume with increasing particle concentration, except for 2 wt. % 47% SiOH particles where a lower initial foam volume can be seen. It is likely that is was due to the aqueous phase becoming very viscous and it being difficult to incorporate bubbles into the aqueous phase by shaking. It can be observed that whilst the overall initial foam volume of foams generated with 47% SiOH particles is higher, the foams collapse within 90 seconds so are extremely unstable. The significantly larger bubble diameter can be seen in the photos of these foams (Figure 3.22 (b)) in comparison to the creamy foam layer of smaller bubbles seen for foams of 20% SiOH, which were stable in sealed vessels for over 1 year.

Optical microscopy images of the foams of 20% SiOH in 20 wt. % ethanol are shown in Figure 3.24. It was not possible to obtain microscopy images of 47% SiOH foams as they were so unstable. Additionally as with particle foams in pure water, the non-spherical shape of the bubbles made it impossible to accurately measure the bubble diameter.

Figure 3.22. Photos of foams generated by hand shaking (30 s) 20 ml of 20 wt. % ethanol containing (a) 20% SiOH fumed silica and (b) 47% SiOH fumed silica. Particle concentration increases from 0.1-2 wt. % left to right. Images taken on a Canon EOS450D immediately after aeration.

Figure 3.23. Average initial foam volume of aqueous foams generated by hand shaking (30 s) 20 ml of 20% SiOH and 47% SiOH fumed silica in 20 wt. % ethanol as a function of particle concentration. Error bars show maximum and minimum values taken from an average of two repeat measurements.
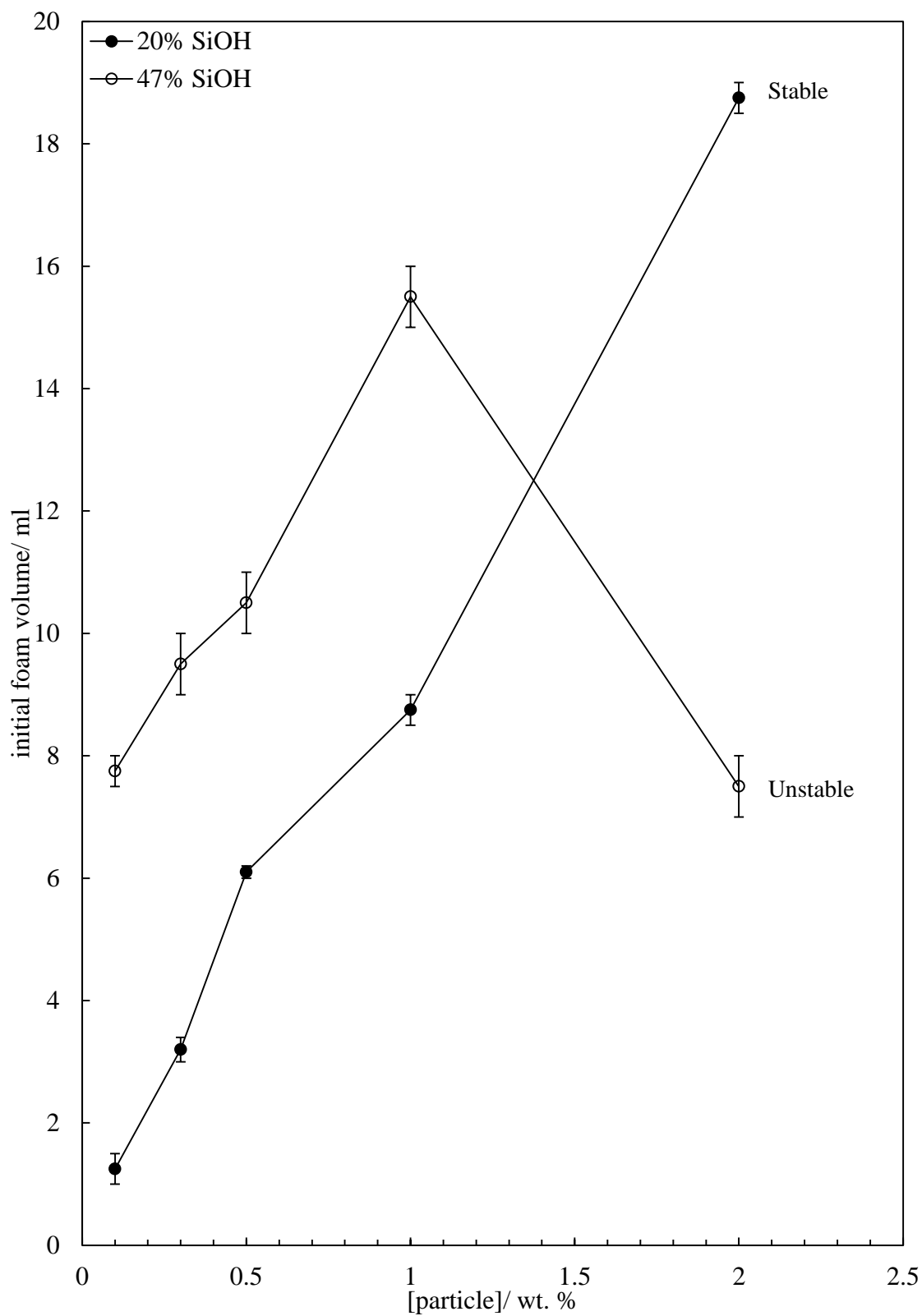
Figure 3.24. Optical microscopy of aqueous foams generated by hand shaking (30s) 20 ml 20% SiOH fumed silica in 20 wt. % ethanol with varying particle concentrations. (a) 0.1 wt. % (b) 0.3 wt. % (c) 0.5 wt. % (d) 1 wt. % (e) 2 wt. %. Scale bar corresponds to 100 μm.
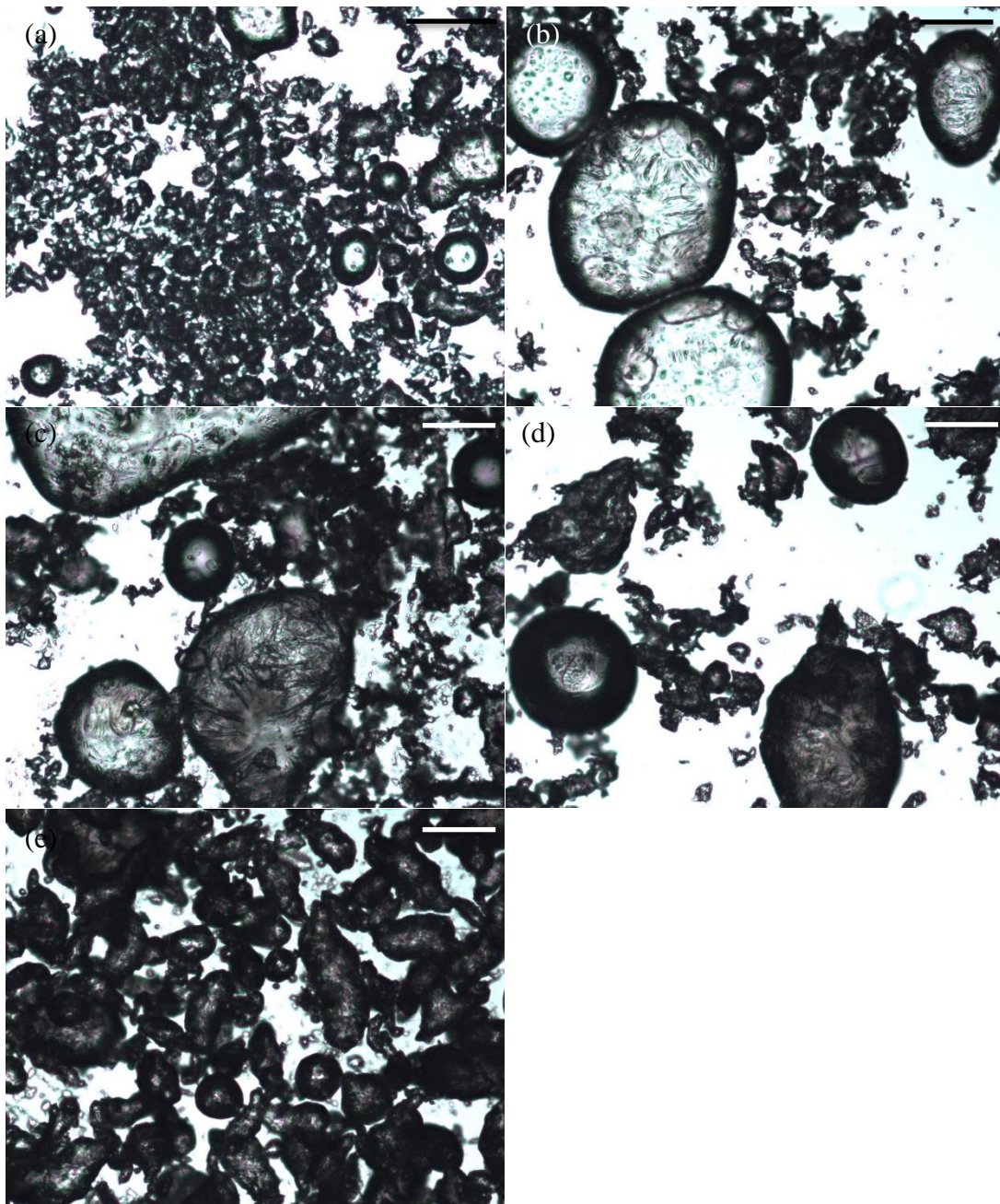
A summary of the foamability and stability (average half-life) of foams stabilised with surfactant and particles alone is given in Table 3.2 and 3.3. Also summarised in these tables is the foamability and stability of the foams generated in aqueous ethanol. The data shown for the ethanol concentration at which the maximum foamability is shown. Overall it can be seen in Table 3.2 that for both of the surfactants in pure water, with increasing surfactant concentration, the foamability and stability of the aerated solutions also increases. As ethanol is introduced into the system, both surfactants pass through a maximum in foamability. This was seen to occur at 30 wt. % and 70 wt. % EtOH for Lamesoft PO65 and Silsurf DI-2510, respectively. However, the stability does not follow the same trend, and maxima in stability (average half-life) pass through maxima at lower ethanol concentrations. In Table 3.3, it can be seen that for 20% SiOH particles, climbing films were generated in pure water but when 20 wt. % ethanol was introduced into the system, foams that were stable to collapse for over 1 year were generated. The volume of these foams was seen to increase with increasing particle concentration. With 47% SiOH particles in pure water, very stable foams were generated that demonstrated increasing initial volume with increasing particle concentration. However, in contrast to that observed for the 20% SiOH particles, with introduction of 20% SiOH to the system, the foams became very unstable and collapsed within 90 seconds.

Table 3.2. Summary of foaming experiments in pure water for foams generated with Lamesoft PO65 and Silsurf DI-2510 in pure water and aqueous ethanol. Foams generated by hand shaking 20 ml solution for 30 s. Average foamability and half-life are shown from three repeats.

[surf.]/ wt. %	Lamesoft PO65				Silsurf DI-2510			
	Foamability/ ml		Half-life/ mins		Foamability/ ml		Half-life/ mins	
	Water	30 wt.% EtOH	Water	30 wt.% EtOH	Water	70 wt.% EtOH	Water	70 wt.% EtOH
2	49.5	76.5	175	9	7.5	64	35	7
1	48	46.5	172.5	5.75	6	48.5	33.75	6.75
0.1	39.5	38	23.5	4.5	5	34.5	3.75	0.45
0.01	8.5	29	21	0.16	0	12	0	11.25
0.001	0	10.5	0	0.16	0	6.5	0	0.45
0.0001	0	10.5	0	0.08	0	0.5	0	0.04

Table 3.3. Summary of foaming experiments in pure water for foams generated with 20% SiOH and 47% SiOH fumed silica particles in pure water and aqueous ethanol solutions. Foams generated by hand shaking 20 ml particle suspension for 30 s. Average foamability and half-life are shown from three repeats.

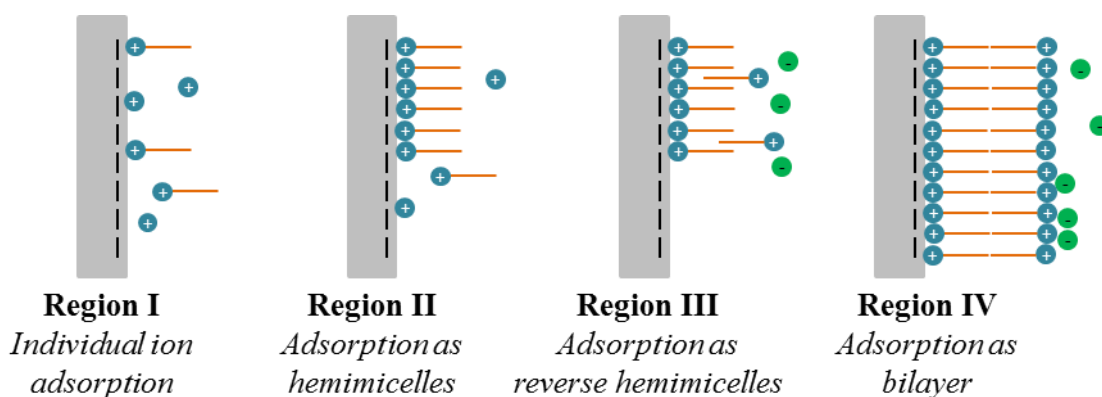| [part.]/ wt. %	20% SiOH				47% SiOH			
	Foamability/ ml		Half-life		Foamability/ ml		Half-life	
	Water	20 wt.% EtOH	Water	20 wt.% EtOH	Water	20 wt.% EtOH	Water	20 wt.% EtOH
2	0	18.75	0	>1 yr	15.25	7.5	>1 yr	<90s
1	0	8.75	0	>1 yr	12.8	15.5	>1 yr	<90s
0.5	0	6.1	0	>1 yr	6	10.5	>1 yr	<90s
0.3	0	3.2	0	>1 yr	4.25	9.5	>1 yr	<90s
0.1	0	1.25	0	>1 yr	2.9	7.75	>1 yr	<90s

3.5   Foaming behaviour of surfactant-particle mixtures

As discussed in Section 3.1, research in the area of aqueous foams stabilised by particle and surfactant mixtures is plentiful, with most of the literature focusing on the electrostatic adsorption of ionic surfactants to charged particle surfaces.[36-39] Work by Binks *et al.* examined the foaming behaviour of didecyldimethylammonium bromide (di-C10DMAB) and negatively charged Ludox silica particles.[36] For the particles alone, no foams were observed, and for the surfactant alone, unstable foams were produced. However, with addition of the surfactant to the particle suspensions, a synergistic relationship was observed whereby foams of a significantly higher stability were produced. Analysis of the supernatant surfactant solution after sedimentation of the particles allowed for calculation of the surfactant adsorption isotherms. It was seen that with increasing surfactant concentration, a gentle increase in the amount of surfactant adsorbed occurred. This was followed by a more significant increase at higher concentrations.

It has been suggested by Fuerstenau and Jia that there are four regions of adsorption (shown in Figure 3.25).[40] Region I; where individual surfactant molecules adsorb by electrostatic interaction of the headgroups. As surfactant concentration increases so that the surface concentration is around the CMC, the adsorbed ions begin to associate into patches of hemimicelles through chain-chain interaction of the adsorbed molecules (Region II). Region III is observed as a reverse in the zeta potential, and electrostatic repulsion causes some of the surfactant molecules to orient themselves in a reverse manner. Region IV is characterised by the formation of a complete bilayer on the solid surface. The scheme is generally accepted throughout the literature and explains adequately the variation in surface wettability of particles functionalised with adsorbed surfactant molecules.

Figure 3.25. Schematic diagram to show four regions of ionic surfactant adsorption to charged solid surface. Figure re-drawn from Reference 40.

Region I
Individual ion adsorption

Region II
Adsorption as hemimicelles

Region III
Adsorption as reverse hemimicelles

Region IV
Adsorption as bilayer

As mentioned earlier, there is significantly less research on the area of the mixture of nonionic surfactant and particles. This section therefore aimed to understand the behaviour of the two commercial surfactants observed (Lamesoft PO65 and Silsurf DI-2510) in the presence of fumed silica particles. It is possible that hydrogen bonding between the nonionic surfactant headgroups and the fumed silica particle surfaces may occur, allowing for a potential enhancement in the foaming properties in comparison to the surfactant solutions alone. Only mixtures of the surfactants and particles in water were explored so that the behaviour could be understood; it was anticipated that incorporating another component (for example, ethanol) into these systems would make it very difficult to understand and deduce explanations for the behaviours observed.

### 3.5.1 *Effect of surfactant concentration*

To investigate the effect of surfactant concentration on the foaming behaviour of 100% SiOH fumed silica particles, 1 wt. % 100% SiOH fumed silica particles were dispersed in surfactant solutions of varying surfactant concentration. Following this, 20 ml of the dispersion was aerated by hand shaking in a 100 cm^3 graduated volumetric cylinder and the foam volume as a function of time was measured. Photos of the foams generated with Lamesoft PO65 and Silsurf DI-2510 are shown in Figure 3.26 (a) and (b). The average initial foam volumes of the dispersions of Lamesoft PO65 and Silsurf DI-2510 as a function of increasing surfactant concentration are shown in Figure 3.27. It can be seen that the addition of particles to both surfactants has no effect at low concentrations (below 0.01 wt. %) but at high concentrations (above 0.1 wt. %) an enhancement in the foamability is observed.

An exception was observed for 1 wt. % Silsurf DI-2510 and 1 wt. % 100% SiOH where the aqueous phase was observed to form a gel-like structure. It is possible that the lower foam volume in this case was due to difficulty in incorporating air bubbles into the higher viscosity aqueous phase. The gel-like continuous phase was only observed in samples of 1 wt. % 100% SiOH. It is clear that some form of interaction occurs between the surfactants and particles, specifically at this surfactant-particle concentration, forming a network-like structure where the viscosity of the aqueous phase was significantly increased. It may have been fruitful to quantify the viscosity of the various solutions as a function of surfactant concentration.

The collapse profiles of the Lamesoft foams as a function of time are shown in Figures 3.28-3.30 where it can be seen that the stability of the foams above 1 wt. % is enhanced in comparison to 1 wt. % surfactant alone. The long term stability of 0.1 wt. % surfactant is also enhanced with the addition of particles so that the foams were more stable than 1 wt. % surfactant alone. The half-lives of the foams are shown in Figure 3.31, where it can be seen that the time taken for half of the initial foam volume to collapse generally increases with increasing concentration, but passes through an apparent minimum at 1 wt. % surfactant. However, even considering this minimum, the half-lives at 1 wt. % with the addition of particles are longer than 1 wt. % surfactant alone.

Figure 3.32 shows optical microscopy of the foams generated. The bubble surfaces are smooth, like those of the surfactants alone, which may indicate that little to no particles have adsorbed to the bubble surfaces, and that possibly the particle surfaces have remained hydrophilic due to poor surfactant adsorption to their surface. The enhancement in stability may be due to particles becoming trapped in the plateau borders of the foam bubbles. The mean bubble diameters as a function of Lamesoft PO65 concentration with and without silica particles are shown in Figure 3.33. As with the foams of surfactant alone, it is difficult to correlate the bubble diameter values to the stability behaviour of the foams generated. Much of the foam collapse in the first 5 minutes of foam generation is due to liquid drainage, which is not reflected in the bubble diameter data. It can be seen in Figure 3.33 that there is little variation in the mean bubble diameter with surfactant concentration, and with the addition of particles (within the error).
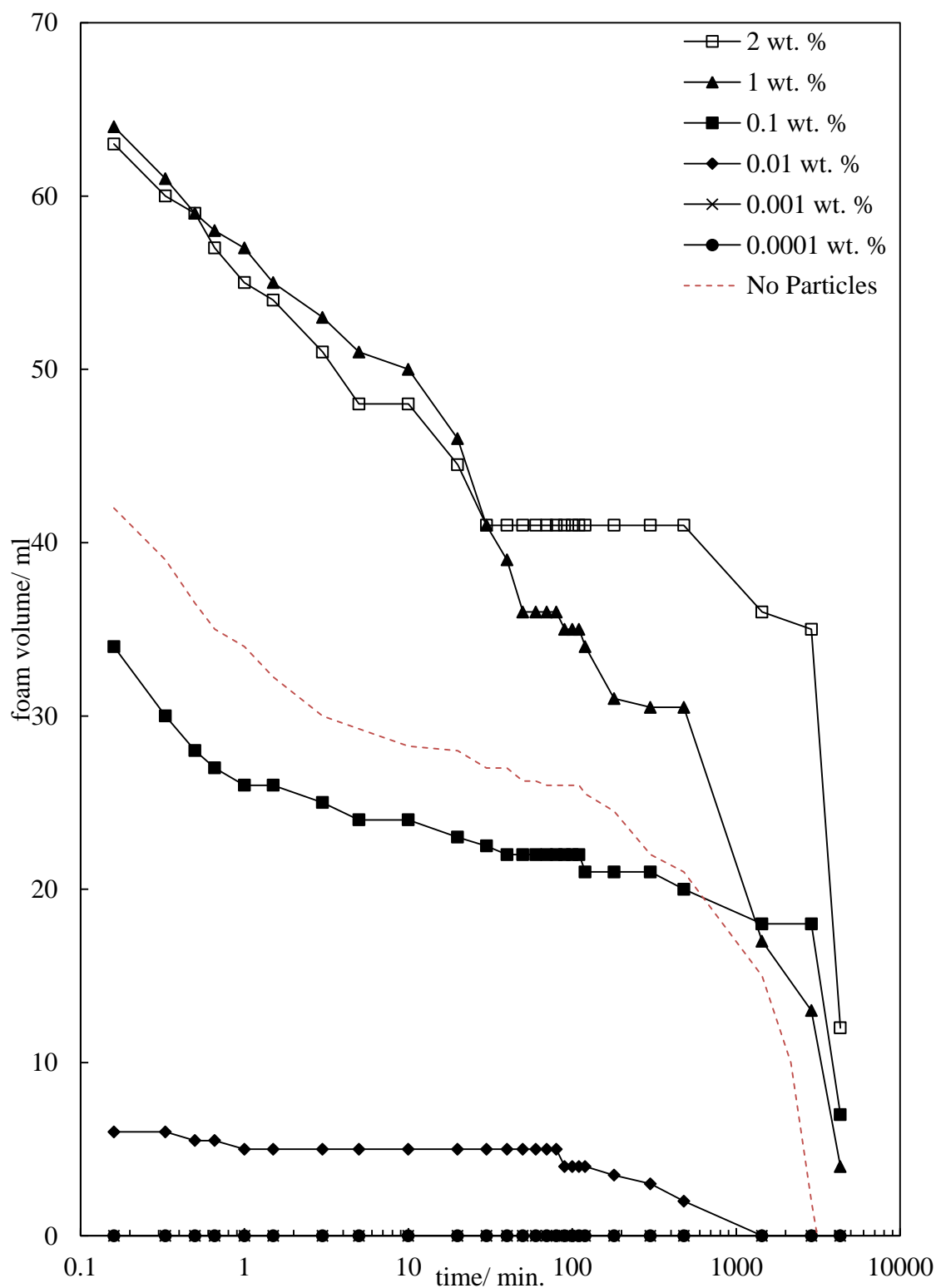
Figure 3.26. Photos of foams generated by hand shaking (30 s) 20 ml of 1 wt. % 100% SiOH fumed silica dispersed in aqueous solutions of (a) Lamesoft PO65 and (b) Silsurf DI-2510 Surfactant concentration increases from 1 × 10^{-4} - 2 wt. % (left to right). Images taken on a Canon EOS 450D immediately after aeration.
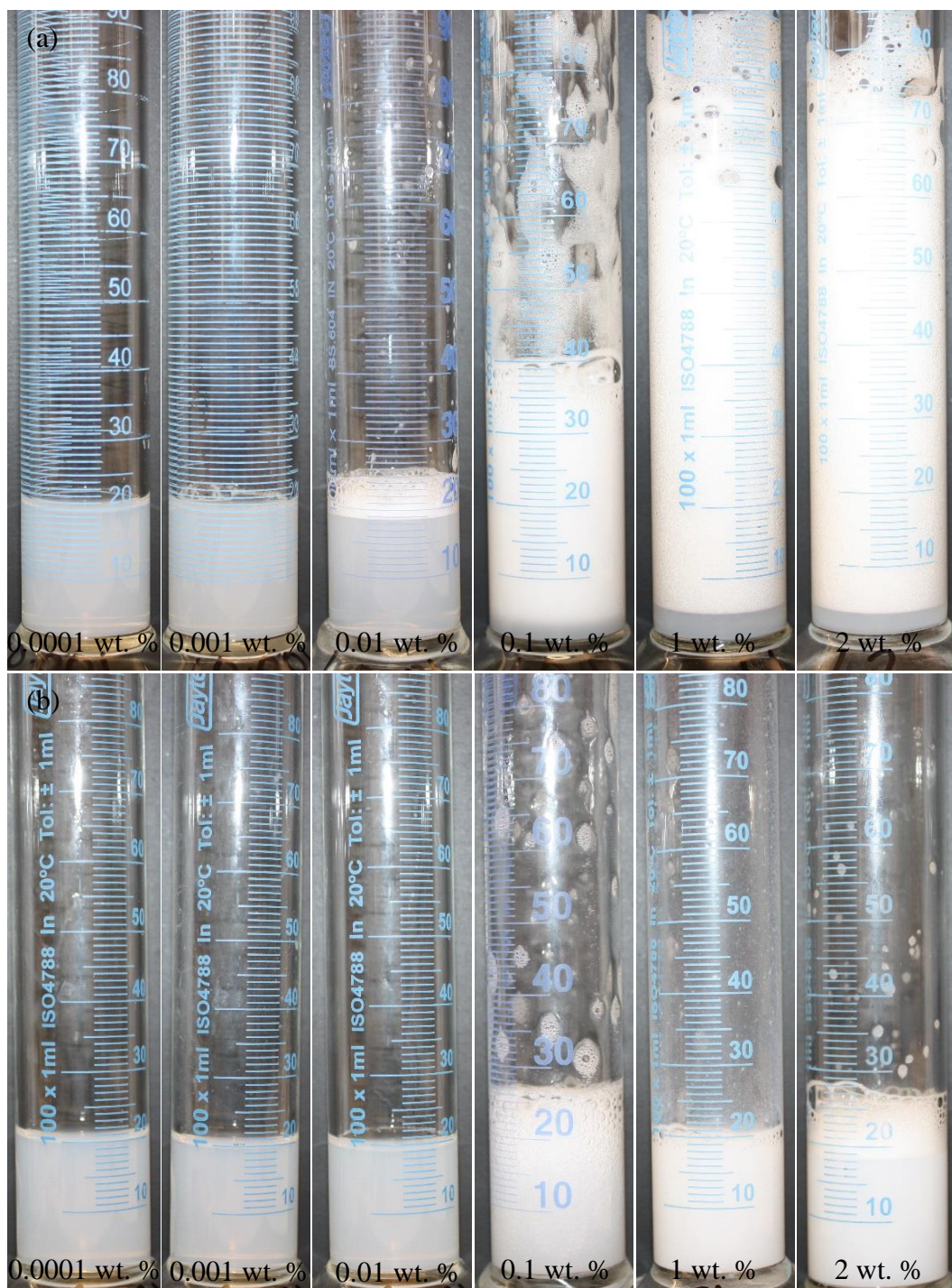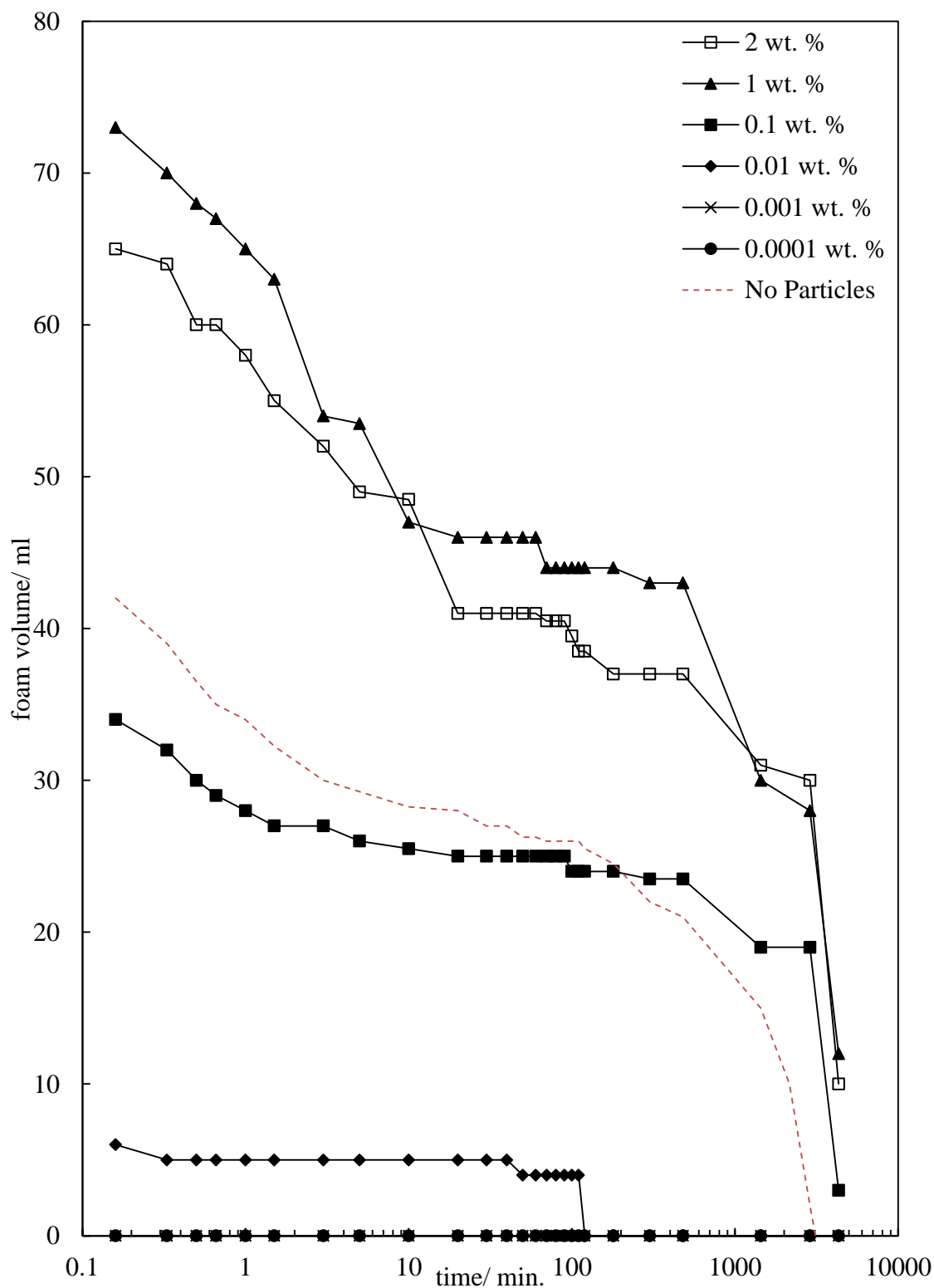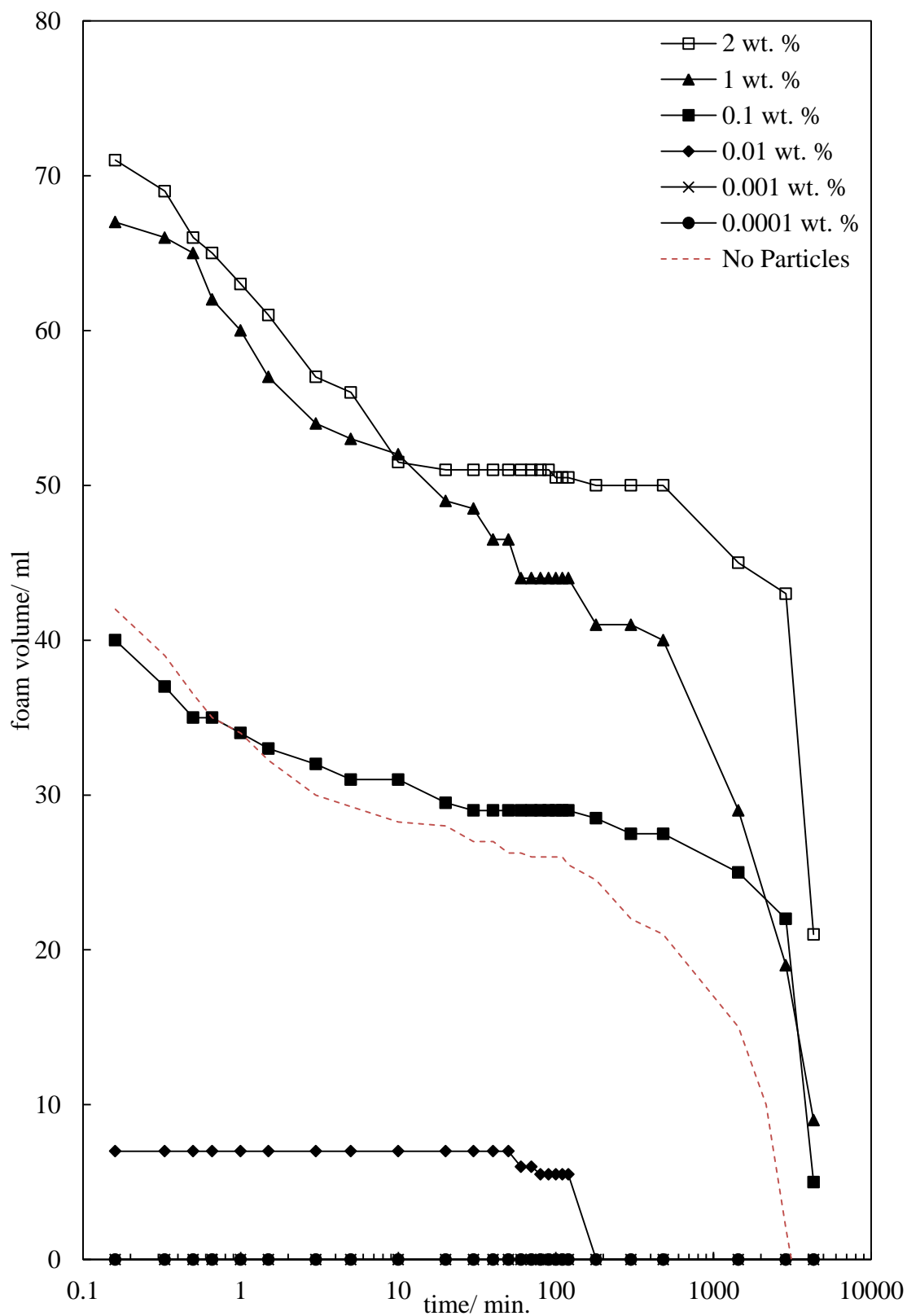
Figure 3.27. Initial foam volume of foams generated from hand shaking (30 s) 20 ml of 1 wt. % 100% SiOH fumed silica dispersed in aqueous solutions of Lamesoft PO65 and Silsurf DI-2510.
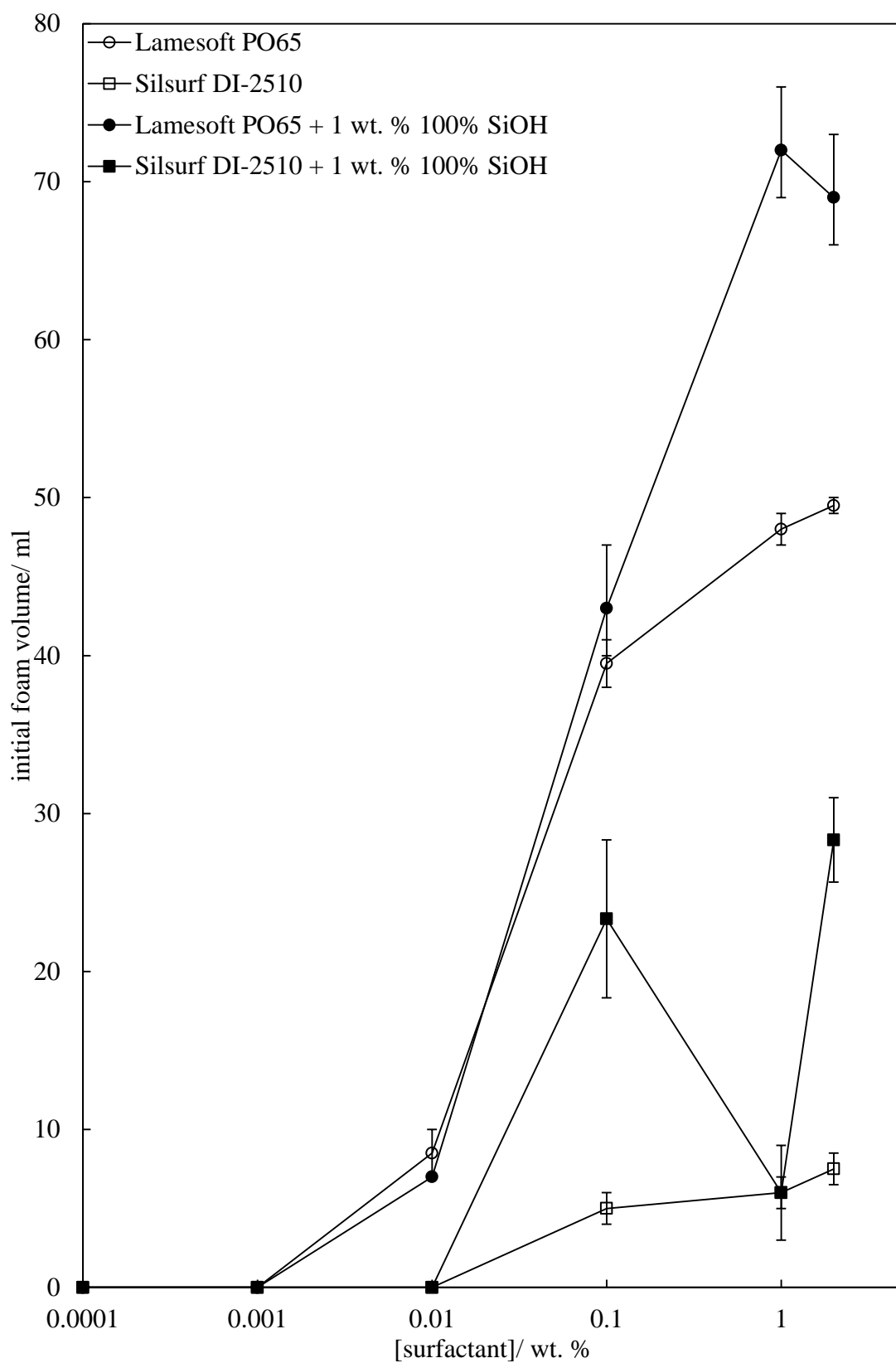
Figure 3.28. Foam volume as a function of time for foams generated by hand shaking (30 s) 20 ml of 1 wt. % 100% SiOH fumed silica dispersed in aqueous solutions of Lamesoft PO65. Run 1 of 3 repeats. Red dashed line shows 1 wt. % Lamesoft PO65 alone.
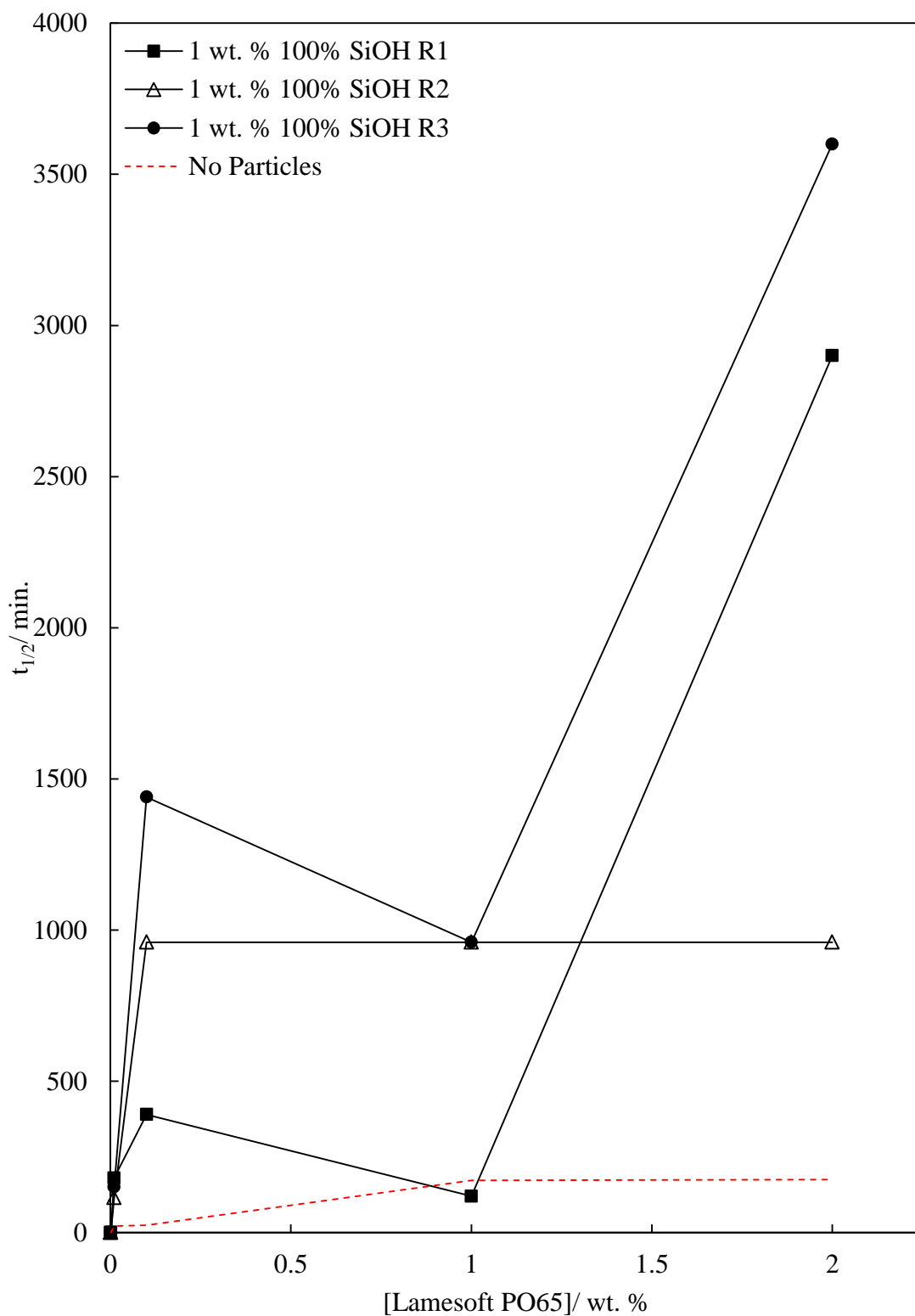
Figure 3.29. Foam volume as a function of time for foams generated by hand shaking (30 s) 20 ml of 1 wt. % 100% SiOH fumed silica dispersed in aqueous solutions of Lamesoft PO65. Run 2 of 3 repeats. Red dashed line shows 1 wt. % Lamesoft PO65 alone.
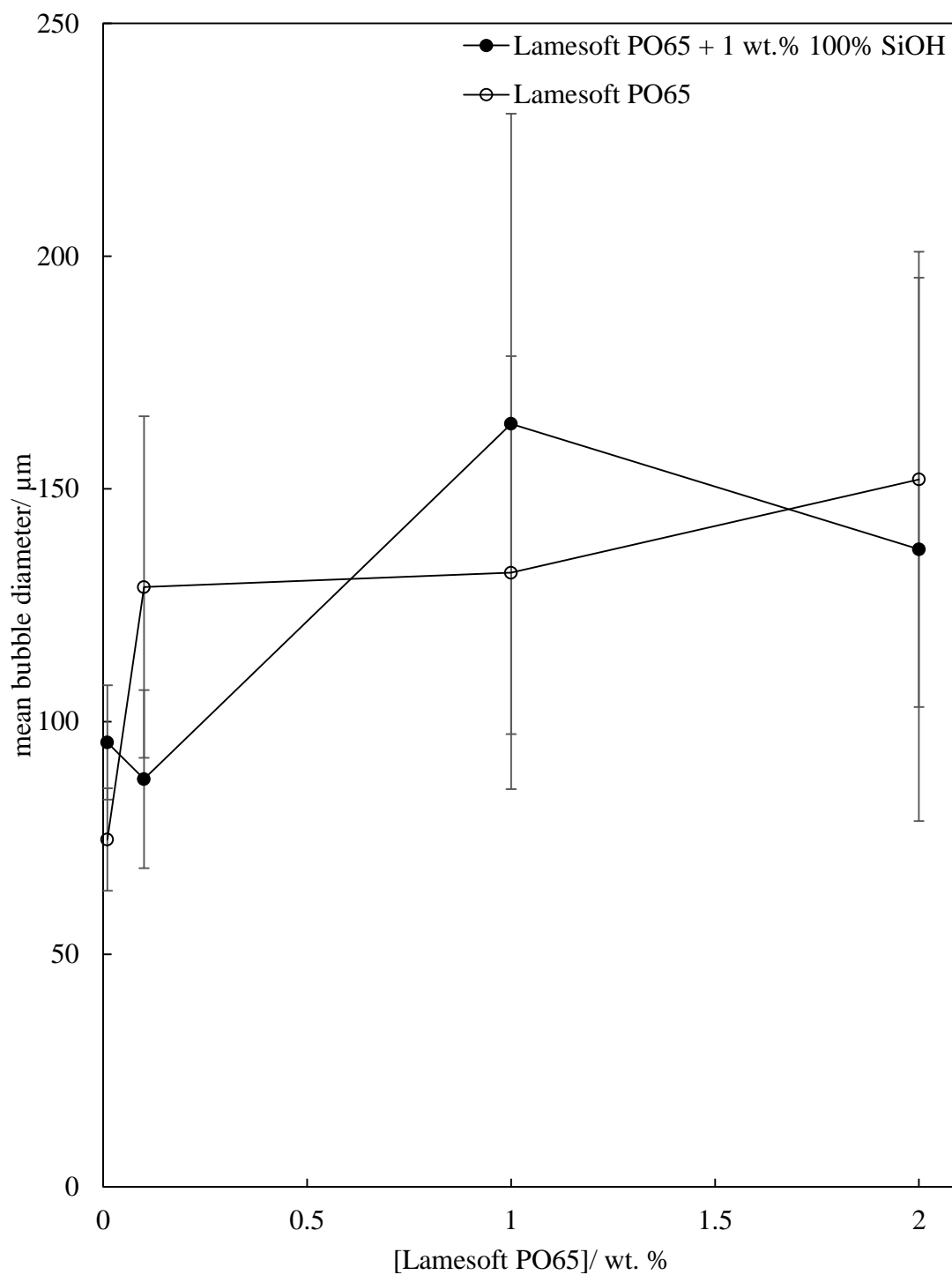
Figure 3.30. Foam volume as a function of time for foams generated by hand shaking (30 s) 20 ml of 1 wt. % 100% SiOH fumed silica dispersed in aqueous solutions of Lamesoft PO65. Run 3 of 3 repeats. Red dashed line shows 1 wt. % Lamesoft PO65 alone.

Figure 3.31. Foam half-life ($t_{1/2}$) as a function of surfactant concentration for foams generated by hand shaking (30 s) 20 ml of 1 wt. % 100% SiOH fumed silica dispersed in aqueous solutions of Lamesoft PO65. Three separate repeat runs and the average half-life for aqueous 1 wt. % Lamesoft PO65 foams with no particles (red dashed line) are shown.

Figure 3.32. Optical microscopy of foams generated by hand shaking (30 s) 20 ml of 1 wt. % 100% SiOH fumed silica dispersed in aqueous solutions of Lamesoft PO65. (a) 1 wt. % Lamesoft PO65 alone, (b) 0.01 wt. % + 1 wt. % particles, (b) 0.1 wt. % + 1 wt. % particles, (b) 1 wt. % + 1 wt. % particles. (b) 2 wt. % + 1 wt. % particles.
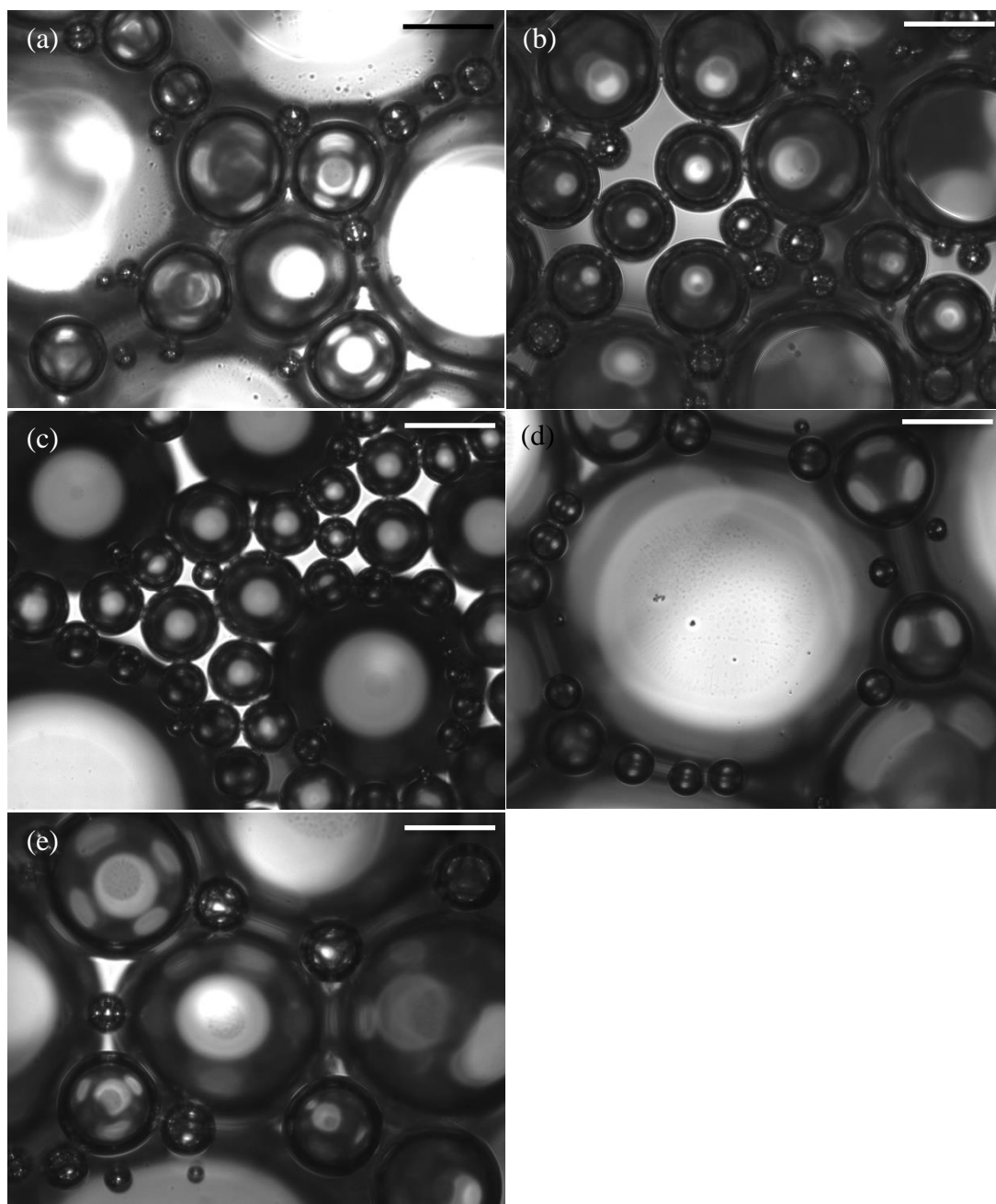
Figure 3.33. Measured average bubble diameter as a function of concentration of Lamesoft PO65 solutions in water with 1 wt. % 100% SiOH particles after aeration by hand shaking 20ml solution for 30s. Mean bubble diameter calculated from at least 40 individual bubble measurements and taken within 5 minutes of foam generation. Error bars show standard deviation.
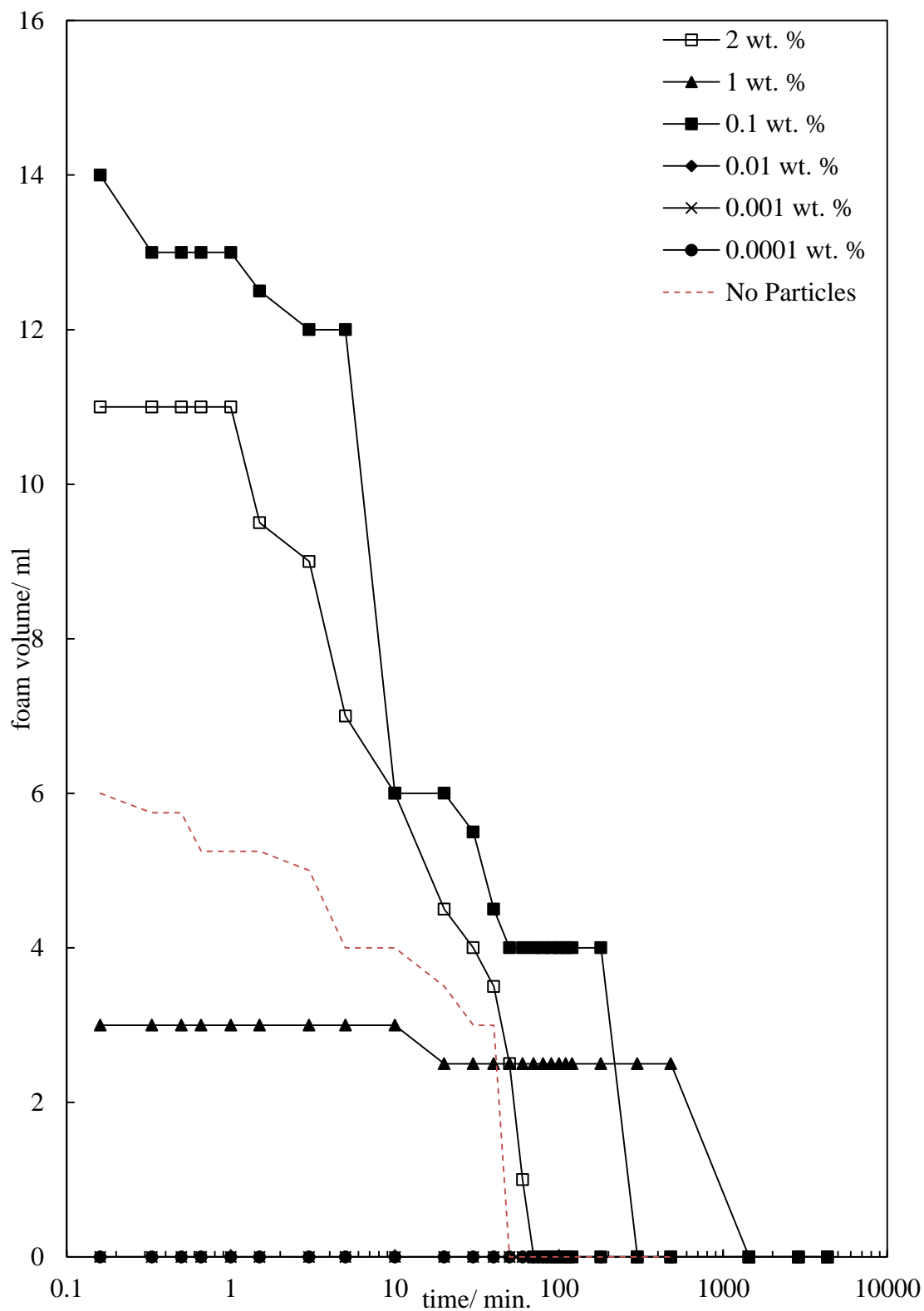
Foam volumes as a function of time for Silsurf DI-2510 foams are shown in Figures 3.34-3.36. Similar to that observed for the Lamesoft PO65 foams, the stability of 0.1 wt. % surfactant is enhanced in comparison to 1 wt. % surfactant alone. Although the 1 wt. % system with particles demonstrated enhanced long-term stability, the foamability was reduced. As mentioned earlier, this particular sample formed a gel/viscous liquid that was difficult to incorporate air into. This increase in viscosity may have been due to the formation of a network between particles and polymeric surfactant molecules.

The half-lives of the foams are shown in Figure 3.37, where a clear maximum in the half-life can be seen at 1 wt. % surfactant for all samples. As liquid drainage is primarily responsible for the initial reduction in the foam volume, it is likely that this maximum is due to there being minimal liquid drainage from the foam due to the increased viscosity of the aqueous phase. At 2 wt. % surfactant, there is a decrease in the half life. If there is surfactant adsorbed to the particle surface, this may be due to the formation of a bilayer of surfactant, rendering the particles hydrophilic again, as suggested in many literature reports. Microscopy (Figure 3.38) and mean bubble diameter measurements (Figure 3.39) shows the bubble diameter to decrease with increasing surfactant concentration, and similarly to the Lamesoft PO65 foams, the bubble surfaces are smooth, and residual particles can be seen in the aqueous phase around the air bubbles. It is complicated to relate the bubble diameter measurements to the stability behaviour of these foams as the bubble diameter does not account for liquid drainage from the foams, particularly in the first few minutes after aeration of the solution has elapsed.

It would be useful for both of these surfactants to carry out an adsorption isotherm to determine whether surfactant has adsorbed to the surface of the particles. However, in this research this experiment posed numerous issues. Primarily, the particle dispersions are very stable and would require ultracentrifugation for very long periods of time to attempt to separate the residual surfactant. Secondly, analysis of these surfactants has proved very challenging. It may be possible to analyse Silsurf DI-2520 using the picrate method[41-43], but as the specific RMM of the structure is unknown (polymeric surfactants have a weight distribution) it would be difficult to determine precise concentrations of surfactant in the supernatant phase. Similarly, the Lamesoft PO65 is a mixture of two surfactants in an unknown ratio that would require separation after centrifugation for successful analysis. As a result of these complexities, these experiments have not been carried out.
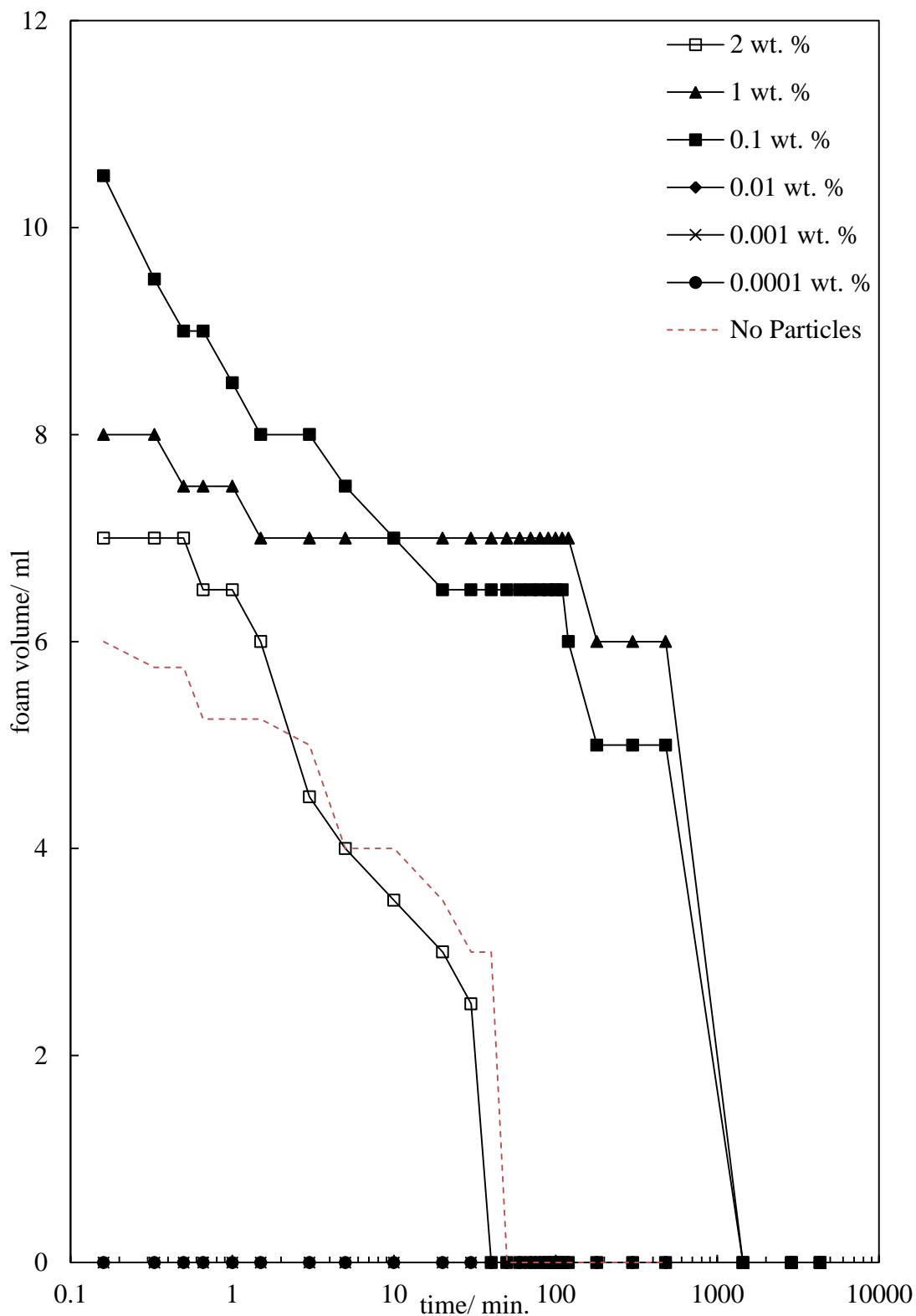
Figure 3.34. Foam volume as a function of time for foams generated by hand shaking (30 s) 20 ml of 1 wt. % 100% SiOH fumed silica dispersed in aqueous solutions of Silsurf DI-2510. Run 1 of 3 repeats. 1 wt. % surfactant alone indicated by dashed line.
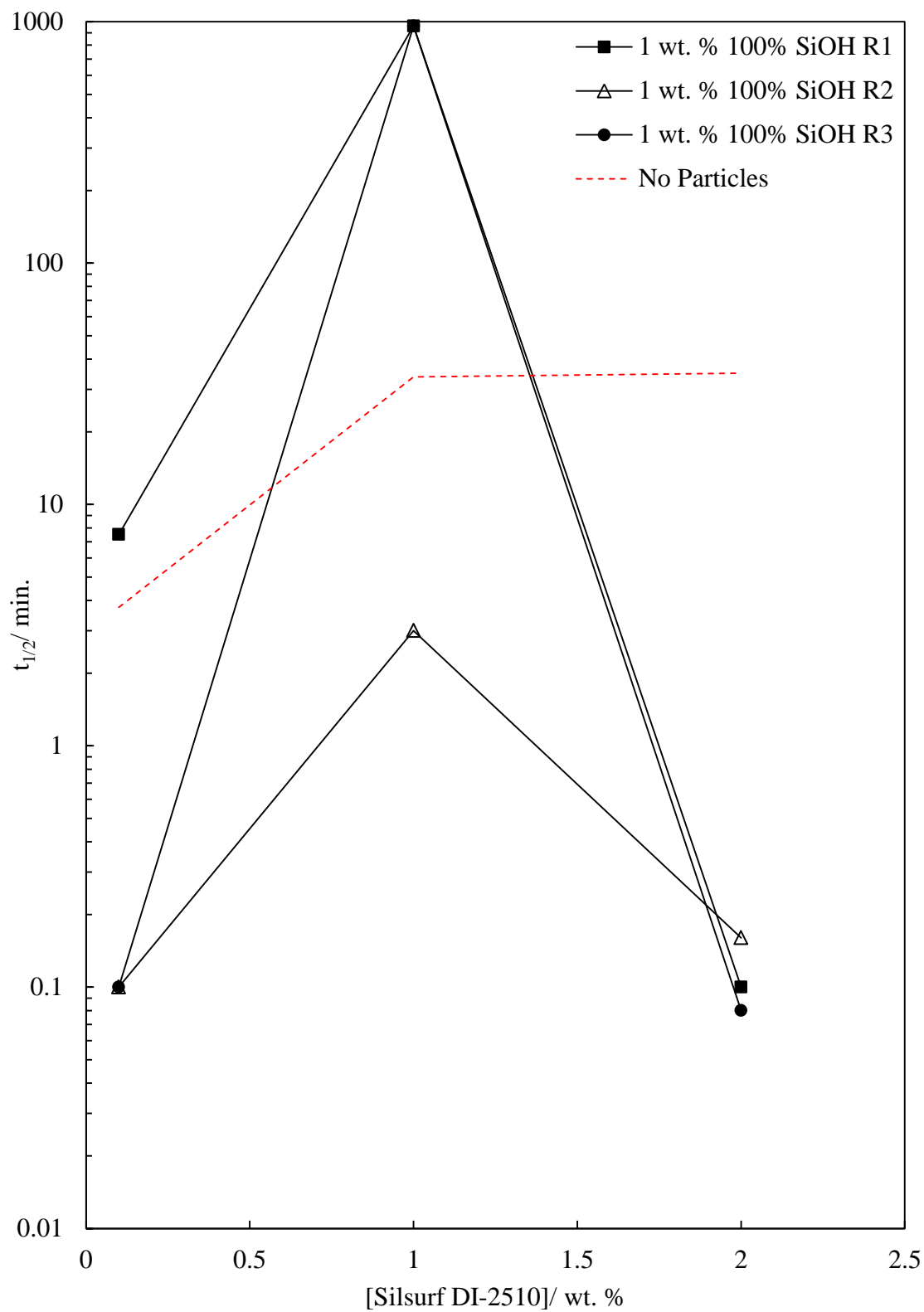
Figure 3.35. Foam volume as a function of time for foams generated by hand shaking (30 s) 20 ml of 1 wt. % 100% SiOH fumed silica dispersed in aqueous solutions of Silsurf DI-2510. Run 2 of 3 repeats. 1 wt. % surfactant alone indicated by dashed line.
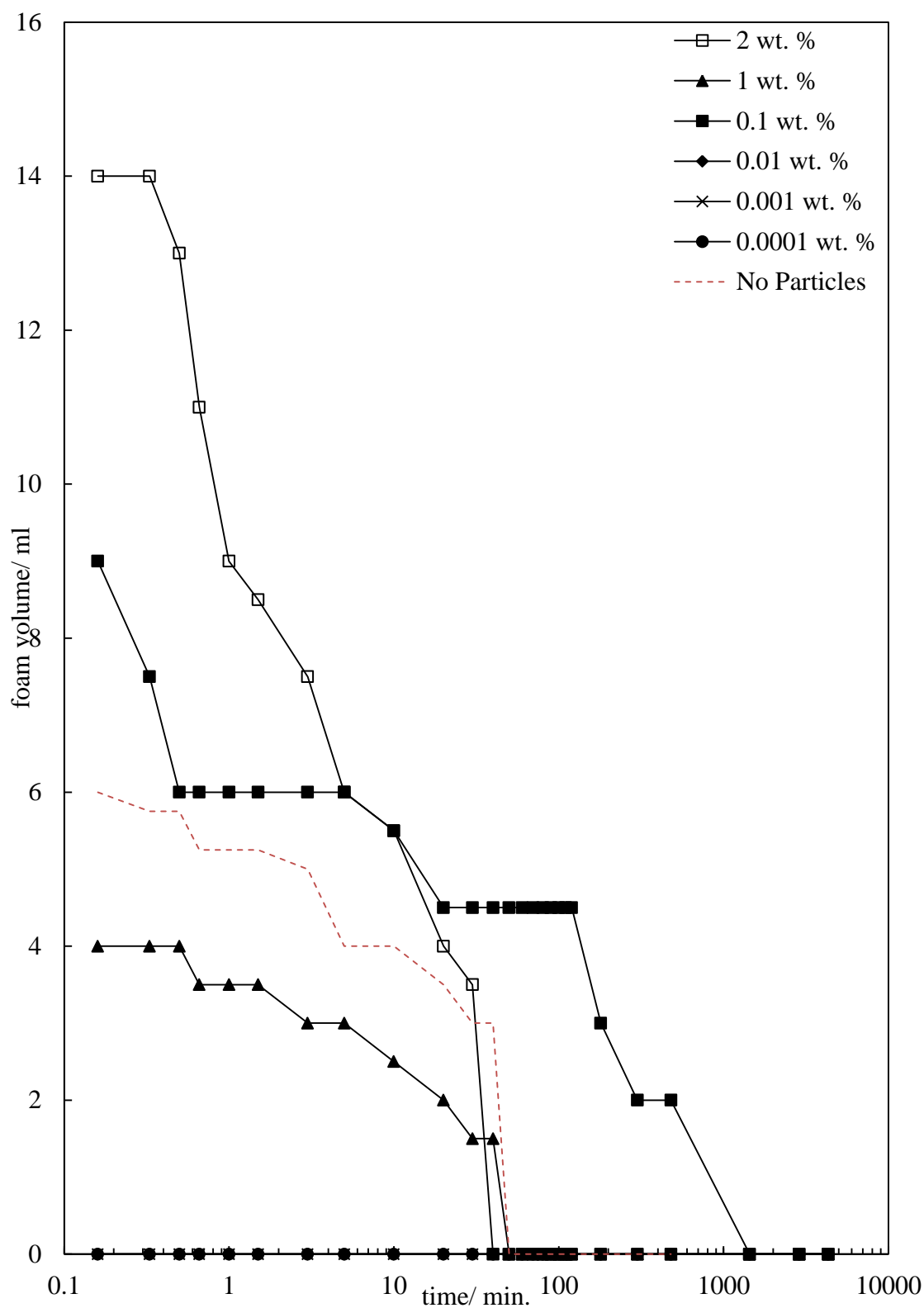
Figure 3.36. Foam volume as a function of time for foams generated by hand shaking (30 s) 20 ml of 1 wt. % 100% SiOH fumed silica dispersed in aqueous solutions of Silsurf DI-2510. Run 3 of 3 repeats. 1 wt. % surfactant alone indicated by dashed line.

Figure 3.37. Foam half-life ($t_{1/2}$) as a function of surfactant concentration (0.1-2 wt. % shown) for foams generated by hand shaking (30 s) 20 ml of 1 wt. % 100% SiOH fumed silica dispersed in aqueous solutions of Silsurf DI-2510. Three separate repeat runs and the average half-life for aqueous 1 wt. % Silsurf DI-2510 foams with no particles (dashed line) are shown.

Figure 3.38. Optical microscopy of foams generated by hand shaking (30 s) 20 ml of 1 wt. % 100% SiOH fumed silica dispersed in aqueous solutions of Silsurf DI-2510. (a) 1 wt. % Silsurf DI-2510 alone (b) 0.1 wt. % surfactant with 1 wt. % particles, (c) 1 wt. % surfactant with 1 wt. % particles and (d) 2 wt. % surfactant with 1 wt. % particles. Scale bar corresponds to 100 μm.
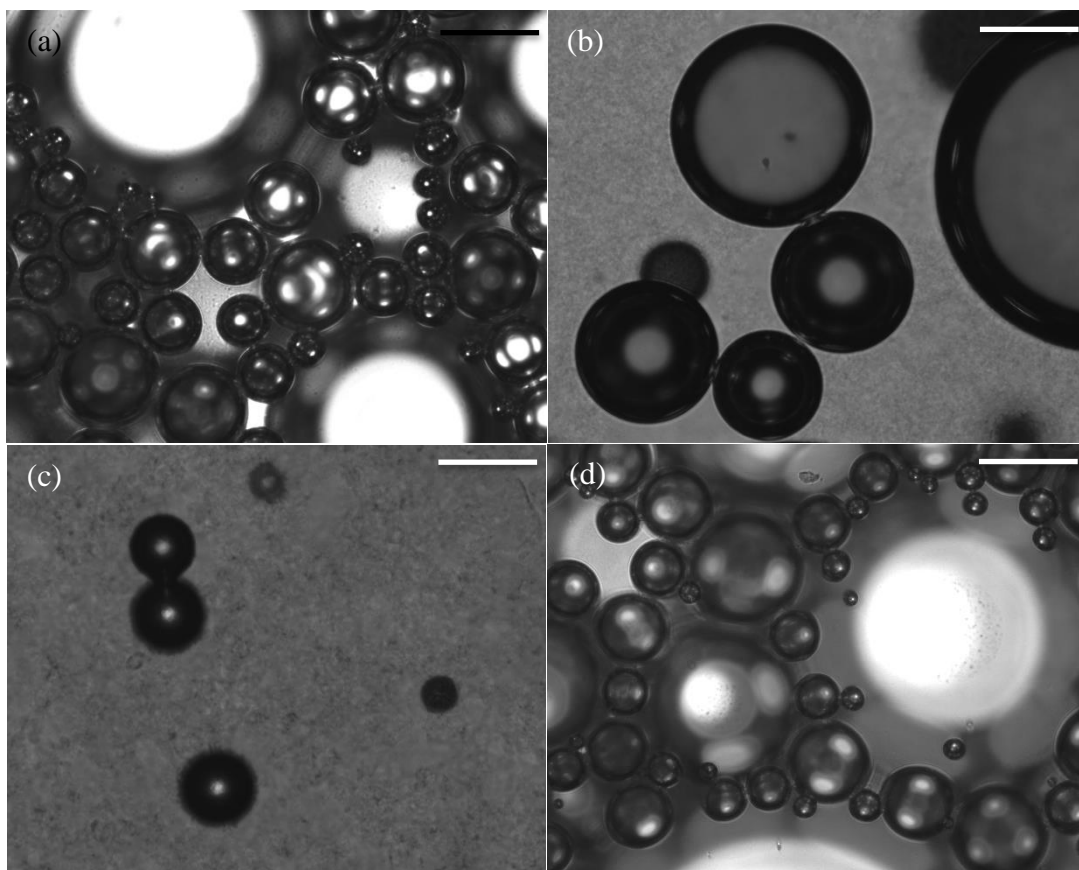
Figure 3.39. Measured average bubble diameter as a function of concentration of Silsurf DI-2510 solutions in water with 1 wt. % 100% SiOH particles after aeration by hand shaking 20 ml solution for 30 s. Mean bubble diameter calculated from at least 40 individual bubble measurements and taken within 5 minutes of foam generation. Error bars show standard deviation.
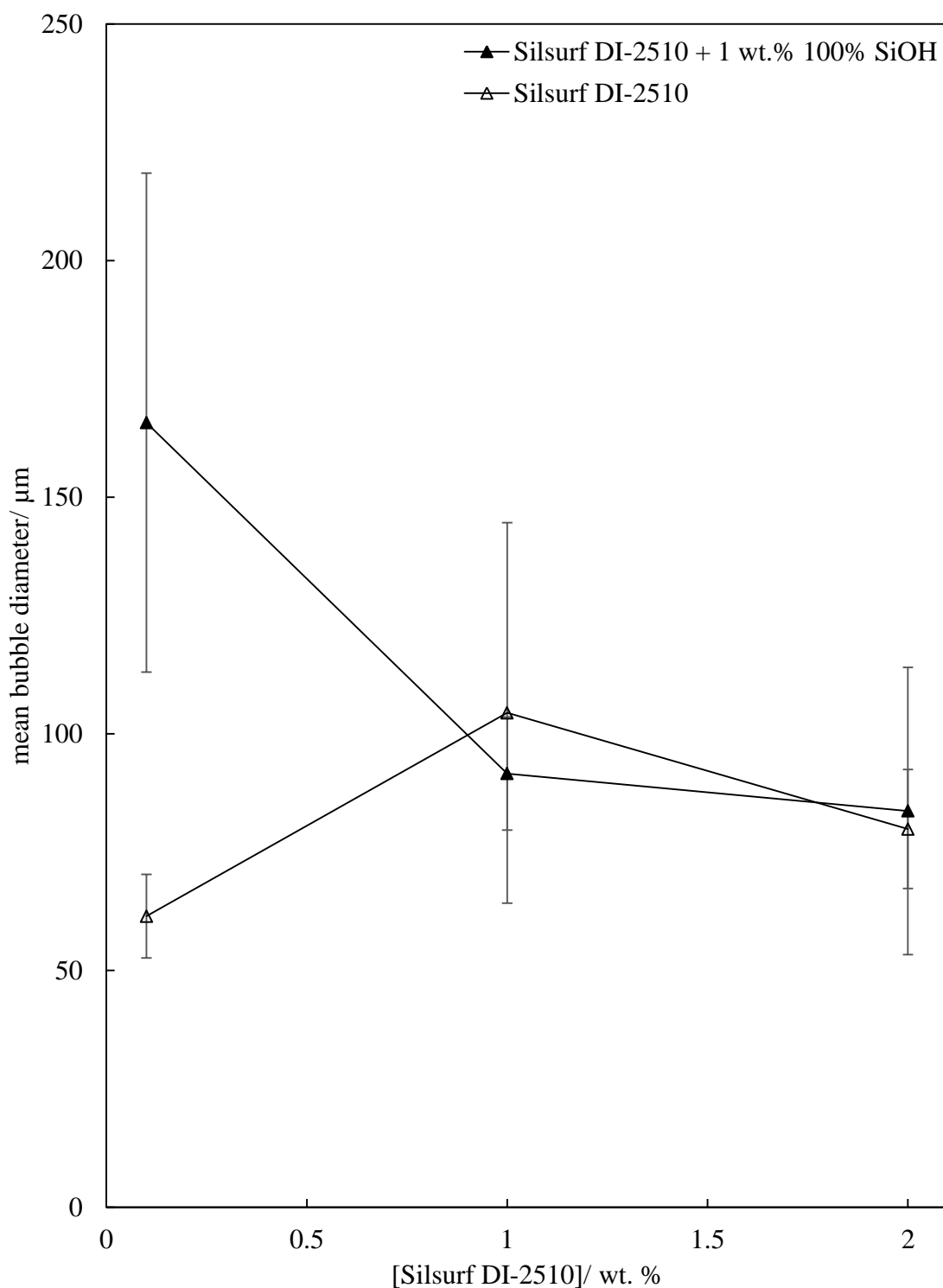
3.5.2 Effect of particle concentration

After investigating the effect of surfactant concentration, it was decided to further investigate these systems by varying the particle concentration in the dispersions. The foaming experiments were repeated with a constant surfactant concentration of 1 wt. % and the particle concentration was varied from 0.1-2 wt. %. Photos of the foams immediately after aeration can be seen in Figures 3.40 (a) and (b). It can be seen that thick, creamy foams were generated upon aeration. A plot of the initial foam volumes of both surfactants as a function of particle concentration can be seen in Figure 3.41. It can be seen that for both surfactants, the addition of particles at any concentration enhances the foamability. However, both surfactants appear to pass through a maximum foamability at 0.1 wt. % particles.

The foam collapse as a function of time plot for Lamesoft PO65 is shown in Figure 3.42. As all of the repeats showed similar collapse profiles, only one plot is shown and the remaining plots can be found in the appendix. It can again be seen that all of the foams demonstrate higher stability than 1 wt. % surfactant alone, additionally when the particle concentration was $\geq$ 0.5 wt. % the foams were stable for over 72 hours. A plot of the foam half-lives as a function of particle concentration is shown in Figure 3.43. The foam half-life is significantly improved with addition of particles and increases with increasing particle concentration, although these experiments have some reproducibility issues. Microscopy images of the foams with increasing particle concentration are shown in Figure 3.44 and the mean bubble diameters are shown in 3.45 for both surfactants. It can be seen that the average bubble diameter has a very wide distribution, as with all other foams generated, this may be due to disproportionation occurring quickly, or even during the microscopy measurements. It can also be seen that there is little variation in the bubble diameter with increasing particle concentration. To relate the bubble diameter measurements to the foam stability (half-life in particular) is complicated due to the fact that bubble diameter measurements do not account for liquid drainage which is a main contributor to the collapse of the foam volume.
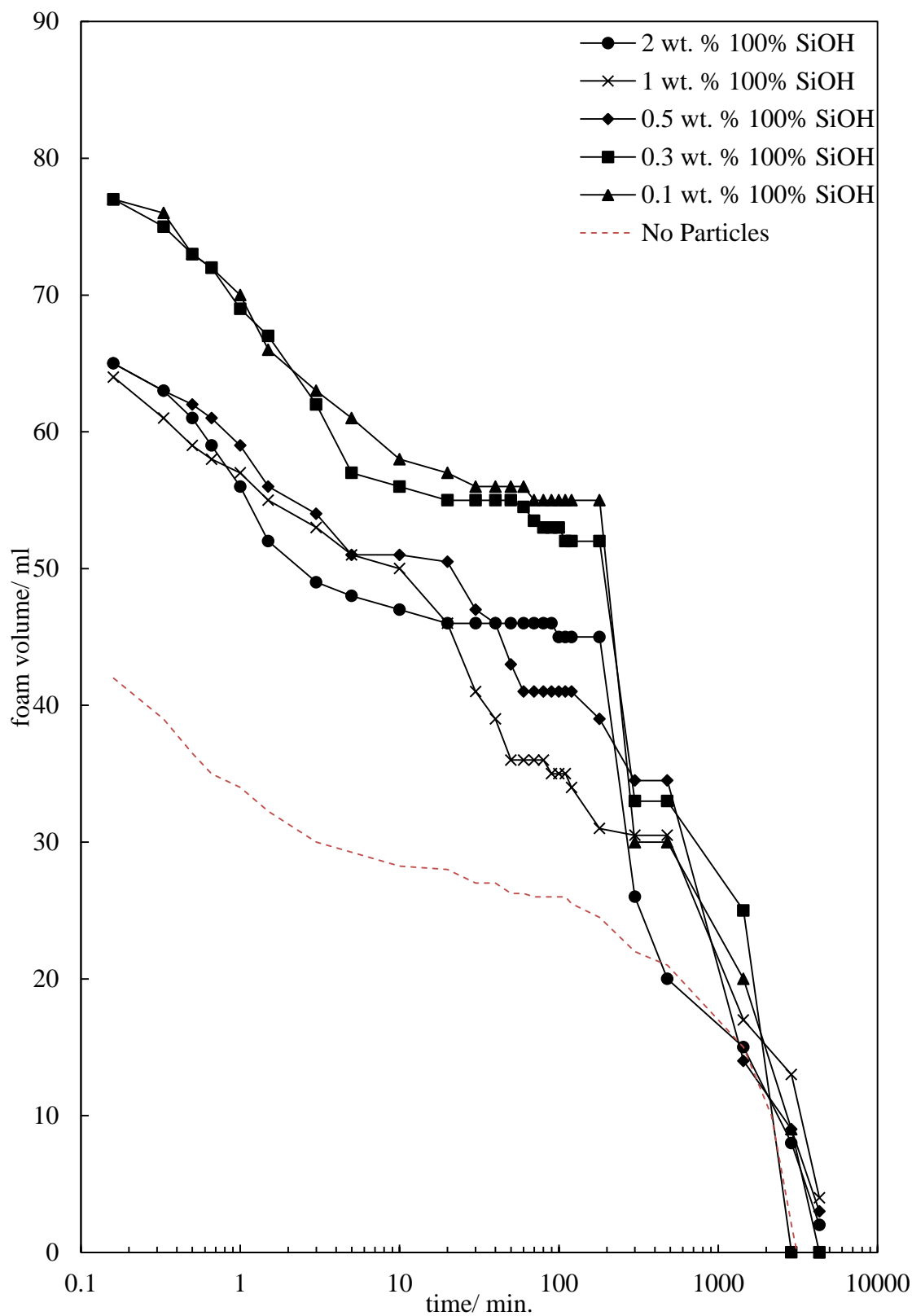
Figure 3.40. Photos of foams generated by hand shaking (30 s) 20 ml of 1 wt. % surfactant with 0-2 wt. % 100% SiOH fumed silica. (a) Lamesoft PO65 (b) Silsurf DI-2510. Images taken on a Canon EOS 450D immediately after aeration.

Figure 3.41. Initial foam volume of foams generated from hand shaking (30 s) 20 ml of 100% SiOH fumed silica dispersed in 1 wt. % aqueous solutions of Lamesoft PO65 and Silsurf DI-2510 as a function of particle concentration.
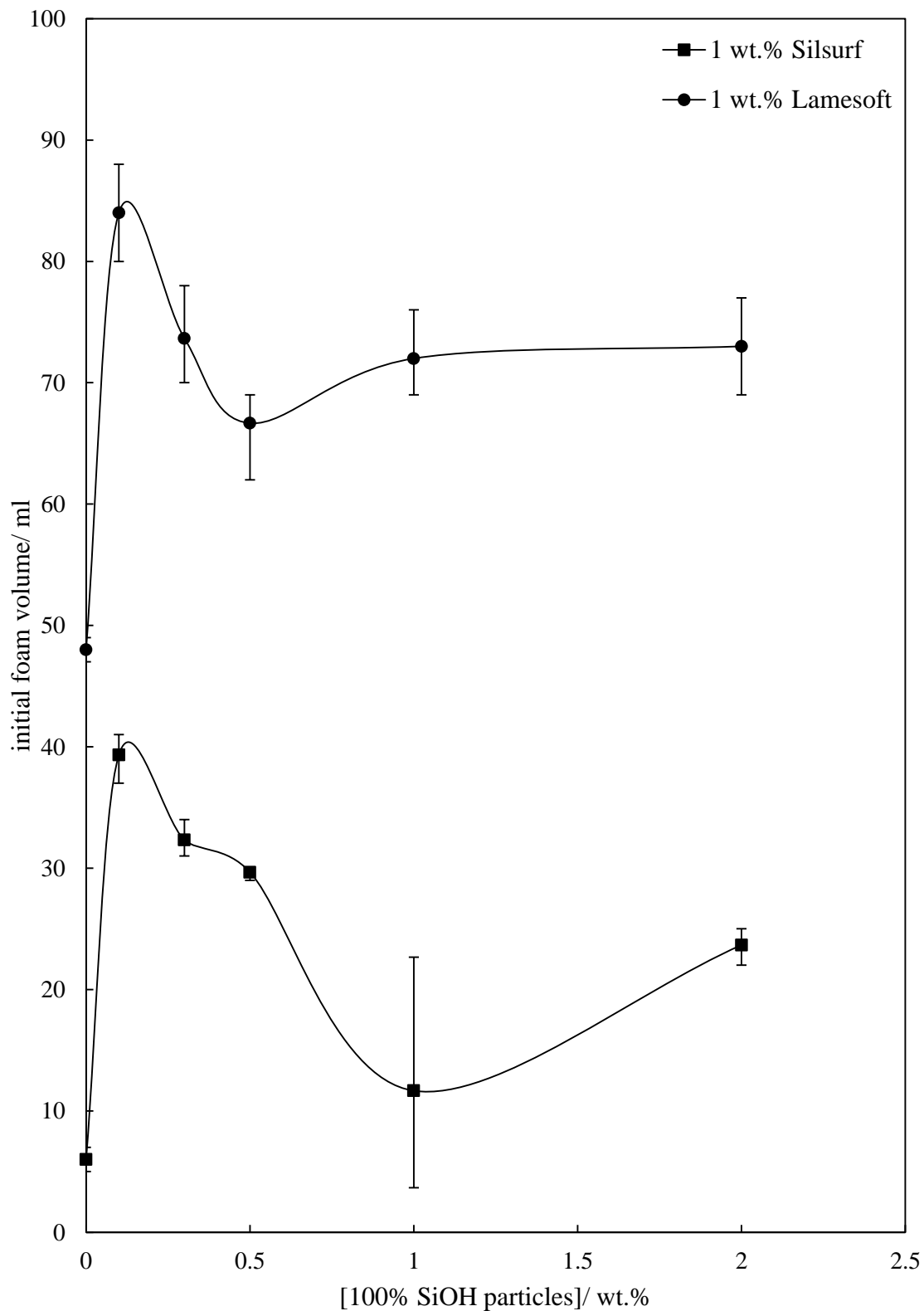
Figure 3.42. Foam volume as a function of time for foams generated by hand shaking (30 s) 20 ml of 1 wt. % Lamesoft PO65 containing 0-2 wt. % 100% SiOH fumed silica particles. Run 1 of 3 repeats. Remaining two repeats are shown in appendix 3.42 (a) and (b).

Figure 3.43. Foam half-life ($t_{1/2}$) as a function of particle concentration for foams generated by hand shaking (30 s) 20 ml of 1 wt. % Lamesoft PO65 containing 0-2 wt. % 100% SiOH fumed silica particles. Three separate repeat runs and the average half-life for 1 wt. % Lamesoft PO65 foam with no particles (dashed line) are shown.
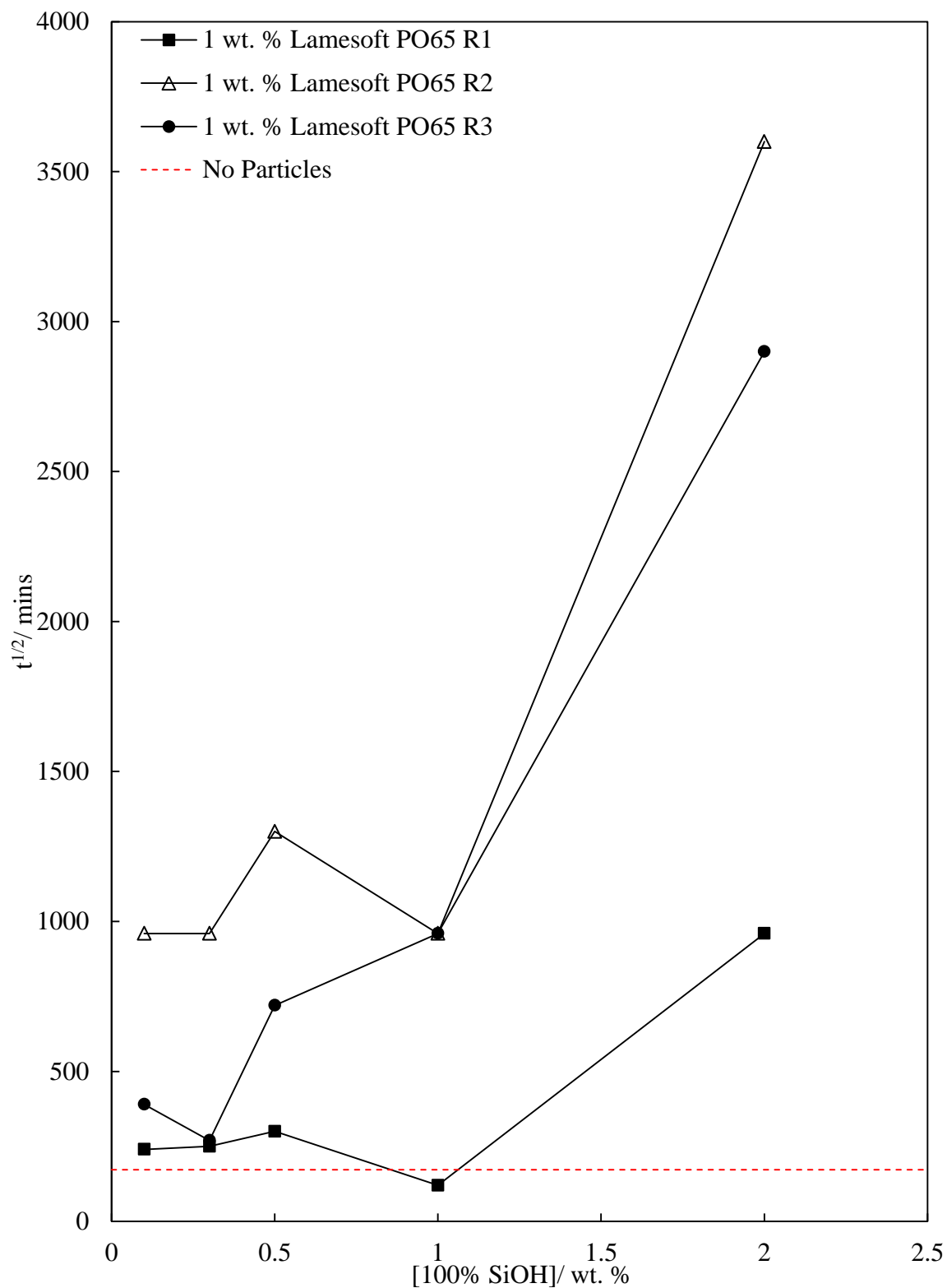
Figure 3.44. Optical microscopy of foams generated by hand shaking (30 s) 20 ml of 1 wt. % Lamesoft PO65 containing 0-2 wt. % 100% SiOH fumed silica particles. (a) 1 wt. % Lamesoft PO65 alone (a) 0.1 wt. % 100% SiOH, (b) 0.3 wt. % 100% SiOH, (c) 0.5 wt. % 100% SiOH, (d) 1 wt. % 100% SiOH and (e) 2 wt. % 100% SiOH. Scale bar corresponds to 100 μm.
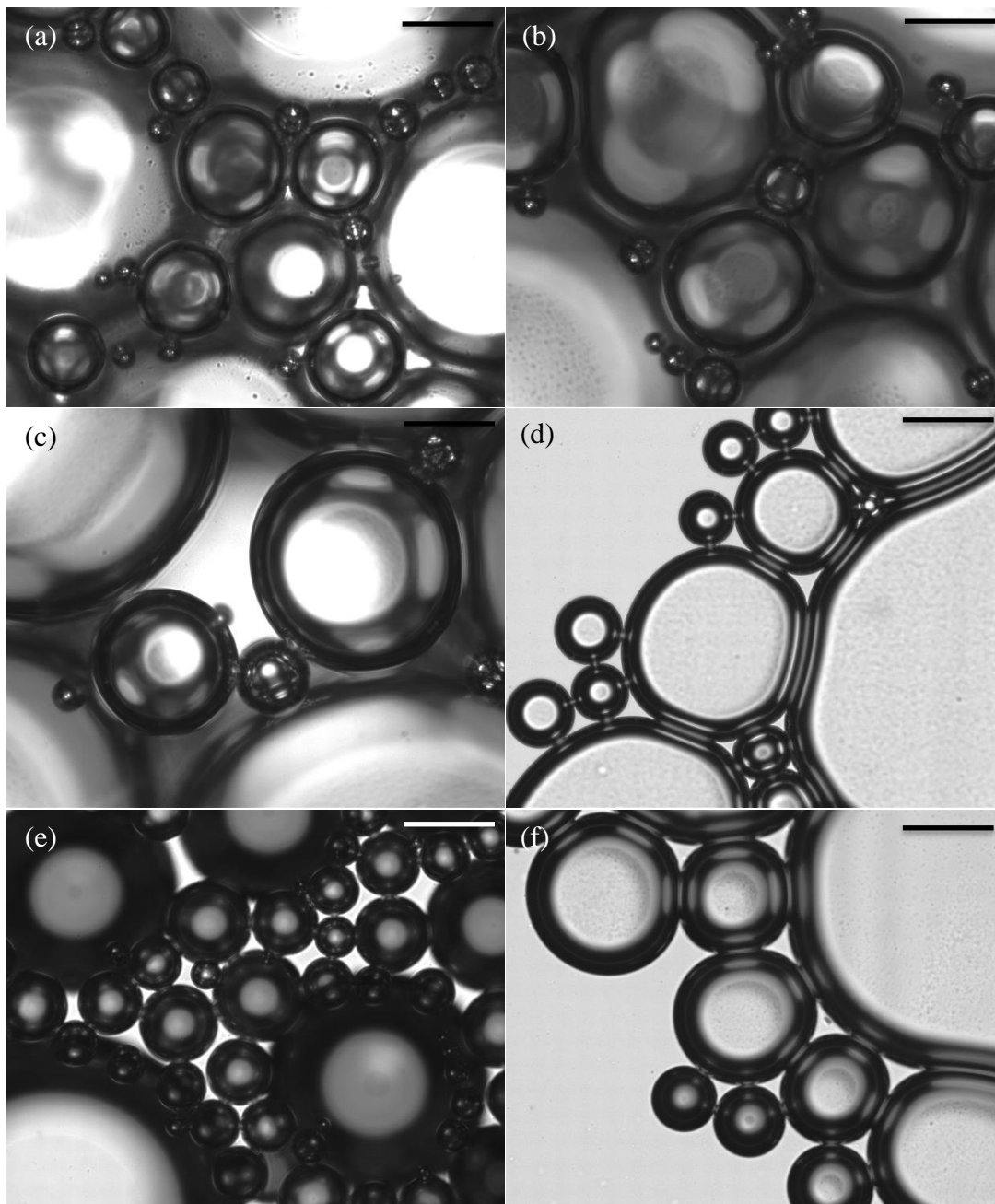
**Figure 3.45.** Measured average bubble diameter as a function of concentration of 100% SiOH fumed silica particles in 1 wt. % Lamesoft PO65 and Silsurf DI2510 solutions in water after aeration by hand shaking 20 ml solution for 30 s. Mean bubble diameter calculated from at least 40 individual bubble measurements and taken within 5 minutes of foam generation. Error bars show standard deviation.
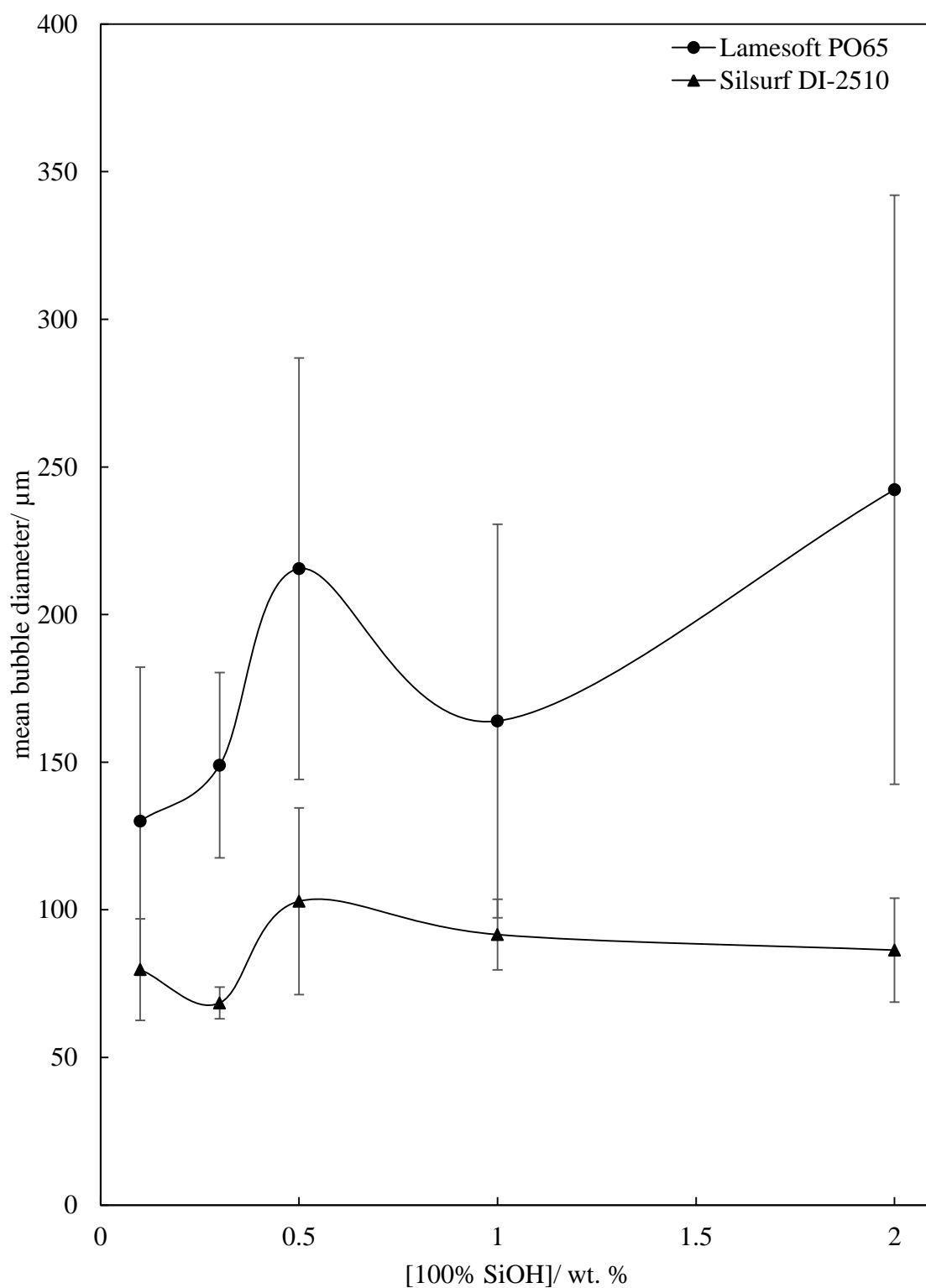
A plot of the foam volume as a function of time for different concentrations of particles in 1 wt. % Silsurf DI-2510 is shown in Figure 3.46. As all of the repeats showed similar collapse profiles, only one plot is shown and the remaining plots can be found in the appendix. It can be seen in these plots that all particle concentrations enhanced the foamability and stability compared to 1 wt. % surfactant alone, with the exception of 1 wt. % particles. As mentioned in the previous section, this system of 1 wt. % 100% SiOH and 1 wt. % Silsurf DI-2510 forms a very viscous liquid, which we have attributed to formation of a polymeric surfactant-particle network. This resulted in difficulty incorporating air into the aqueous phase and the low volume of foam produced also demonstrated poor long-term stability. The foams of 2 wt. % particles demonstrated excellent stability of over 72 hours. The foam half-lives are plotted in Figure 3.47 and show an interesting trend where by the half-life of all foams passes through a minimum at 0.3-0.5 wt. % particles. Optical microscopy of the foams (Figure 3.48) show that at high concentrations of particles (1 and 2 wt. %) the particles are visible in the aqueous phase, this may demonstrate that there is poor attachment of the particles to the bubble surfaces.

Figure 3.46. Foam volume as a function of time for foams generated by hand shaking (30 s) 20 ml of 1 wt. % Silsurf DI-2510 containing 0-2 wt. % 100% SiOH fumed silica particles. Run 1 of 3 repeats. Remaining two repeats are shown in appendix 3.46 (a) and (b).

137
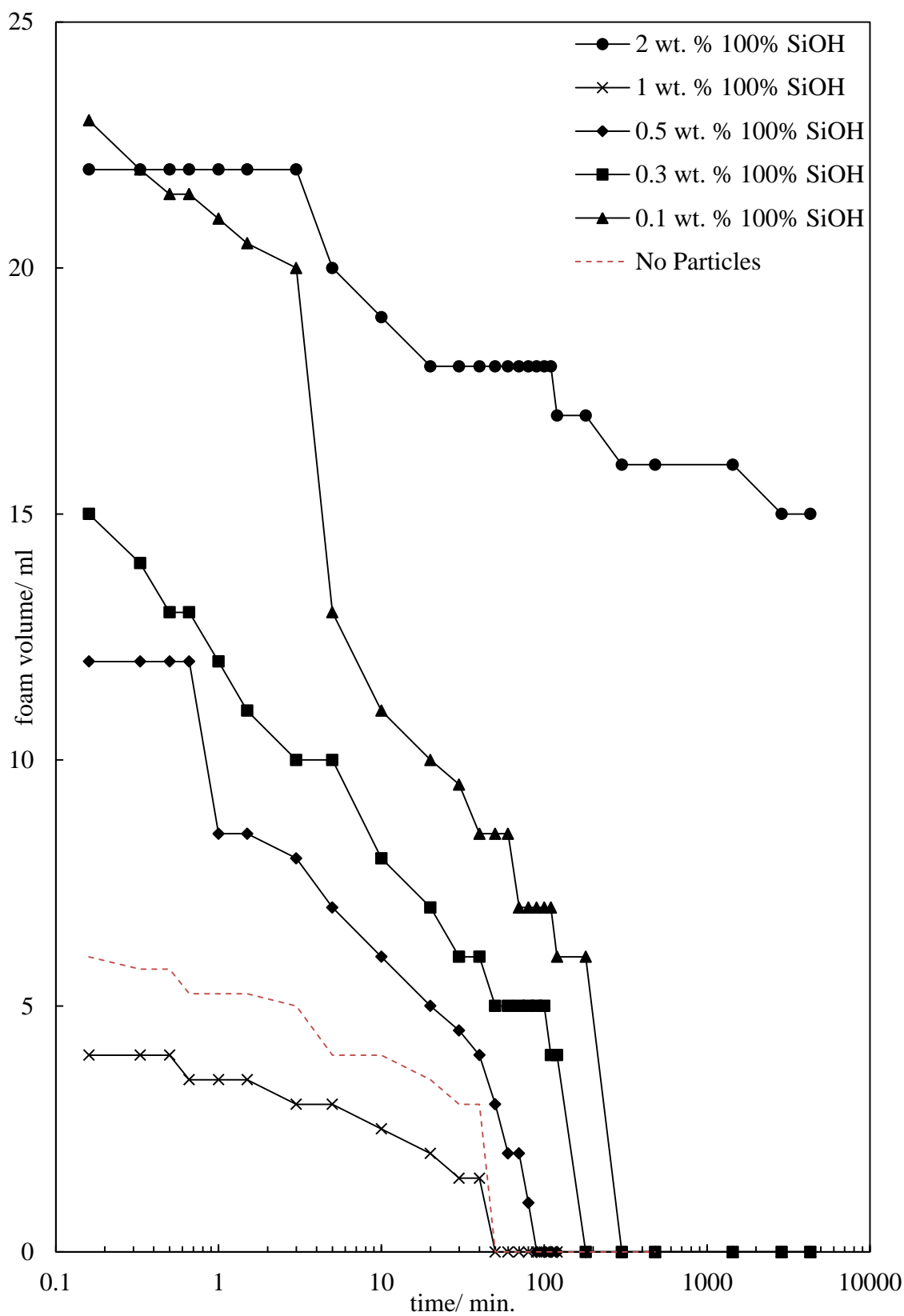
Figure 3.47. Foam half-life ($t_{1/2}$) as a function of particle concentration for foams generated by hand shaking (30 s) 20 ml of 1 wt. % Silsurf DI-2510 containing 0-2 wt. % 100% SiOH fumed silica particles. Three separate repeat runs and the average half-life for 1 wt. % Silsurf DI-2510 foam with no particles (dashed line) are shown.
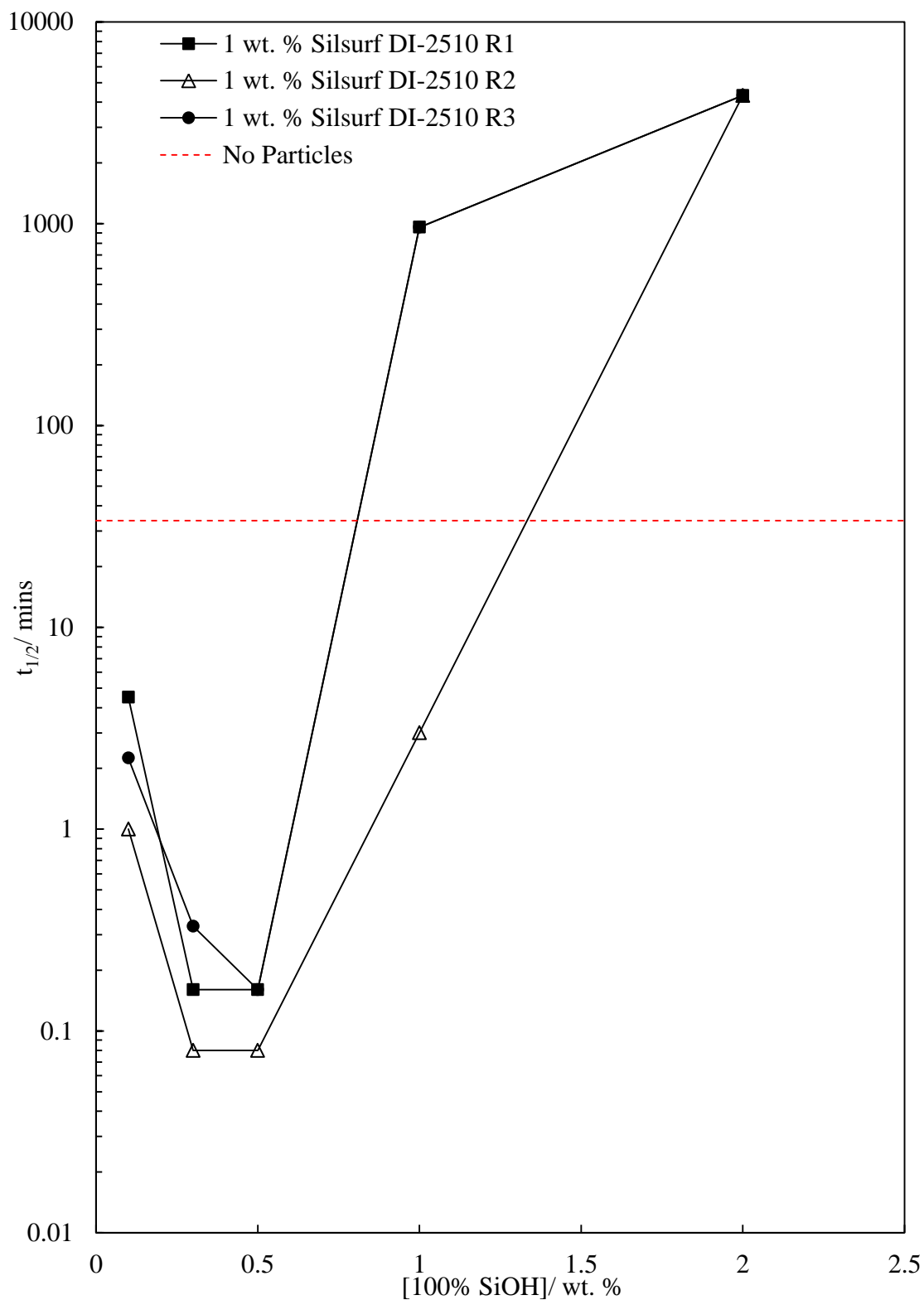
Figure 3.48. Optical microscopy of foams generated by hand shaking (30s) 20 ml 1 wt. % Silsurf DI-2510 containing 0-2 wt. % 100% SiOH fumed silica particles. (a) 1 wt. % Silsurf DI-2510 alone (b) 0.1 wt. % 100% SiOH, (c) 0.3 wt. % 100% SiOH, (d) 0.5 wt. % 100% SiOH, (e) 1 wt. % 100% SiOH and (f) 2 wt. %. Scale bar corresponds to 100 μm.
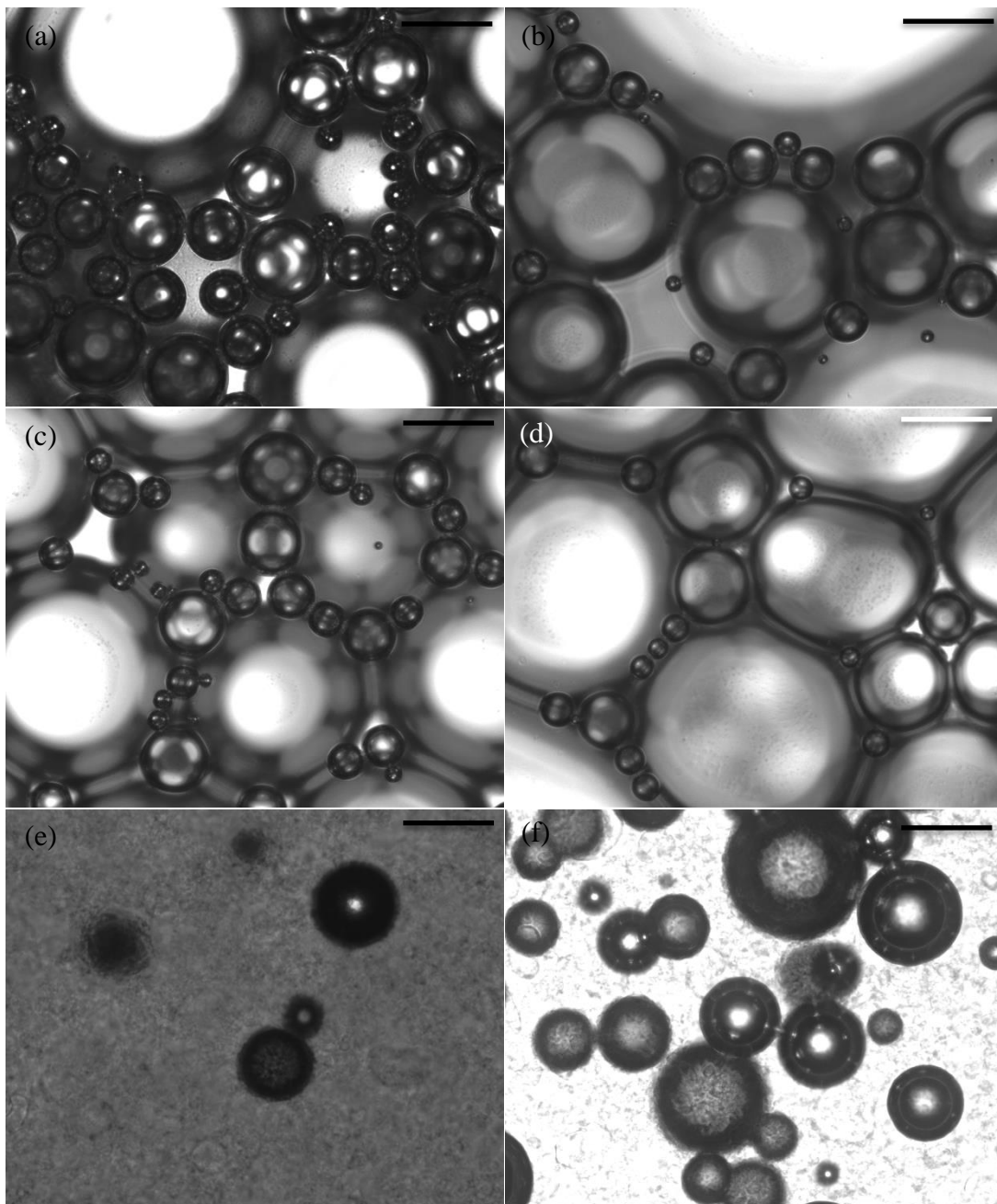
3.5.3   *Effect of particle hydrophobicity*

Finally, the effect of particle hydrophobicity was investigated. Aeration of these particles in pure water demonstrated that 100% SiOH particles do not foam, 47% SiOH systems produced stable foams and 14% SiOH produced climbing films. These particles were dispersed in 1 wt. % surfactant solutions and aerated as in previous experiments. Photos of the foams generated with Lamesoft PO65 and Silsurf DI-2510 can be seen in Figures 3.49 (a) and (b). Additionally a plot of the initial foam volumes of both surfactant systems as a function of particle hydrophobicity is shown in Figure 3.50. Interestingly, the surfactants behave completely differently when the particle hydrophobicity is varied. For Lamesoft PO65, increasing the particle hydrophobicity causes the foam volume to be reduced. Conversely, Silsurf DI-2510 foams are enhanced with increasing particle hydrophobicity.

It was observed initially that in pure water 20% SiOH (most hydrophobic) particles are not wetted by the liquid. This is also the case for 20% SiOH in surfactant solutions, they initially do not wet the particles. However, upon aeration of the surfactant solutions, the particles become incorporated into the liquid, contributing to the foam volume. In pure water, only climbing films were observed. The enhancement in foamability (seen for Silsurf DI-2510) may be due to the particle contact angle being reduced enough to enter the liquid, as a result of the reduced surface tension of the aqueous phase. The variation in foamability between the surfactants may be due to differences in adsorption of these surfactants to the hydrophobic particle surfaces.

 Foam collapse as a function of time for all three particle types with Lamesoft PO65 is plotted in Figure 3.51. As all of the repeats showed similar collapse profiles, only one plot is shown, the remaining plots can be found in the appendix. The reduction in foamability and stability with the addition of 20 wt. % SiOH particles is clear from these figures. Additionally, $t_{1/2}$ for foams generated with 20, 47 and 100% SiOH particles and Lamesoft PO65 are plotted Figure 3.52, again a clear increase in stability of the foams as the hydrophobicity of the particles is reduced is clear. In a study by Aveyard *et al.* thin films of 0.2 mM cetyl trimethylammoniumbromide (CTAB) were shown to be ruptured after introduction of rods coated with octadecyltrichlorosilane (OTS) of contact angle over 90°.[44] This is known throughout industry whereby hydrophobic particles are often used as anti-foams. It is possible that the introduction of the hydrophobic particles in the Lamesoft PO65 ruptured foam films, acting as antifoams.

A plot of foam collapse as a function of time for foams generated with Silsurf DI-2510 and 20, 47 and 100% SiOH particles is shown in Figure 3.55. As all of the repeats showed similar collapse profiles, only one plot is shown and the remaining plots can be found in the appendix. The collapse data seen for 100% SiOH particles where a plateau in the foam volume can be seen is a true reflection of the behaviour of this system. As previously mentioned, for the system of 1 wt. % 100% SiOH in 1 wt. % Silsurf DI-2510, a viscous material was formed, which was difficult to aerate, aeration of this suspension resulted in a foam of low volume and low bubble density (seen in microscopy images in Figure 3.57). The slow collapse of this aerated suspension is likely a consequence of there being very few bubbles to coalesce and disproportionate, it is possible that the bubbles that were generated became "trapped" in the thick viscous network of particles and surfactant. The half-life plot is shown in Figure 3.56. From these graphs it can be shown that although the initial foamability seems to be enhanced with the addition of hydrophobic particles, the stability of the foams actually follows the same trend observed for Lamesoft PO65 foams. Microscopy images (Figures 3.53 and 3.57) of both surfactant foams demonstrate that with hydrophobic particles (20 and 47% SiOH) the bubble surfaces are less spherical and have textured, rippled surfaces, indicating some particles have adsorbed at the bubble surface. It is possible that irrespective of the adsorption of surfactant molecules to the particle surfaces, the partially hydrophobic particles (47% SiOH) may adsorb to the bubble surfaces alone and enhance the stability. Additionally, the hydrophilic particles (100% SiOH) may block plateau borders in the foam structure and enhance the foam stability. This may explain the relative stability of the foams generated with particles of varying hydrophobicity (for both surfactants) being of the order 100>47>20% SiOH. The mean bubble diameters for both surfactants as a function of particle hydrophobicity are shown in Figure 3.54. There appears to be a slight increase in bubble diameter with increasing particle hydrophilicity, which may correlate with the foam $t_{1/2}$ values (more hydrophilic particles produce more stable foams). However the error on the bubble diameter measurements is large due to high polydispersity of the bubbles. This high polydispersity may occur from disproportionation of the bubbles during the sample preparation for microscopy.

Figure 3.49. Images of foams generated by hand shaking (30 s) 20 ml of 1 wt. % surfactant with 1 wt. % fumed silica (20-100% SiOH) (a) Lamesoft PO65 and (b) Silsurf DI-2510. Images taken on a Canon EOS450D immediately after aeration.

Figure 3.50. Average initial foam volume of foams generated from hand shaking (30s) 20 ml 100% SiOH fumed silica dispersed in 1 wt. % aqueous solutions of Lamesoft PO65 and Silsurf DI-2510 as a function of particle hydrophobicity. Particle hydrophobicity ranges from 20-100% SiOH groups on particle surface. Average initial foam volumes of Lamesoft PO65 and Silsurf DI-2510 alone are indicated by red and blue dashed lines, respectively. Error bars indicate maximum and minimum values from 3 repeat measurements.
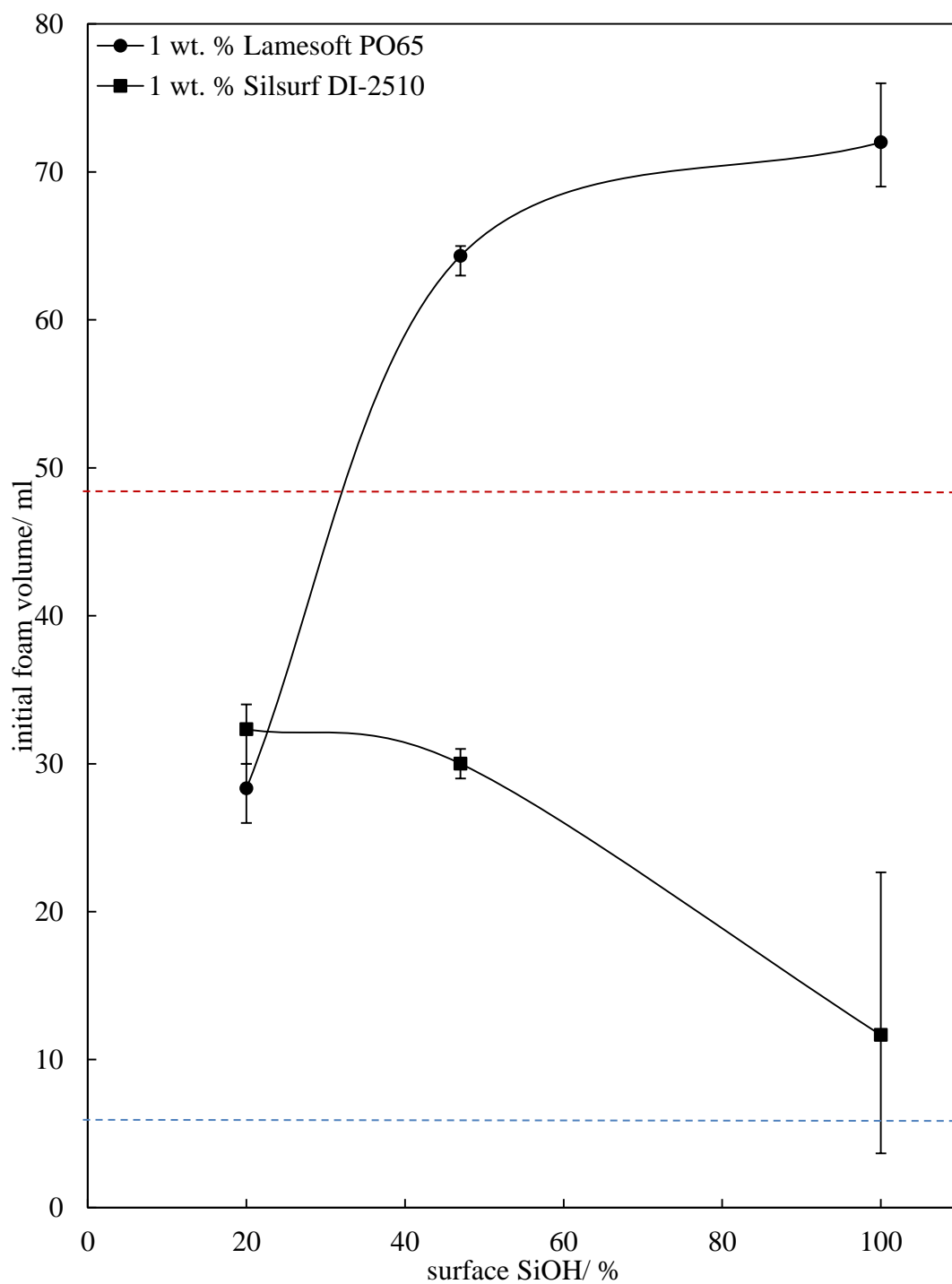
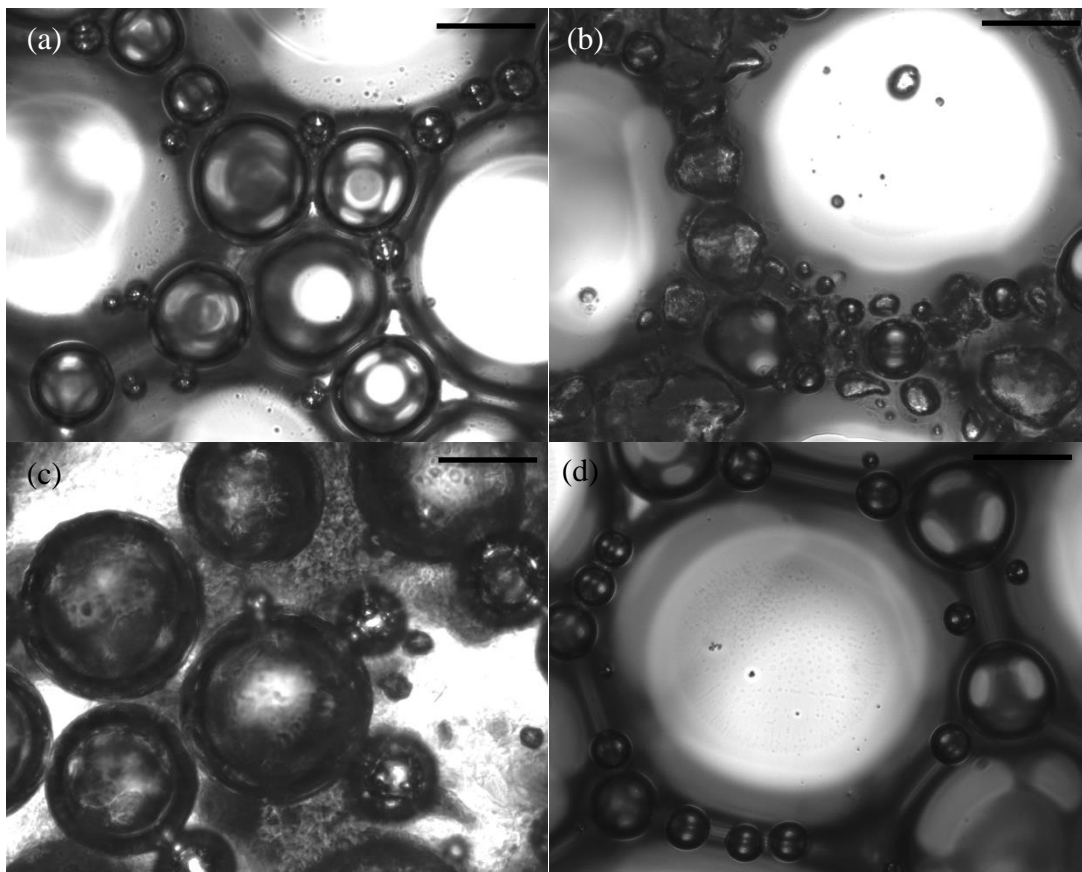**Figure 3.51.** Foam volume as a function of time for foams generated by hand shaking (30s) 20 ml 1 wt. % Lamesoft PO65 containing 1wt. % fumed silica particles. Particle hydrophobicity is varied from 20-100% surface SiOH groups. Run 1 of 3 repeats. Remaining two repeats are shown in appendix 3.51 (a) and (b).
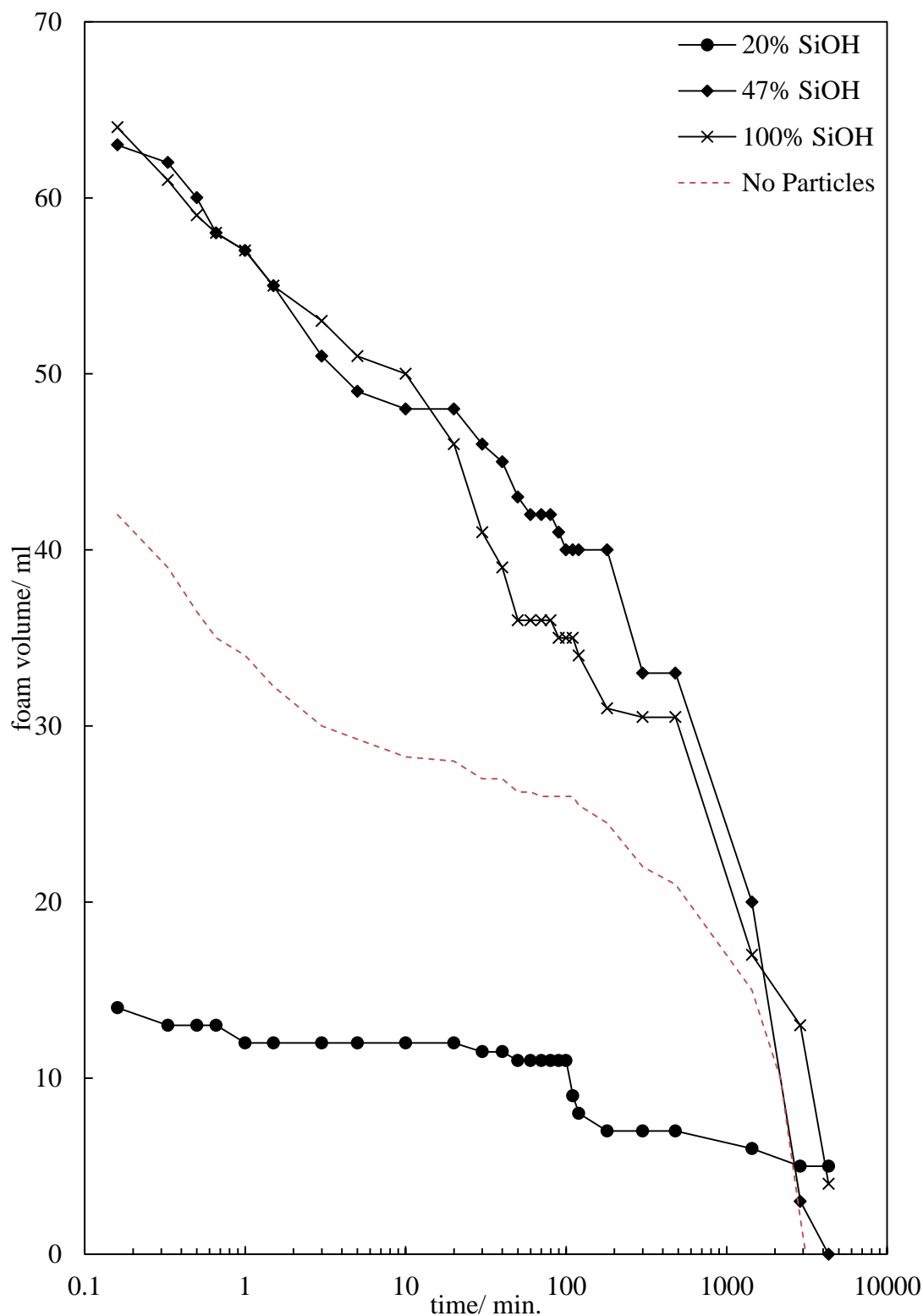
Figure 3.52. Foam half-life ($t_{1/2}$) as a function of particle hydrophobicity for foams generated by hand shaking (30 s) 20 ml of 1 wt. % Lamesoft PO65 containing 1wt. % fumed silica particles. Particle hydrophobicity is varied from 20-100% surface SiOH groups. Three separate repeat runs and the average half-life for 1 wt. % Lamesoft PO65 foam with no particles (dashed line) are shown.
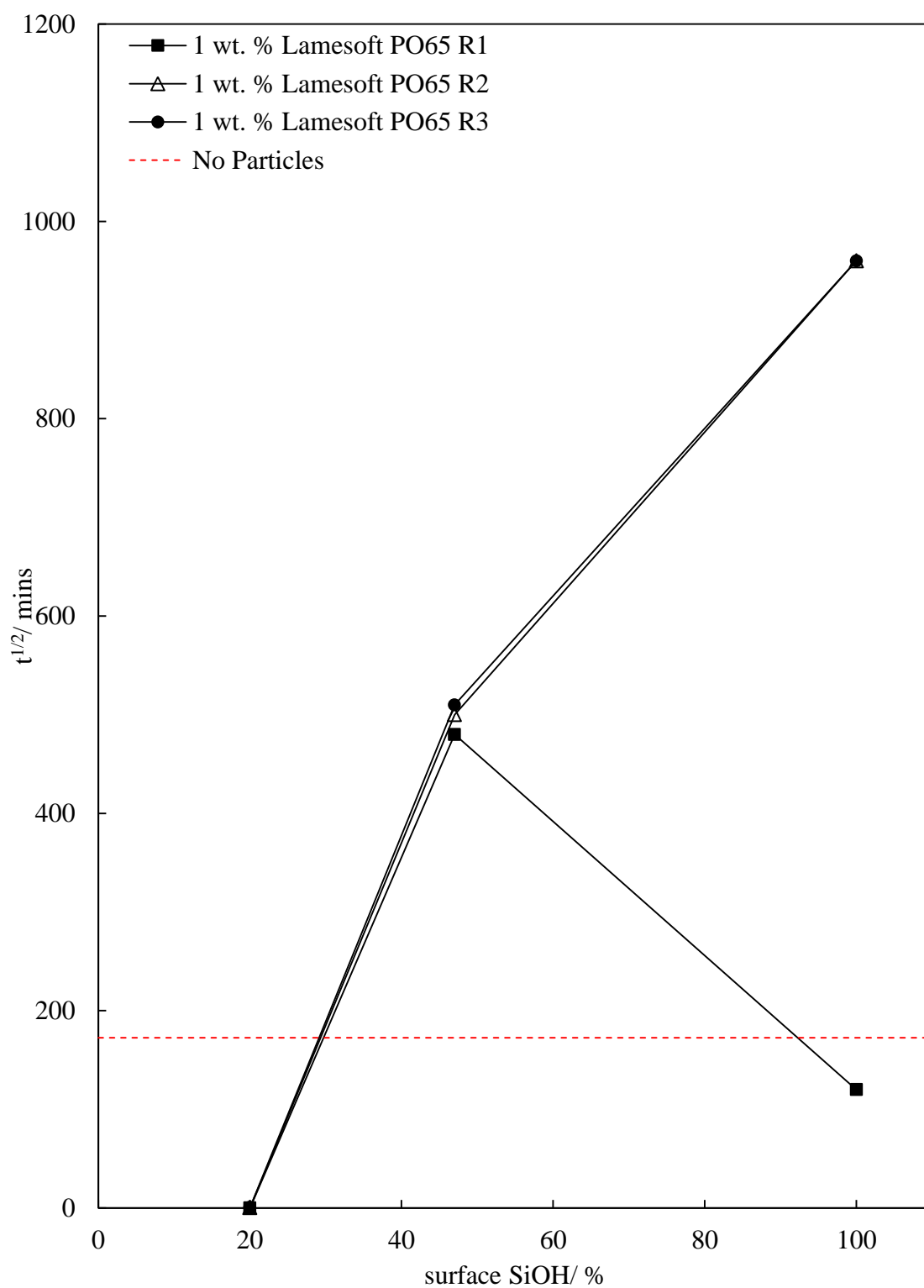
Figure 3.53. Optical microscopy of foams generated by hand shaking (30s) 20 ml 1 wt. % Lamesoft PO65 containing 1 wt. % fumed silica particles. Particle hydrophobicity is varied from 20-100% surface SiOH groups. (a) 1 wt. % Lamesoft PO65 alone (b) 20% SiOH, (c) 47% SiOH and (d) 100% SiOH. Scale bar corresponds to 100 μm.

Figure 3.54. Measured average bubble diameter as a function of hydrophobicity of 1 wt. % fumed silica particles in 1 wt. % Lamesoft PO65 and Silsurf DI2510 solutions in water after aeration by hand shaking 20 ml solution for 30 s. Mean bubble diameter calculated from at least 40 individual bubble measurements and taken within 5 minutes of foam generation. Error bars show standard deviation.

Figure 3.55. Foam volume as a function of time for foams generated by hand shaking (30 s) 20 ml of 1 wt. % Silsurf DI-2510 containing 1wt. % fumed silica particles. Particle hydrophobicity is varied from 20-100% surface SiOH groups. Run 1 of 3 repeats. Remaining two repeats are shown in appendix 3.55 (a) and (b).
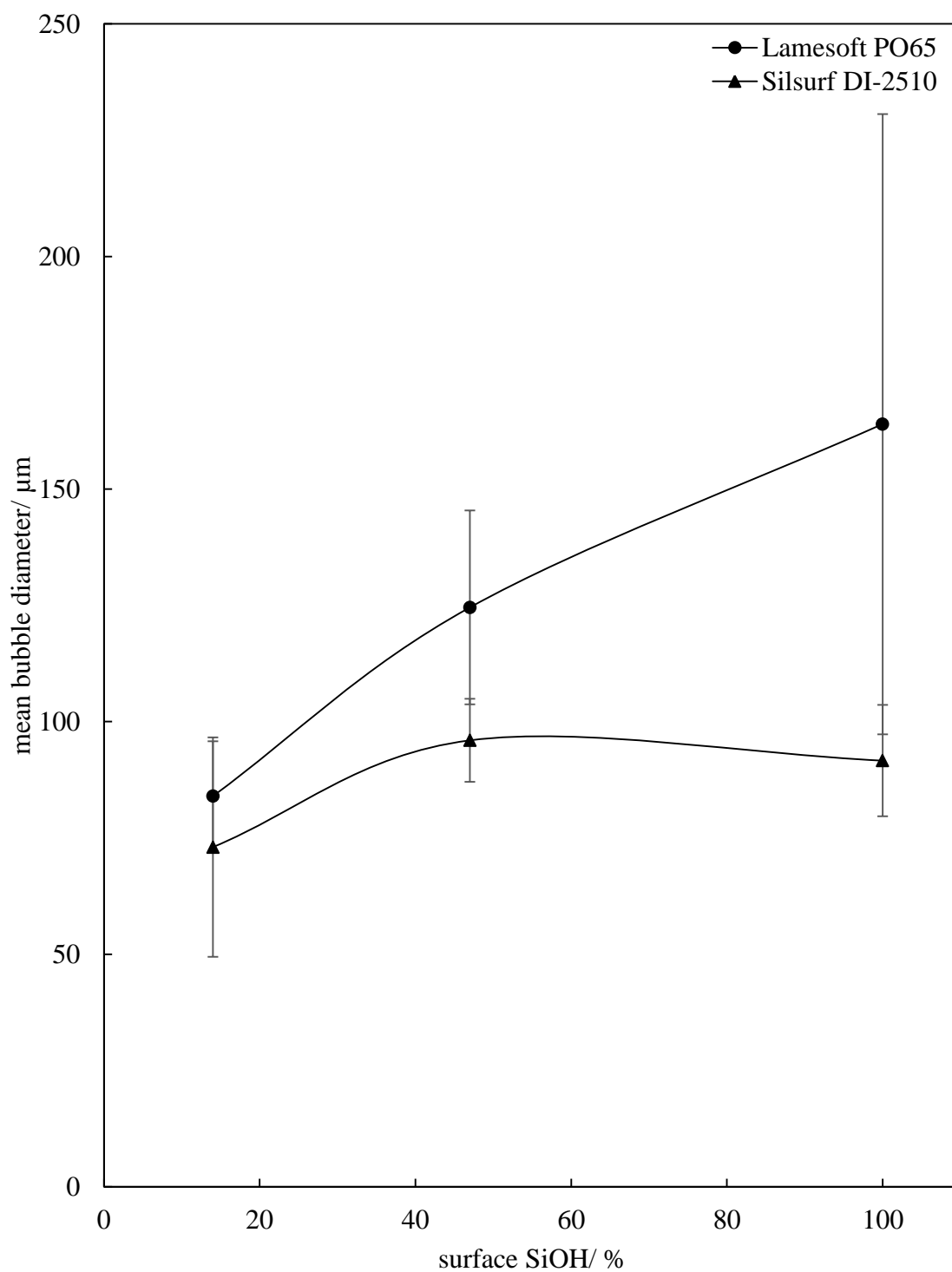
Figure 3.56. Foam half-life ($t_{1/2}$) as a function of time for foams generated by hand shaking (30s) 20 ml 1 wt. % Silsurf DI-2510 containing 1wt. % fumed silica particles. Particle hydrophobicity is varied from 20-100% surface SiOH groups. Three separate repeat runs and the average half-life for 1 wt. % Silsurf DI-2510 foam with no particles (dashed line) are shown.
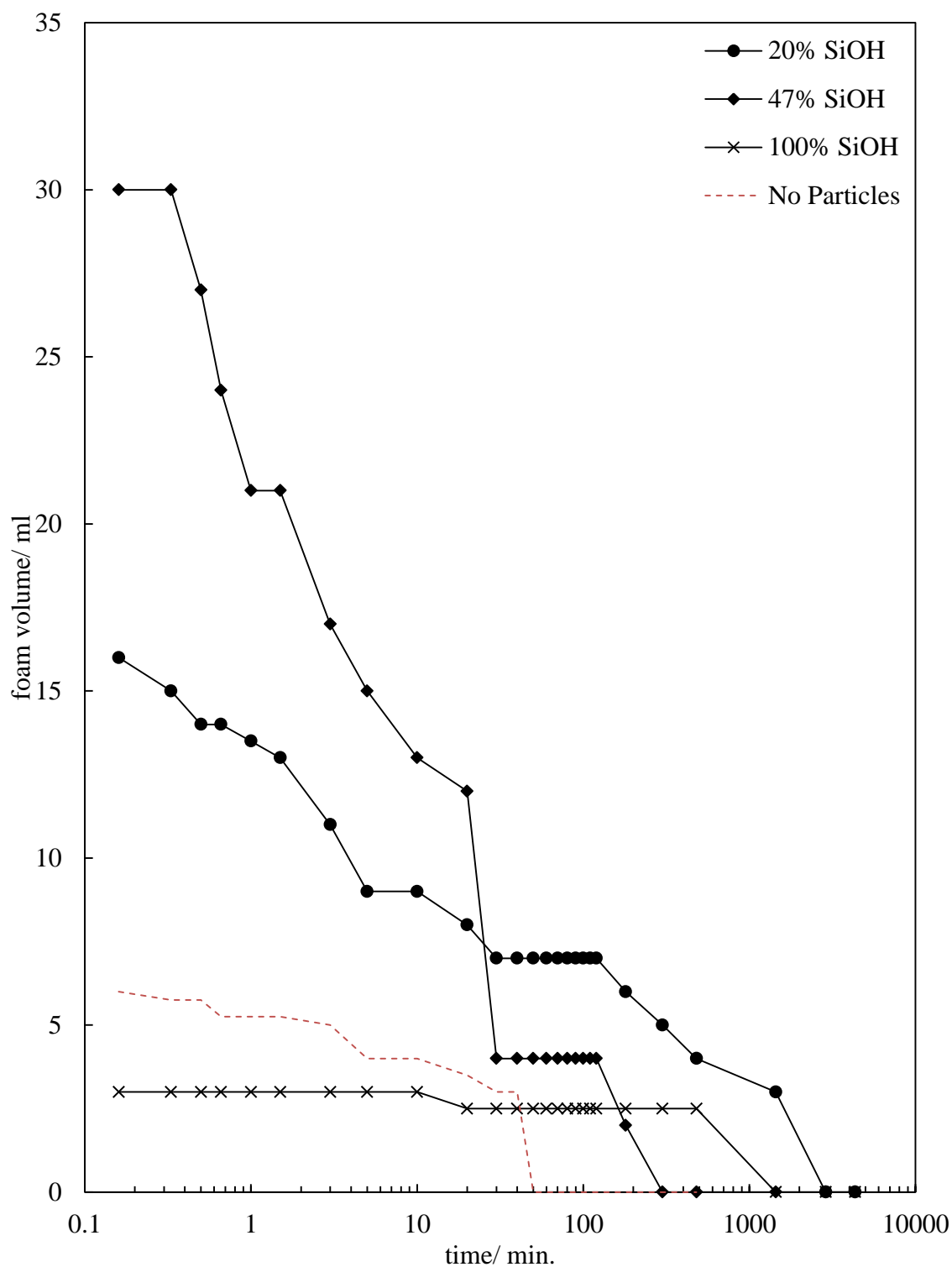
Figure 3.57. Optical microscopy of foams generated by hand shaking (30 s) 20 ml of 1 wt. % Silsurf DI-2510 containing 1 wt. % fumed silica particles. Particle hydrophobicity is varied from 20-100% surface SiOH groups. (a) 1 wt. % Silsurf DI-2510 alone (b) 20% SiOH, (c) 47% SiOH and (d) 100% SiOH. Scale bar corresponds to 100 μm.
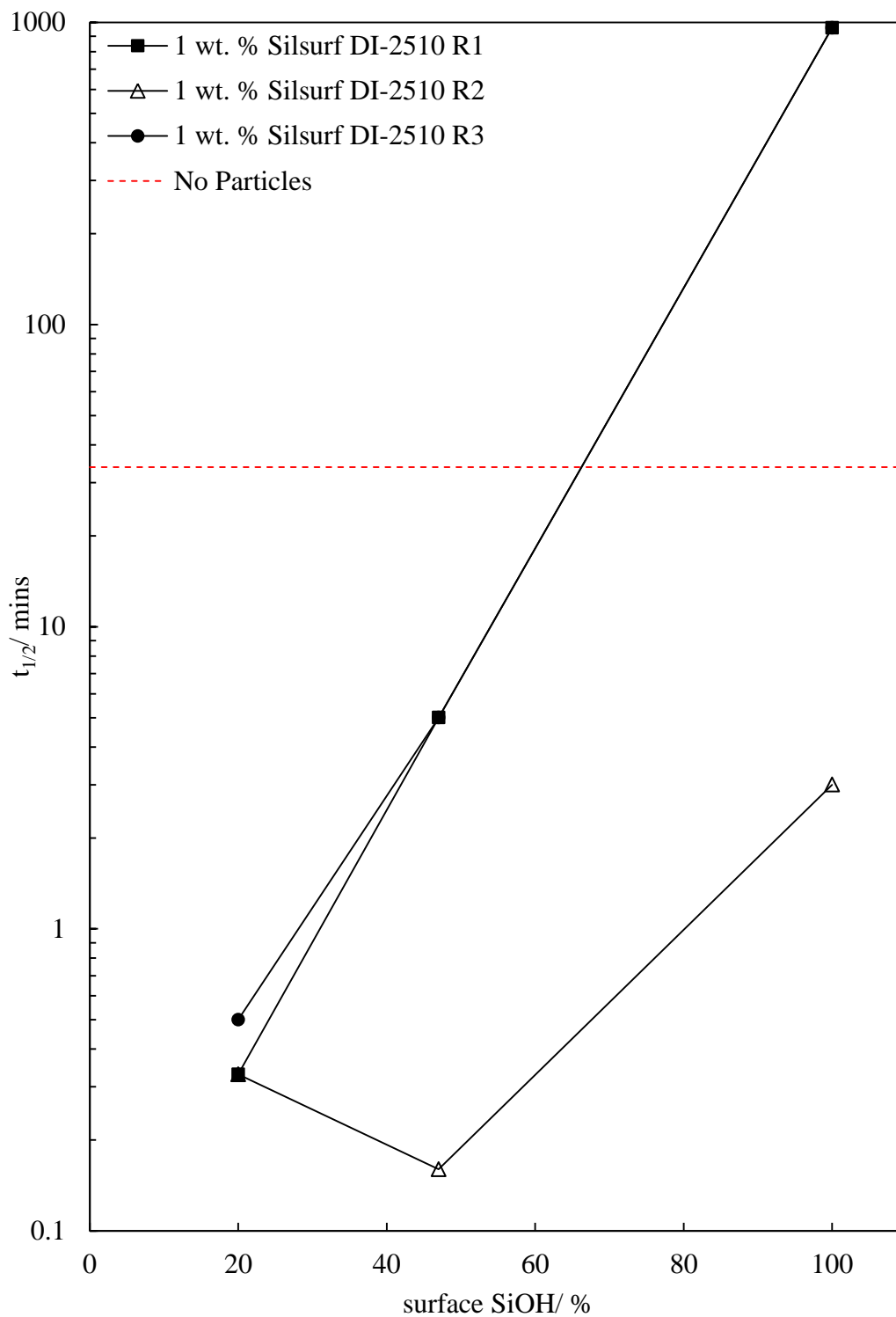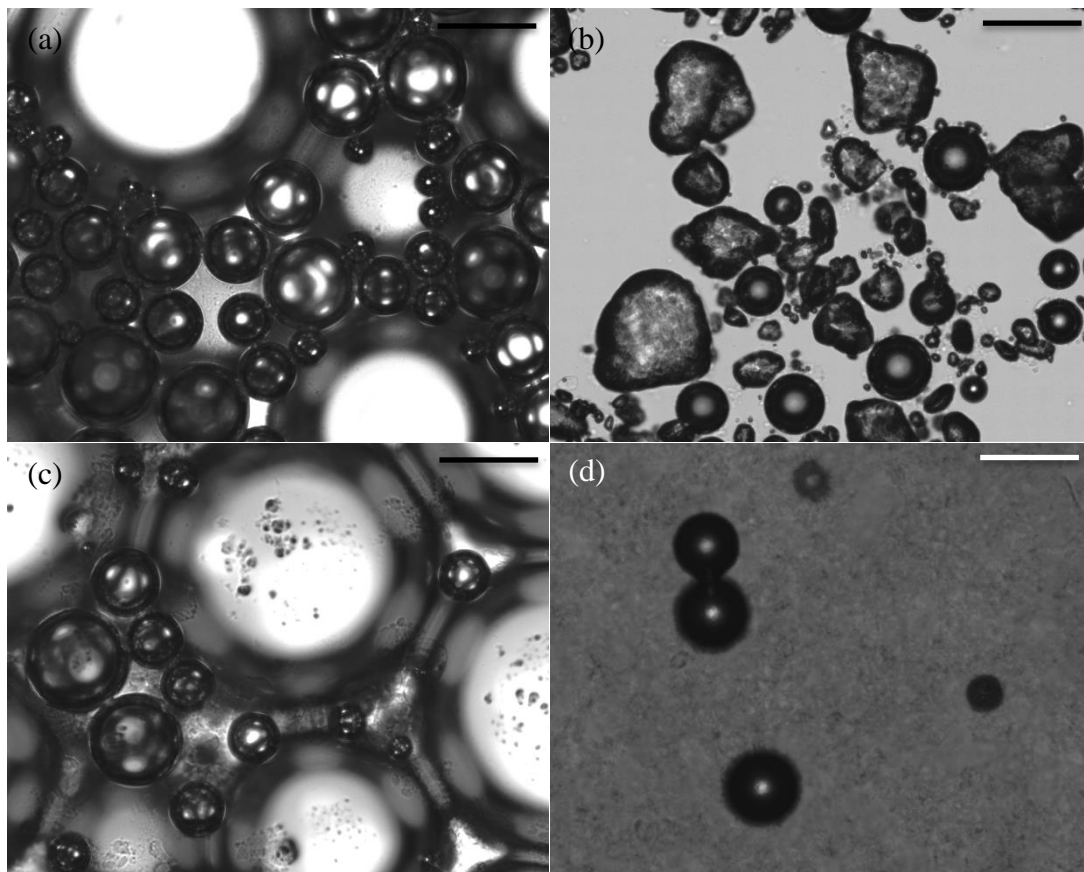
Figure 3.58 shows the advancing contact angles of aqueous surfactant drops in air on both hydrophilic and hydrophobic glass slides. It can be seen that for aqueous solutions of both surfactants on a hydrophobised glass slides, the contact angle continually decreases with increasing surfactant concentration. This may suggest that the surfactant adsorbs to the hydrophobic surface via their hydrophobic tails, rendering the surface hydrophilic. However, with the hydrophilic glass slides, both surfactants pass through a slight maximum contact angle with increasing surfactant concentration. This maximum occurs at 0.001 wt. % for Lamesoft PO65 and at 1 wt. % for Silsurf DI-2510. This may indicate the adsorption of surfactant to the hydrophilic surface rendering it hydrophobic. As the surfactant concentration increases it may be possible that a bilayer of surfactant adsorbs via hydrophobic chain-chain interactions, with their heads exposed to the solution, decreasing the contact angle.

Figure 3.58. Advancing contact angles of sessile drops (10 µl) of surfactant solutions in air on hydrophobic (top) and hydrophilic (bottom) glass slides as a function of surfactant concentration. Dashed lines in both graphs indicate contact angle of pure water. Hydrophobic surfaces prepared by reacting glass slides to maximum extent with 0.1 ml DCDMS vapour for 1 hour. Hydrophilic slides are cleaned untreated glass slides.
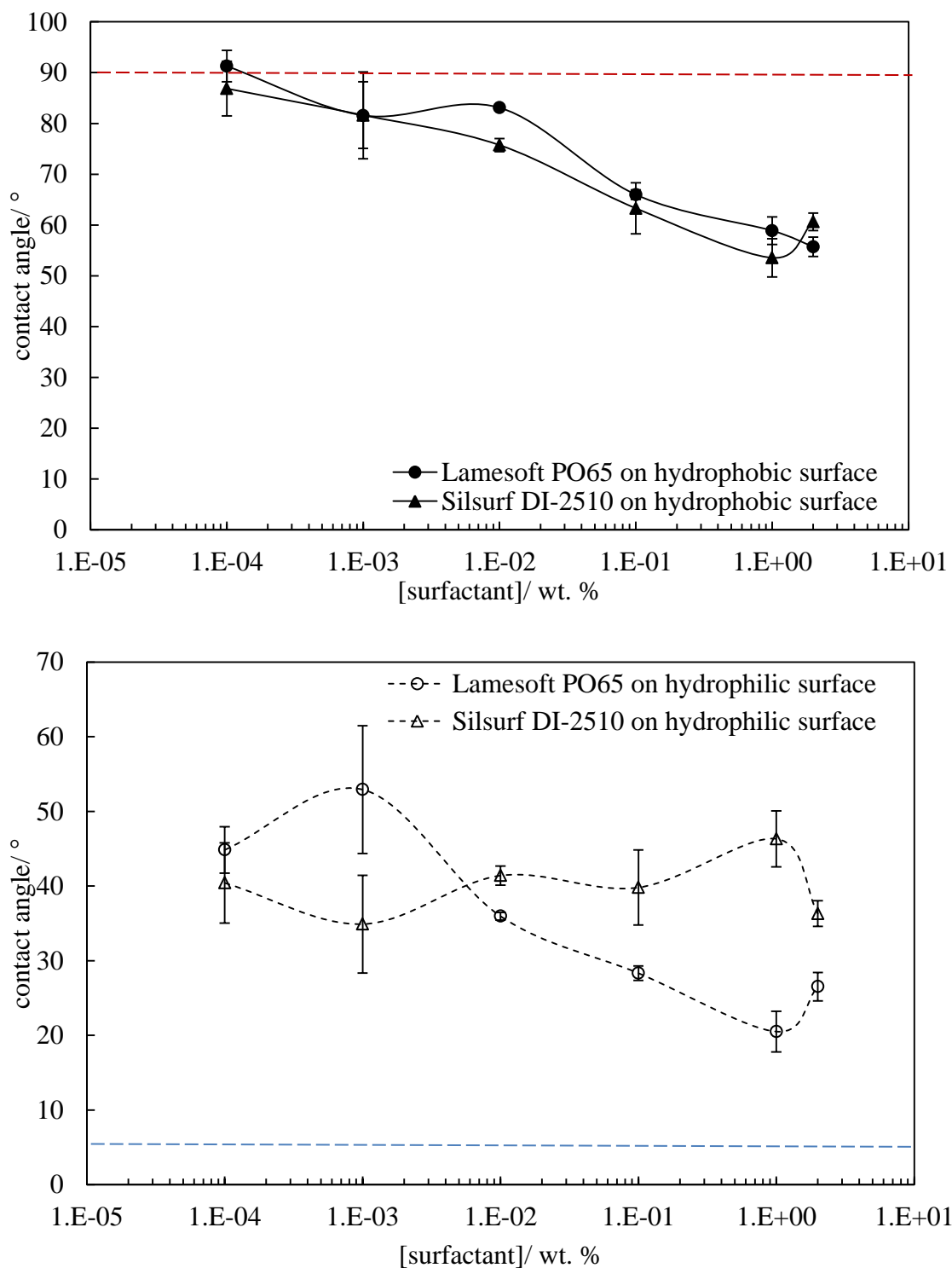
3.6 Summary

This chapter has presented a systematic investigation into the foaming properties of two commercial grade nonionic surfactants. Their behaviour in the bulk solution and upon aeration of the bulk solution has been investigated in pure water and with the addition of ethanol. It was found that for pure water, the CMC's of the surfactants were found to be 0.0023 and 0.01 wt. % for Lamesoft PO65 and Silsurf DI-2510, respectively. Upon addition of 20 wt. % ethanol to the aqueous phase, the CMC values were altered so that the CMC for Lamesoft PO65 increased to 0.003 wt. %, and the CMC for Silsurf DI-2510 increased to 0.08 wt. %. These variations in CMC were attributed to better solvation of surfactant molecules due to presence of alcohol, which reduced the hydrophobic effect between surfactant molecules and therefore reduced the driving force for adsorption to the interface and micellisation.

The foaming properties (foamability and stability) of the surfactants in pure water and 20 wt. % ethanol were shown to increase with increasing surfactant concentration. Both surfactants showed a maximum in foamability at an optimum concentration of ethanol, this being 30 wt. % ethanol for Lamesoft PO65 and 70 wt. % ethanol for Silsurf DI-2510. However, maxima in stability of aqueous ethanol surfactant foams were observed at lower ethanol concentrations.

The effect of addition of particles to the aqueous phase was investigated by dispersing fumed silica into aqueous solutions of the two surfactants. The effect of surfactant concentration, particle concentration and particle hydrophobicity were investigated. It was seen that with the addition of 1 wt. % 100% SiOH to surfactant solutions of varying concentration, foams were only formed above the CMC, as observed with the solutions of the surfactant alone. The foamability, half-lives and total collapse times of the foams were seen to be enhanced by the addition of particles to the aqueous phase. An exception was observed for the system of 1 wt. % 100% SiOH and 1 wt. % Silsurf DI-2510, whereby a viscous gel-like aqueous phase was generated, resulting in poor foam volume with low stability. The addition of 0.1-2 wt. % hydrophilic fumed silica particles to 1 wt. % surfactant solutions enhanced the foamability at all particle concentrations. The stability of foams was also enhanced.

The effect of particle hydrophobicity was investigated by generating foams of 1 wt. % surfactant and 1 wt. % silica particles with a varying percentage of silanol groups on their surface. It was seen that the two surfactants behaved very differently, increasing the particle hydrophobicity in Lamesoft PO65 foams proved detrimental to the foamability, possibly because the hydrophobic particles act as antifoaming agents, rupturing surfactant films in the foam structure. However, the Silsurf DI-2510 foams were shown to be enhanced with the increase in particle hydrophobicity, potentially due to the surface modification of particles by surfactant adsorption or due better wetting of the most hydrophobic particles by the low surface tension of the surfactant solution. As the particles became wetted, they may have been able to adsorb to the interface alone providing significant stability. For future studies, analysis of the surfactant structures would be beneficial. Additionally some experiments to determine if there is any adsorption of the surfactant molecules to the particle surfaces would be valuable.

3.7   References

1. L.L. Shramm, Emulsions, Foams and Suspensions Fundamentals and Applications, 2005, Wiley VCH, Weinheim.

2. Z. Du, M.P. Bilbao-Montoya, B.P. Binks, E. Dickinson, R. Ettelaie and B.S. Murray, *Langmuir*, 2003, **19**, 3106.

3. E. Dickinson, R. Ettelaie, T. Kostakis and B.S. Murray, *Langmuir*, 2004, **20**, 8517.

4. B.P. Binks and T.S. Horozov, *Angew. Chem. Int. Ed.*, 2005, **44**, 3722.

5. A. Stocco, E. Rio, B.P. Binks and D. Langevin, *Soft Matter*, 2011, **7**, 1260.

6. H. Jin, W. Zhou, J. Cao, S.D. Stoyanov, T.B.J. Blijdenstein, P. W. N. de Groot, L. N. Arnaudov and E. G. Pelan, *Soft Matter*, 2012, **8**, 2194.

7. B.S. Murray, K. Durga, A. Yusoff and S.D. Stoyanov, *Food Hydrocoll.*, 2011, **25**, 627.

8. Z.-G. Cui, Y.-Z. Cui, Z. Chen and B.P. Binks, *Langmuir*, 2010, **26**, 12567.

9. B. Tigges, T. Dederichs, M. Moller, T. Liu, W. Richtering and O. Weichold, *Langmuir*, 2010, **26**, 17913.

10. F. Carn, A. Colin, O. Pitois, M. Vignes-Adler and R. Backov, *Langmuir*, 2009, **25**, 7847.

11. B.P. Binks, A.J. Johnson and J.A. Rodrigues, *Soft Matter*, 2009, **6**, 126.

12. K.P. Sharma, V.K. Aswal and G. Kumaraswamy, *J. Phys. Chem. B*, 2010, **114**, 10986.

13. Q. Zhou and P. Somasundaran, *J. Colloid Interface Sci.*, 2009, **331**, 288.

14. L. Zhang, P. Somasundaran and C. Maltesh, *J. Colloid Interface Sci.*, 1997, **191**, 202.

15. S. Zhang, D. Sun, X. Dong, C. Li and J. Xu, *Colloids Surf. A*, 2008, **324**, 1.

16. S. Yusuf, M. Manan and M.Z. Jaafar, *Iranica J. Energy & Envir.*, 2013, **4**, 8.

17. C. Lens, J.J. Lucchini and P. Grascha, *Can. J. Infection Control*, 2011, **26**, 21.

18. G. Vásquez, E. Alvarez and J.M. Navaza, *J. Chem. Eng. Data.*, 1995, **40**, 611.

19. G.T. Barnes and I.R. Gentle, *Interfacial Science: an introduction*, 2nd Ed.. Oxford University Press, New York, 2011.

20. D.J. Shaw, *Introduction to Colloid & Surface Chemistry*, 4th Ed., Butterworth-Heinemann, Oxford, 1992.

21. P. Stevenson, *Foam Engineering Fundamentals and Applications*, Wiley-Blackwell, East Sussex, 2012.

22. S. Javadian, H. Gharibi, B. Sohrabi, H. Bijanzadeh, M.A. Safarpour and R. Behjatmanesh-Ardakani, *J. Mol. Liq.*, 2008, **137**, 74.

23. P. Becher, *J. Colloid Interface Sci.*, 1965, **20**, 728.

24. N. Nikishido, Y. Moroi, H. Uehara and R. Matuura, *Bull. Chem. Soc. Japan*, 1974, **47**, 2634.

25. J.R. Wegner and C.A. Littau, *Dimethicone surfactants are PEG-8 to PEG-12 linear dimethicone surfactants; C2-C4 alcohol and water; hand and skin care product; microbiocides*, 2010, US 7842725 B2.

26. S. Samanta and P. Ghosh, *Chem. Eng. Sci.*, 2011, **66**, 4824.

27. P.D.I. Fletcher and B.L. Holt, *Langmuir*, 2011, **27**, 12869.

28. H-L. Cheng and S.S. Velankar, *Colloids Surf. A*, 2008, **315**, 275.

29. B.P. Binks, J.H. Clint, P.D.I. Fletcher, T.J.G. Lees and P. Taylor, *Chem. Commun.*, 2006, 33, 3531.

30. U.T. Gonzenbach, A.R. Studart, E. Tervoort and L.J. Gauckler, *Angew. Chem. Int. Ed.*, 2006, **45**, 3526.

31. R.G. Alargova, D.A. Warhadpande, V.N. Paunov and O.D. Velev, *Langmuir*, 2004, **20**, 10371.

32. Y. Q. Sun and T. Gao, *Metall. Mat. Trans. A*, 2002, **33A**, 3285.

33. B.P. Binks, *Curr. Opin. Colloid Interface Sci.*, 2002, **7**, 21.

34. B.M. Somosvári, N. Babcsán, P. Bárczy and A. Berthold, *Colloids Surf. A*, 2007, **309**, 240.

35. J.A. Rodrigues, E. Rio, J. Bobroff, D. Langevin and W. Drenckhan, , *Colloids Surf. A*, 2011, **384**, 408.

36. B.P. Binks, M. Kirkland and J. A. Rodrigues, *Soft Matter*, 2008, **4**, 2373.

37. B.P. Binks, L. Isa and A.T. Tyowua, *Langmuir*, 2013, **29**, 4923.

38. Q. Liu, S. Zhang and J. Xu, *Colloids Surf. A*, 2010, **355**, 151.

39. A. Maestro, E. Guzmán, E. Santini, F. Ravera, L. Liggieri, F. Ortega and R. G. Rubio, *Soft Matter*, 2012, **8**, 837.

40. D.W. Fuerstenau and R. Jia, *Colloids Surf. A*, 2004, **250**, 223.

41. L. Favretto and F. Tunis, *Analyst*, 1976, **101**, 198.

42. L. Favretto, B. Stancher and F. Tunis, *Analyst*, 1980, **105**, 833.

43. L. Favretto, B. Stancher and F. Tunis, *Int. J. Envir. Anal. Chem.*, 1983, **14**, 201.

44. R. Aveyard, B.P. Binks, P.D.I. Fletcher, T.G. Peck and C.E. Rutherford, *Adv. Colloid Interface Sci.*, 1994,

CHAPTER 4

BEHAVIOUR OF MONODISPERSE FLUORINATED SILICA PARTICLES AT AN AQUEOUS ETHANOL-AIR INTERFACE

4.1 Introduction

Chapter 3 explored the foaming behaviour of two commercial aqueous surfactant solutions in the presence of particles and in ethanol. The addition of ethanol to the surfactant systems alone was seen to enhance the foamability within a certain concentration range of ethanol. The behaviour of fumed silica particles alone in the presence of aqueous ethanol was similar, in that it was not possible to generate foams above a certain ethanol concentration. It is understood that this is likely due to variation in the contact angle of the particles at the interface as the surface tension of the liquid-air interface is varied; as demonstrated by Young's equation:[1]

$$\cos\theta = \frac{\gamma_{pa} - \gamma_{pw}}{\gamma_{aw}}$$

(4.1)

where θ is the three-phase contact angle and γ_{pa}, γ_{pw}, γ_{aw} are the interfacial tensions of particle-air, particle-water and air-water interfaces, respectively.

Encapsulation of liquids of varying surface tension are of particular interest in the current work. Bormashenko has shown that encapsulation of aqueous ethanol in liquid marbles of polytetrafluoroethylene (PTFE), polyvinylidene fluoride (PVDF) and polyethylene particles is possible, but only up to a maximum concentration of 21% ethanol.[2] It was also reiterated in this work that encapsulation of high surface tension liquids (such as water and glycerol) is relatively simple. More recent work by Binks and Tyowua has demonstrated encapsulation of fairly low surface tension liquids (oils of surface tension >27 mN m^{-1}) by fluorinated clay particles.[3] Additionally, Lai *et al.* have demonstrated the potential of fluorinated titanate "nanobelts" for encapsulation of many liquids.[4] The liquid marbles generated demonstrated great mechanical stability and robustness, and could encapsulate aqueous metal salts and dyes for gas sensing applications. It is therefore understood that particles of lower surface energy are required for encapsulation of liquids of low surface tension.[5-7] This chapter therefore aims to investigate the relationship between particle hydrophobicity and colloidal systems generated when ethanol is introduced into the aqueous phase.

Monodisperse silica particles of relatively large diameter have been used, so that the contact angle of these particles can be measured directly by the film calliper method.[8] It is clear from the literature in this area that the controlled hydrophobisation of silica surfaces using fluoroalkylchlorosilanes is not simple. Many parameters need to be considered, such as the concentration of silane, the reagent phase, solvent dryness, temperature and time of the reaction. Additionally the functionality of the fluoroalkylchlorosilane has significance for how the silanes will attach to the solid surface, as shown in Figure 4.1.

Figure 4.1. Depiction of various methods of attachment of polyfunctional alkylchlorosilanes to a silica surface comprising silanol groups. Image from reference 9.
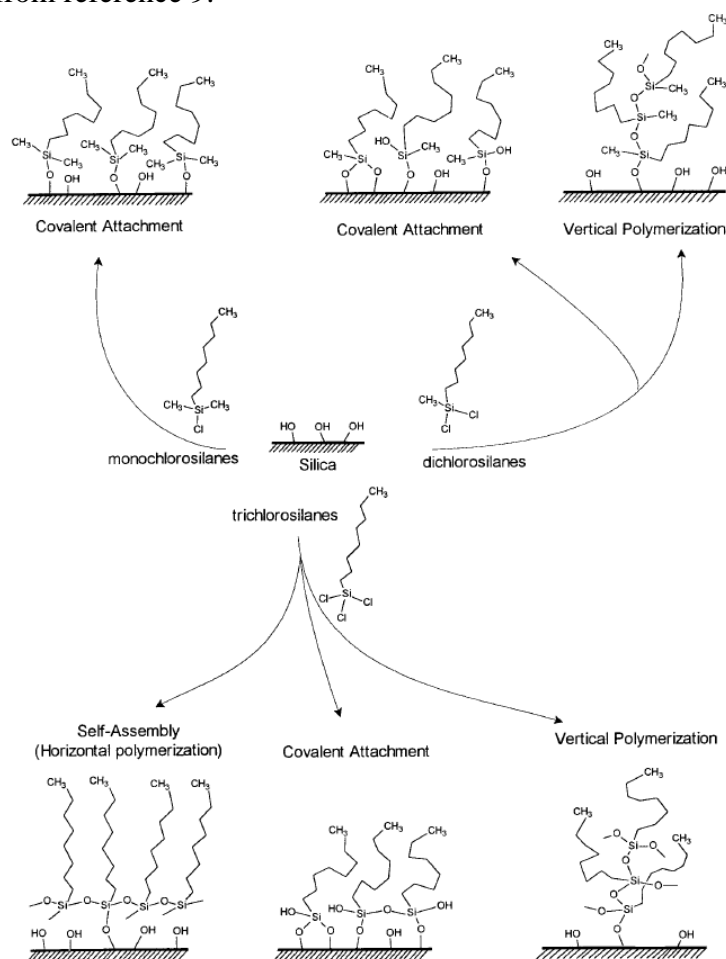
4.2   Experimental

To develop a protocol for hydrophobisation of silica particles with fluoroalkylchlorosilane, firstly a range of experiments were carried out on glass slides (following procedure described in Section 2.2.6.2). A variety of reaction parameters (including solvent type, duration, reagent functionality and addition of amines to the reaction) were investigated so that optimal conditions for the fluorination reaction could be determined. Once an optimal set of conditions for the reaction had been determined, a range of 2 μm diameter monodisperse silica particles were then hydrophobised in toluene for two hours under controlled temperature. The particle hydrophobicity was varied by changing the concentration of the selected fluoroalkylchlorosilane following the technique described in Section 2.2.6.3. The contact angles of these particles at an-air water and aqueous ethanol-air interface were then measured by the film calliper method. A detailed explanation of the film calliper method is given in Chapter 2. The behaviour of the particles spread at horizontal interfaces and upon aeration was then investigated. Further to this the influence of ethanol introduction to the aqueous phase was observed. The systems were further characterised by optical microscopy and freeze-fracture SEM.

4.3   Optimisation of fluorination

A preliminary investigation was carried out on glass slides, whereby glass slides were treated under a variety of different experimental conditions. The effect of reagent phase and functionality (monochloro- or dichloro- functionality), solvent, time and concentration of silane was investigated. The effect of pre-addition of various amines was also investigated. The contact angle of a sessile drop of water in air was then measured on the fluorinated surface.

4.3.1.   *Contact angles of water drops on glass slides hydrophobised with fluoroalkylchlorosilanes*

4.3.1.1   Effect of reagent functionality and concentration

Two fluoroalkylchlorosilanes were used, one comprising two chlorine groups (1H, 1H, 2H, 2H-perfluorooctylmethyldichlorosilane) and the other comprising one chlorine group (1H, 1H, 2H, 2H-perfluorooctyldimethylchlorosilane). A study into the fluorination of silicon wafers using dichloro- and trichloroalkylsilanes by Fadeev and McCarthy discussed many features of these reactions.[9,10] It was shown that trifunctional organosilanes have higher reactivity than their monofunctional counterparts. Additionally, they can polymerise in the presence of water, giving rise to a variety of potential surface structures (shown in Figure 4.1). Glass slides were hydrophobised by reaction of both types of silane (in toluene) at ambient temperature for 72 hours. The extent of hydrophobisation was assessed by measuring the contact angle of water drops on the slides in air. Figure 4.2 shows the advancing contact angle of a 10 μl water drop on glass slides in air. It can be seen that the contact angle increases with the increase of silane concentration from 6.8×10^{-5}-6.8×10^{-4} M but reaches an almost constant value at higher concentrations. Furthermore, when examining the functionality the silanes, the dichlorofluoroalkylsilane was seen to demonstrate a consistently higher contact angle. The contact angle obtained at the highest concentration of dichlorofluoroalkylsilane was 111°, while that of the monochloro-functional silane was 85°. These results suggest that the dichloro-functional silane of a more efficient hydrophobising agent than the monochloro-functional silane. This is in contradiction with what has been observed by others, that monochloroalkyl silanes produce more hydrophobic and homogeneous surfaces.[11]

In our case, it seems possible that the additional methyl group on the monochlorosilane imparts some element of steric hindrance for further incoming reagent molecules, thus leading to a lower density of fluoroalkyl chains grafted onto the glass surface. In addition, some surface cross-linking of the dichlorofluoroalkylsilane may shield some of the residual hydrophilic surface silanol groups from the probe liquid. Fadeev and McCarthy who found that surface silanol groups of silicon wafers treated with monochloroalkylsilanes were shielded from penetrating water by hydrophobic monolayers.[10] Although there couldn't have been any cross-linking between these monofunctional silanes, it is understood that formation of a monolayer (whether strongly bound to the surface, or its neighbouring silanes) can shield surfaces from probe fluids. There also may be some surface roughness as a result of unpredictable polymerisation between the difunctional silane molecules, which has also been suggested by Fadeev and McCarthy who proposed that multi-functional fluoroalkylchlorosilanes can generate a surface topography that can affect the contact angle hysteresis. Polymerisation cannot occur in the case of the monochlorosilane, therefore giving more homogeneous surfaces after hydrophobisation.

Figure 4.2.   Effect of silane functionality on contact angle of 10 µl sessile water drop in air on glass slides treated with 1H, 1H, 2H, 2H-perfluorooctylmethyldichlorosilane and 1H, 1H, 2H, 2H-perfluorooctyldimethylchlorosilane for 72 h at ambient temperature as a function of reagent concentration. Error bars show standard deviation from an average of 9 measurements.
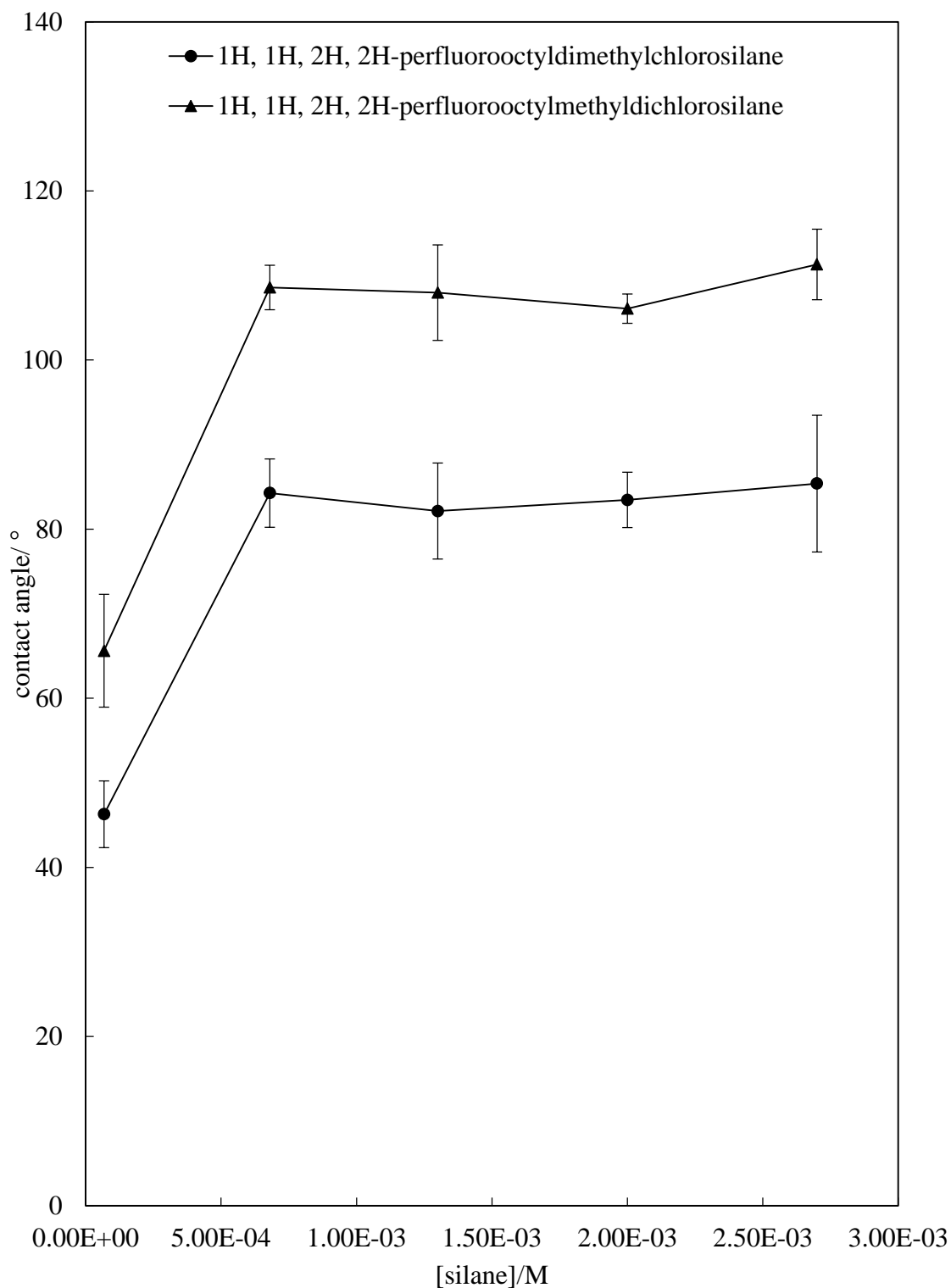
4.3.1.2   Effect of reagent phase

According to Fadeev and McCarthy,[10] the highest contact angles on glass slides treated with alkyldimethylchlorosilane were obtained in the vapour phase (at elevated temperature). To test this, glass slides have been hydrophobised in the vapour phase by placing the slides in a closed vessel with a volume of 120 cm^3 together with different amounts of neat monochlorofluoroalkylsilane. The results for the contact angles obtained after 72 hours of hydrophobisation are summarised in Table 4.1. It is seen that the contact angle values are almost identical irrespective of the volume of silane used (except the small decrease at the largest volume). This suggests that even the smallest volume of silane used (20 µl) has been in excess sufficient to achieve the maximum hydrophobicity.

Table 4.1.   Contact angles of 10 µl water drops on glass slides in air measured after gas phase hydrophobisation of the slides using different volumes of neat silane (1H, 1H, 2H, 2H-perfluorooctyldimethylchlorosilane) at room temperature for 72 hours.

Volume of silane used/ mL	Contact angle/ °
0.002	88.8 ± 5.7
0.02	93.5 ± 3.7
0.04	93.4 ± 3.0
0.06	96.5 ± 2.0
0.08	86.1 ± 6.3

4.3.1.3   Effect of solvent dryness in liquid phase hydrophobisation

Much of the literature has discussed the use of anhydrous toluene as a solvent, and that the presence of moisture within the reaction between the silica surface and alkylchlorosilane can result in uncontrollable polymerisation of the silane, causing an unpredictable surface coating. To investigate this further, toluene dried to varying extents was used as a solvent for the fluoroalkylchlorosilane. Anhydrous toluene, calcium hydride dried toluene, analytical grade toluene, and toluene dried over molecular sieves were used by dissolving 1H, 1H, 2H, 2H-perfluorooctyldimethylchlorosilane at a concentration of 6.8×10^{-4} M and allowing to react at ambient temperature for 72 hours. The contact angles of the glass slides prepared under these conditions are shown in Figure 4.3. It can be seen that the highest contact angles were obtained for solutions prepared with anhydrous toluene, additionally the smallest hysteresis between advancing and receding contact angles was observed for this sample. It was not possible to quantify the water content of the different solutions; this would have been beneficial information in order to deduce the quantity of water between each grade of toluene. Water content in each sample could have been determined by Karl Fisher titration had this equipment been available. It is also possible that despite the slides being dried in an oven, stored in a vacuum oven and transferred quickly to a vessel flushed with nitrogen gas, that some water molecules may have condensed onto the glass slide surfaces. Carrying out the entire slide drying process in an inert atmosphere may have enabled for a higher level of control of the moisture content on the glass slide surfaces.

Figure 4.3.   Effect of toluene grade on contact angle of 10 μl sessile water drop in air on glass slide treated with 6.8×10^{-4} M of 1H, 1H, 2H, 2H-perfluorooctyldimethylchlorosilane for 72 h at ambient temperature. Error bars show standard deviation from an average of 9 measurements.

165
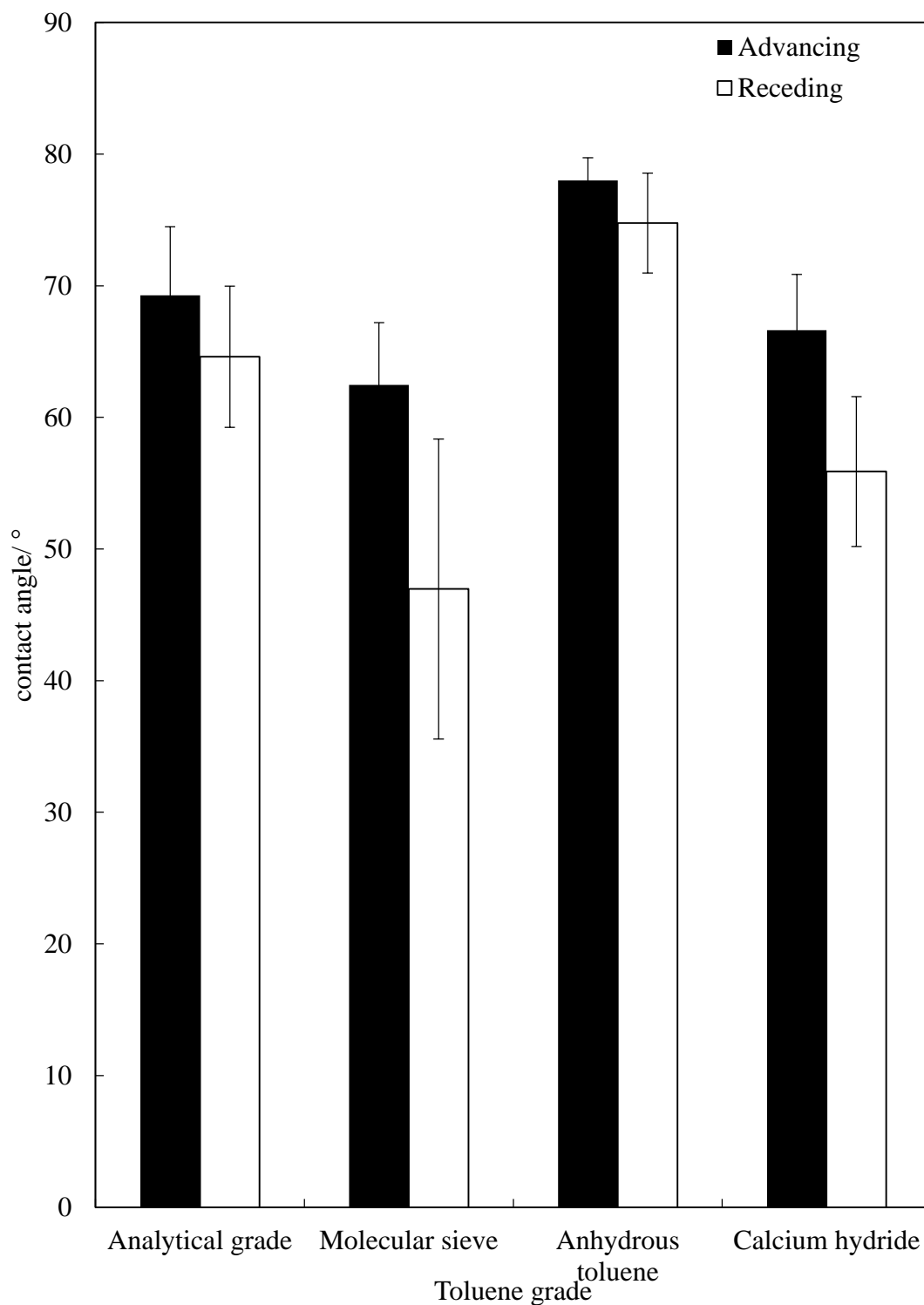
4.3.1.4   Effect of amine treatment prior to hydrophobisation

Much of the literature covering the area of fluorination of silica surfaces concerned the utilisation of amine based compounds as a precursor to addition of alkylchlorosilanes.[11-15] Most studies demonstrated that by exposing the surface to an amine for a period of time prior to the addition of the alkylchlorosilane, could enhance the grafting density of the silane to the surface. Tripp and Hair proposed a mechanism by which this process may occur (shown in Figure 4.4).

Figure 4.4.   Proposed mechanism of attachment by Tripp and Hair[15] of ammonia promoted attachment of trichlorosilane to silanol coated surface.
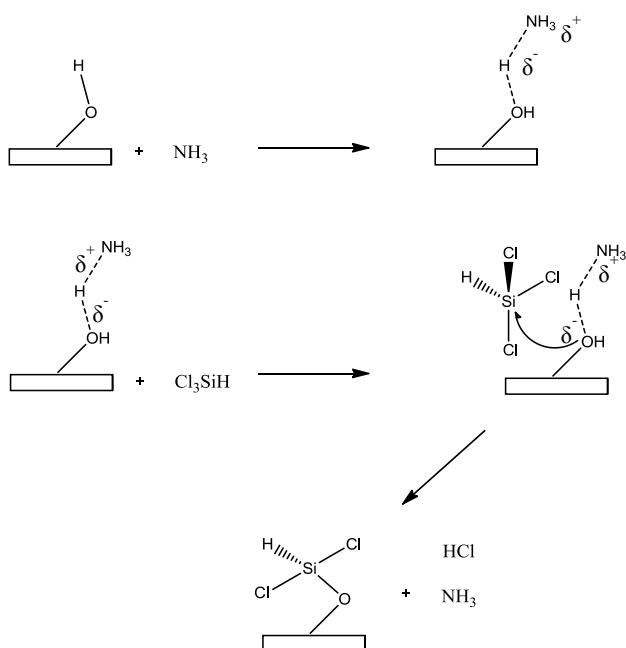

It can be seen in Figure 4.5 that the adsorption of ammonia to the surface silanol groups results in the oxygen of the hydroxyl becoming more nucleophilic, attracting the silicon of the trichlorosilane and promoting the formation of the siloxane bond. Kanan *et al.* have suggested that amines catalyse a direct reaction of alkoxysilanes with surface silanol groups[14] by using a two-step process. In the first step, the amine is exposed to the silica surface and forms a strong hydrogen bond, the vessel is then evacuated to remove any excess amine. In the second step, the incoming alkoxysilane reacts with the hydrogen bonded silanol groups, resulting in strong Si-O-Si linkages between the silane and the silica surface. Figure 4.5 shows the effect of pre-addition of 0.5 ml triethylamine, pyridine or ammonium hydroxide on the contact angle of glass slides treated with 1.3×10^{-3} M 1H, 1H, 2H, 2H-perfluorooctyldimethylchlorosilane and 1H, 1H, 2H, 2H-perfluorooctylmethyldichlorosilane for 72 hours.

The glass slides were exposed to 0.5 ml of the neat amine vapour for 1 hour in a sealed 120 cm^3 glass jar, ensuring the liquid did not directly contact the glass slides. The slides were then transferred to a separate glass jar containing the silane solution and allowed to react at ambient temperature for 72 hours.

It can be seen that in all cases except triethylamine, the pre-addition of an amine appears to enhance the grafting density of fluoroalkylchlorosilane to the glass slide surface, resulting in higher contact angle. Pyridine was shown to enhance the attachment of reagent to the surface most effectively, giving an increase in contact angle both fluoroalkylchlorosilanes of around 8-10°. Ammonium hydroxide was seen to have a modest effect in the case of the monochlorosilane, but a more pronounced effect in the case of the dichlorosilane, increasing the contact angle by around 14°.

Figure 4.5. Effect of pre-addition of amines in the vapour phase at a volume of 0.5 ml on the advancing contact angle of water sessile drop in air on slides reacted with 1.3×10^{-3} M of 1H, 1H, 2H, 2H-perfluorooctyldimethylchlorosilane and 1H, 1H, 2H, 2H-perfluorooctylmethyldichlorosilane for 72 hours. Error bars show standard deviation taken from an average of 9 measurements.
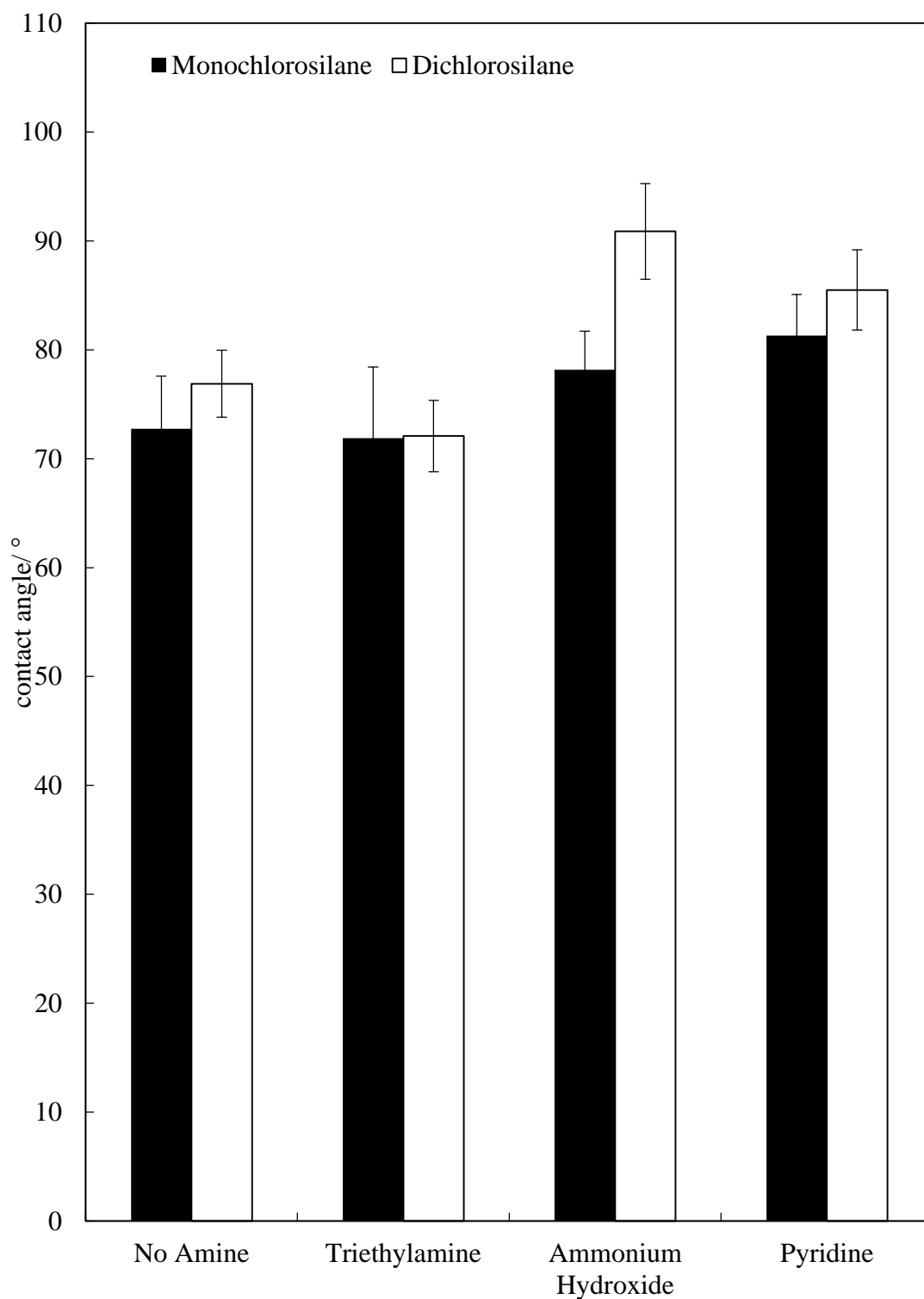
4.3.1.5 Effect of reaction time

Throughout the literature, and specifically in work by Fadeev and McCarthy[9,10] and Campos *et al.*[11] very long reaction times (up to 72 hours, or 3 days) have been specified as necessary to achieve maximum bonding densities of chloroalkylsilanes. It is suggested that reactions at the solid-solution surface are very slow in the later stages of the reaction and so to achieve maximum bonding density of silane to the solid surface, it is required to leave the reaction to proceed for a long time period. Figure 4.6 shows the effect of reaction time on the advancing contact angle of glass slides treated with 1H, 1H, 2H, 2H-perfluorooctyldimethylchlorosilane in bulk solution and the vapour phase.

It can be seen that maximum grafting density is achieved within 2 hours for the vapour phase, however the reaction between solution and solid surface is significantly slower, and maximum grafting density is observed after 24 hours, which is still faster than suggested in the literature. However for the nature of the current work, it was not necessary to achieve maximum grafting density, as the intention was to vary the contact angle.

To proceed, from the work carried out on optimising the reaction parameters it was decided to use the dichlorofluoroalkylsilane in anhydrous toluene over a range of concentrations, treated at 25°C (controlled) for two hours for surface silanisation of the silica particles. As mentioned previously, it was not necessary to achieve maximum bonding density, and this has been the intention of much of the literature presented to date. Therefore it was decided that no pre-addition of amine was required and that a two-hour treatment period was sufficient. A range of silica particles of varying hydrophobicity would be prepared and the hydrophobicity tailored by concentration of silane. The rate of silane reacting with the silica surface should be faster for more concentrated solutions, and so more silane should graft to the surface in the two-hour reaction period for more concentrated solutions.

Figure 4.6. Effect of reaction time on contact angle of 10 µl sessile water drop on glass slide hydrophobised with 6.8×10^{-4} M of 1H, 1H, 2H, 2H-perfluorooctyldimethylchlorosilane in anhydrous toluene or 0.5 ml neat reagent. Error bars show standard deviation from an average of 9 measurements.
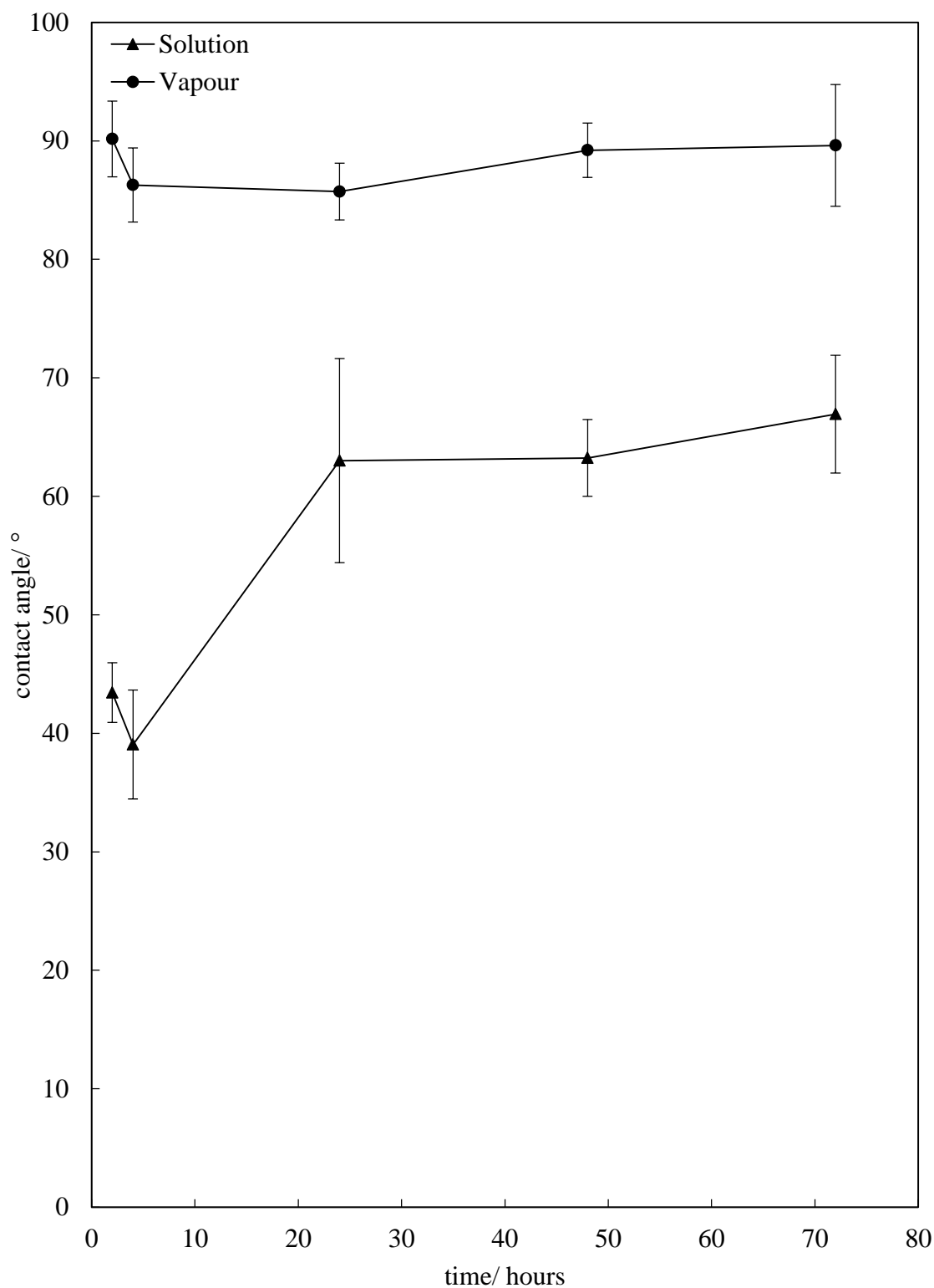
4.4 Contact angles of silica particles hydrophobised with fluorosilanes

The aim of this work was to produce a range of fluorinated particles with varying hydrophobicity and to then explore their behaviour at a liquid-air interface with reduced surface tension. The contact angle at the liquid-air interface of the particles prepared was measured directly using the film calliper method. Further exploration of the lateral interactions between particles spread at the liquid-air interface was explored by optical microscopy. Finally the colloidal systems generated by these particles were investigated by aerating under high shear conditions.

The particle contact angle is plotted as a function of the reagent concentration in Figure 4.7. It can be seen that the particle contact angle increases with increasing silane concentration and is significantly higher than that of raw silica particles ($19.4 \pm 4.7°$, dashed line on Figure 4.7). At concentrations of silane above 3.4×10^{-4} M the particle contact angle was not measurable by the film calliper method. The aqueous films broke immediately after particle bridging, thus indicating that the particles had contact angles above 90°, represented by the arrows on Figure 4.7.

This work concerns the behaviour of solid particles at air-liquid interfaces of varying surface tension and the purpose of investigating fluorinated particles was to explore their behaviour when ethanol is introduced into the aqueous phase. Therefore, the particle contact angle in the presence of ethanol in the aqueous phase was measured. The results obtained are shown in Figure 4.8. Where a continual reduction in particle contact angle for both unhydrophobised and hydrophobised silica particles is seen as the concentration of ethanol in the continuous phase is increased. A similar trend to that in Figure 4.8 has been observed for the contact angle of polystyrene latex particles. Hence the addition of ethanol to the aqueous phase leads to a significant reduction of the contact angle, thus making the particles more hydrophilic. This is clearly seen in Figure 4.7 for the silica particles hydrophobised with different concentrations of fluorosilane. The addition of 15 wt. % ethanol to the water phase has reduced the contact angle of silica particles of varying hydrophobicity including those having contact angles above 90°. For example, the contact angle of silica particles hydrophobised at 6.8×10^{-4} M was decreased from above 90° in pure water to 74.1° with addition of 15 wt. % ethanol.

It is known from the work of Koretsky and Kruglyakov[16] and more recently, Levine *et al.*[17] that the minimum energy of particle detachment from the air-liquid interface into either the water (equation 4.2) or air phase (equation 4.3) can be given by:

$$\Delta G_{dw} = \pi r^2 \gamma_{la} (1 - cos\theta)^2 \tag{4.2}$$

$$\Delta G_{da} = \pi r^2 \gamma_{la} (1 + cos\theta)^2 \tag{4.3}$$

where *r* is the particle radius, γ_{la} is the surface tension of the liquid-air interface and θ is the three-phase particle contact angle. Equations 4.2 and 4.3 can be combined to give:

$$\Delta G_d = \pi r^2 \gamma_{la} (1 - |cos\theta|)^2 \tag{4.4}$$

It is therefore possible to calculate the energy of particle detachment from the interface as a function of contact angle, and of surface tension of the aqueous phase. This is shown as a function of contact angle of the particles measured in pure water in Figure 4.9. There is a clear increase in the minimum energy of particle detachment from the interface as the contact angle is increased. This is supported throughout the literature[18,19] and it is understood with confidence that the minimum energy of detachment of particles from a fluid-fluid interface passes through a maximum at 90°.[1] Additionally, the minimum energy of particle detachment as a function of surface tension of the aqueous phase is shown in Figure 4.9 for particles treated with 6.8×10^{-6} M of fluorosilane. It can be seen that as the surface tension of the system is increased, the energy of particle detachment is also increased. This is in keeping with findings of Davies *et al.* who found that detachment energy of a neutrally wetting particle ($\theta = 90$) increased as the surface tension of a liquid-liquid interface increased.[20] It is important to note however that despite the energy of detachment from the interface being reduced when the particle contact angle is reduced; the energy of detachment is still many orders of magnitude larger than the thermal energy (kT) and so will not affect the strength of attachment over the range discussed.

Figure 4.7. Particle contact angle at aqueous ethanolic-air interface as a function of 1H, 1H, 2H, 2H-perfluorooctylmethyldichlorosilane concentration. Particles are 2 μm diameter monodisperse silica treated at $24 \pm 0.1°C$ for two hours, measured using film calliper method. Error bars show standard deviation of at least 70 individual particle measurements. Dashed line indicates contact angle of unhydrophobised silica particle ($19.4 \pm 4.7°$) and arrow indicates a contact angle of over 90°.
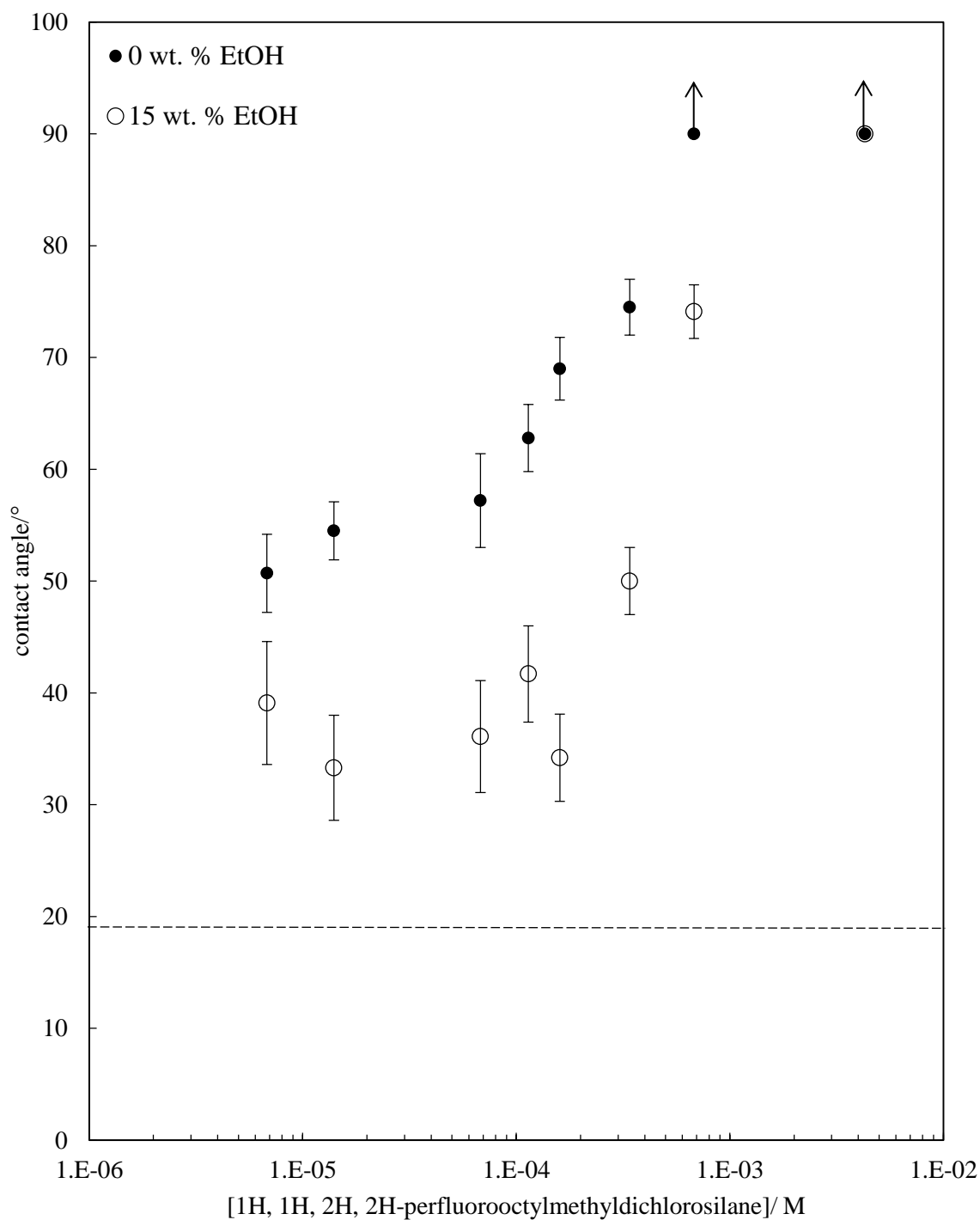
Figure 4.8. Particle contact angle at the air-water interface as a function of ethanol concentration. Particles are 2 μm diameter monodisperse silica before (squares) and after (triangles) treatment with 1H, 1H, 2H, 2H-perfluorooctylmethyldichlorosilane and 2.9 μm diameter sulfate latex particles. Particles measured using film calliper method. Error bars show standard deviation of at least 70 individual particle measurements.
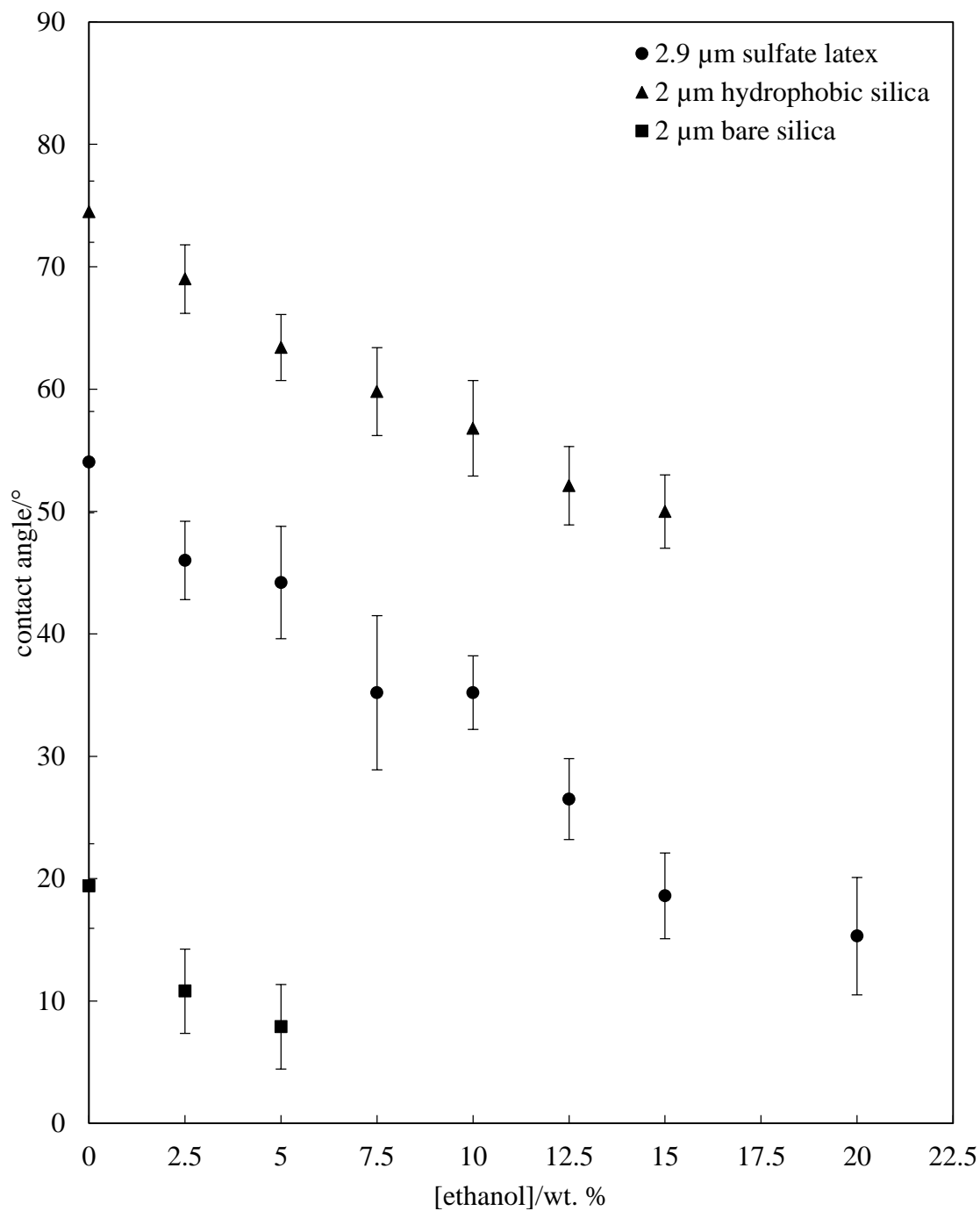
Figure 4.9. Minimum energy of detachment of a 2 μm diameter silica particle treated with 1H, 1H, 2H, 2H-perfluorooctylmethyldichlorosilane as a function of contact angle of the particle at an air-water interface. Calculated from Equation 4.4.
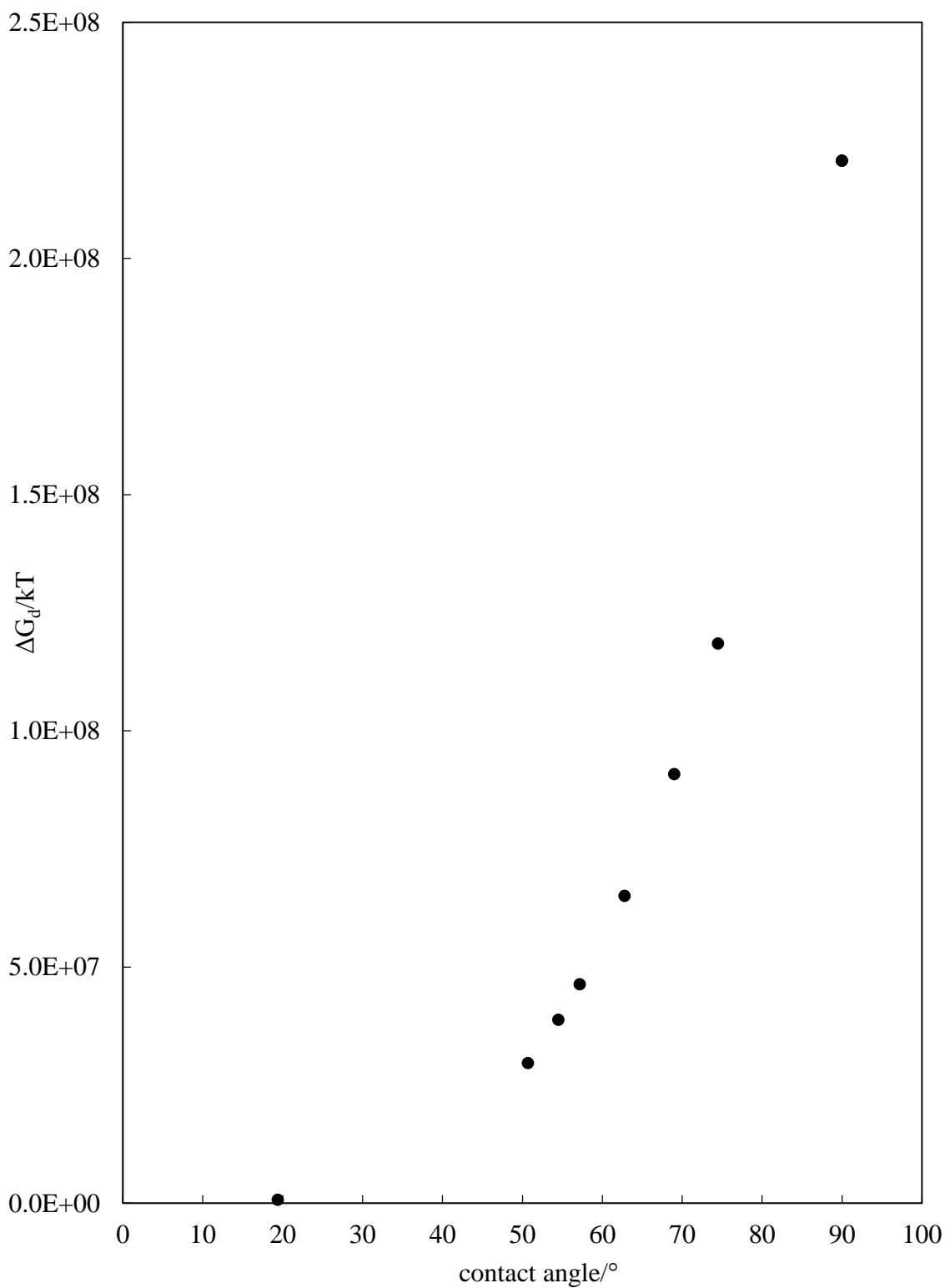
Figure 4.10. Minimum energy of detachment of a 2 µm diameter silica particle treated with 1H, 1H, 2H, 2H-perfluorooctylmethyldichlorosilane as a function of surface tension of the particle at an aqueous ethanol-air interface. Calculated from equation 4.4.
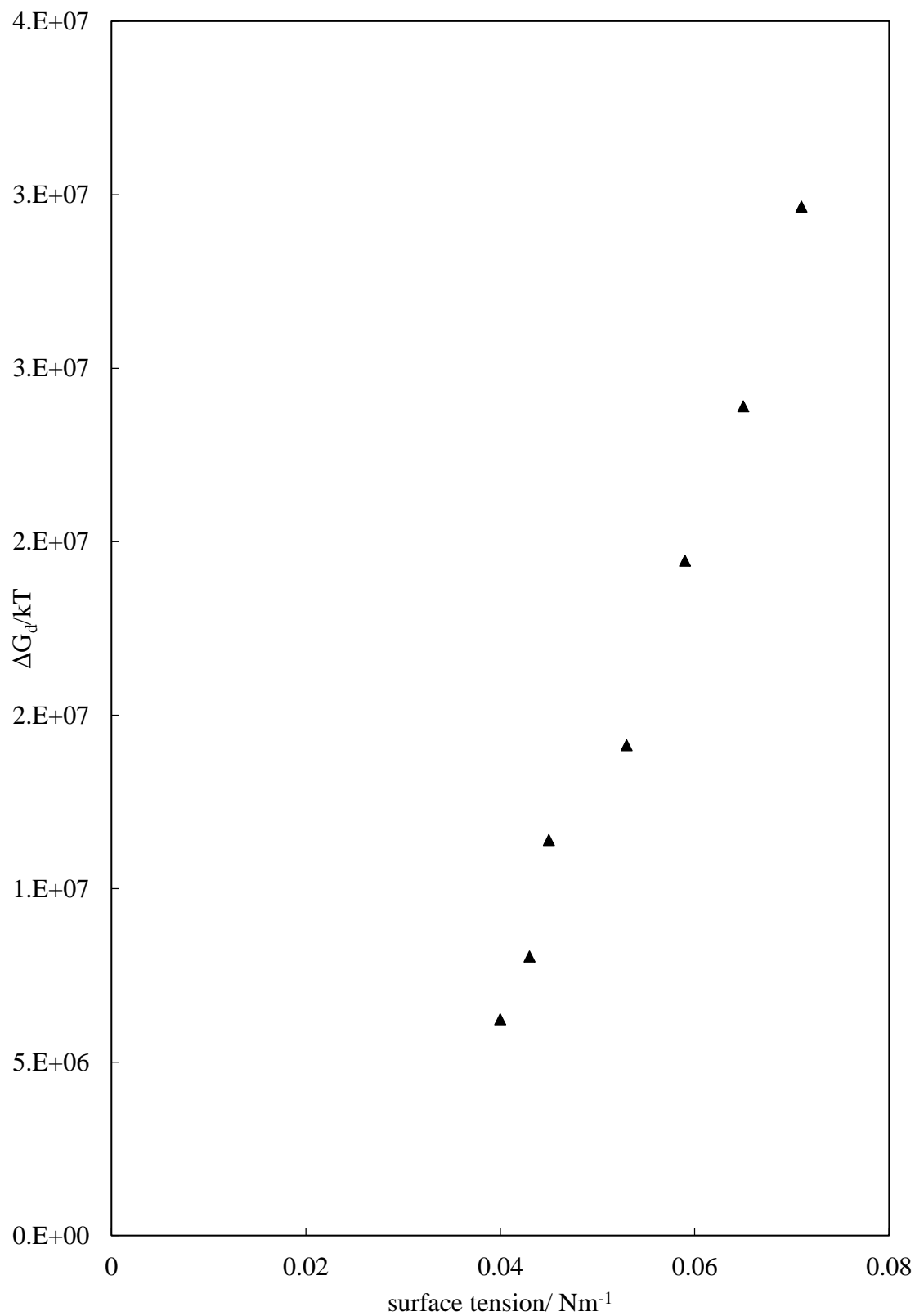
4.4.1 Behaviour of particles at planar air-water interfaces

The behaviour of particles spread at a planar air-water interface was investigated by optical microscopy. Particle dispersed in a spreading suspension (2 wt. % particles in 50:50 methanol:water) were spread at the interface in relatively dilute amounts (25 µl) in a small dish containing water and their behaviour at the interface observed. Optical microscopy images of the particle monolayers with increasing particle hydrophobicity are shown in Figure 4.12. It is seen that the particles with contact angles smaller than 90° form large aggregates at the interface (a-f). The monolayers of particles with contact angles above 90° are less aggregated (g, h). There are a significant number of single particles which show some degree of ordering, better seen in Figure 4.12 (h). This suggests that there is significant long-range repulsion between hydrophobic particles with contact angles larger than 90°. Similar behaviour of silica particles hydrophobised with dichlorodimethylsilane to different extents has been observed by Horozov *et al.* at the octane-water interface.[21] They found disordered, aggregated monolayers of particles with contact angles less than 115°, but well-ordered monolayers of very hydrophobic particles with contact angles larger than 115°.

Strong repulsion between very hydrophobic silica particles at the air-water interface has also been reported by Horozov and Binks.[22] Well-ordered particle monolayers stable against aggregation were observed and the interparticle distances were larger than three particle diameters. The strong long-range repulsion between very hydrophobic particles has been attributed to residual charges at the particle-oil (air) interface, leading to unscreened Coloumbic repulsion through the non-polar phase (oil or air).[23,24] An alternative explanation for the long-range repulsion between latex particles at the air-water interface was suggested by Pieranski,[25] who observed so called "two dimensional colloidal crystals" of polystyrene latex spheres trapped at an air-water interface and suggested that the asymmetric electric double layer around the particle surface in contact with the water created an effective dipole. The electric dipoles from adjacent particles interact through the non-polar phase (air) thus leading to long-range unscreened electrostatic repulsion between particles.

Horozov *et al.* observed only a weak short-range repulsion between partially hydrophobic silica particles at the octane-water interface.[26] The repulsion was mediated through the water because it disappeared by adding even small amounts of electrolyte to the water phase. In contrast, the long-range order of the monolayers of very hydrophobic silica particles at the octane-water interface has not been affected even when 1 M NaCl was present in the water. They concluded that the electrostatic repulsion between very hydrophobic particles is mediated through the non-polar oil phase. These two extreme cases are illustrated in Figure 4.11.

Figure 4.11. Schematic diagram showing the origin and strength of electrostatic interactions between hydrophilic particles (left) and hydrophobic particles (right).

Short-range repulsion (through water)   Long-range repulsion (through air)

Hydrophilic   Hydrophobic particles
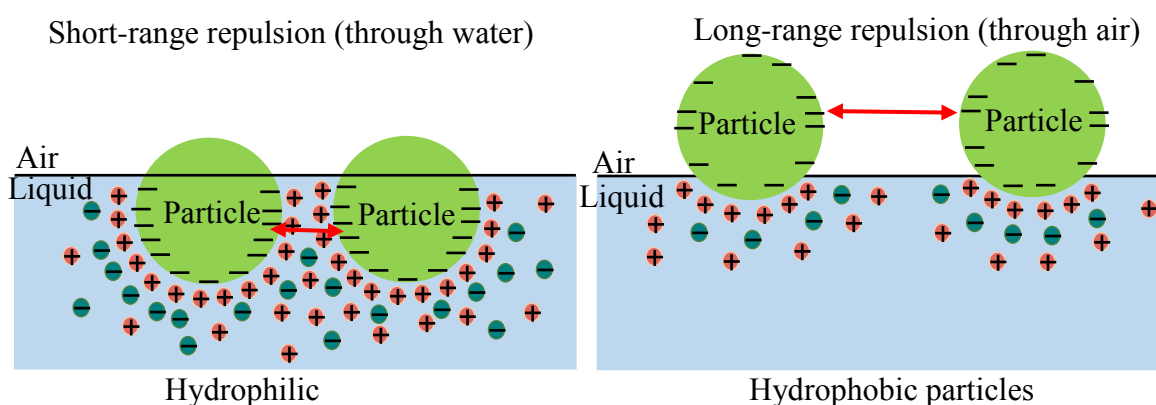
Figure 4.12. Optical microscopy images of 2 wt. % particle suspension spread (25 µl) at horizontal air-water interface with increasing hydrophobicity. Particles are 2 µm diameter silica particles treated with 1H, 1H, 2H, 2H-perfluorooctylmethyldichlorosilane. (a) 6.8×10^{-6} M, $\theta = 51 \pm 3°$ (b) 1.4×10^{-5} M, $\theta = 54 \pm 3°$ (c) 6.8×10^{-5} M, $\theta = 57 \pm 4°$ (d) 1.14×10^{-4} M, $\theta = 63 \pm 3°$ (e) 1.6×10^{-4} M, $\theta = 69 \pm 3°$ (f) 3.4×10^{-4} M, $\theta = 74 \pm 2°$ (g) 6.8×10^{-4} M, $\theta \geq 90°$ (h) 4.3×10^{-3} M, $\theta \geq 90°$. Scale bar corresponds to 30 µm.
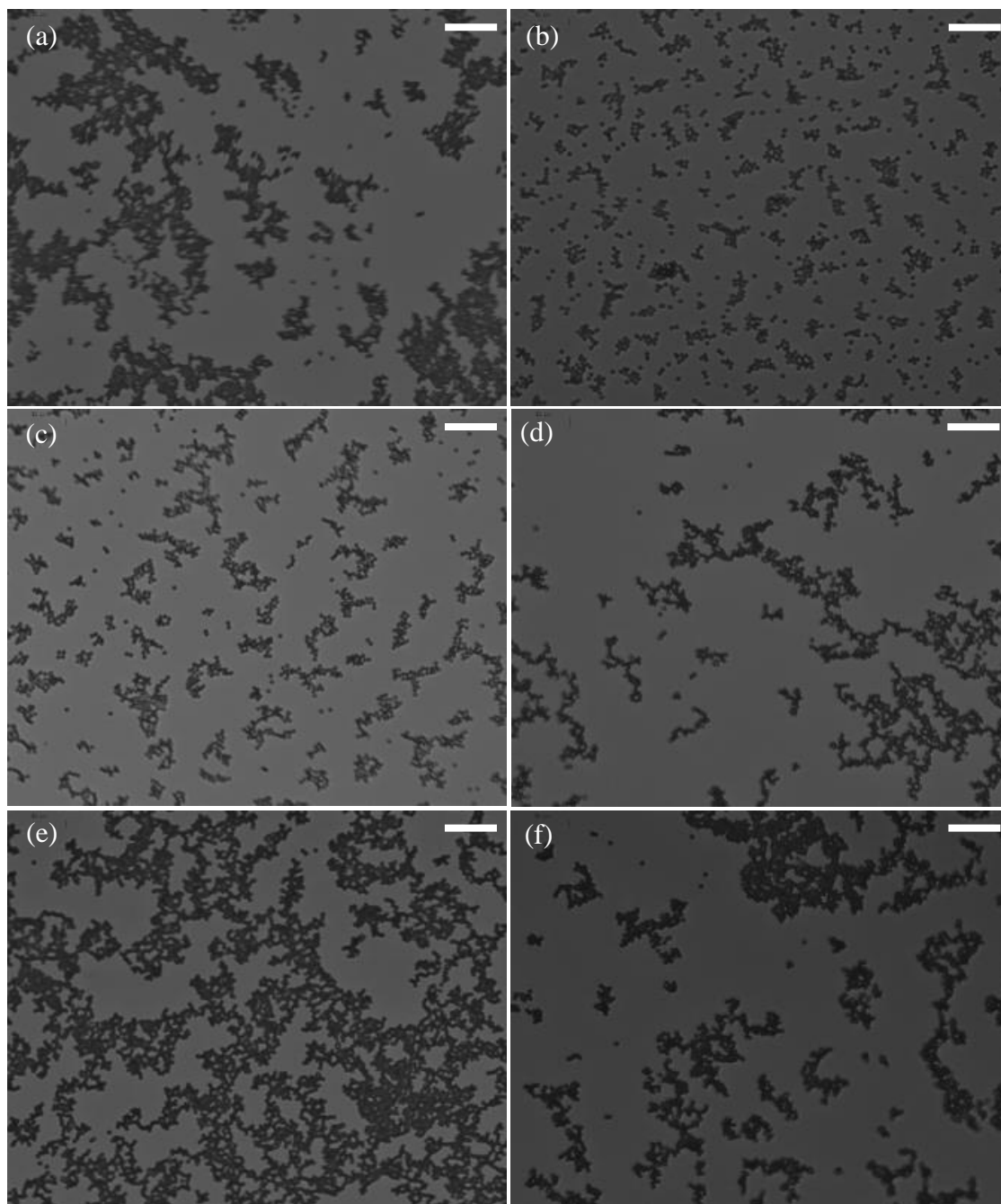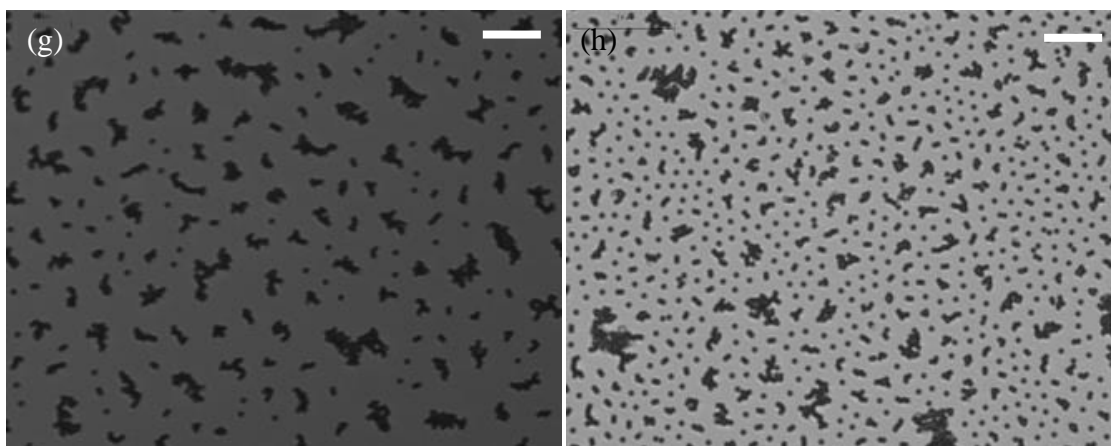
To investigate the effect of the solvent on interactions across the horizontal air-water interface, the concentration of ethanol in the aqueous phase was increased from 0-15 wt. %. Corresponding film calliper measurements on these particles demonstrate that increasing the concentration of ethanol in the aqueous phase effects a reduction in the particle contact angle. Therefore, it is expected that the repulsion due to residual charges at the particle-air interface (Figure 4.11, right) will be reduced because a smaller portion of the particle surface will be exposed to the air.

Optical microscopy of the particles investigated are shown in Figure 4.13. For the least hydrophobic particles (6.8×10^{-6} M) over a range of ethanol concentrations (0-7.5 wt. % EtOH) it was seen that at low ethanol concentrations, the particles aggregated heavily at the interface. As the concentration of ethanol was increased the particles became better dispersed in the aqueous phase but the particle layer was not stable. It was not possible to obtain images above 7.5 wt. % ethanol as the particles moved too fast for the camera to obtain clear images. Focusing on the particles at the interface also became challenging. Images of the two most hydrophobic particles spread in 15 wt. % ethanol are shown in Figure 4.13 (d) and (e). It can be seen that although there are areas of the monolayer where the particles are heavily aggregated, there was still ordering and long-range repulsion between particles. Contact angles of particles hydrophobised with 6.8×10^{-4} M and 4.3×10^{-3} M in 15% ethanol were 74.1° and ≥90°, respectively. Contact angle measurements as a function of ethanol concentration showed a continual decrease in the particle contact angle with increasing ethanol concentration, indicating the particles became more wetted at higher ethanol concentrations. The particle aggregation at higher ethanol concentrations can be justified by the reduced contact angle; more of the particle surface is immersed in the liquid, and therefore any inter-particle repulsion may be screened by counter-ions in solution.

Figure 4.13. Optical microscopy images of a 2 wt. % particle suspension spread (25 µL) at a horizontal air-aqueous ethanol interface. Particles are 2 µm diameter silica particles hydrophobised to varying extents with 1H, 1H, 2H, 2H-perfluorooctylmethyldichlorosilane. (a) 6.8×10^{-6} M in 7.5 wt. % ethanol, $\theta = 45 \pm 6°$ (b) 1.14×10^{-4} M in 15 wt. % ethanol, $\theta = 42 \pm 4°$ (c) 3.4×10^{-4} M in 15 wt. % ethanol, $\theta = 50 \pm 3°$ (d) 6.8×10^{-4} M in 15 wt. % ethanol, $\theta = 74 \pm 2°$ (e) 4.3×10^{-3} M in 15 wt. % ethanol, $\theta \geq 90°$. Scale bar corresponds to 30 µm.
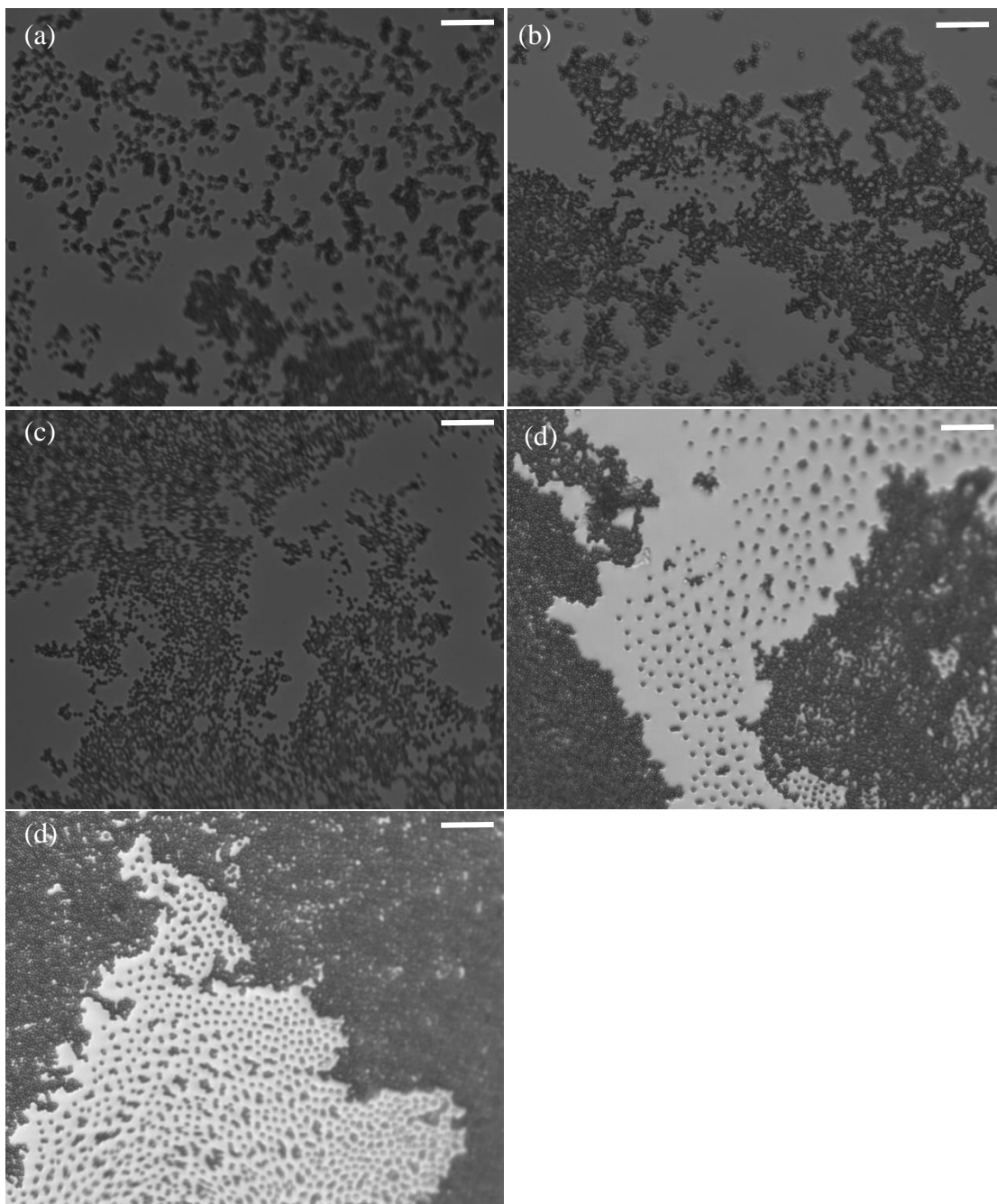
4.5   Foaming of aqueous suspensions of fluorinated silica particles

It is known that particle-stabilised foams exhibit a significant enhancement in stability. Some studies have reported long-term stability of particle-stabilised foams of over a year. The foaming properties of the fluorinated silica particle suspensions in pure water, and then with the addition of 15 wt. % ethanol to the aqueous phase was investigated. This concentration of ethanol was selected as this was the maximum concentration of ethanol with which it was possible to measure the particle contact angles (thin film was unstable above concentrations of 15 wt. %).

4.5.1   Foaming of particle suspensions in pure water

The foaming behaviour of fluorinated particle suspensions was examined by dispersing 5 wt. % particles in 5 ml water with an ultrasound bath for five minutes. The suspensions were then aerated by homogenisation with an Ultra-Turrax homogeniser (8 mm head, 13'000 r.p.m.) for a total of 60 seconds. Particles with lower hydrophobicity were completely dispersed in water while those hydrophobised with a concentration of silane above 6.8×10^{-5} M were seen to sit on top of the fluid and not disperse at all. After homogenisation, the height of the layer formed on top of the particle suspension was recorded and measured at regular time intervals. In some cases (at low particle hydrophobicity) the top layer was found to be foam. However, with more hydrophobic particles, an inverted powder-like material was formed on top of the liquid layer. As the foam volume was very small, the foam volume was calculated by analysing the images with Image-J software. Images of the suspensions immediately after aeration and 24 hours after aeration are shown in Figures 4.14 and 4.15, respectively.

The initial volume of foam as a function of silane concentration (particle hydrophobicity) is shown in Figures 4.18, 4.19 and 4.20. It can be seen that as the particle hydrophobicity increases there is a general trend for an increase in the foam volume, although as can be seen from the two repeats carried out, the foam volumes are irreproducible. Above a silane concentration of 3.4×10^{-4} M (corresponding to a particle contact angle of 74.5°) a phase inversion of the system was observed, from an air-in-water (foam) system to a water-in-air (or so-called "dry water") system. Phase inversion was observed in both samples.

This is due to the increased hydrophobicity of the particles causing an inversion of the curvature of the air-water interface to accommodate the increased particle contact angle. It is unusual for the inversion of the curvature of the interface to be effected by a particle contact angle lower than 90°. A possible explanation for this is that the contact angle measured by the film calliper method is actually closer to the receding contact angles than the equilibrium contact angle, and there may be a significant contact angle hysteresis for the particles measured. Therefore, the equilibrium particle contact angles may be higher than the values obtained from the film calliper method. It is clear from cryo-SEM images in Figure 4.17 that for particles with low contact angles, foams with monolayers of particles at their interfaces can be seen. At higher contact angles (particles treated with 3.4×10^{-4} M and above), drops of water-in-air coated by a single layer of particles can be observed. Optical microscopy of the top layer is shown in Figure 4.16. The bubbles have a textured dimpled surface indicative of particle adsorption, further supported by the cryo-SEM images.

An interesting feature of these particle-stabilised foams is their instability relative to particle-stabilised foams reported in the literature and in Chapter 3 of this work. Particle-stabilised foams are known to have long-term stability of many months or even years. All of the foams produced here had fully collapsed within 10 days. Even after 24 hours a visible coarsening of the foam layers can be seen (Figure 4.15). Work by Abkarian *et al.* investigated the stabilising effects of particles adsorbed to air bubble surfaces and the role of particles in halting the dissolution of bubbles into the aqueous phase. The researchers used surface evolver calculations of negatively charged latex particles[27] at an air-water interface. It was shown that as time progresses after aeration had elapsed, the bubbles deform from spherical shapes to form multi-faceted structures as a result of losing gas from areas of the interface uncovered, these non-spherical bubbles remain stable to further dissolution. This multi-faceted structure results in and overall mean curvature of the bubble becoming zero; zero mean curvature is a consequence of the fluid-fluid interface around each particle surface being deformed to a saddle-shape. The zero mean curvature of the system causes the Laplace pressure of the bubbles to become zero, and therefore the driving force for bubble dissolution is arrested. Therefore the stability of foam bubbles against disproportionation is due to (i) the strong particle attachment to the bubble surface and (ii) vanishing Laplace pressure because of the zero mean curvature of the liquid interface between particles on the bubble surface due to the reduction of the bubble volume resulting from gas dissolution.

The first requirement is very important because the bubble shrinking generates significant mechanical stresses in the particle monolayer covering the bubble. The results presented here suggest that the particles have been gradually expelled from the surface of the shrinking bubbles resulting in poor stability of the foams against disproportionation. This is supported by the fact that faceting of the bubbles was not observed. Ejection of solid particles from particle monolayers during their compression in a Langmuir trough has also been reported in the literature.[28] Although the energy of particle detachment (ejection) from the air-water interface is large for micron sized particles, the mechanical stress in the compressed particle monolayer is not homogenous and its local values may exceed that required for particle ejection if the cohesion with the surrounding particles is not very strong. These hypotheses require further investigation in order to reveal the factors behind the poor stability of foams observed in the present study.
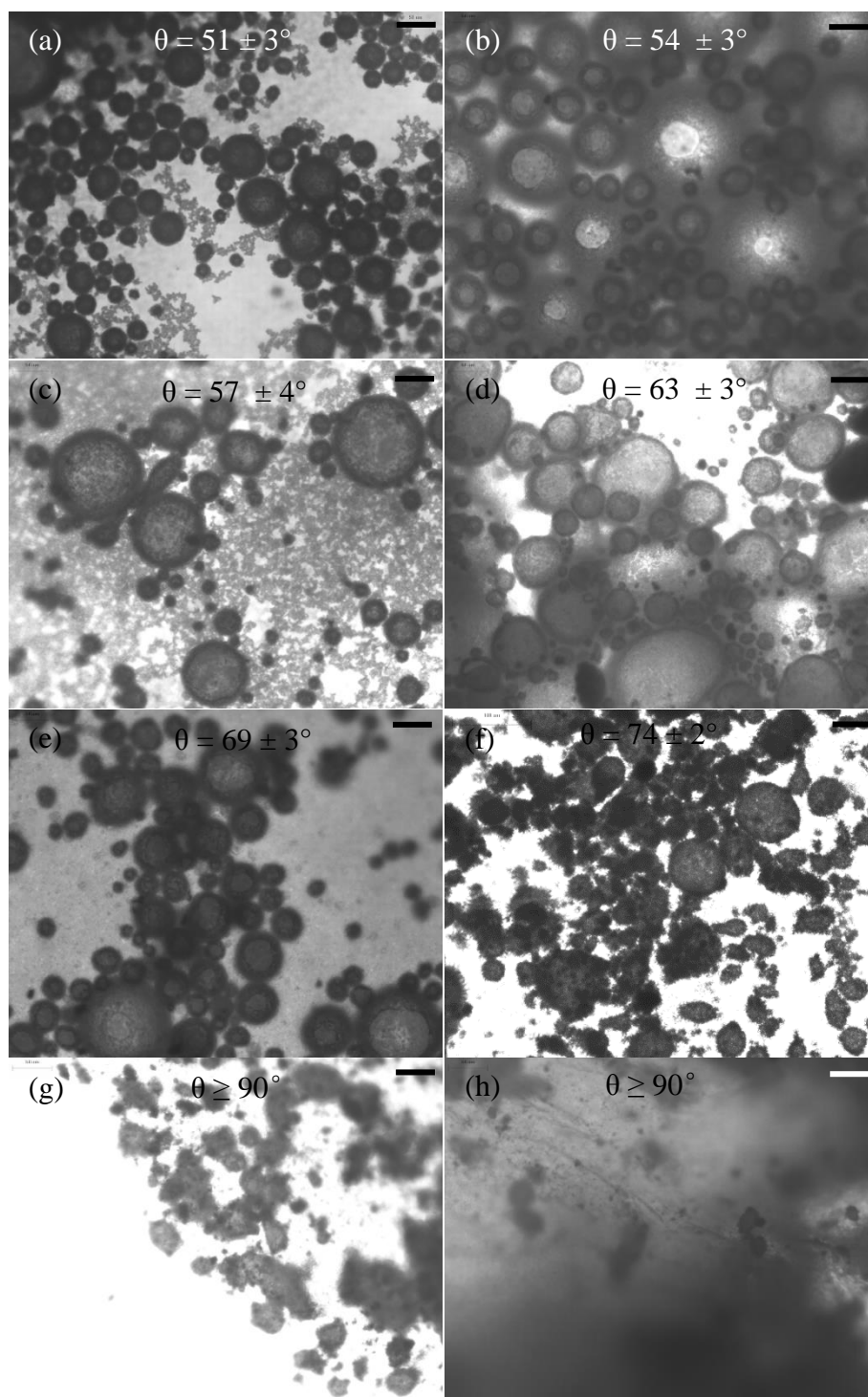
Figure 4.14. Images of aerated particle suspensions generated with 5 wt. % 2 µm diameter silica particles (hydrophobised to varying extents with 1H, 1H, 2H, 2H-perfluorooctylmethyldichlorosilane) in 5 ml water. Suspensions aerated for 60 seconds by homogenisation. Images taken using a Canon EOS450D camera at t=0.
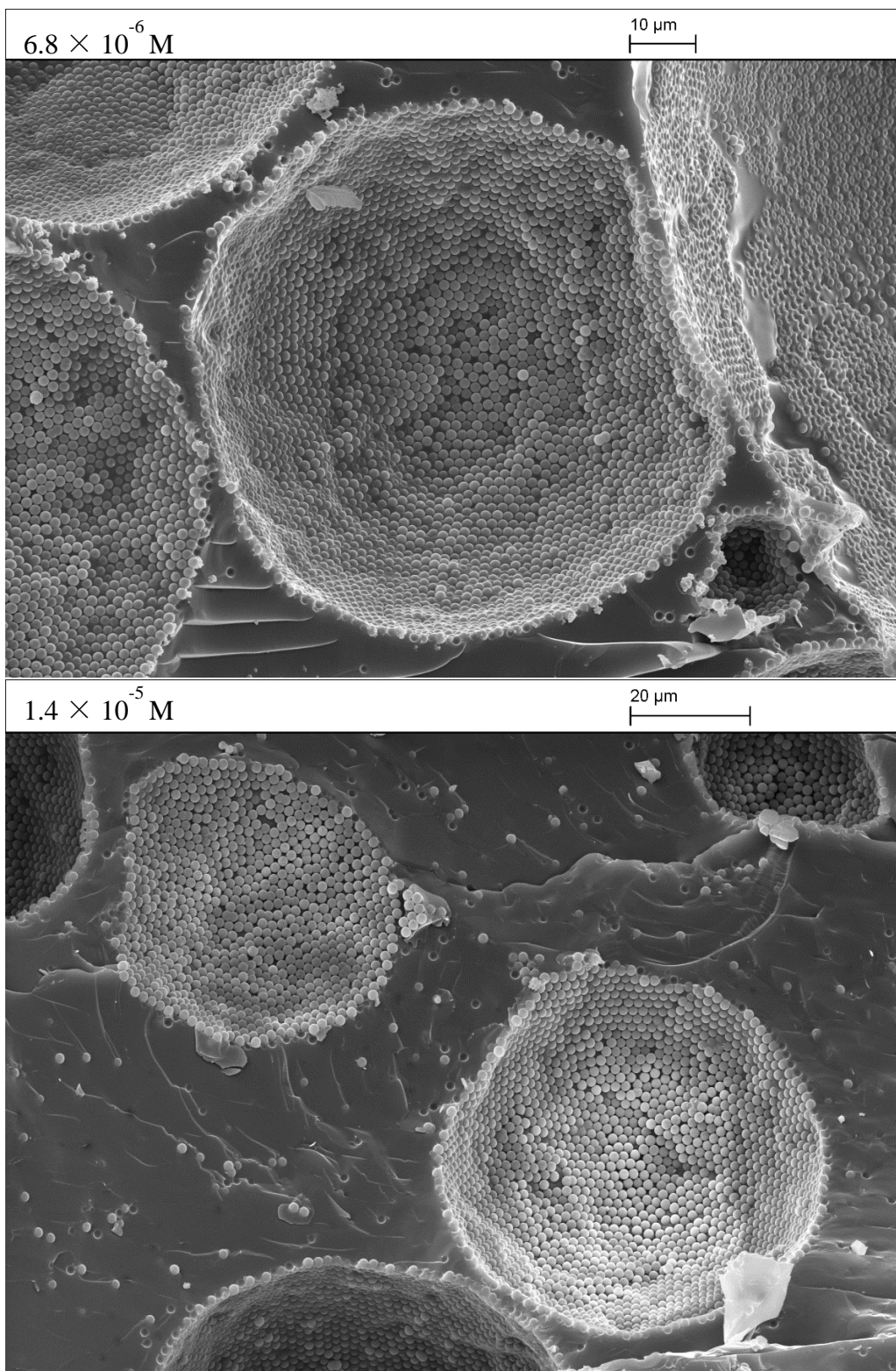
Figure 4.15. Images of aerated particle suspensions generated with 5 wt. % 2 µm diameter silica particles (hydrophobised to varying extents with 1H, 1H, 2H, 2H-perfluorooctylmethyldichlorosilane) in 5 ml water. Suspensions aerated for 60 seconds by homogenisation. Images taken using a Canon EOS450D camera at t=24 hours.
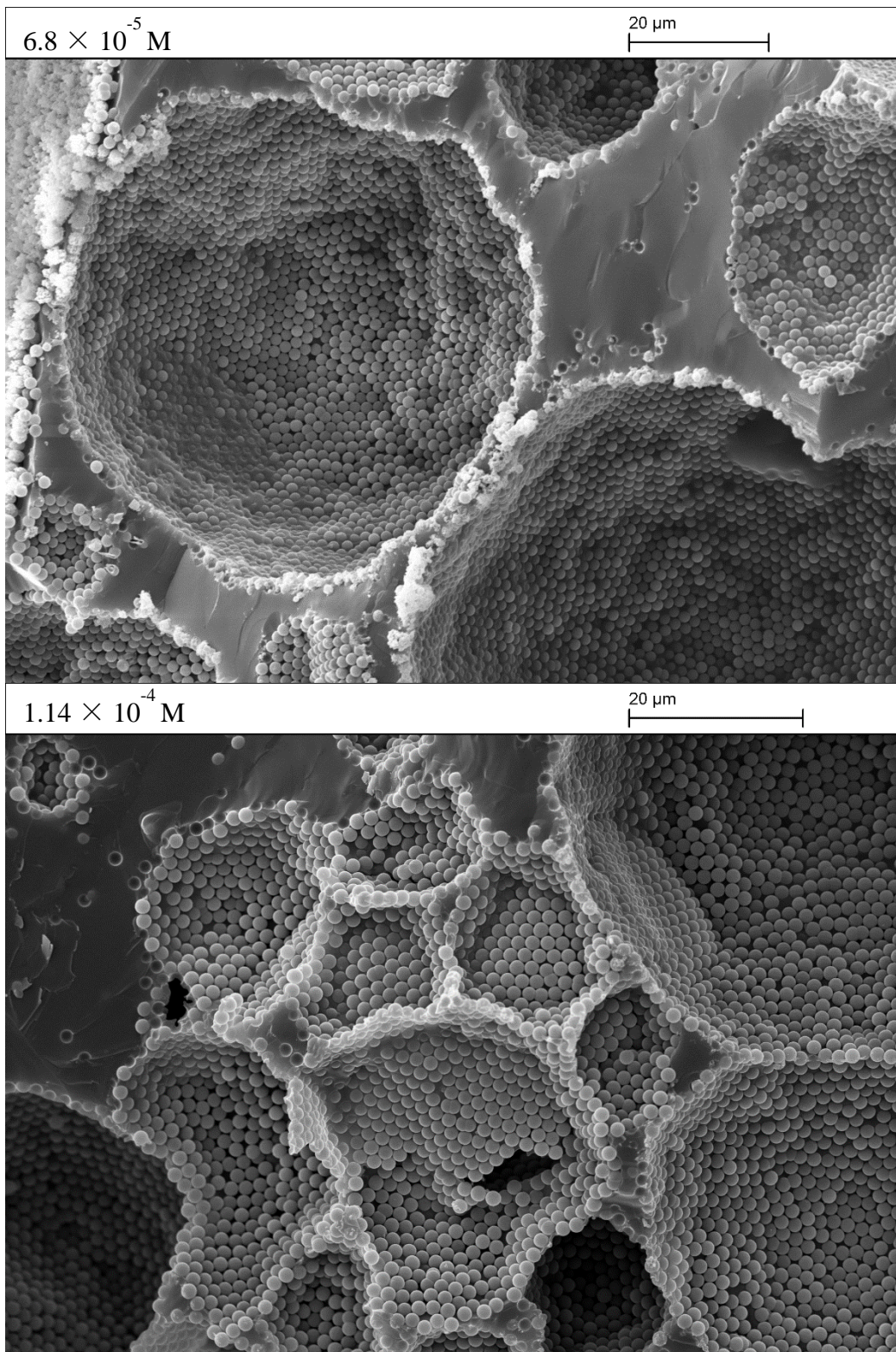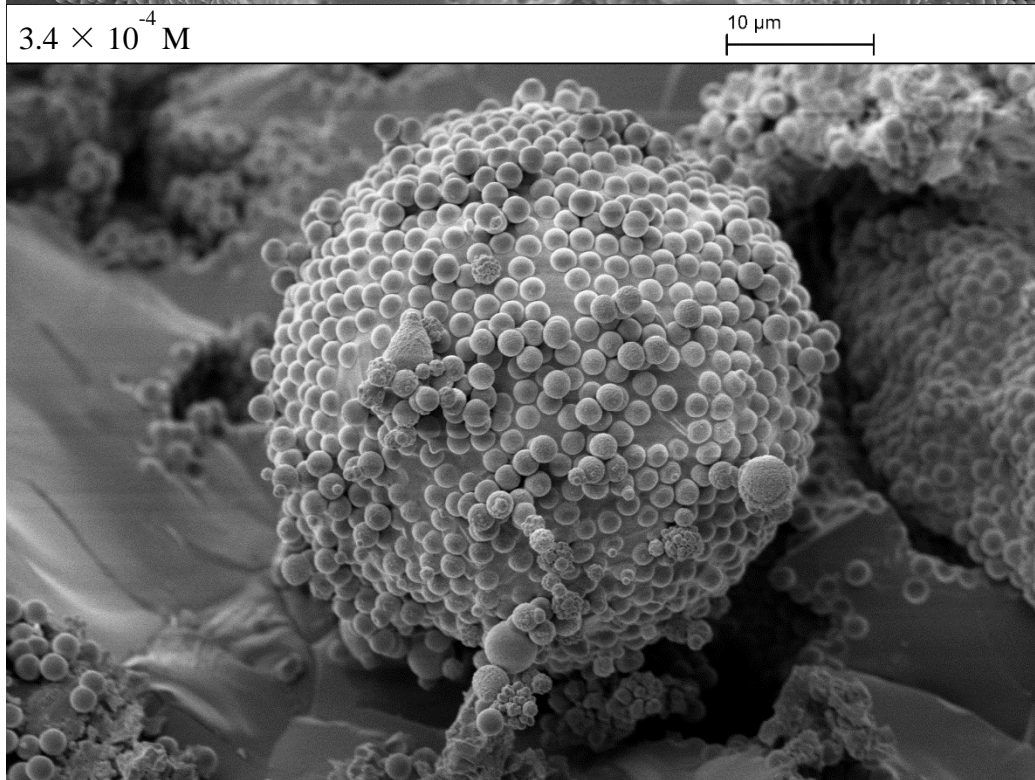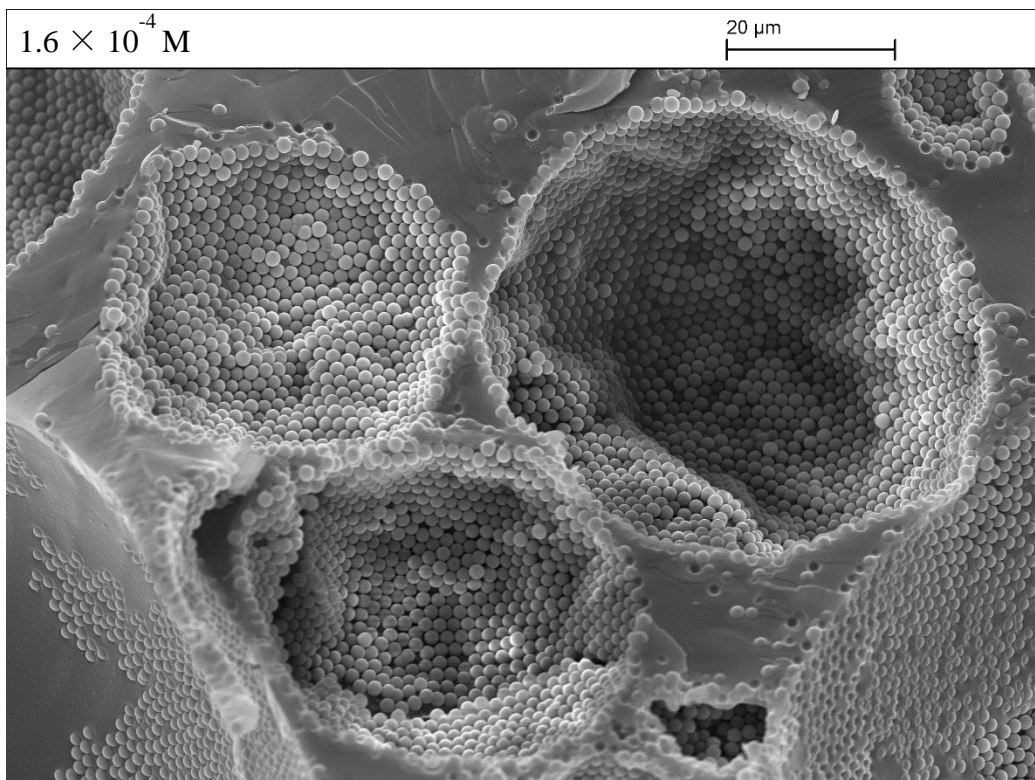
Figure 4.16. Optical microscopy of aerated particle suspensions of 5 wt.% 2 μm diameter silica particles (hydrophobised to varying extents with 1H, 1H, 2H, 2H-perfluorooctylmethyldichlorosilane) in 5 ml water. Suspensions aerated for 60 seconds by homogenisation. Images taken within 5 minutes of aeration. (a) 6.8×10^{-6} M, (b) 1.4×10^{-5} M, (c) 6.8×10^{-5} M, (d) 1.14×10^{-4} M, (e) 1.6×10^{-4} M (f) 3.4×10^{-4} M, (g) 6.8×10^{-4} M and (h) 4.3×10^{-3} M. Scale bar corresponds to 50 μm.
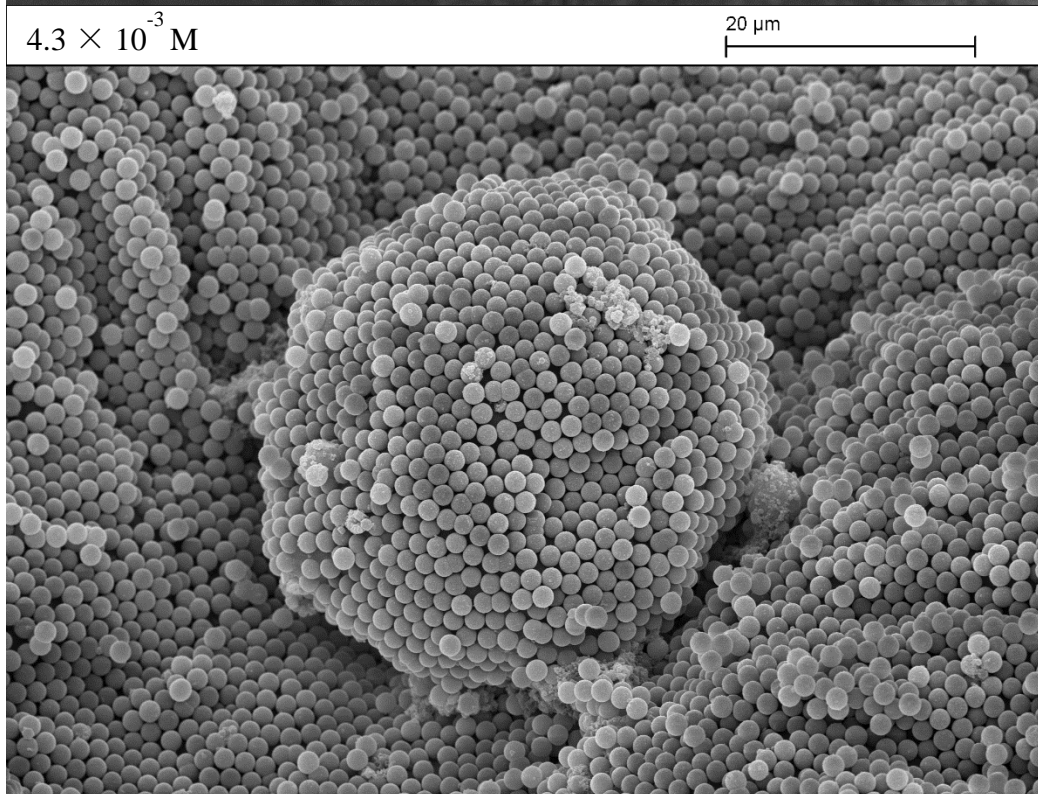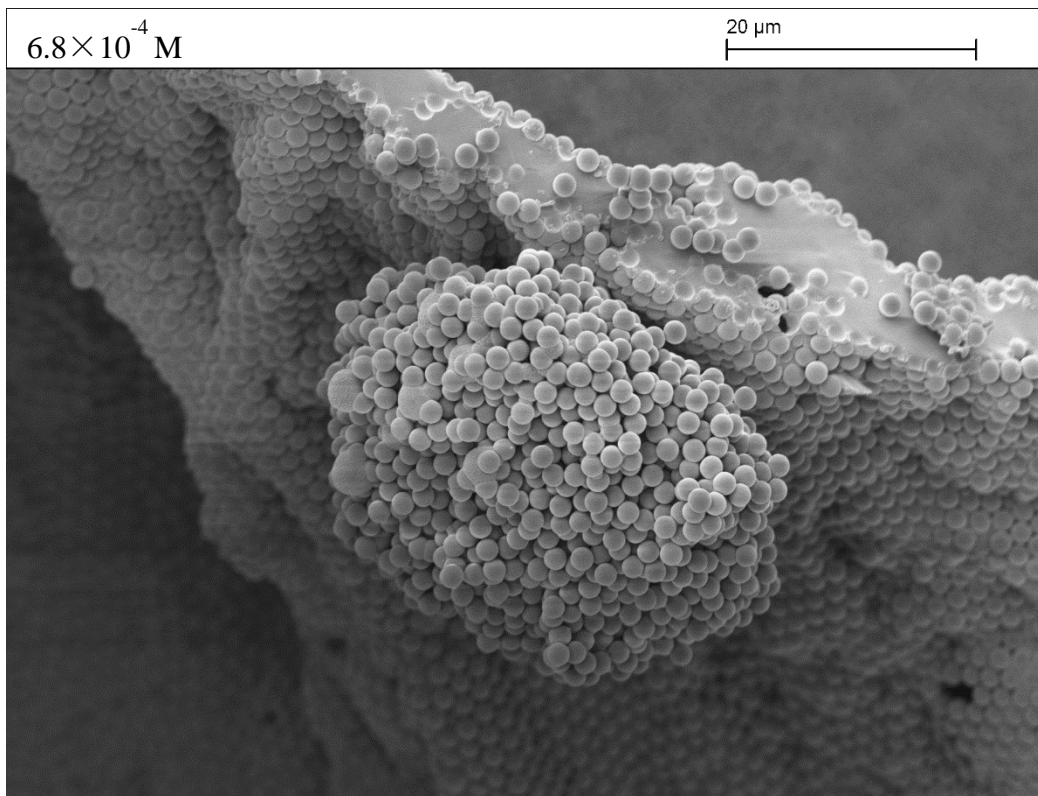
Figure 4.17. Freeze-fracture cryo-SEM images of aerated particle suspensions generated with 5 wt. % 2 μm diameter silica particles (hydrophobised to varying extents with 1H, 1H, 2H, 2H-perfluorooctylmethyldichlorosilane) in 5 ml water. Suspensions aerated for 60 seconds by homogenisation. Samples frozen within 15 minutes of aeration. All cryo-SEM carried out by Tony Sinclair at The University of Hull, U.K.

6.8 × 10^{-5} M   20 μm

1.14 × 10^{-4} M   20 μm

1.6 × 10^{-4} M   20 µm

3.4 × 10^{-4} M   10 µm

190

6.8×10^{-4} M   20 µm

4.3 × 10^{-3} M   20 µm

Figure 4.18. Foam volume as a function of particle hydrophobicity of aerated particle suspensions with 5 wt. % 2 μm diameter silica particles (hydrophobised to varying extents with 1H, 1H, 2H, 2H-perfluorooctylmethyldichlorosilane) in 5 ml water. Samples homogenised for 60 seconds. Foam volume at t = 0 and t =24 h are shown. Run 1 of 2 repeats shown. Error bars show maximum and minimum values from 2 repeats.
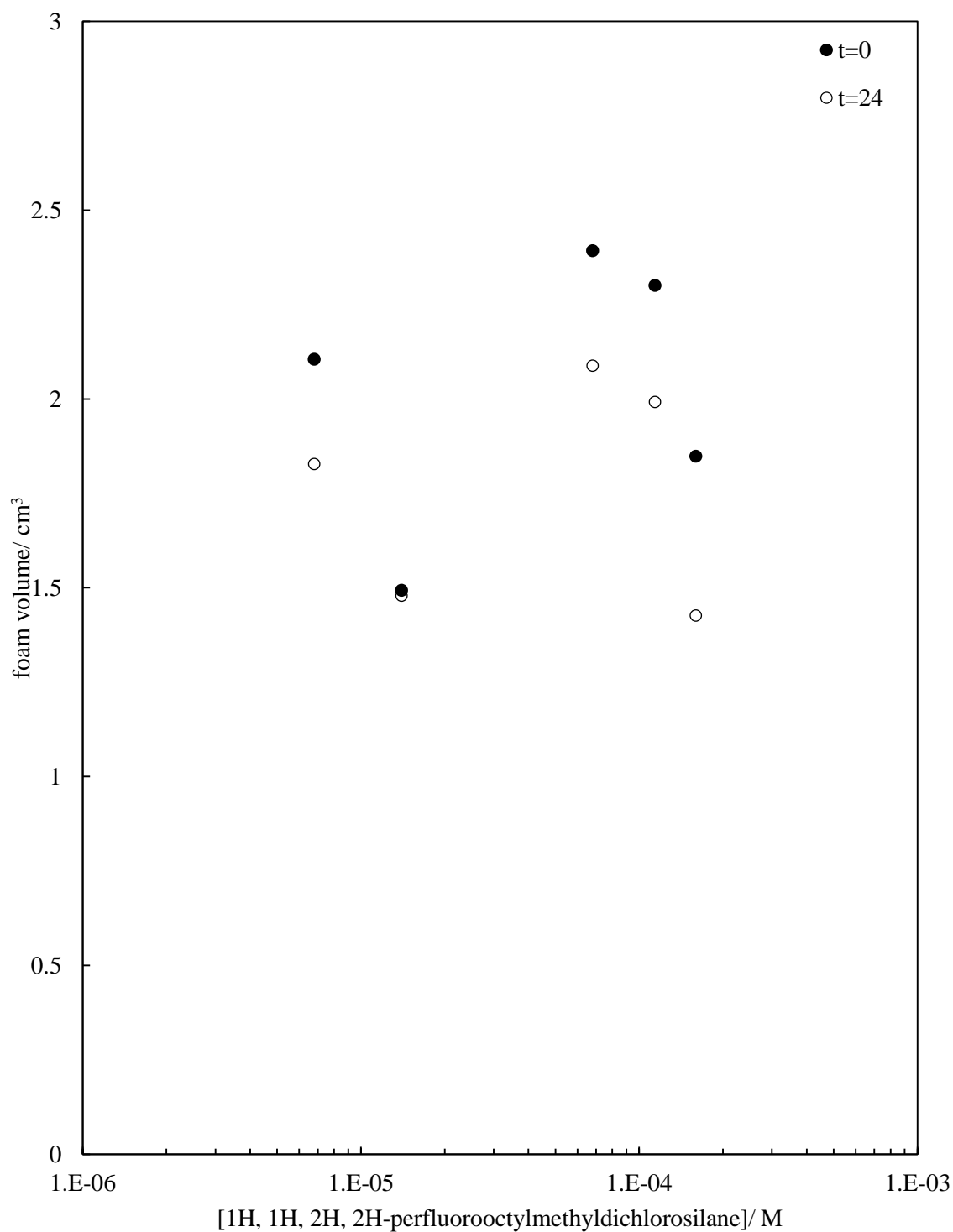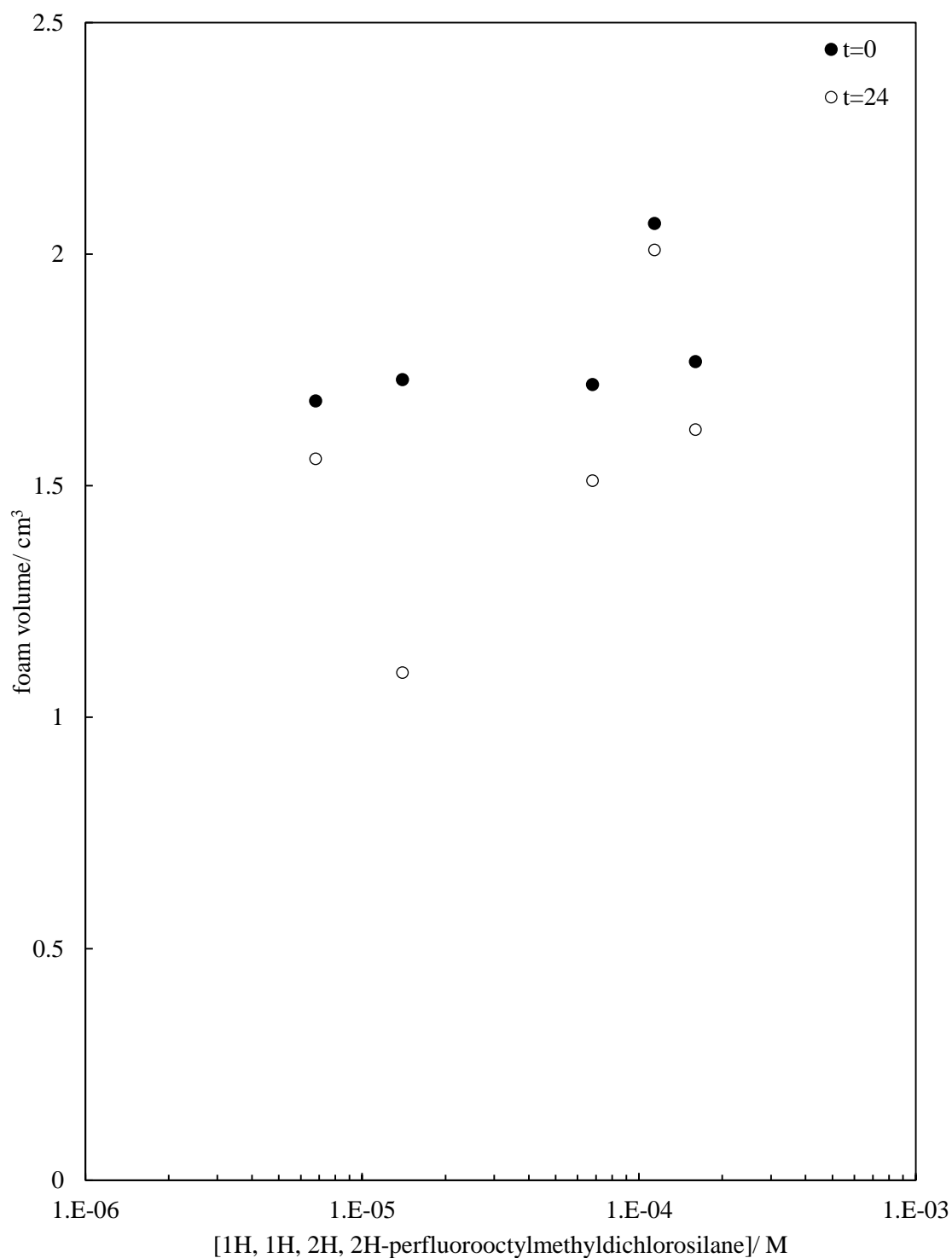
Figure 4.19. Foam volume as a function of particle hydrophobicity of aerated particle suspensions with 5 wt. % 2 μm diameter silica particles (hydrophobised to varying extents with 1H, 1H, 2H, 2H-perfluorooctylmethyldichlorosilane) in 5 ml water. Samples homogenised for 60 seconds. Foam volume at t = 0 and t =24 h are shown. Run 2 of 2 repeats shown. Error bars show maximum and minimum values from 2 repeats.
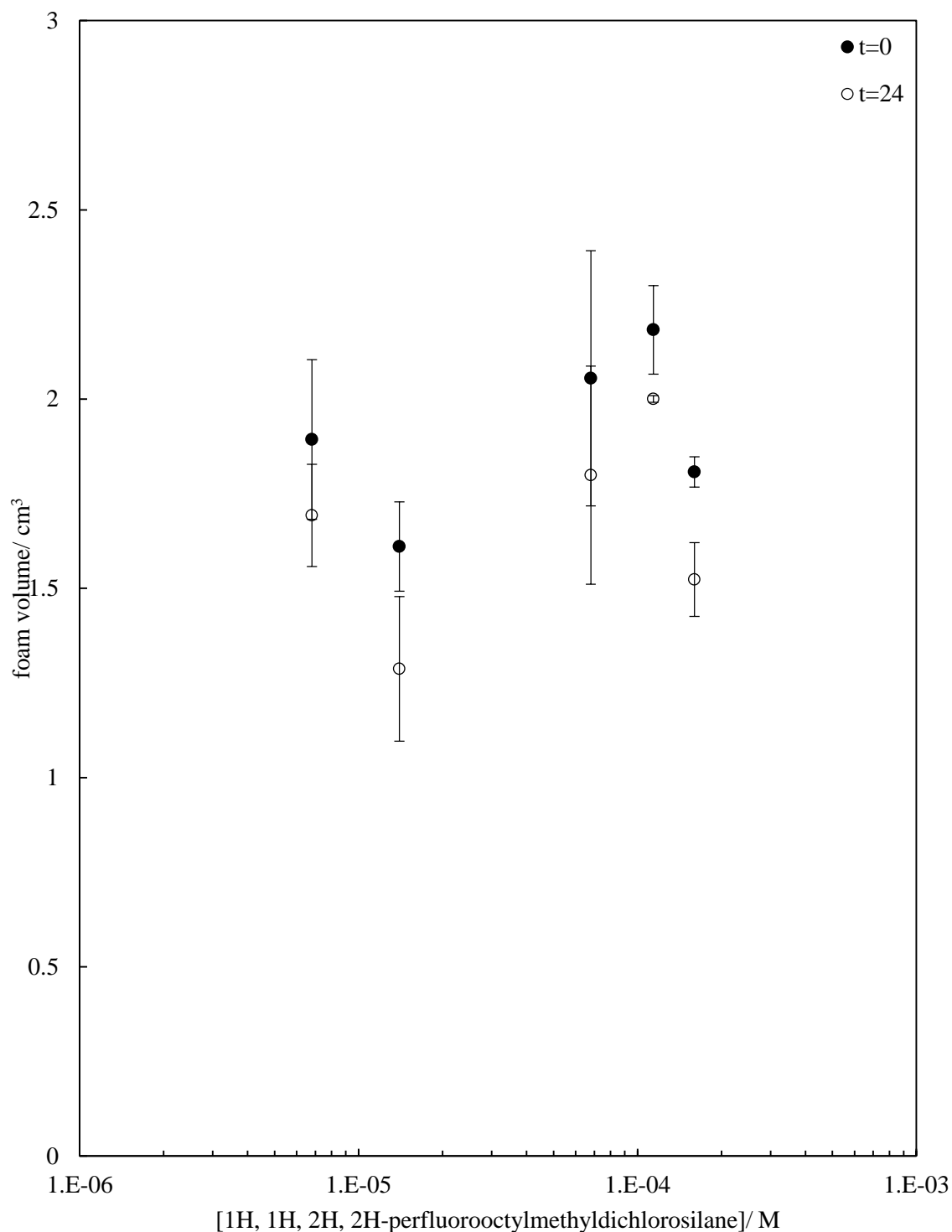
Figure 4.20. Average foam volume as a function of particle hydrophobicity of aerated particle suspensions with 5 wt. % 2 μm diameter silica particles (hydrophobised to varying extents with 1H, 1H, 2H, 2H-perfluorooctylmethyldichlorosilane) in 5 ml water. Samples homogenised for 60 seconds. Foam volume at t = 0 and t =24 h are shown. Average values from 2 repeats shown. Error bars show maximum and minimum values from 2 repeats.

Table 4.2. Time taken for full collapse of all aerated particle suspensions generated. System comprised 5 wt. % 2 μm diameter silica particles (hydrophobised to varying extents with 1H, 1H, 2H, 2H-perfluorooctylmethyldichlorosilane) in 5 ml water. Samples aerated for 60 seconds by homogenisation. Full collapse of the upper layer is defined as the time at which there was no longer a complete layer covering the surface of the liquid.

Sample	Type of system generated	Collapse time (Run 1)	Collapse time (Run 2)
6.8×10^{-6} M	Air-in-water	7 days	7 days
1.4×10^{-5} M	Air-in-water	3 days	3 days
6.8×10^{-5} M	Air-in-water	8 days	8 days
1.14×10^{-4} M	Air-in-water	9 days	9 days
1.6×10^{-4} M	Air-in-water	10 days	9 days
3.4×10^{-4} M	Water-in-air	> 2 months	> 2 months
6.8×10^{-4} M	Water-in-air	> 2 months	> 2 months
4.3×10^{-3} M	Water-in-air	> 2 months	> 2 months

4.5.2 *Aqueous-ethanol particle foams*

The foaming behaviour of the fluorinated particles were then investigated with addition of 15 wt. % ethanol to the aqueous phase. It has been shown in Section 4.4 that the addition of 15 wt. % ethanol to the aqueous phase effects an average contact angle reduction of 21.5°. It is therefore expected that this reduction in the particle contact angle will have some consequences on the particle behaviour at the aqueous ethanol-air interface. The foaming experiments carried out in pure water were repeated in 15 wt. % ethanol, where it was observed upon adding the aqueous phase to the dry particles that at a silane concentration of 3.4×10^{-4} M, the particles were no longer wet by the liquid. This was the same in pure water. Images of the foams generated can be seen in Figures 4.21 and 4.22 taken at t=0 and t=24 hours, respectively. Similarly to the foams observed in water, a change in the bubble size can be seen visibly with time, this may be due to coarsening (or disproportionation) or coalescence. Cryo-SEM (Figure 4.23) imaging of the foams shows that adding 15 wt. % ethanol to the system effects a phase inversion of the most hydrophobic particle systems. In pure water these particles generated dry water systems. However, with 15 wt. % ethanol in the aqueous phase particles coated with 3.4×10^{-4} M and 6.8×10^{-4} M fluorosilane generated foams instead of dry water systems. Only the most hydrophobic particles (4.3×10^{-3} M) generated a dry water-like system, however this was deemed to be in between a foam and a dry powder. Images from SEM show the sample comprises liquid drops coated with particles, trapped inside particle-stabilised air bubbles Therefore this system could be referred to as a water-in-air-in-water system, similar to a double emulsion. It is anticipated that if the ethanol concentration were to be further increased, the system would invert to an aqueous-ethanol foam.

The initial foam volumes of two repeat samples are shown in Figure 4.24 and 4.25. The initial foamability of the systems in ethanol prove to be higher than in comparison to foams generated in pure water, the initial foam volume is almost double in the case of 15 wt. % ethanol. The reproducibility of the foams was also better in 15 wt. % ethanol than pure water. The particles were more easily wet and dispersed in the ethanol samples, so this may have meant more particles were available for transport to the newly generated foam interface. A graph comparing the average initial foam volume in pure water and 15 wt. % ethanol is shown in Figure 4.27. The long term stability of the foams generated with 15 wt. % ethanol showed significantly higher than the systems of pure water. The full collapse times for the systems generated are shown in Table 4.3.

The research of Somosvari *et al.* investigated the stabilisation of ethanol foams using PVC particles,[29] and to our knowledge is the only other study available in the literature discussing the stabilisation of ethanol foams with particles alone. It was found that as the concentration of ethanol was increased, the foam volume generated decreased. This is the opposite to what has been observed in the current work, whereby addition of 15 wt. % ethanol to the aqueous phase effected a doubling of the initial foam volume. It was found additionally, that the contact angle of the PVC particles decreased as the concentration of ethanol increased, which is in concordance with the findings presented. The researchers found it was not possible to generate foams above 70 wt. % ethanol.

Figure 4.21. Images of aerated particle suspensions generated with 5 wt. % 2 μm diameter silica particles (hydrophobised to varying extents with 1H, 1H, 2H, 2H-perfluorooctylmethyldichlorosilane) in 5 ml 15 wt. % ethanol. Suspensions aerated for 60 seconds by homogenisation. Images taken using a Canon EOS 450D camera at t=0.
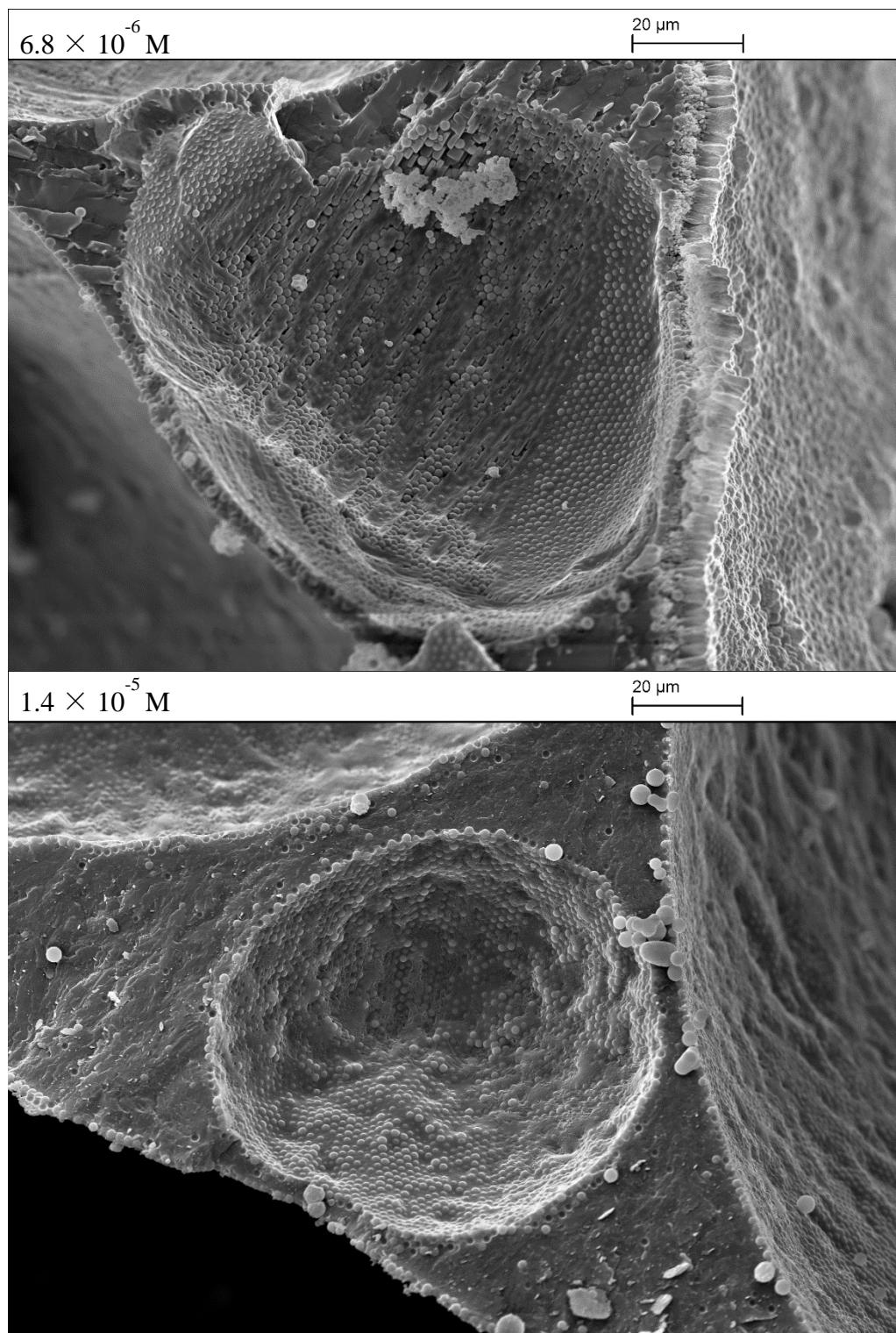
Figure 4.22. Images of aerated particle suspensions generated with 5 wt. % 2 μm diameter silica particles (hydrophobised to varying extents with 1H, 1H, 2H, 2H-perfluorooctylmethyldichlorosilane) in 5 ml 15 wt. % ethanol. Suspensions aerated for 60 seconds by homogenisation. Images taken using a Canon EOS 450D camera at t=24 hours.
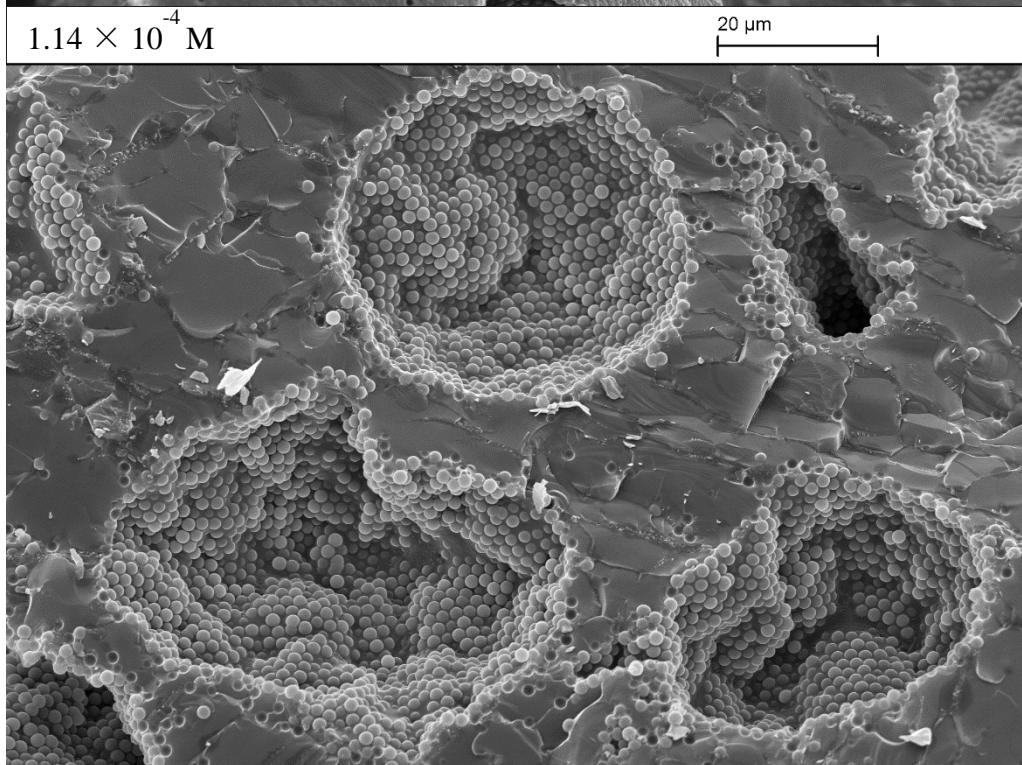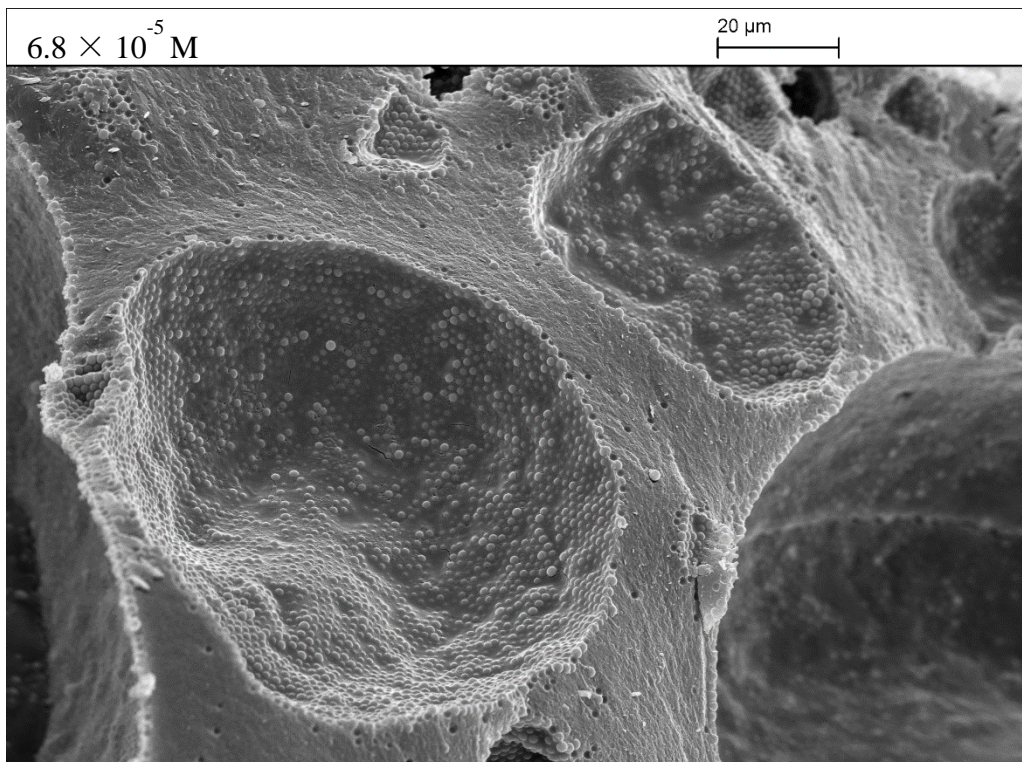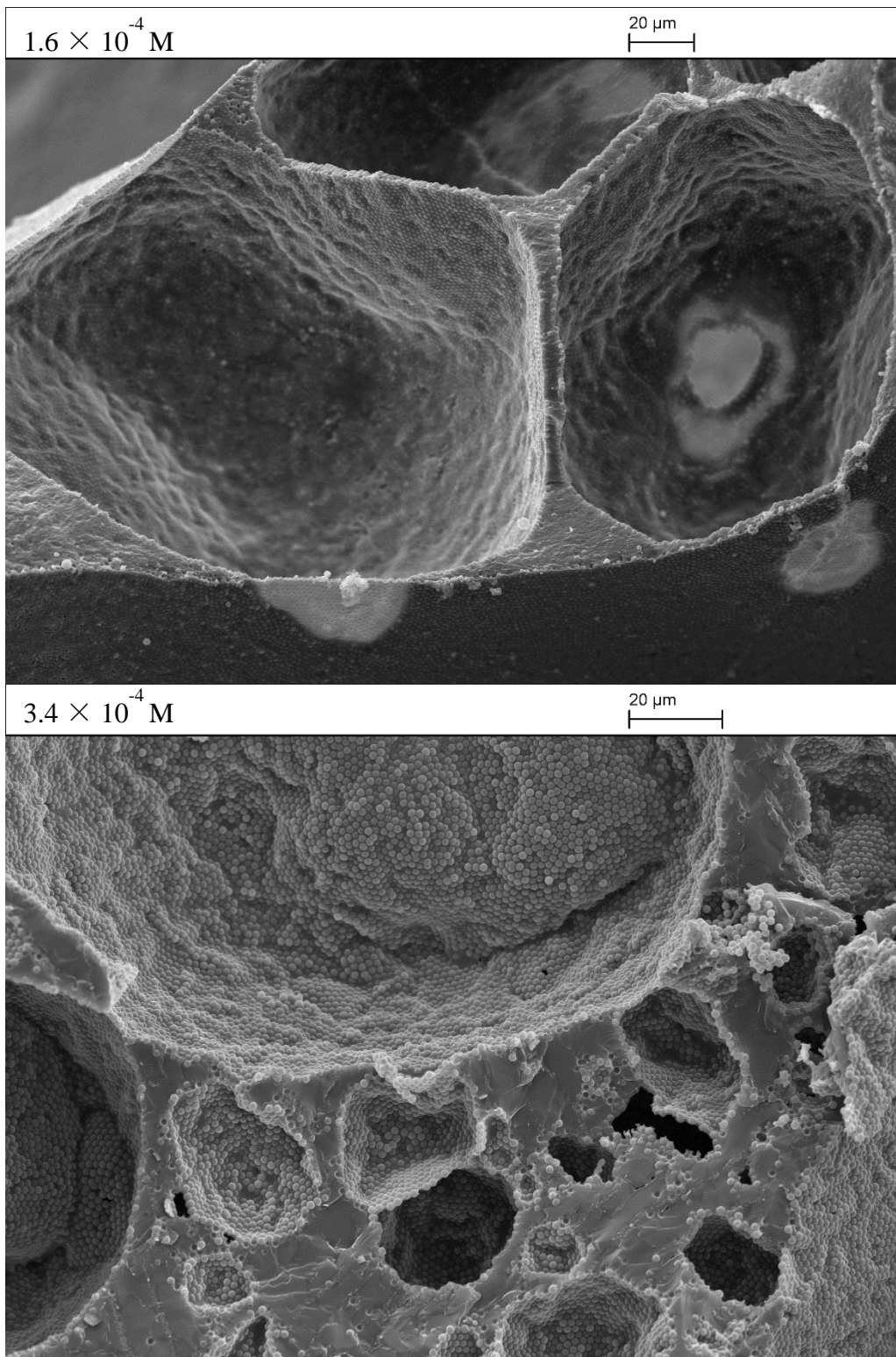
Figure 4.23. Freeze-fracture cryo-SEM images of aerated suspensions generated with 5 wt.% 2 μm diameter silica particles (hydrophobised to varying extents with 1H, 1H, 2H, 2H-perfluorooctylmethyldichlorosilane)in 5 ml 15 wt. % ethanol. Suspensions aerated for 60 seconds by homogenisation. Samples frozen within 15 minutes of aeration. All cryo-SEM carried out by Tony Sinclair at The University of Hull, U.K.

6.8×10^{-6} M

20 μm

1.4×10^{-5} M

20 μm

6.8 × 10^{-5} M   20 μm

1.14 × 10^{-4} M   20 μm

1.6 × 10^{-4} M   20 μm

3.4 × 10^{-4} M   20 μm

6.8 × 10^{-4} M   20 µm

4.3 × 10^{-3} M   20 µm
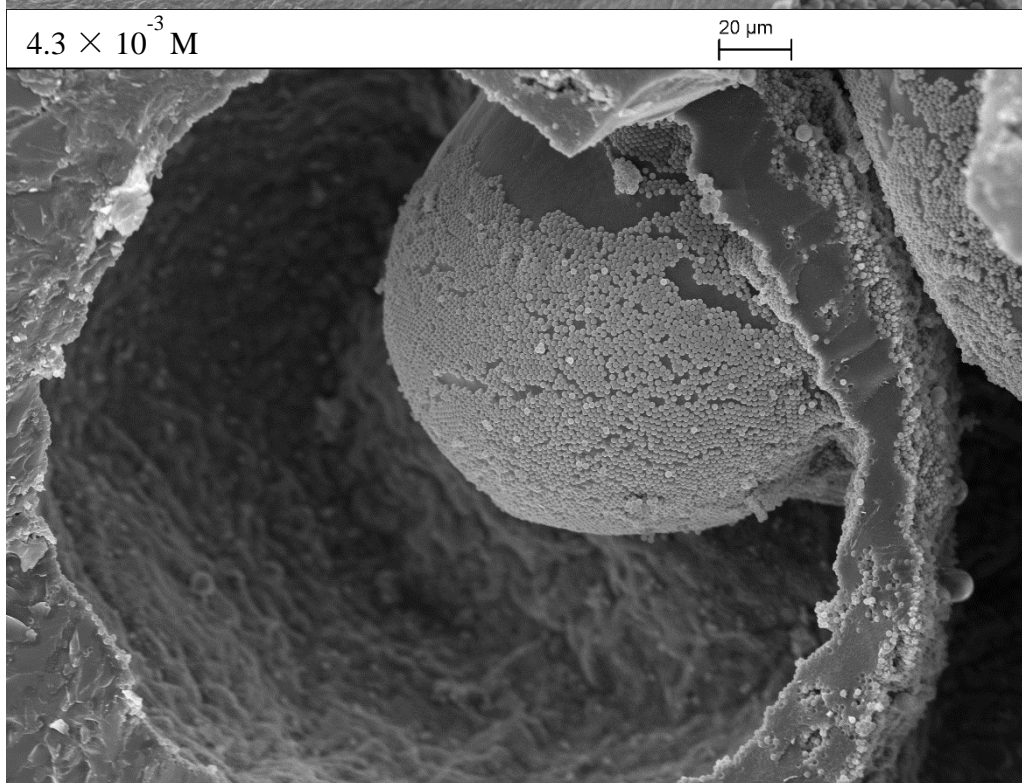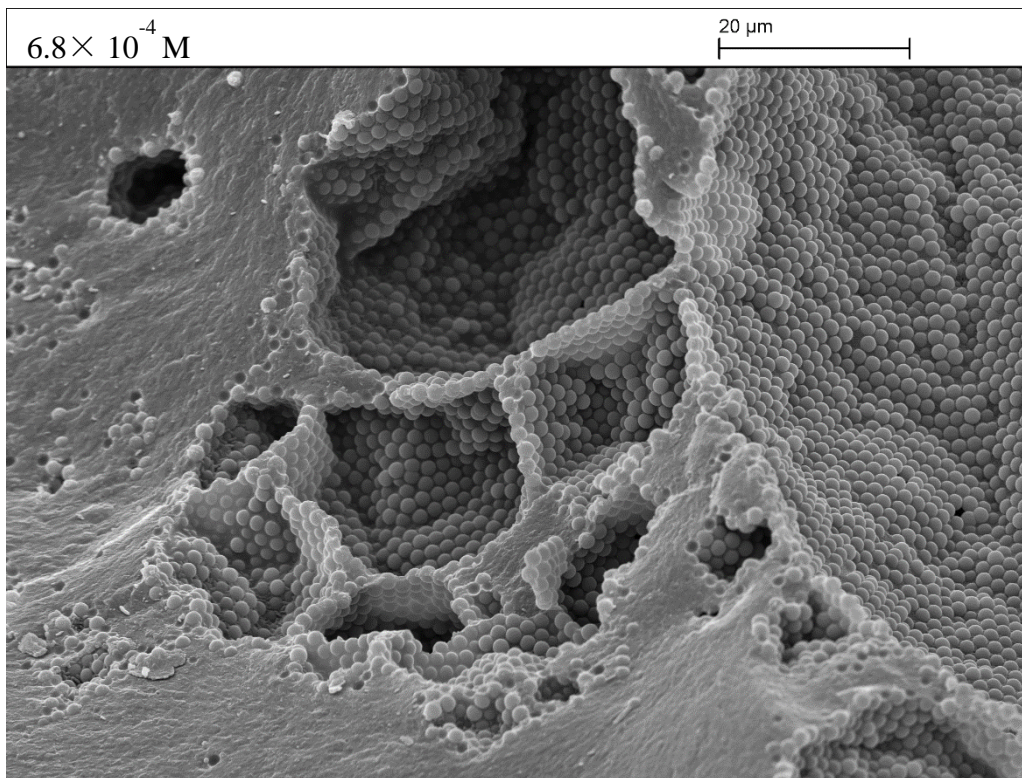
Figure 4.24. Foam volume as a function of particle hydrophobicity of aerated particle suspensions generated with 5 wt. % 2 μm diameter silica particles (hydrophobised to varying extents with 1H, 1H, 2H, 2H-perfluorooctylmethyldichlorosilane) in 5 ml 15 wt. % ethanol. Foams aerated for 60 seconds by homogenisation. Foam volumes at t = 0 and t =24 h are shown. Run 1 from 2 repeats shown.

Figure 4.25. Foam volume as a function of particle hydrophobicity of aerated particle suspensions generated with 5 wt. % 2 μm diameter silica particles (hydrophobised to varying extents with 1H, 1H, 2H, 2H-perfluorooctylmethyldichlorosilane) in 5 ml 15 wt. % ethanol. Foams aerated for 60 seconds by homogenisation. Foam volumes at t = 0 and t =24 h are shown. Run 2 from 2 repeats shown.
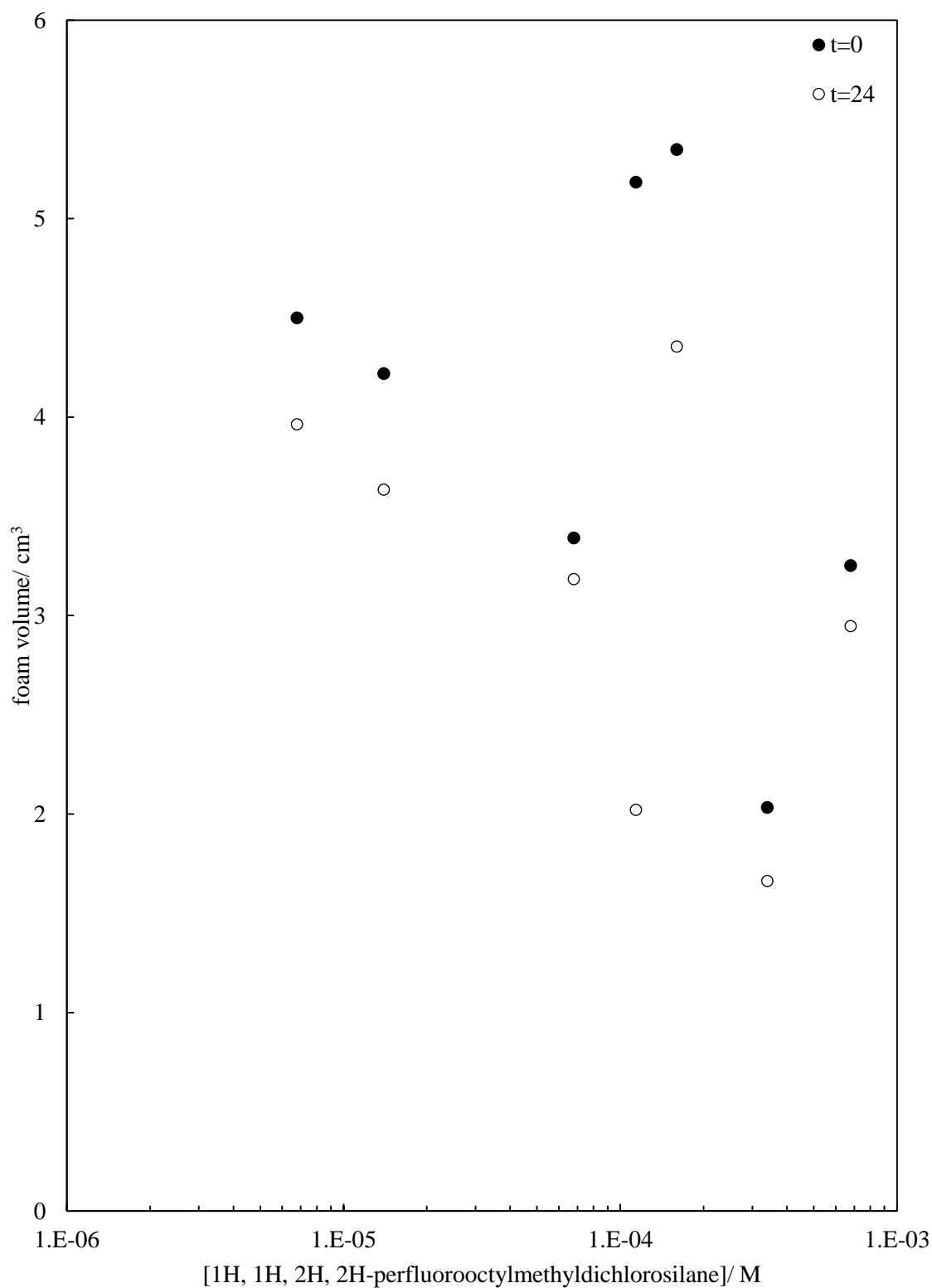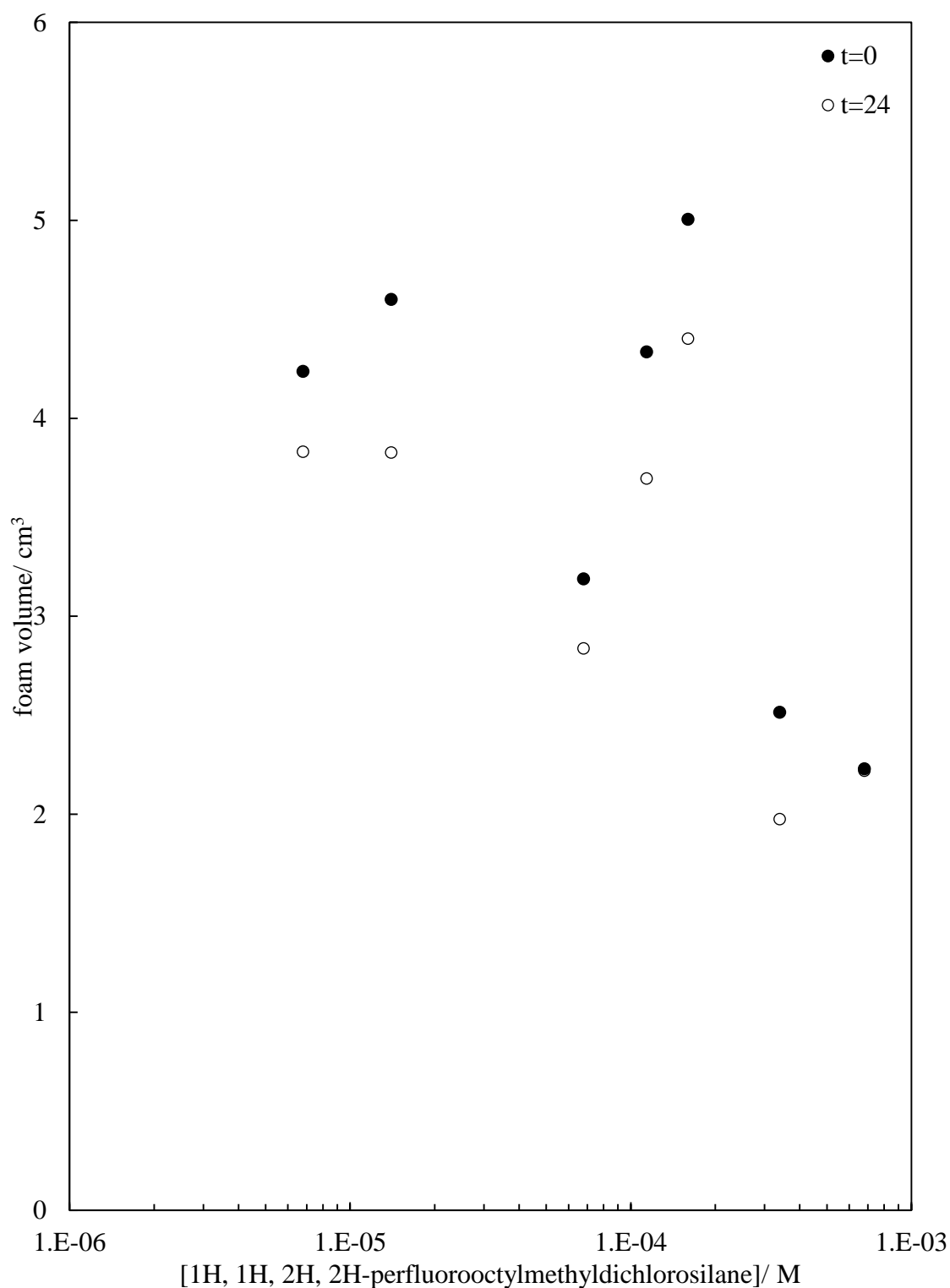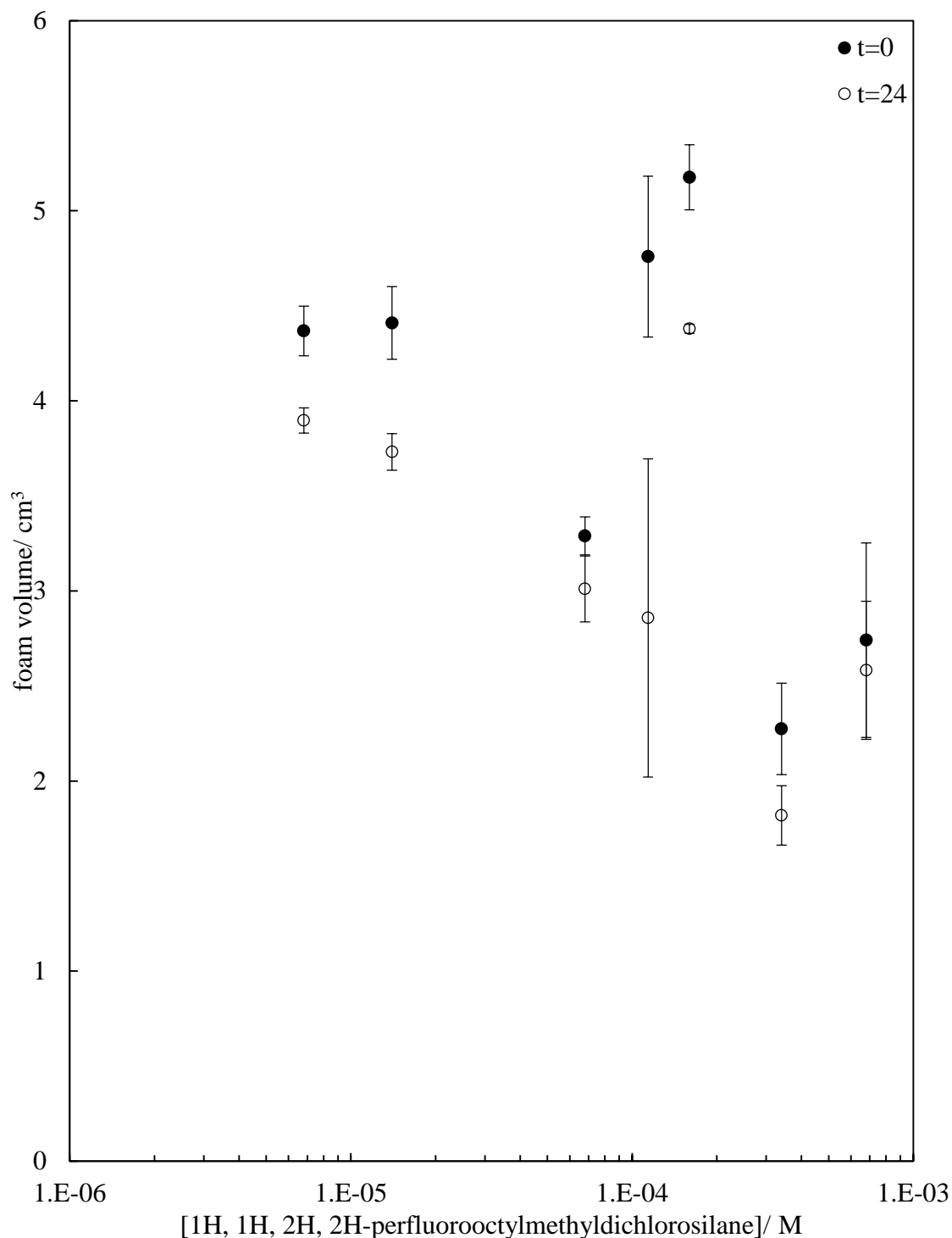
Figure 4.26. Average foam volume as a function of particle hydrophobicity of aerated particle suspensions generated with 5 wt. % 2 μm diameter silica particles (hydrophobised to varying extents with 1H, 1H, 2H, 2H-perfluorooctylmethyldichlorosilane) in 5 ml 15 wt. % ethanol. Foams aerated for 60 seconds by homogenisation. Foam volumes at t = 0 and t =24 h are shown. Average of 2 repeats shown. Error bars show maximum and minimum values from 2 repeat measurements.

Figure 4.29. Comparison of average foam volume as a function of particle hydrophobicity of aqueous foams generated with 5 wt. % 2 μm diameter silica particles (hydrophobised to varying extents with 1H, 1H, 2H, 2H-perfluorooctylmethyldichlorosilane)in 5 ml water/15 wt. % ethanol. Foams aerated for 60 seconds by homogenisation. Foam volumes at t = 0 are shown. Average values from 2 repeats shown and error bars show maximum and minimum values.
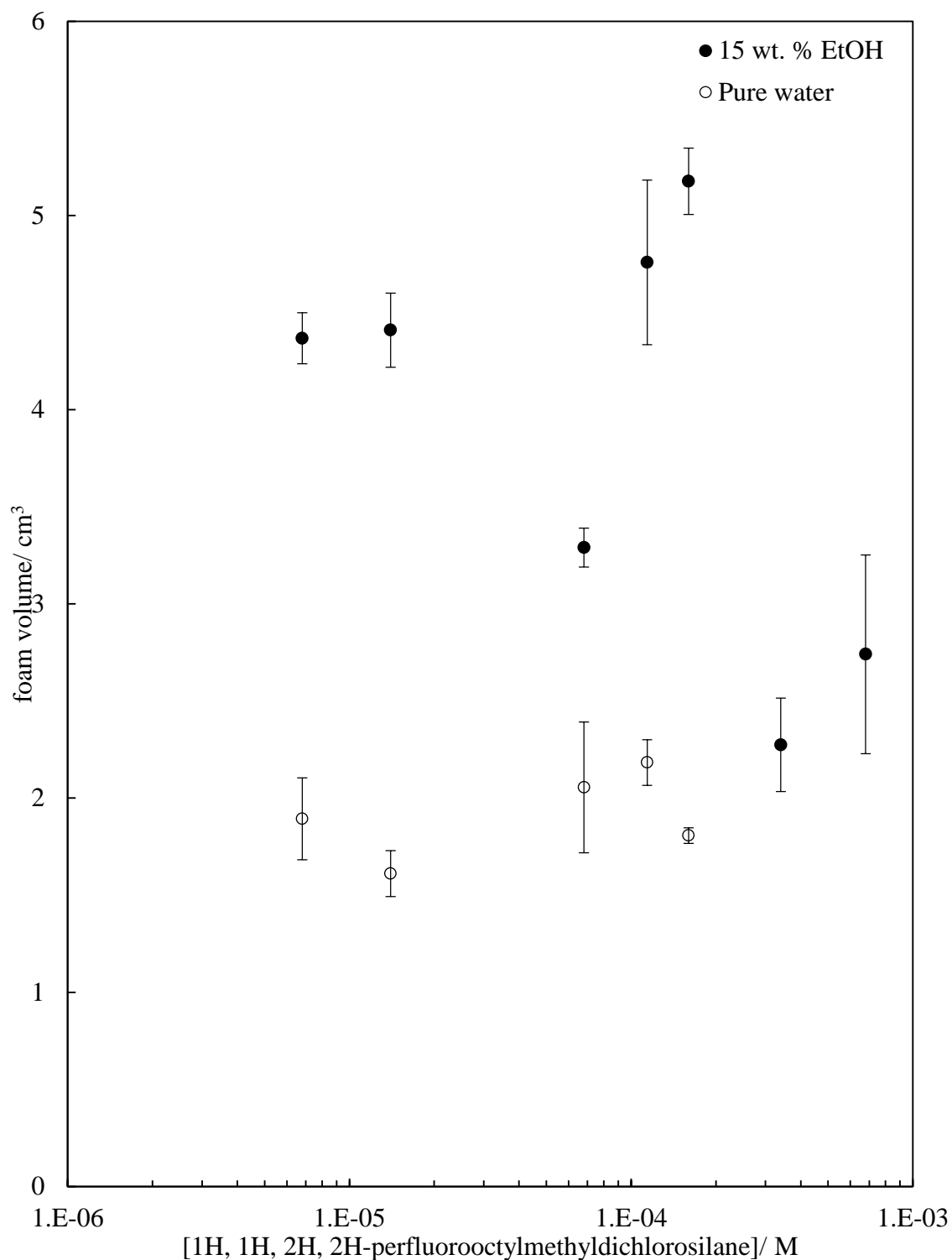
Table 4.3. Time taken for full collapse of all aerated particle suspensions generated. System comprised 5 wt. % 2 μm diameter silica particles (hydrophobised to varying extents with 1H, 1H, 2H, 2H-perfluorooctylmethyldichlorosilane) in 5 ml 15 wt. % ethanol. Suspensions aerated for 60 seconds by homogenisation. Full collapse of the upper layer is defined as the time at which there was no longer a complete layer covering the surface of the liquid.

Sample	Type of system generated	Collapse time (Run 1)	Collapse time (Run 2)
6.8×10^{-6} M	Air-in-water	42 days	44 days
1.4×10^{-5} M	Air-in-water	43 days	44 days
6.8×10^{-5} M	Air-in-water	47 days	46 days
1.14×10^{-4} M	Air-in-water	48 days	49 days
1.6×10^{-4} M	Air-in-water	48 days	49 days
3.4×10^{-4} M	Air-in-water	57 days	54 days
6.8×10^{-4} M	Air-in-water	>3 months	>3 months
4.3×10^{-3} M	Water-in-air	>3 months	>3 months

4.6   Summary

This chapter aimed to investigate the fluorination of monodisperse silica particles and to characterise their behaviour at fluid-fluid interfaces of air-water and aqueous ethanol-air. An initial investigation into the controlled silanisation of glass slide surfaces was investigated to allow for generation of a protocol to allow for controlled hydrophobisation of monodisperse, micron-sized silica particles. It was discovered that fluoroalkylchlorosilanes with di-chloro functionality provide coatings of higher hydrophobicity. Additionally, carrying out the fluorination in the vapour phase results in more hydrophobic surfaces but it was not possible to tailor the surface hydrophobicity this way. The effect of pre-addition of amines was investigated and it was found that addition of pyridine resulted in higher contact angles of the glass surfaces by promoting attachment of the fluorosilane.

Using the protocol developed, a range of eight different silica particle samples was prepared by varying the concentration of fluorosilane in the bulk solution (anhydrous toluene). The contact angle of these particles at the air-water interfaces was measured directly using the film calliper method and found to range from 50.7° to >90°. The contact angles were then measured in aqueous ethanol up to a concentration of 15 wt. % ethanol. Above this concentration the thin liquid film was unstable. It was seen that addition of ethanol effected a contact angle reduction in all cases.

The lateral interactions of the particles spread at air-water and aqueous ethanol-air was studied by spreading monolayers and observing them with optical microscopy. It was seen that the most hydrophobic silica particles formed repulsive arrays at the air-water interfaces. With addition of ethanol to the aqueous phase, particles of all concentrations became aggregated due to the reduction in contact angle at the interface. However, some regions of the monolayers spread with the two most hydrophobic particles displayed some aggregation, and some areas of the monolayers demonstrated the formation of repulsive arrays.

Finally, foams of these particles were generated by homogenisation at a particle concentration of 5 wt. %. Inconsistent foaming was seen in pure water, and the foams generated showed poor stability (uncharacteristic of particle-stabilised foams) with all foams collapsing within 10 days. Above concentrations of 1.6×10^{-4} M the systems were seen to phase-invert and form stable dry powders of liquid drops in air coated with a layer of particles. Foams of 15 wt. % aqueous ethanol showed improved foamability and stability, despite showing visible coarsening of foam bubbles. Phase inversion of dry water systems observed at 3.4×10^{-4} M and 6.8×10^{-4} M was effected by addition of ethanol, so that these systems formed aqueous particle-stabilised foams.

In 15 wt. % ethanol, the most hydrophobic particles formed an intermediate system of particle-stabilised dry powders inside particle-stabilised air-bubbles. The work carried out in this chapter provides an essential understanding to the effect of varying the surface tension of the aqueous phase on particles of varying hydrophobicity. The properties observed in this chapter, particularly the contact angles and behaviour on aeration have significant implications in the generation of dry water systems encapsulating various liquids and active agents.

4.7   References

1. B. P. Binks and T. S. Horozov, Colloidal Particles at Liquid Interfaces, 2006, Cambridge University Press, Cambridge.

2. E. Bormashenko, R, Balter and D. Aurbach, *J. Colloid. Interface. Sci.*, 2012, **384**, 157.

3. B. P. Binks and A. T. Tyowua, *Soft Matter*, 2014, **10**, 578.

4. Y. Lai, Y. Tang, J. Huang, H. Wang, H. Li, D. Gong, X. Ji, J. Gong, C. Lin, L. Sun and Z. Chen, *Soft Matter*, 2011, **7**, 6313.

5. B. P. Binks and A. T. Tyowua, *Soft Matter*, 2013, **9**, 834.

6. P. Aussillous and D. Quéré, *Nature*, 2001, **411**, 924.

7. Y. Lai, H. Zhou, Z. Zhang, Y. Tang, J. W. C. Ho, J. Huang, Q. Tay, K. Zhang, Z. Chen and B. P. Binks, *Part. Part. Syst. Charact.*, 2014, 1.

8. T. S. Horozov, D. A. Braz, P. D. I. Fletcher, B. P. Binks and J. H. Clint, *Langmuir*, 2008, **24**, 1678.

9. A. Y. Fadeev and T. J. McCarthy, *Langmuir*, 2000, **16**, 7268.

10. A. Y. Fadeev and T. J. McCarthy, *Langmuir*, 1999, **15**, 3759.

11. R. Campos, A. J. Guenther, T. S. Haddad and J. M. Mabry, *Langmuir*, 2011, **27**, 10206.

12. L. D. White and C. P. Tripp, *J. Colloid. Interface. Sci.*, 2000, **227**, 237.

13. L. D. White and C. P. Tripp, *J. Colloid. Interface. Sci.*, 2000, **232**, 400.

14. S. M. Kanan, W. T. Y. Tze and C. P. Tripp, *Langmuir*, 2002, **18**, 6623.

15. C. P. Tripp, P. Kazmaier and M. L. Hair, *Langmuir*, 1996, **12**, 6407.

16. A. F. Koretsky and P. M. Kruglyakov, *Izv. Sib. Otd. Akad. Nauk USSR*, 1971, **2**, 139.

17. S. Levine, B. D. Bowen and S. J. Partridge, *Colloids. Surf.*, 1989, **38**, 325.

18. D. J. Shaw, Introduction to Colloid and Surface Chemistry 4th Ed., 1991, Butterworth-Heineman Ltd., Oxford.

19. J. C. Berg, Wettability, 1993, Marcel Dekker Inc., New York.

20. G. B. Davies, T. Kruger, P. V. Coveney and J. Harting, *J. Chem. Phys.*, 2014 **141**, 154902.

21. T. S. Horozov, R. Aveyard, J. H. Clint and B. P. Binks, *Langmuir*, 2003, **19**, 2822.

22. T. S. Horozov and B. P. Binks, *Colloids Surf. A,* 2005, **267**, 64.

23. R. Aveyard, J. H. Clint, D. Nees and N. Quirke, *Langmuir*, 2000, **16**, 8820.

24. R. Aveyard, J. H. Clint, D. Nees and V. N. Paunov, *Langmuir*, 2000, **16**, 1969.

25. P. Pieranski, *Phys. Rev. Let.*, 1980, **45**, 569.
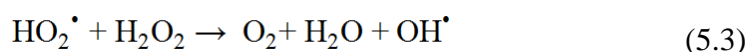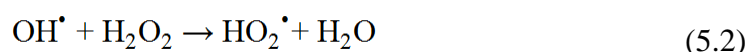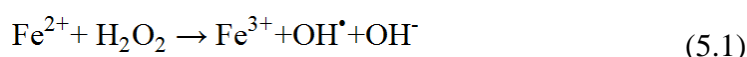
26. T. S. Horozov, R. Aveyard, B. P. Binks and J. H. Clint, *Langmuir*, 2005, **71**, 7405.

27. M. Abkarian, A. B. Subramaniam, S-H. Kim, R. J. Larsen, S-M. Yang and H. A. Stone, *Phys. Rev. Let.*, 2007, **99**, 188301.

28. S. Bordács, A. Agod and Z. Hórvölgyi, *Langmuir*, 2006, **22**, 6944.

29. B. M. Somosvari, N. Babcsan, P. Barczy and A. Berthold, *Colloids Surf. A,* 2007, **309**, 240.

CHAPTER 5
ENCAPSULATION OF FENTON REACTION COMPONENTS IN DRY WATER

5.1   Introduction

The primary industrial aim of this research is to develop a novel hand sanitiser comprising two separate components that are required to be kept separate until the point of use. The Fenton reaction was discovered in 1894 by Fenton[1,2] and describes the catalytic decomposition of hydrogen peroxide by iron (II) salts (Fe^{2+} + H_2O_2). The Fenton reaction has been used widely as a method for destroying hazardous organic pollutants.[3-5] However, there is widespread controversy surrounding the exact mechanism of the reaction[6] and various mechanisms have been proposed.[7-9] The work of Haber and Weiss,[8] and Haber and Willstäter [10] suggested the following mechanism:

$$Fe^{2+} + H_2O_2 \rightarrow Fe^{3+} + OH^{\bullet} + OH^{-} \tag{5.1}$$

$$OH^{\bullet} + H_2O_2 \rightarrow HO_2^{\bullet} + H_2O \tag{5.2}$$

$$HO_2^{\bullet} + H_2O_2 \rightarrow O_2 + H_2O + OH^{\bullet} \tag{5.3}$$

$$Fe^{2+} + OH^{\bullet} \rightarrow Fe^{3+} + OH^{-} \tag{5.4}$$

However, in 1950 Barb *et al.* suggested a new mechanism for the reaction, in which Fe^{2+} is regenerated[9] which is now the most widely accepted mechanism of the Fenton reaction. The reaction mechanism is commonly abbreviated to the following throughout the literature:

$$Fe^{2+} + H_2O_2 \rightarrow Fe^{3+} + HO^{\bullet} + HO^{-} \tag{5.5}$$

$$Fe^{3+} + H_2O_2 \rightarrow Fe^{2+} + HOO^{\bullet} + H^{+} \tag{5.6}$$
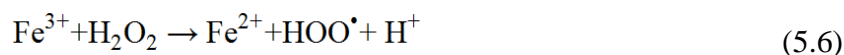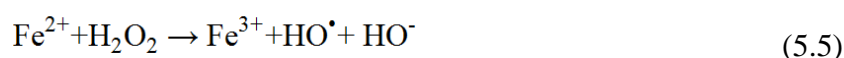
Other work has suggested the formation of intermediate iron species, such as the ferryl ion,[11] FeO^{2+}, for example. However it was highlighted by Dunford in his review of the various Fenton mechanisms, that controversy still surrounds the Fenton reaction today. A review by Sawyer *et al.*[12] and work by Goldstein and Meyerstein[13] both support the notion that hydroxyl radicals are not formed in the Fenton reaction. Yet, the mechanisms of Haber and Weiss, Barb *et al.* and more recent publications by Walling[14-16] all support the concept that hydroxyl radicals are intermediate species in the Fenton reaction.

The biocidal effects of the Fenton reaction are well known, and some researchers have suggested that the toxicity of hydrogen peroxide (to bacteria) alone is due to the initiation of the Fenton reaction by reaction with *in vivo* iron salts contained within bacterial cells.[17-19] The research of Repine *et al.* supported the production of hydroxyl radicals to be the reason for biocidal activity of the Fenton reaction by demonstrating the addition of hydroxyl scavengers inhibited destruction of bacterial cells by the Fenton reagents. It is understood that the production of hydroxyl radicals in biological systems can effect cell death by a number of mechanisms; namely, by causing damage to cell proteins, DNA, membrane lipids and by transducing cell signalling processes.[20]

It is additionally known that despite the traditional Fenton reaction comprising the redox of Fe^{2+}; that the degradation of hydrogen peroxide can be catalysed by many other metal ions of multiple redox states. Examples of such elements are chromium, cerium, cobalt, copper and manganese[21] which are defined as "Fenton-like" reagents. A primary issue for the iron-catalysed traditional Fenton reaction is the necessity to strongly acidify the reagents to enable solubilisation of the iron salts. This issue is eradicated by using soluble salts of other transition metal ions, which can operate efficiently at neutral pH.

The Fenton-like reaction of copper with hydrogen peroxide has been investigated in depth and the reactivity of both monovalent (Cu^+) and divalent (Cu^{2+}) oxidation copper oxidation states show very similar reactivity towards hydrogen peroxide as iron. The mechanism proposed for the Fenton-like reaction of copper (II) with hydrogen peroxide is:

$$Cu^{2+} + H_2O_2 \rightarrow Cu^+ + HO_2^{\bullet} + OH^- \tag{5.7}$$

$$Cu^+ + H_2O_2 \rightarrow Cu^{2+} + HO^{\bullet} + HO^- \tag{5.8}$$
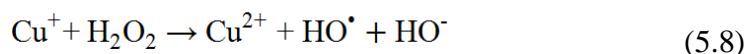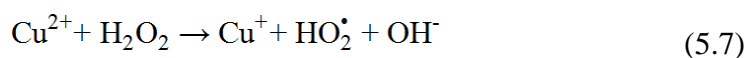
Additionally, the increased solubility of copper (II) salts should mean that the copper-catalysed Fenton reaction should operate over a broader pH range.[21] The study of the copper-based Fenton-like reaction has been measured by many researchers and techniques for measuring the reaction usually comprise analysis of a reagent with time whilst being exposed to the Fenton-like reagents.[22-28] The work of Salem[26] investigated the degradation of bromophenol blue with the Cu^{2+}/H_2O_2 system.

Measurement of the UV-visible adsorption of the dye after addition of the reagents revealed the rate of the reaction to be dependent (first-order) on the concentration of H_2O_2. The bromophenol blue was unaffected by addition of H_2O_2 alone, but with the addition of the copper catalyst, complete colour removal of the dye was observed. Gabriel *et al.* monitored the degradation of phenanthrene, fluoranthene and pyrene with the copper (II)-hydrogen peroxide, Fenton-like system.[28] It was found that within one day, a mixture of 10 mM copper sulfate ($CuSO_4$) and 100 mM H_2O_2, 80% of the analytes had degraded completely. Thin Layer Chromatography of the solutions with time confirmed the presence of various products for each compound analysed, indicating they had been broken down by the Fenton reaction.

It is clear that the Fenton-like reaction of copper (II) with hydrogen peroxide is effective in reducing organic compounds, however the aim of this research concerns the antimicrobial efficacy of the Fenton reaction. Dittmar *et al.* published work in 1930 discussing the germicidal effects of inorganic salts with hydrogen peroxide on *Escherichia coli* and *Staphylococcus aureus*.[29] It was observed that whilst hydrogen peroxide alone had a growth restricting effect on both types of bacteria; the addition of Cu^{2+} salts caused the same reduction in growth in the same time, but at much lower hydrogen peroxide concentrations.

Work by Bayliss and Waites also demonstrated the addition of Cu^{2+} salts to colonies of *Clostridium bifermentans* with hydrogen peroxide increased the lethal effect of the hydrogen peroxide by a factor of around 3000.[30] Further to this, analysis of DNA bases of calf thymus DNA were exposed to Cu^{2+} or Fe^{2+} and H_2O_2 showed exposure to copper to degrade DNA to a higher extent than iron.[31]

It is intended in this work to utilise the Fenton-like system of Cu^{2+}/H_2O_2 for the application of a novel hand sanitiser that is kinder to skin than ethanol-based equivalent sanitisers. The primary issue and challenge with this system therefore, is how to maintain separation of the two Fenton components until point of use. The industrial sponsor would like to investigate a more novel technology, specifically dry water.

Dry water comprises small liquid drops coated with a layer of hydrophobic particles and was discovered (and subsequently patented) by DeGussa in 1968.[32] The invention received attention at the time due to its potential cosmetic applications, but was rediscovered in 2006 in the Surfactant and Colloid group, Hull, U.K. by Binks and Murakami.[33]

The dry powder is formed by blending 5% hydrophobic fumed silica with 95% water under high shear, the resulting dry, fluffy, free-flowing powder can remain stable for many years, and releases the encapsulated liquid by shearing. The aim of this chapter is to therefore study the potential for the encapsulation of the aqueous Fenton components (Cu^{2+}/H_2O_2) in the form of dry water. The intention is that the encapsulated components can be used as a carrier until point of use of the product. Once the product is sheared on the skin, the contents of the dry powder will be released the Fenton reaction can proceed *in situ* on the skin surface, killing any bacteria present. Figure 5.1 shows a schematic of the concept of encapsulation of the aqueous Fenton components in the format of dry water.

This chapter therefore explores the Fenton reaction itself, and parameters that can affect the rate of the Fenton reaction, such as pH and concentration of the individual components. The potential for encapsulation of the Fenton components is explored by attempting to generate dry water with a variety of different formulations. Finally, the antimicrobial efficacy of the formulations is investigated on *Escherichia coli* colonies, *in vitro* and *in vivo*.

5.2 Experimental

In order to study the kinetics of the Fenton reaction, the progress of the reaction has been tracked via the degradation of a dye molecule, Naphthol Blue Black (NBB). It is known that the wavelength at which the maximum absorption of this dye occurs (Lamda max, or λ_{max}) is 618 nm, and therefore studies using UV-visible spectrophotometry have been carried out as a function of time. The effect of concentration of both the Fenton reagents (copper sulfate) on the rate of degradation of the dye molecule have been investigated. Furthermore, the effect of the solution pH on the rate has been investigated. The potential for encapsulation of the aqueous Fenton components has been studied, along with other potential additives (such as moisturisers and fragrances). Finally the *in vitro* and *in vivo* anti-microbial efficacy of the formulations as aqueous solutions and dry powders has been carried out on *Escherichia coli* bacteria. All microbiology experiments have been carried out in externally accredited microbiology labs with Lisa Powell at Deb Group Ltd. (Derby, U.K) and with Tina Bradley and Martin Wilkinson at Queen Elizabeth Hospital (Birmingham, U.K.).

5.3   Monitoring of Fenton reaction

It was important to confirm the occurrence of the Fenton reaction upon mixing of copper (II) sulfate and hydrogen peroxide. Many methods exist for the monitoring and measurement of the Fenton reaction, but experiments which have aimed to track the direct generation of hydroxyl radicals are difficult, as the radicals are so short-lived. Many studies have used techniques such as electron spin resonance spectroscopy with spin trapping[34,35] and analysis of products formed from Fenton oxidation of probe compounds.[36] However, other studies have shown the use of dye degradation methods to be a relatively straight-forward method for testing the rate of consumption of H_2O_2, and therefore the rate of production of hydroxyl radicals. These methods usually comprise the use of a dye molecule, which upon mixing with the Fenton reagents is degraded by the production of hydroxyl radicals. Therefore the rate of the degradation of the dye (as monitored by UV-visible spectrometry) is directly related to the rate of production of hydroxyl radicals. A method comprising the use of copper sulfate, hydrogen peroxide and Naphthol Blue Black (NBB) was used, whereby the degradation of the dye molecule was tracked by measuring the absorbance change with time, at a wavelength of 618 nm (the lambda max, λ_{max} of the NBB dye).

### 5.3.1   Effect of concentration of Fenton reagents

Initially the effect of varying the concentration of each of the different components of the reaction was investigated. Initial concentrations of 10 mM $CuSO_4$ and 100 mM H_2O_2 were used, as suggested in multiple other studies.[27,28] As the copper is catalytic and is regenerated, a much smaller concentration of copper is required in comparison with the hydrogen peroxide.

Figure 5.1 shows the calibration graph for NBB dye, by a plot of absorbance as a function of dye concentration. A linear relationship can be seen, and the molar absorption coefficient (ε) is constant, indicating the dye obeys the Beer-Lambert law:[37]

$$A = \varepsilon \, l \, c \tag{5.9}$$

where A is the absorbance, l is the path length of the cuvette and c is the concentration of the analyte. Figure 5.2 shows reduction in absorbance of NBB dye as a function of time for various different concentrations of H_2O_2 in 10 mM $CuSO_4$.

Figure 5.1. Calibration graph of Napthol Blue Black Dye (NBB) plotting absorbance as a function of concentration. Samples measured at 618 nm (λ_{max} of NBB) using a Perkin-Elmer Lambda 25 UV-Visible spectrophotometer.

$y = 0.0681x$
$R^2 = 0.9983$

absorbance

[Naphthol Blue Black]/ μM
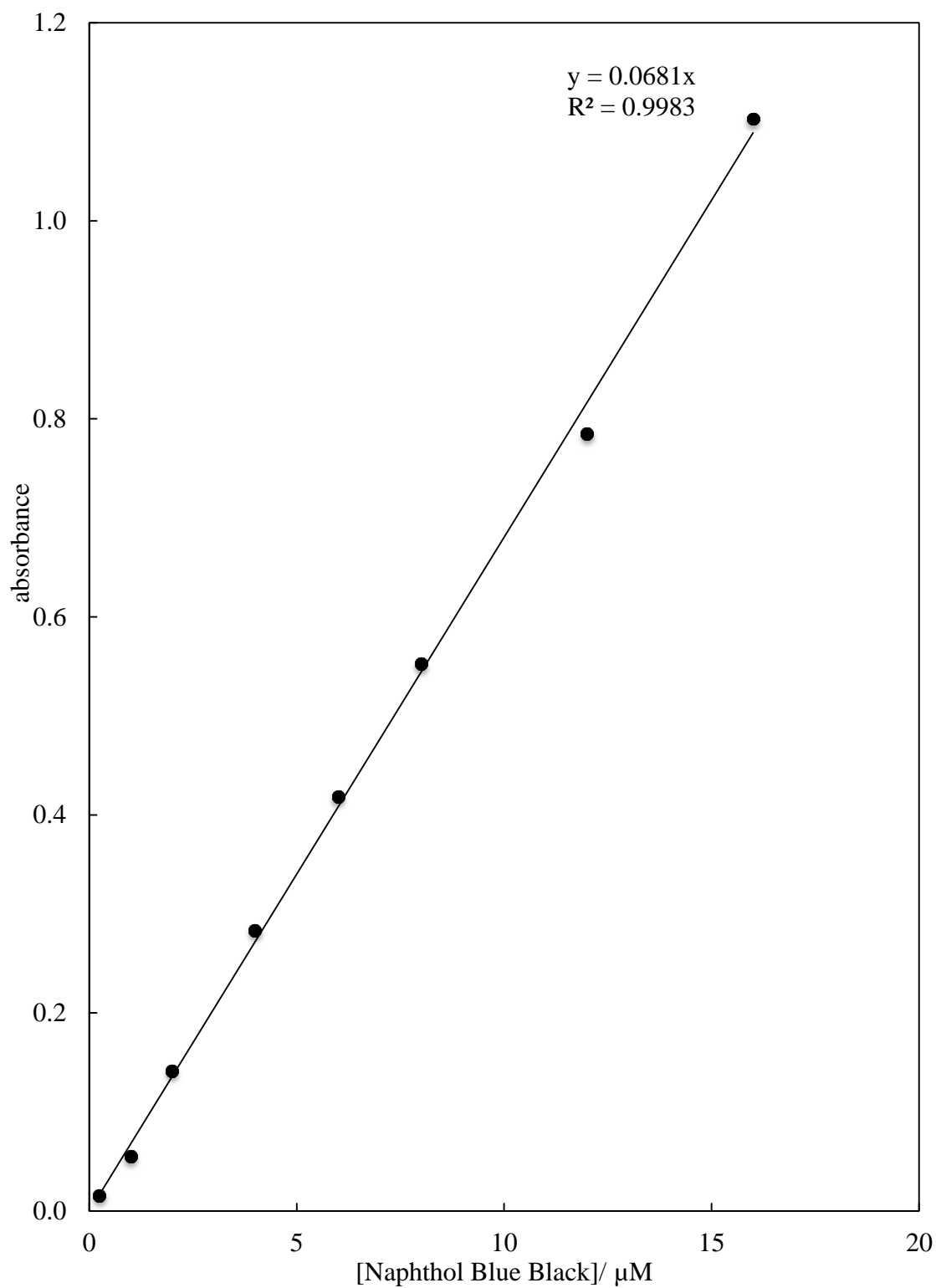
Figure 5.2. Plot of absorbance as a function of time measured at 618 nm. Samples are 2 ml 16 µM NBB + 0.7 ml 10 mM $CuSO_4$ + 0.7 ml 0-100 mM H_2O_2. Measured using a Perkin-Elmer Lambda 25 UV-Visible spectrophotometer with a Helma quartz cuvette (path length, 10 mm) held at 25 ± 0.1 °C.
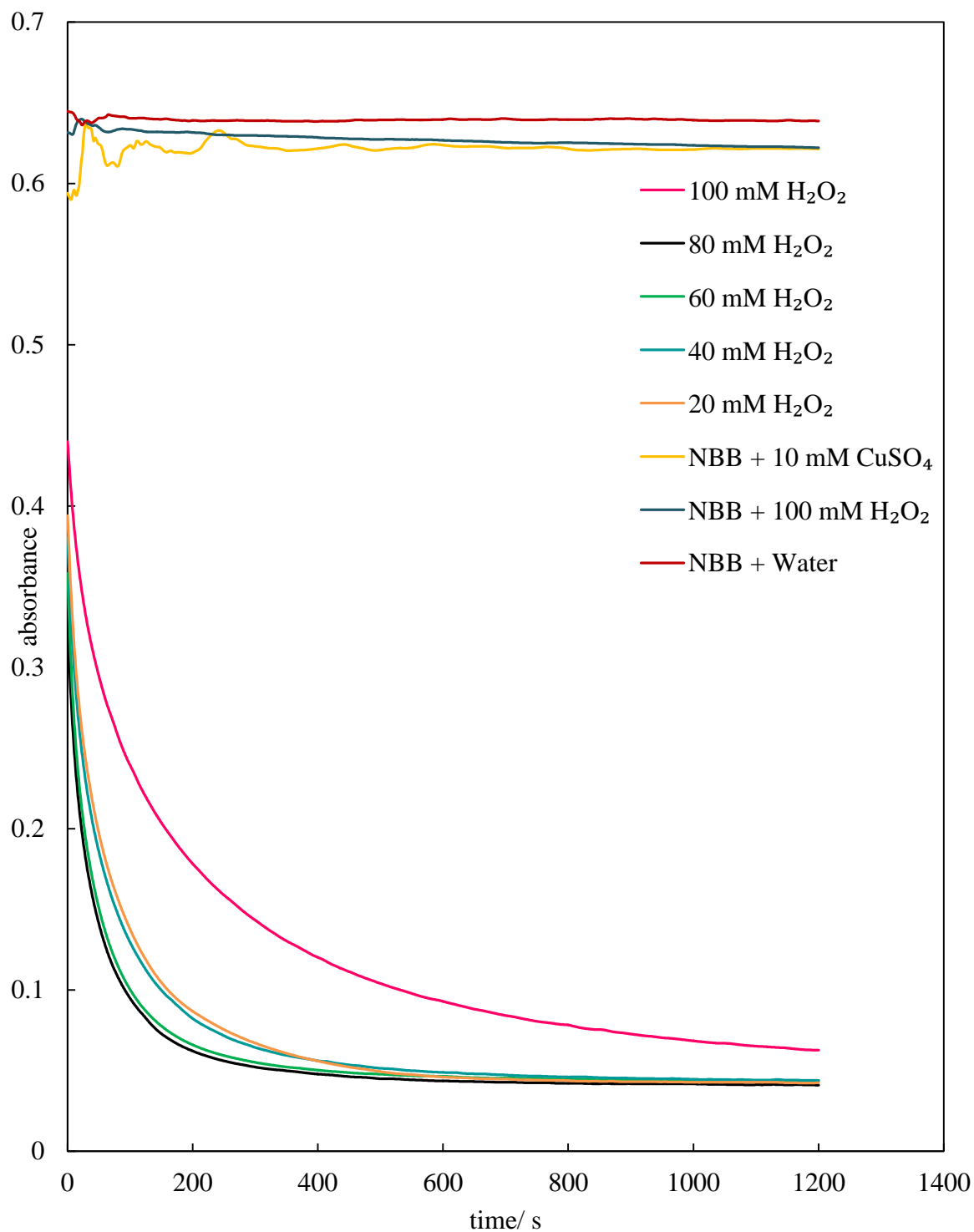
Figure 5.3. Plot of absorbance as a function of time measured at 618 nm. Samples are 2 ml 16 µM NBB + 0.7 ml 100 mM H_2O_2 + 0.7 ml 0-10 mM $CuSO_4$. Measured using a Perkin-Elmer Lambda 25 UV-Visible spectrophotometer with a Helma quartz cuvette (path length, 10 mm) held at 25 ± 0.1 °C.
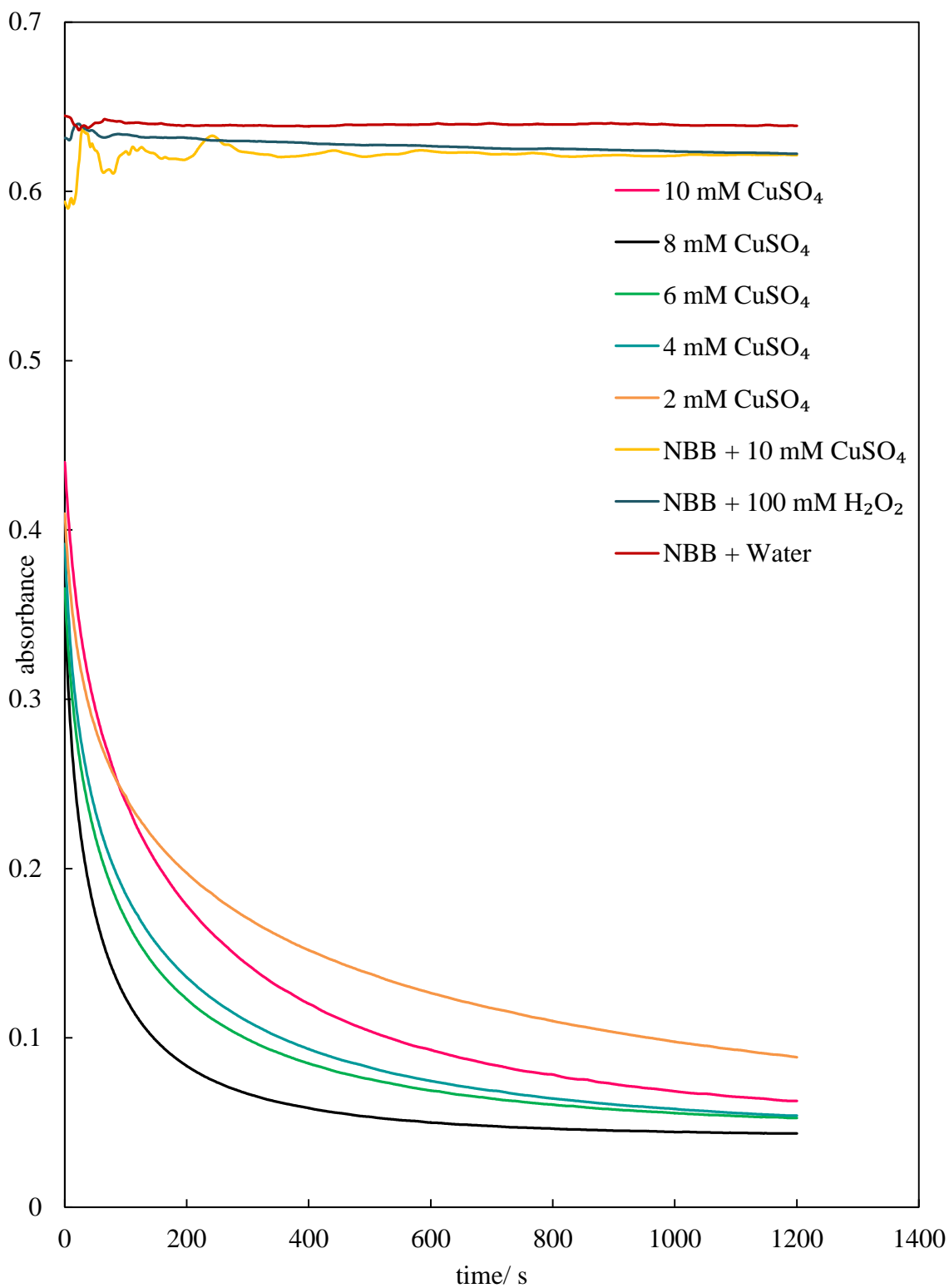
From these graphs, the dye absorbance was converted to concentrations using the calibration plot in Figure 5.1 and the Beer-Lambert law. The molar absorptivity coefficient was found to be $0.066 \pm 0.005 \ \mu M^{-1} \ cm^{-1}$. Figures of the dye concentration as a function of time are shown in Figure 5.5 and 5.7. It can be seen that in all samples whereby the Fenton reagents are added to the dye solution, a rapid decrease in the dye concentration as a function of time occurs. For control samples, there is no dye degradation at all. Some fluctuation around the control sample of copper sulfate and NBB dye can be seen, this may have been due to some interaction between the dye and copper sulfate, or possibly poor/incomplete mixing between the two before the spectrum was obtained. As only one spectrum for the control sample was obtained, it is recommended that for future work, more spectra are obtained to clarify if this is a true effect or a result of incomplete mixing. Images of the cuvettes filled with test solution prior to, and after reaction can be seen in Figure 5.4. A distinct colour change of the sample (dark blue to pink) is observed for addition of all Fenton reagents (Figure 5.4 (b)), at all concentrations. For samples of the dye mixed with copper sulphate, hydrogen peroxide and water alone (Figure 5.4 (c)), no colour change was observed. It is clear that the degradation of the dye results in molecular fragments which maintain some absorbance in the visible range of the electromagnetic spectrum. The initial reaction rates were calculated by equation 5.10:

$$\text{Initial rate} = -\frac{\Delta[\text{NBB}]}{\Delta t}$$

(5.10)

Where $\Delta[\text{NBB}]$ is the difference in concentration between t=0 and t=60 s (Δt). The time range was selected as 60 seconds as the initial rate of the reaction in this time period is relevant for the application as a hand sanitiser. If a fast reaction rate is not achieved in this time period, the product may not have good application as a hand sanitiser where the product is usually applied for a maximum of 60 seconds.

Plots of the initial reaction rates are shown in Figures 5.6 and 5.8, where the concentrations of H_2O_2 and $CuSO_4$ are varied independently. It can be seen that the initial reaction rate initially increases with the addition of H_2O_2 and $CuSO_4$. In both reactions where the concentration of H_2O_2 and $CuSO_4$ were varied independently, it can be seen that the initial reaction rate passes through a slight maximum at 60 mM H_2O_2 and 8 mM $CuSO_4$, respectively. However, above the lowest concentrations of both reagents (2 and 20 mM $CuSO_4$ and H_2O_2, respectively) the initial reaction rate varies only very slightly. It should be noted this data was calculated from only one run, and therefore the experimental error may be larger than the observed variation in reaction rate with reagent concentration. For future work it is recommended to collect a larger quantity of data to support the observations made.

Figure 5.4. Images of cuvettes containing 2 ml 16 µM NBB dye and 1.4 ml Fenton reagents, or water after 20 minutes analysis in UV-visible spectrophotometer. (a) Appearance of all samples prior to analysis (b) after addition of 10 mM $CuSO_4$ and 100 mM H_2O_2 (c) after addition of 100 mM H_2O_2 only.

Figure 5.5. NBB concentration as a function of time measured at 618 nm. Samples are 2 ml 16 μM NBB + 0.7 ml 10 mM $CuSO_4$ + 0.7 ml 0-100 mM H_2O_2. Measured using a Perkin-Elmer Lambda 25 UV-Visible spectrophotometer with a Helma quartz cuvette (path length, 10 mm) held at 25 ± 0.1 °C.
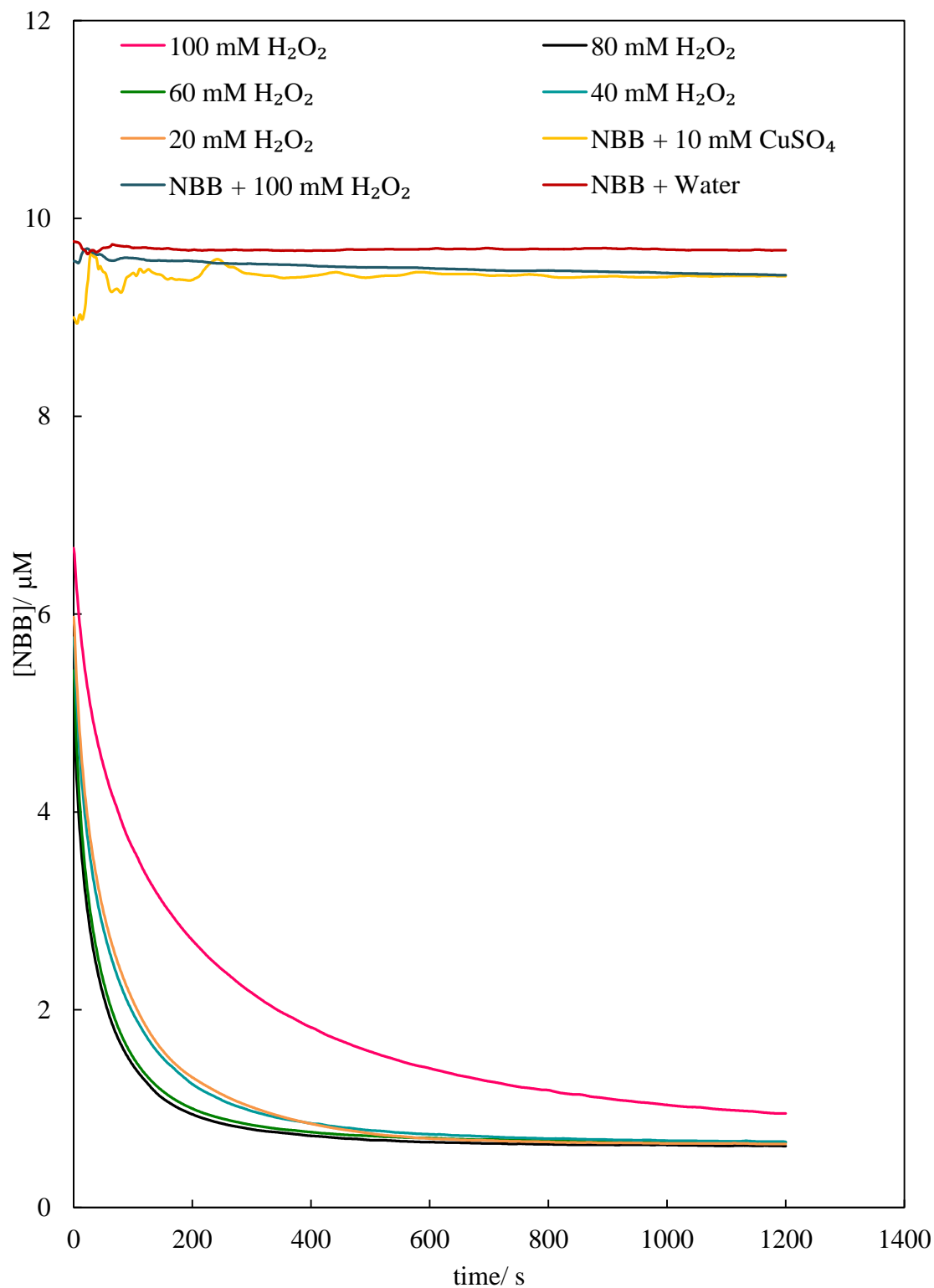
Figure 5.6. Initial rate of degradation of 2 ml 16 uM NBB dye as a function of hydrogen peroxide concentration. Samples are 2 ml 16 μM NBB + 0.7 ml 10 mM CuSO$_4$ + 0.7 ml 0-100 mM H$_2$O$_2$. Initial rate calculated from change in [NBB] from t = 0-60 seconds.
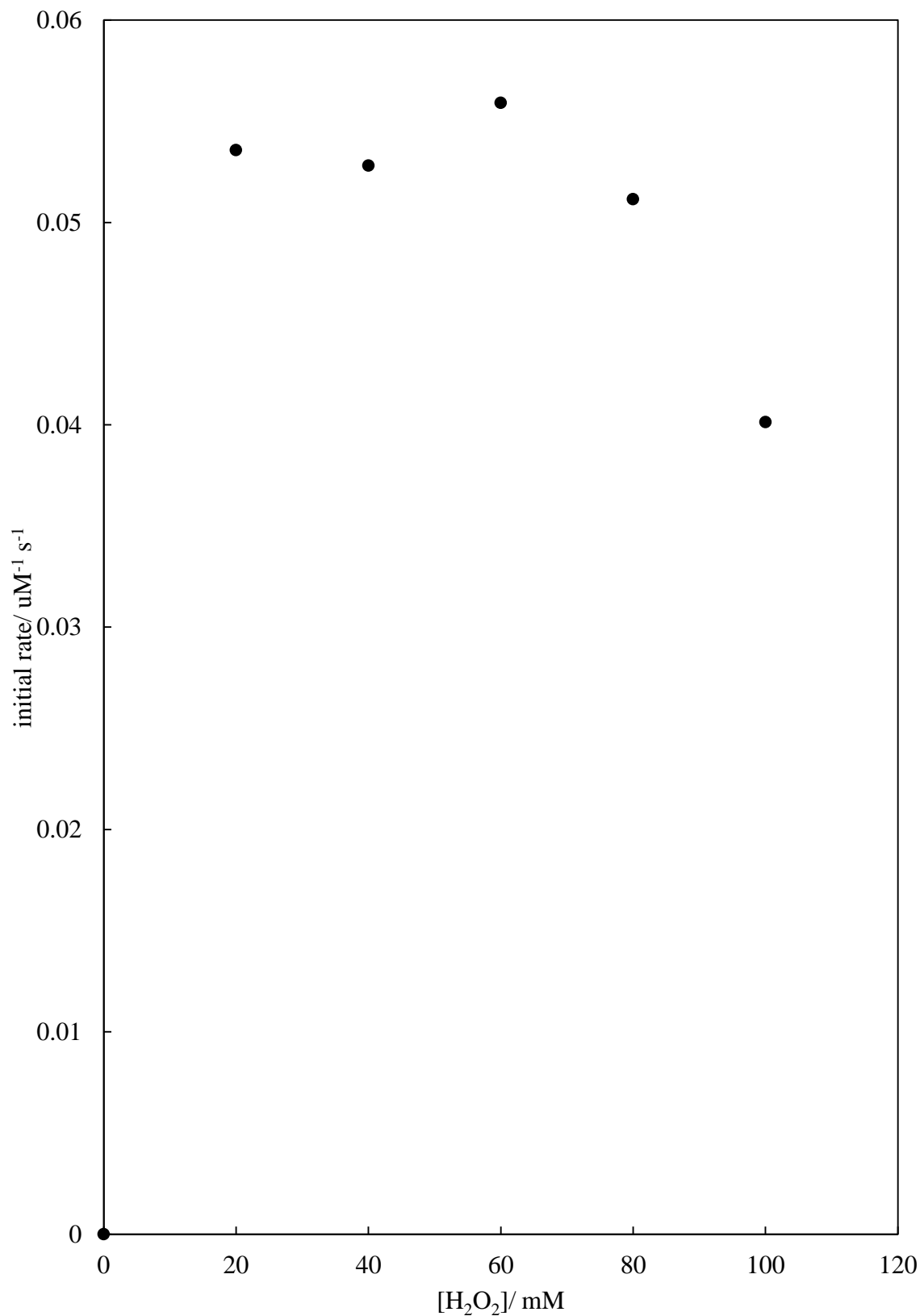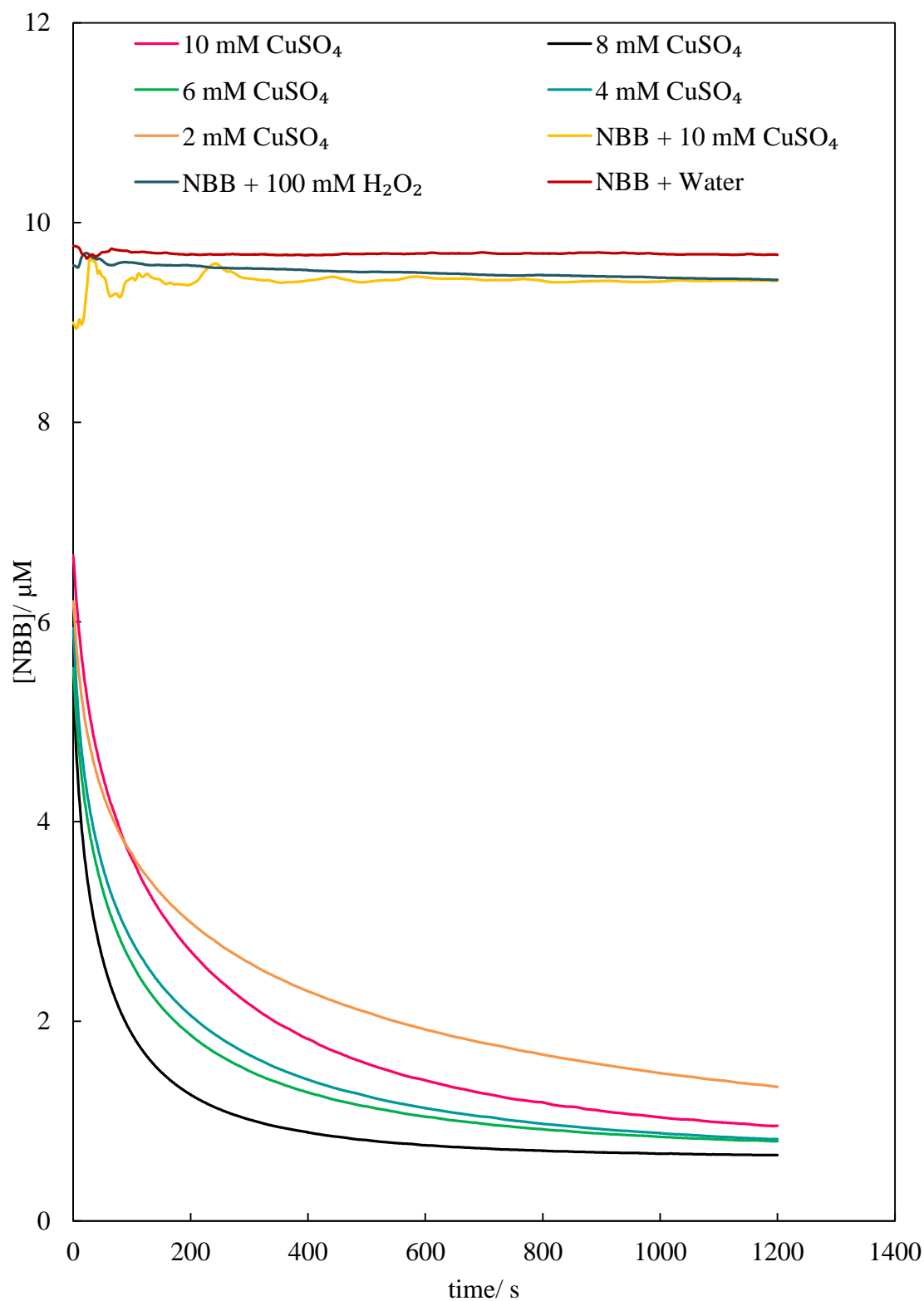
Figure 5.7. NBB concentration as a function of time measured at 618 nm. Samples are 2 ml 16 μM NBB + 0.7 ml 100 mM H_2O_2 + 0.7 ml 0-10 mM $CuSO_4$. Measured using a Perkin-Elmer Lambda 25 UV-Visible spectrophotometer with a Helma quartz cuvette (path length, 10 mm) held at 25 ± 0.1 °C.

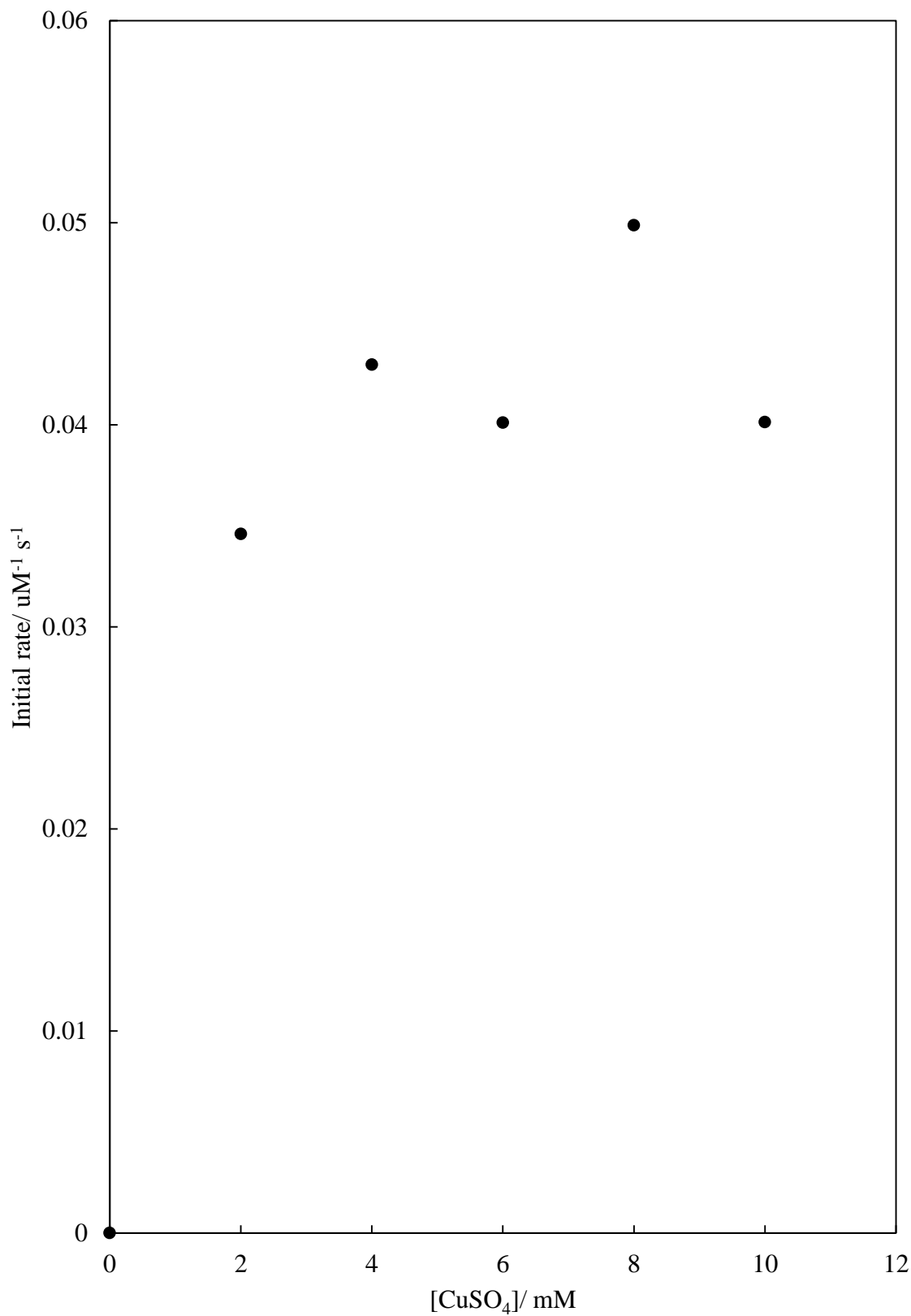**Figure 5.8.** Initial rate of degradation of 2 ml 16 uM NBB dye as a function of copper sulfate concentration. Samples are 2 ml 16 μM NBB + 0.7 ml 100 mM H_2O_2 + 0.7 ml 0-10 mM $CuSO_4$. Initial rate calculated from change in [NBB] from t = 0-60 seconds.

5.3.2   Effect of pH

The effect of pH in the traditional Fenton reaction using an iron catalyst is well known, with much research suggesting that the optimum pH for the Fenton reaction is under acidic conditions.[38,39]

The conditions for the copper-catalysed Fenton-like reaction are very different from those observed for iron systems. The general consensus and understanding from the literature is that copper catalysed systems work optimally at neutral pH, and can operate over a broad range of pH values.[40-42] It has been suggested in some studies that this is due to the reaction mechanism being altered at different pH values. To confirm this, the effect of the pH on the rate of degradation of NBB dye with 10 mM $CuSO_4$ and 100mM H_2O_2 acidified with phosphoric acid was investigated. The pH of the reaction is of interest as it is well known that many bacteria possess an enzyme called catalase. Catalase is contained within many bacterial, and human cells and acts as a defence to protect cells against hydrogen peroxide.[43] It is necessary to acidify the Fenton reagents in order to deactivate/denature bacterial catalase,[44] and additionally stabilise the hydrogen peroxide.

Figure 5.9 shows the percentage reduction in the absorbance of NBB after exposure to the Fenton reagents for 20 minutes. It can be seen that with increasing pH the amount of dye consumed/degraded also increased. Figure 5.10 and 5.11 show the decrease in NBB absorbance and concentration with time. From Figure 5.11, the initial rate of the reactions as a function of pH were calculated using equation 5.10 and the values of initial reaction rate are shown in Figure 5.12. It can be seen that there is a continual increase in the reaction rate as the pH is increased, indicating that the progression of the reaction occurs at an optimal pH of around 4-5. It has been suggested by Shah *et al.* that the addition of acid to the Fenton system could possibly alter the reduction potential of copper (II) so that the copper ions may disfavour reaction with peroxide.[27] These researchers also suggested the possibility for the addition of acids to block the available sites on copper where hydrogen peroxide may interact.

Figure 5.9. Percentage reduction in the absorbance at 618 nm of 2 ml 16 µM NBB dye after exposure to 0.7 ml 10 mM $CuSO_4$ and 0.7 ml 100 mM H_2O_2 over a pH range of 1-4.7 for 20 minutes. Samples measured using a Perkin-Elmer Lamda 25 UV-Visible spectrophotometer and a Helma quartz cuvette with 10 mm path length held at 25 ± 0.1 °C.
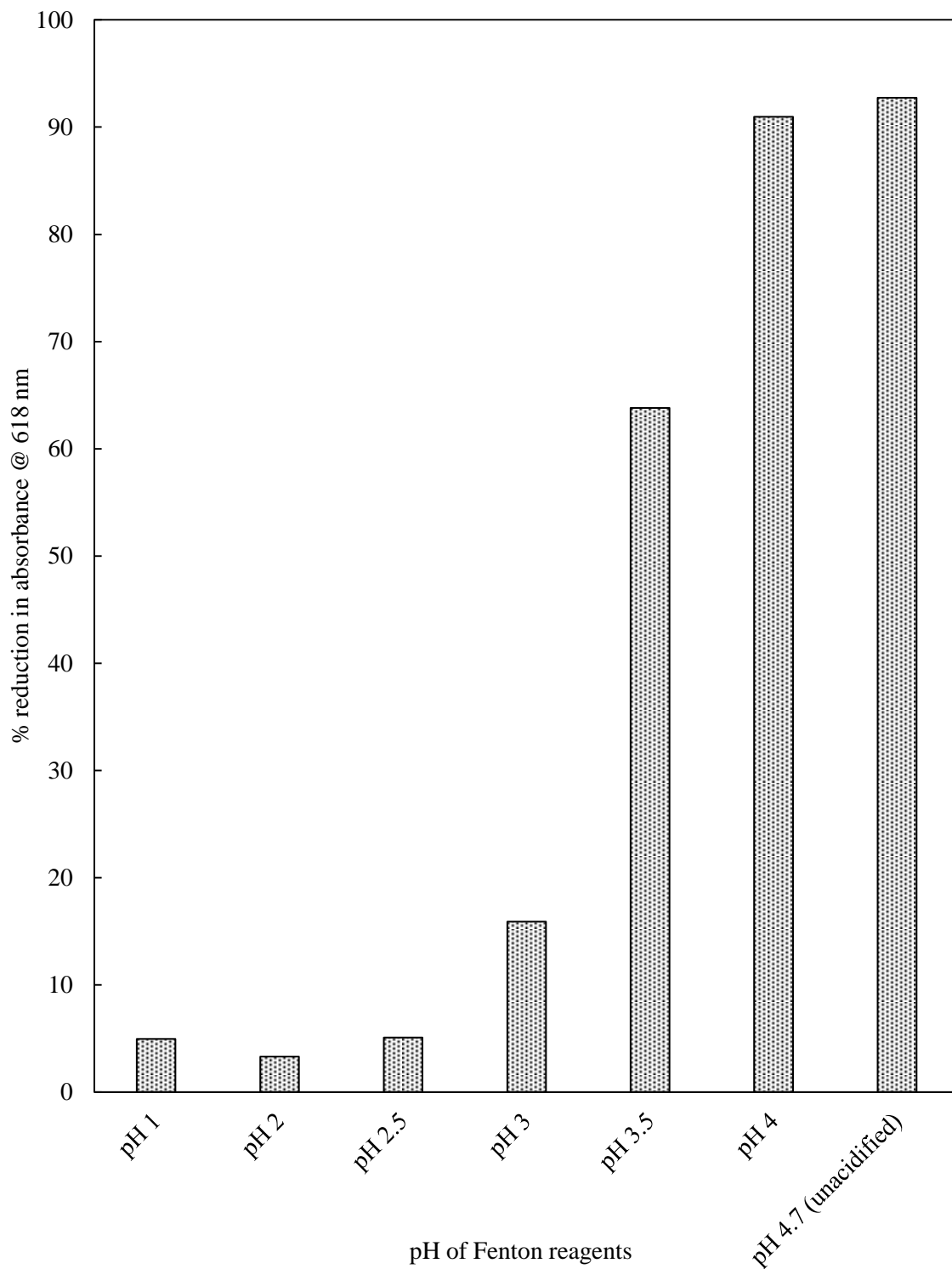
Figure 5.10. Plot of NBB absorbance as a function of time measured at 618 nm. Samples are 2 ml 16 μM NBB + 0.7 ml 100 mM H_2O_2 + 0.7 ml 10 mM $CuSO_4$ acidified over a range of pH values. Measured using a Perkin-Elmer Lambda 25 UV-Visible spectrophotometer with a Helma quartz cuvette (path length, 10 mm) held at 25 ± 0.1 °C.
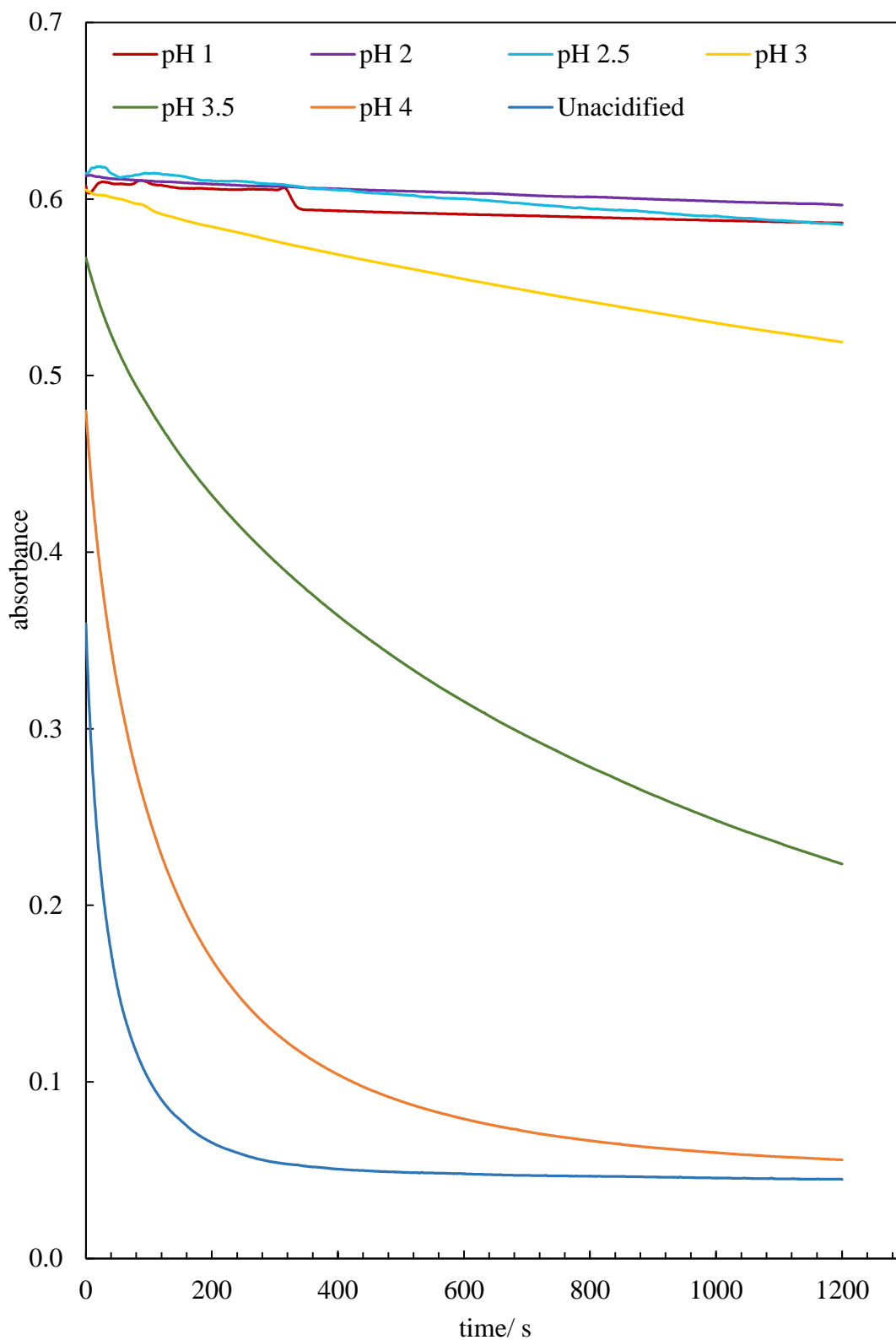
Figure 5.11. Plot of NBB concentration as a function of time measured at 618 nm. Samples are 2 ml 16 μM NBB + 0.7 ml 100 mM H_2O_2 + 0.7 ml 10 mM $CuSO_4$ acidified over a range of pH values. Measured using a Perkin-Elmer Lambda 25 UV-Visible spectrophotometer with a Helma quartz cuvette (path length, 10 mm) held at 25 ± 0.1 °C.
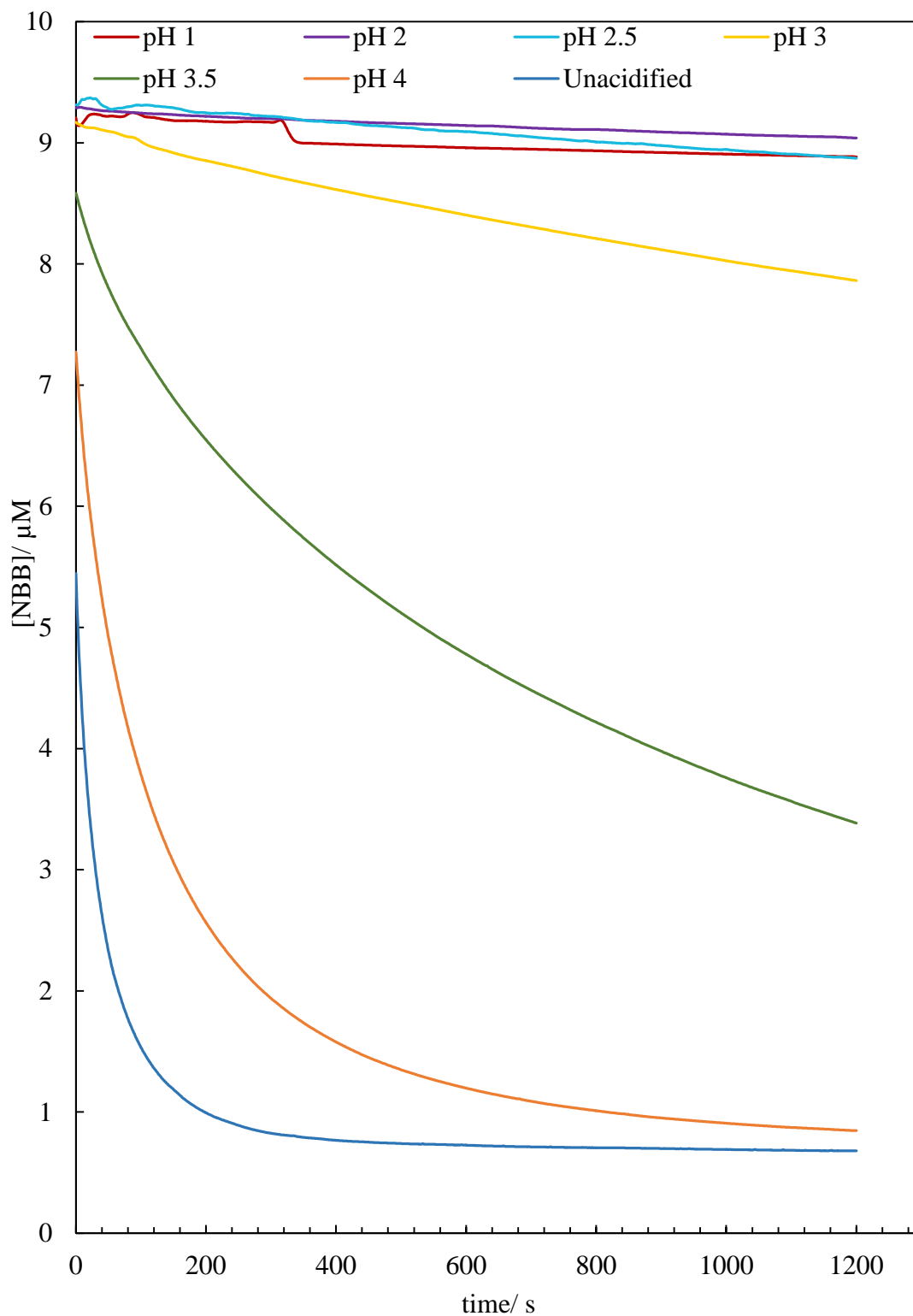
Figure 5.12. Initial reaction rate as a function of pH for the reaction of 2 ml 16 µM NBB dye + 0.7 ml 10 mM CuSO₄ + 0.7 ml H₂O₂ at 25 ± 0.1 °C. Initial rate calculated from concentration reduction of NBB dye from t = 0-60 seconds.

5.4 Encapsulation studies of potential formulations

It was necessary to determine the limits of encapsulation for various different liquids. It has been elucidated from the work presented in Chapter 4, that the contact angle of particles at a liquid-air interface is reduced when the surface tension of the aqueous phase is reduced. Therefore the addition of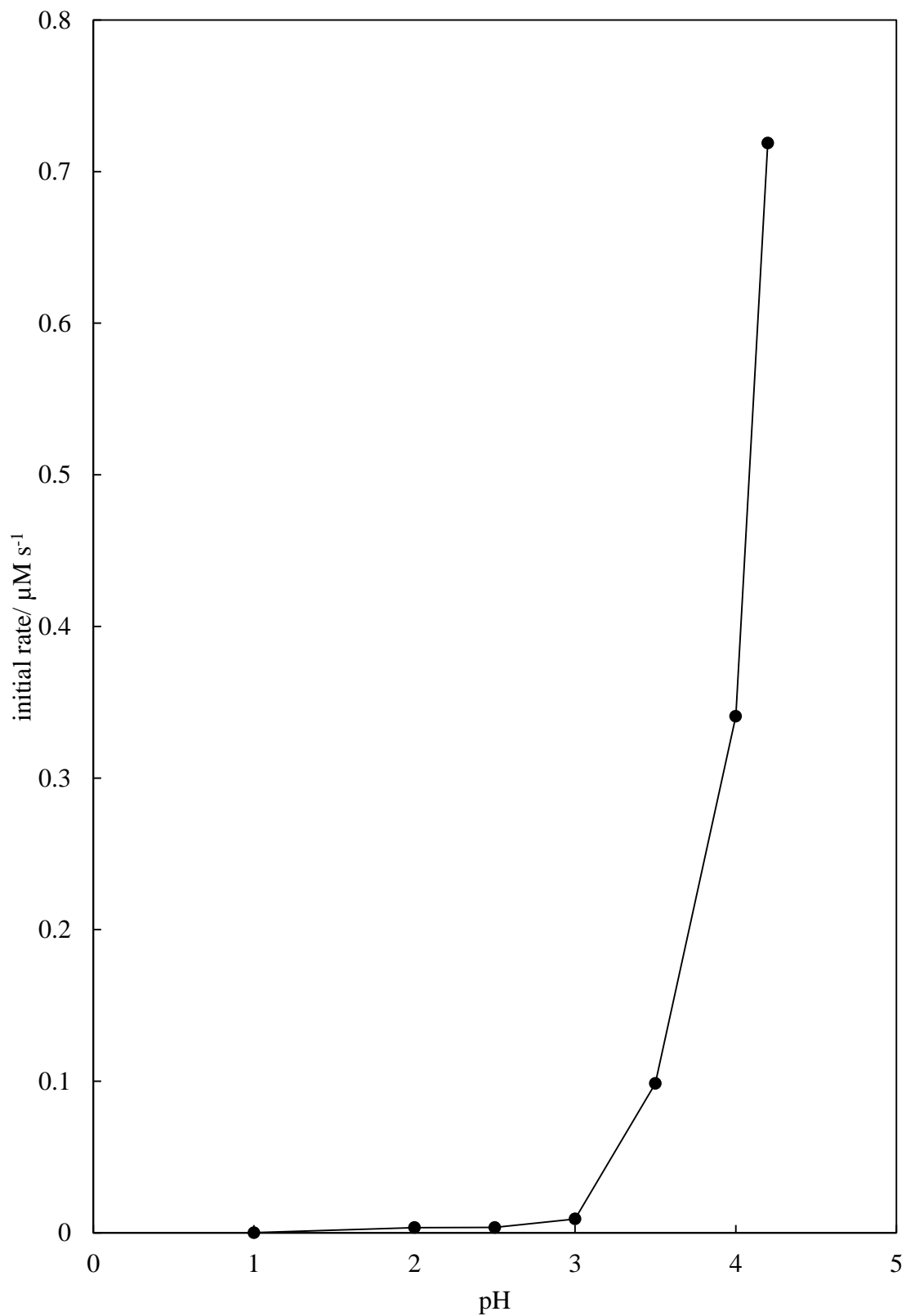 surface tension lowering components to the aqueous phase may destabilise the encapsulated system, as demonstrated in the studies of Binks *et al.*[45] and Bormashenko.[46] In these studies it was demonstrated that the addition of surface-active compounds (such as surfactants and alcohol) to systems of dry water and liquid marbles, destabilised the systems. As copper sulfate and hydrogen peroxide are not surface-active reagents, it is expected that the addition of these reagents to the system will not affect the stability. However, it is of interest to explore the addition of other reagents, such as emollients and fragrances to test the viability of the dry water structure.

A range of samples were prepared by dissolving in water, and then attempting to encapsulate in dry water format. Results of these tests can be seen in Table 5.1. for multiple different potential formulations. It can be seen that as expected, the addition of components that do not demonstrate significant surface activity do not affect the stability of the dry water system. However, the addition of components such as alcohols and surfactants cause the dry water system to invert to a foam.

Table 5.1   Table to summarise findings of dry water screening tests of various different formulations. Samples prepared by blending 95g water containing multiple components (detailed in table below) with 5g of 20% SiOH (hydrophobic) fumed silica particles for 30 seconds.

Sample		Dry water produced?	Notes
Reagent	Mass used/ g		
Hydrogen peroxide	1.95	✔	Dry powder formed, releases contents upon shearing.
Phosphoric acid	1.14		
Water	92.00		
Hydrogen peroxide	3.80	✔	Dry powder formed, releases contents upon shearing.
Phosphoric acid	1.54		
Water	89.68		
Hydrogen peroxide	5.71	✔	Dry powder formed, releases contents upon shearing.
Phosphoric acid	0.77		
Water	88.51		
Hydrogen peroxide	7.64	✔	Dry powder formed, releases contents upon shearing.
Phosphoric acid	0.54		
Water	86.83		
Copper sulfate	1.92	✔	Dry powder formed, releases contents upon shearing.
Phosphoric acid	0.96		
Water	92.12		
Copper sulfate	3.80	✔	Dry powder formed, releases contents upon shearing.
Phosphoric acid	1.53		
Water	89.66		
Copper sulfate	5.72	✔	Dry powder formed, releases contents upon shearing.
Phosphoric acid	1.10		
Water	88.37		

Formulation	Dry water produced?	Notes	Formulation
Copper sulfate Phosphoric acid Water	7.61 0.60 86.60	✔	Dry powder formed, releases contents upon shearing.
Hydrogen peroxide Glycerol Phosphoric acid Water	1.90 4.74 0.76 87.61	✔	Dry powder formed, releases contents upon shearing. Sensation after shearing on skin leaves softer feeling on skin surface.
Hydrogen peroxide Glycerol Phosphoric acid Water	1.91 19.00 1.68 72.44	✔	Sensation after shearing on skin leaves softer feeling on skin surface, more so than with 5% glycerol formulation.
Hydrogen peroxide Lauramine oxide Phosphoric acid Water	1.93 5.72 1.82 85.55	✘	A wet foam was formed which had completely collapsed after 90 minutes. Liquid drained from foam was milky white, indicating presence of particles.
Hydrogen peroxide Glycerol Polyquat-7 Phosphoric acid Water	1.91 4.77 1.05 1.52 85.80	✘	Soufflé-foam generated, creamy texture.
Hydrogen peroxide Glycerol Butylene glycol Phosphoric acid Water	1.90 4.76 2.92 1.31 84.16	✔	Substance formed a dry powder but visually larger drops and not as free-flowing as dry water. Felt soft when applied and sheared on skin.

Formulation	Dry water produced?	Notes	Formulation
Hydrogen peroxide	1.92	✖	Soufflé-foam generated, creamy texture.
Glycerol	4.85		
Butylene glycol	2.76		
Polyquat-7	1.14		
Phosphoric acid	1.01		
Water	83.33		
Copper sulphate	1.91	✖	Soufflé-foam generated, creamy texture.
Ethanol	4.67		
Phosphoric acid	1.00		
Water	87.44		
Hydrogen peroxide	1.89	✔	Dry powder formed, releases contents upon shearing. Sensation after shearing on skin leaves softer feeling on skin surface, skin surface has pleasant fragrance.
Glycerol	4.85		
"Mountain mist" fragrance	0.06		
Phosphoric acid	1.26		
Water	86.94		

5.5   Anti-bacterial efficacy testing

As the application of the Fenton reaction in this study is an anti-bacterial sanitiser, the anti-bacterial efficacy of the copper-catalysed Fenton reaction was investigated. An initial *in vitro* study was carried out by measuring the effect of addition of aqueous Fenton reagents to a vessel containing a known inoculum of *Escherichia coli* bacteria. After this, an *in vivo* study of application of the Fenton reagents to the skin surface contaminated with *E. coli* was carried out. The use of volunteers allowed for the encapsulated Fenton reagents to be studied (dry powder could be sheared on the skin).

Escherichia coli is a Gram-negative, rod-shaped bacteria. Gram-negative bacteria are named so, as the cells do not retain a Gram stain after rinsing (stain comprises purple dye and iodine). Gram-negative bacteria are colourless after rinsing with alcohol, but retain a safranin dye stain, which gives the bacteria a characteristic pink colour. Conversely, Gram-positive bacteria retain the purple dye, so appear purple.[47] The cell wall structure of these two different classifications of bacteria are responsible for their staining behaviour. The cell wall of Gram-negative bacteria consists of a few layers of peptidoglycan (comprising N-acetylglucosamine bound to N-acetylemuramic acid by a β-1,4 linkage). The peptidoglycan layer is additionally bound to a lipoproteins, lipopolysaccharides and phospholipids in the outer membrane. Due to the small amount of peptidoglycan in the cell wall, Gram-negative bacteria are more susceptible to mechanical breakage. However, the outer lipid layer of the cell membrane provides protection against phagocytosis, detergents, heavy metals, bile salts, dyes and certain antibiotics. Figure 5.13 the various structures comprising the cell wall of a Gram-negative bacteria.[43]

Figure 5.13.   Schematic representation of the cell wall structure of a Gram-negative bacterium.
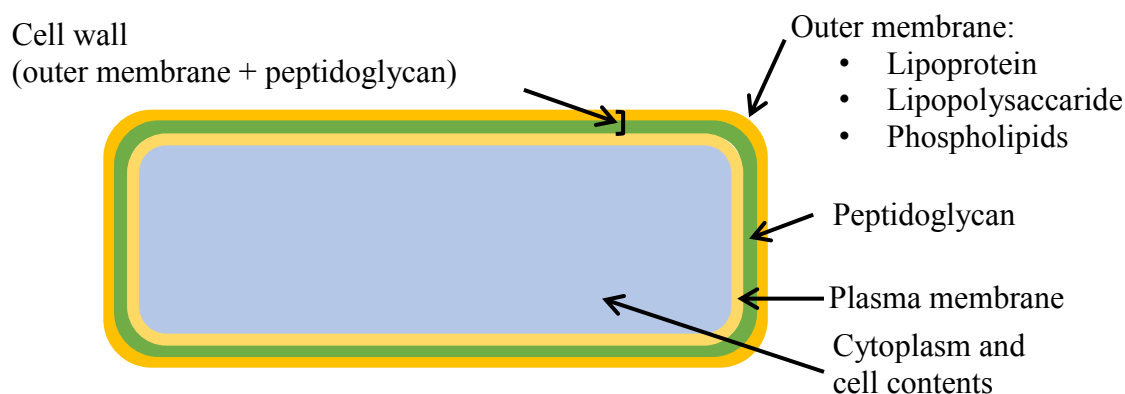
5.5.1 *In vitro studies*

The *in vitro* study was carried out in microbiology laboratories at the Sponsor Company (Deb Denby Site, U.K.). An EN 1040 test was carried out. In brief, 8 ml of the test solution (in the case of the Fenton components, 4 ml of each reagent) along with 1 ml deionised water was added to a 1 ml suspension of 1×10^8 cfu ml^{-1} *E. coli*. This means that there were 1×10^8 bacterial cells (or "colony forming units", cfu) per millilitre of suspension. The reagents were shaken with the inoculum for the specified test time (30 or 60 seconds) and then passed through a membrane filter and rinsed with membrane rinse fluid (Tween 80 surfactant solution). The filters used allowed for bacterial cells to be trapped directly on the membrane, which was then transferred to an agar plate and incubated for 48 hours at 37.5 ± 0.5 °C. The colonies formed on the membrane after this time were then counted by eye, and the reduction in the number of bacterial cells was reported as a log reduction calculated by:

$$\text{Log reduction} = \log_{10}\left(\frac{A}{B}\right)$$

(5.11)

Where A is the number of viable organisms before treatment and B is the number of viable organisms after treatment.

Figure 5.14 shows the effect of addition of various Fenton reagents to a 1×10^8 cfu ml^{-1} *E. coli* after 60 seconds exposure, where the effect of concentration and pH of the reagents was investigated. As for *in vitro* testing it is not possible to test encapsulated liquids (e.g. dry water) only solutions have been tested. It can be seen that irrespective of the pH, copper sulfate alone shows around a 4.5 log reduction, so has some anti-bacterial efficacy alone. As expected the efficacy of hydrogen peroxide alone is strongly affected by pH, at low pH the bacterial catalase is denatured and so cannot consume the H_2O_2, therefore the H_2O_2 shows significant efficacy at low pH. However, the relationship between the Fenton reagents and pH can be seen clearly, whereby increasing the pH results in a higher bacterial kill. In fact up to an 8 log reduction in the bacteria is seen at pH 4, demonstrating all bacteria in the suspension were killed. This is in keeping with the findings of the kinetic studies of the Fenton reaction between copper sulfate and hydrogen peroxide, whereby the rate of the reaction is slower at lower pH.

Figure 5.14. Log reduction of 1×10^8 cfu ml^{-1} inoculum of *E. coli* after 60 second exposure to various concentrations of Fenton solutions (Copper sulfate, CuSO$_4$ and hydrogen peroxide, H$_2$O$_2$) at pH values 2-4. Sample membranes plated on tryptone soya agar plates and incubated at 32.5 ± 2.5 °C for 48 hours.
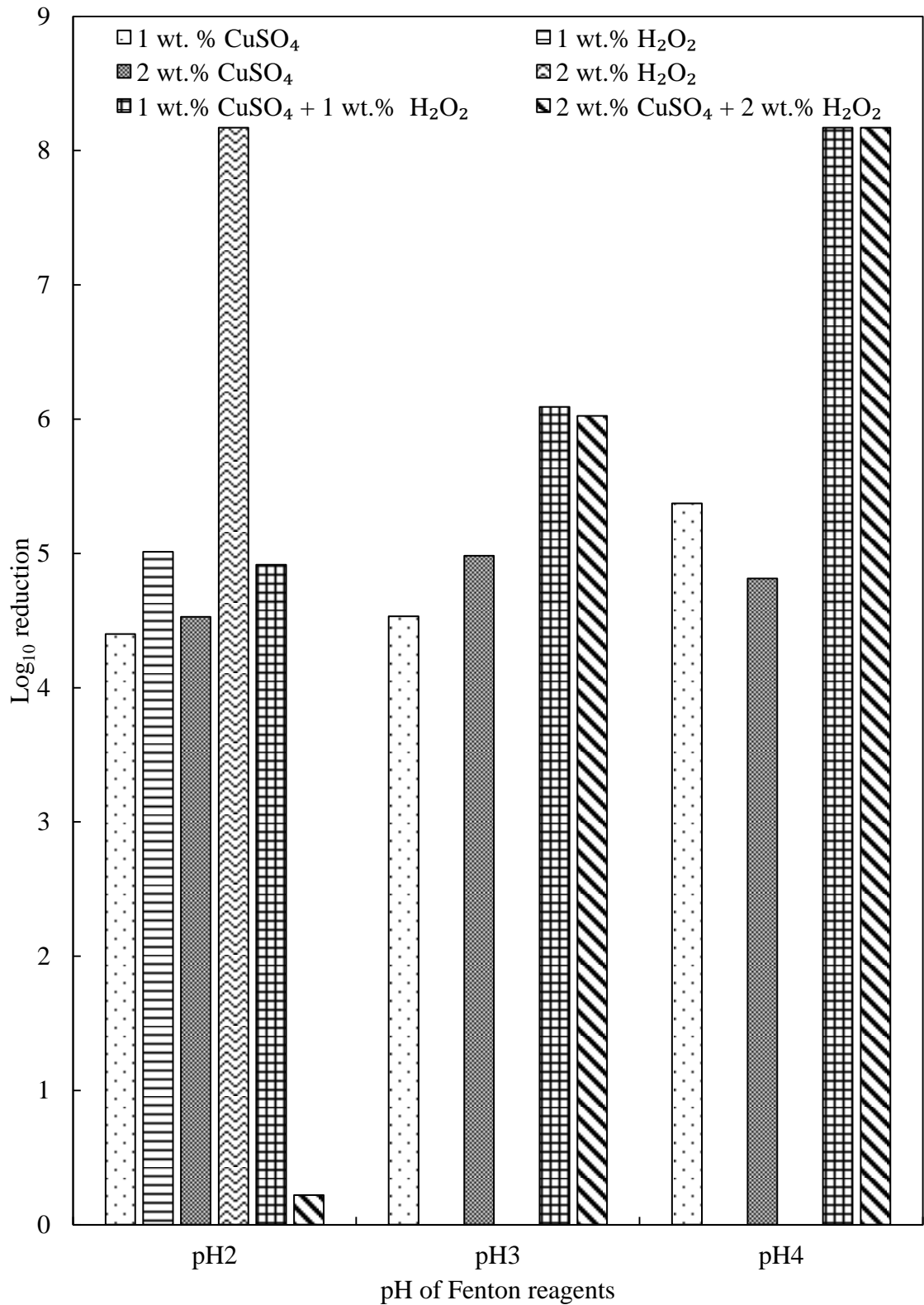
5.5.2   In vivo studies

To test the potential application for the encapsulated Fenton reaction as a hand sanitiser, it was necessary to carry out *in vivo* studies on the skin surface of volunteers. This technique allowed for testing the dry powder formulations, as the participants could shear the dry powder on their hands. *In vivo* testing was carried out at an external CPA accredited lab (Clinical Microbiology Services, Queen Elizabeth Hospital, Birmingham) using an EN1500 test standard. The test in brief comprised contaminating clean hands by immersing into 1 L of 1×10^8 cfu ml^{-1} *E.coli* for 5 seconds and allowing to air dry for 3 minutes. The "pre-count" was then carried out by immersing the finger tips in a tryptone soya agar broth contained in petri dishes. The test product (3 ml) was then applied to the skin in two separate batches of 1.5 ml and rubbed into the skin surface by the volunteer following a 5-step hand washing standard. The "post-count" was carried out by then immersing the fingertips in petri dishes containing tryptone soya agar broth and a neutralising agent to neutralise the reaction. The samples were then diluted and plated on agar plates, then incubated for 48 hours at 37.5 ± 0.5 °C.

Figures 5.15 and 5.16 show the log reduction in *E.coli* after exposure to Fenton reagents in liquid and dry powder format for 60 seconds at pH 2 and 4, respectively. Figure 5.17 shows a comparison of the bacterial efficacy at both pH values. It can be seen that despite pH having a pronounced effect in the *in vitro* and kinetic studies, it appears to have little effect in the *in vivo* studies. It should be noted though that although the pH dependency of the Fenton reaction did not translate to the *in vivo* experiments, this study was a preliminary study was only carried out on a sample size of five volunteers. Additionally, the results are not very promising when comparing the efficacy of the Fenton mixture to the reference sample. The mixture of the reagents shows an improved efficacy in comparison to the control solutions alone, but there is a significant loss of efficacy when the solutions are applied to the skin as an encapsulated powder. It is thought that this was due to difficulty in applying the mass of powder to the skin as there was a significant loss of sample due to the light, fluffy texture of the dry water. Some consideration would need to be given to the safety and toxicity of the use of fumed silica particles in a skin care formulation due to the potential for respiratory irritation associated with their use.

Figure 5.15. Log reduction of 1×10^8 cfu ml^{-1} inoculum of *E. coli* after 60 second exposure to Fenton reagents in solution and dry water format at pH 2. Samples plated on tryptone soya agar plates and incubated at 32.5 ± 2.5 °C for 48 hours. Error bars show standard deviation from an average of five volunteers.
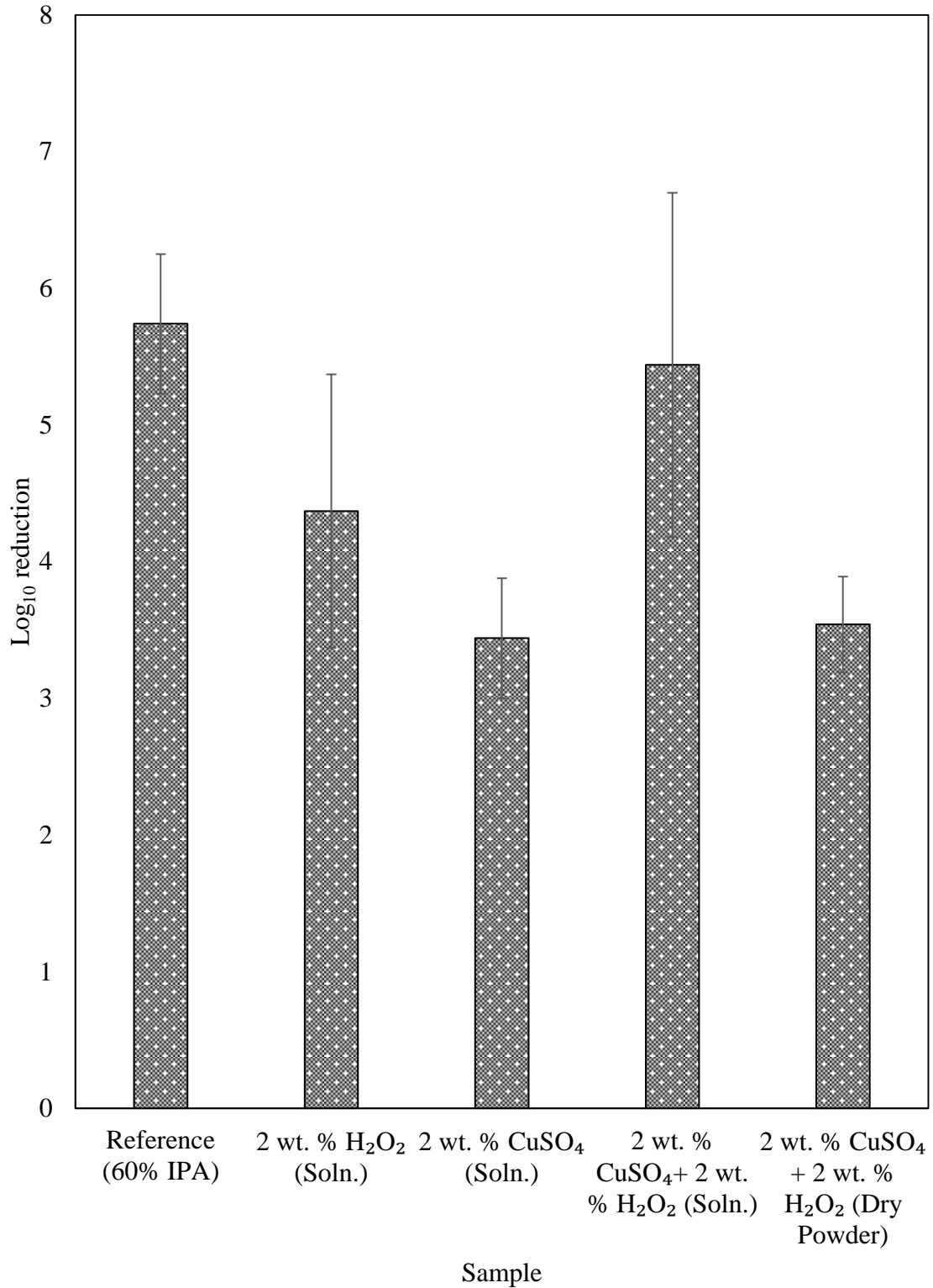
Figure 5.16. Log reduction of 1×10^8 cfu ml^{-1} inoculum of *E. coli* after 60 second exposure to Fenton reagents in solution and dry water format at pH 4. Samples plated on tryptone soya agar plates and incubated at 32.5 ± 2.5 °C for 48 hours. Error bars show standard deviation from an average of five volunteers.
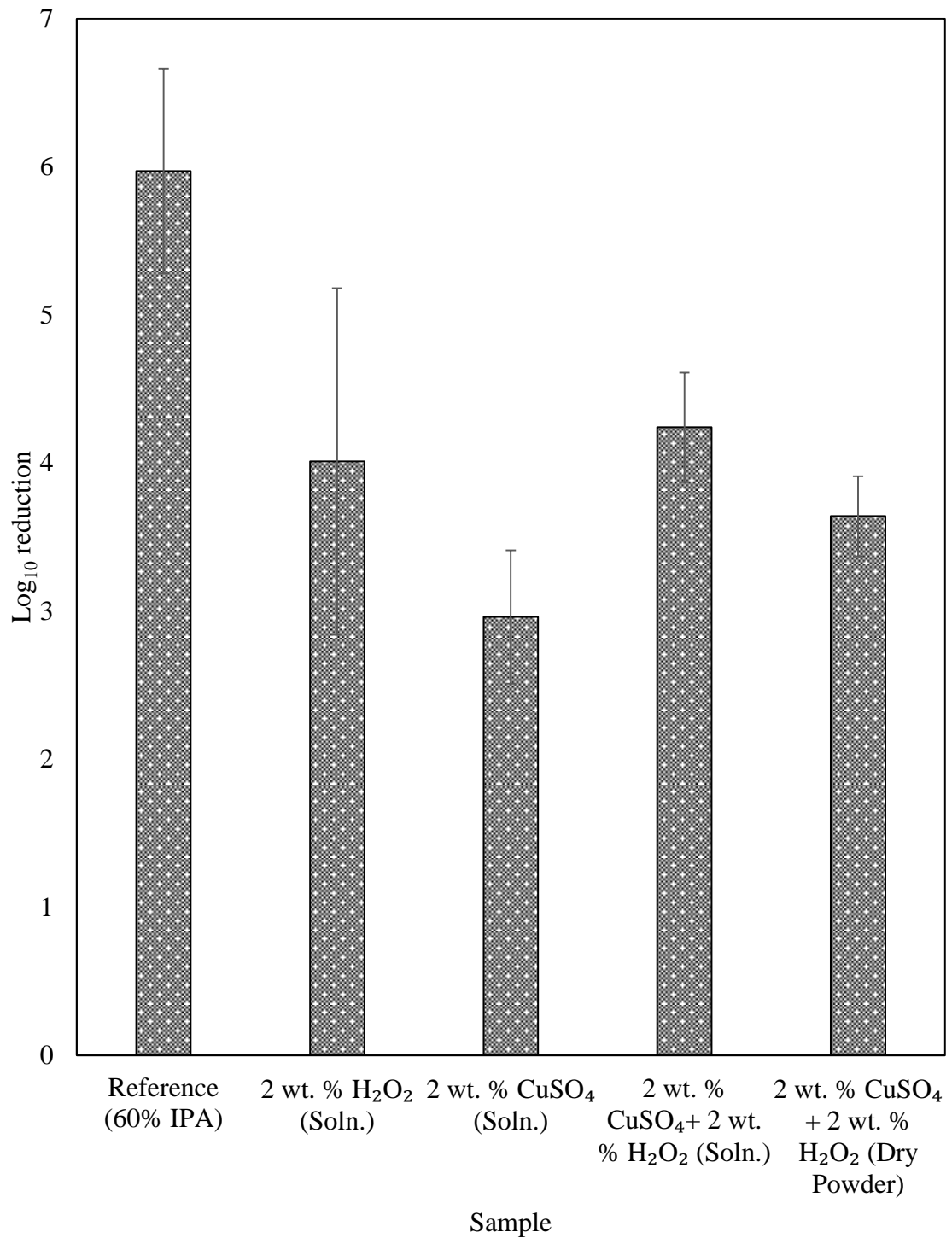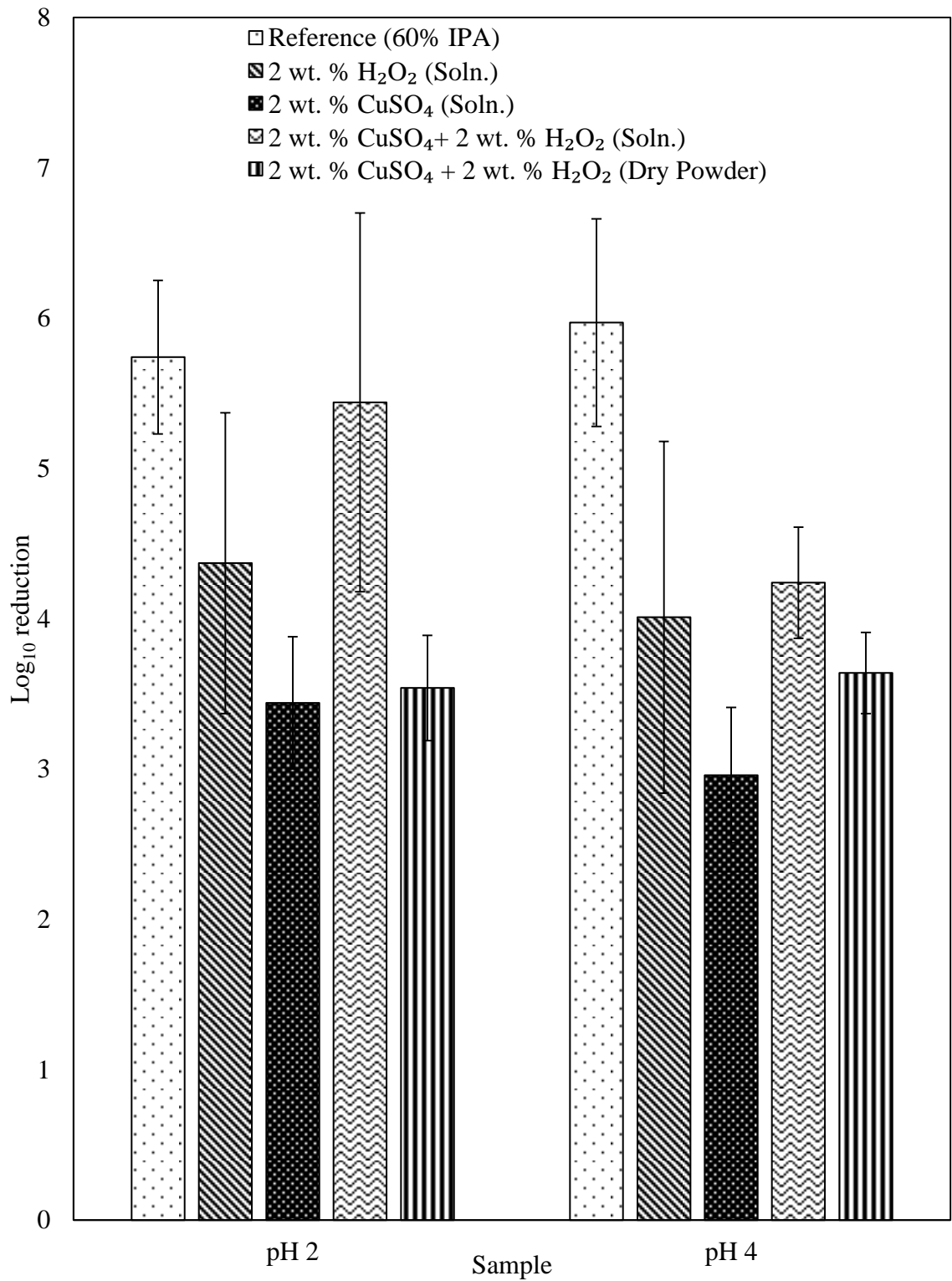
Figure 5.17. Comparison of log reduction of 1×10^8 cfu ml^{-1} inoculum of *E. coli* after 60 second exposure to Fenton reagents at pH 2 and 4. Samples plated on tryptone soya agar plates and incubated at 32.5 ± 2.5 °C for 48 hours. Error bars show standard deviation from an average of five volunteers.

5.6   Stability of formulations

As mentioned earlier, the requirement to acidify the Fenton solutions is not only for the purpose of deactivating the bacterial catalase, but for stabilising the hydrogen peroxide, which degrades rapidly alone, meaning that without acidification, the final product would have a poor shelf life. In all of the results presented, phosphoric acid has been used as a stabilising acid, however the industrial sponsor were keen to investigate the potential of other acids as stabilising agents. Therefore, the effect of phosphoric, maleic and citric acids on stabilising a solution of 2 wt % hydrogen peroxide under accelerated conditions is shown in Figure 5.19. It can be seen that the citric acid is a poor stabiliser of hydrogen peroxide, imparting no stability at all, in comparison to the control sample of hydrogen peroxide alone. However, the remaining two acids were effective at stabilising the hydrogen peroxide so have application for stabilising agents in the final formulation.

Figure 5.19. Concentration of 4 g (in 400 g water) of hydrogen peroxide (initial concentration 2 wt.%) in the presence of maleic, citric and phosphoric acids as a function of time under accelerated conditions (70 °C). Samples taken from 0-25 days after preparation. Error bars show maximum and minimum values from an average of 2 repeat measurements.
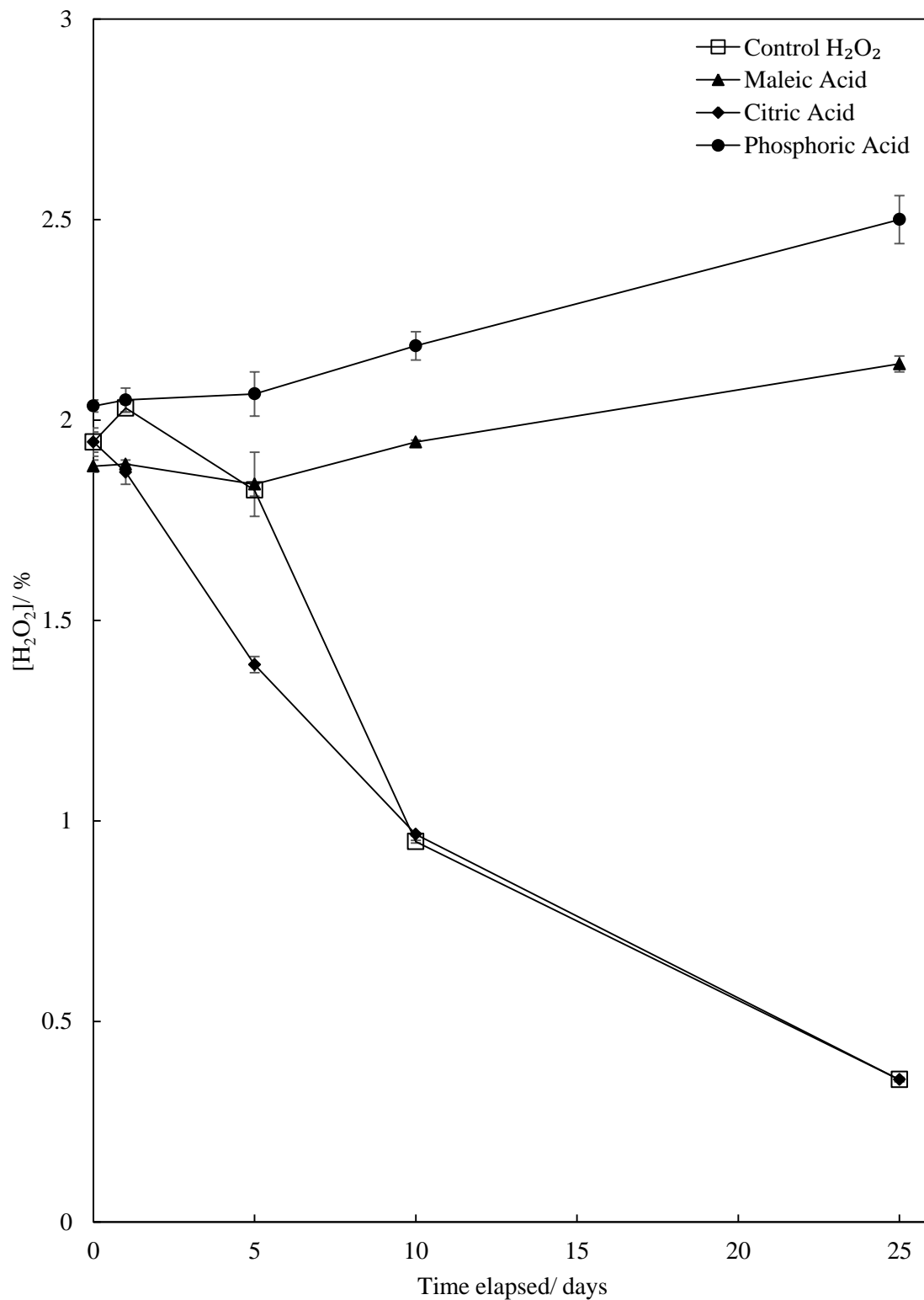
5.7 Summary

This chapter aimed to investigate the kinetics and application of the copper-catalysed Fenton-like reaction for use in a novel encapsulated hand sanitiser. Initially, the kinetics of the reaction were investigated by a dye degradation method using UV-Visible spectrophotometry. It was found that at all concentrations of Fenton reagents investigated at neutral pH, the probe dye was degraded rapidly (within 5 minutes). The initial rate of the reactions was determined by measuring the concentration change in NBB dye for the first 60 seconds of the reaction. It was found that when the concentration of both copper sulfate and hydrogen peroxide were varied independently, the initial rate of the reaction increased with addition of the Fenton reagents, but only varied slightly with increasing concentration. The rate for both reagents passed through a slight maximum at 60 mM and 8 mM for hydrogen peroxide and copper sulfate, respectively. The effect of pH on the initial reaction rate was then investigated, where it was found that the reaction had a strong dependence on pH, with the rate dropping significantly as the pH was reduced. This behaviour has been observed throughout the literature although there is no consensus over why the pH causes such a strong effect on the rate of the Fenton reaction. Some studies have suggested the mechanism of the reaction switches from one that produces hydroxyl radicals at low pH to one that produces intermediate copper species of high valency. Other research has suggested the addition of acid alters the reduction potential of copper, reducing its ability to react with peroxide molecules.

A brief investigation into the encapsulation potential for various different components was carried out. It was found that the addition of components to the aqueous phase that altered the surface tension of the liquid significantly (such as alcohols and surfactants) caused the dry water systems to phase-invert to aqueous foams. This finding is not surprising given the findings from Chapter 4, whereby the contact angle of hydrophobic particles was shown to decrease with decreasing surface tension of the aqueous phase.

An important feature of the novel hand sanitiser concept is not only the encapsulation aspect, but also the antimicrobial efficacy. Therefore, *in vitro* and *in vivo* studies were carried out to investigate the potential antimicrobial efficacy of the aqueous solutions and encapsulated powdered Fenton reagents on *E. coli* bacteria. The *in vitro* study demonstrated a significant enhancement of the bacterial kill at higher pH values (around pH 4) where an 8 log reduction was observed. This supported the findings of the kinetic studies where a strong pH dependence of the reaction rate was shown. However, the *in vivo* studies showed a different pattern. Firstly, there was a significant loss in the efficacy of the solutions when applied to a skin surface, to around 4.5 logs at pH 4. There was further loss of bactericidal efficacy when the Fenton reagents were applied to the skin as a dry powder. It is suggested that this may have been due to loss of the powder on application. The test standard requires 3 ml of liquid, the equivalent mass of this in dry water format is a large volume of powder, which was difficult to apply to the skin surface without spillage. However, there was some efficacy of the powder and some reduction in the amount of bacteria killed. To progress the system, it may be necessary to adapt the encapsulated concentrations so that a lower mass of powder is required. It is additionally possible that the hydrophobic silica itself acts as a barrier on the skin for the reagents to access the bacteria contaminated on the skin surface. It may also be possible to deliver the powder in a different format, such as suspended in a gel, although the behaviour of dry water in these systems is not known.

5.8   References

1. H.J.H. Fenton, *J. Chem. Soc. Trans.*, 1894, **65**, 899.

2. K. Barbusiński, *Chemia Dydaktyka Ekologica Metrologica*, 2009, **14**, 101.

3. C. P. Huang, C. Dong and Z. Tang, *Waste Manage.*, 1993, **13**, 361.

4. E. Neyens and J. Baeyens, *J. Hazard. Mat.*, 2003, **B98**, 33.

5. S.H. Lin, C. M. Lin and H.G. Leu, *Water Res.*, 1999, **33**, 1735.

6. K. Barbusiński, *Ecol. Chem. Eng. S*, 2009, **16**, 347.

7. H.B. Dunford, *Coord. Chem. Rev.*, 2002, **233**, 311.

8. F. Haber and J. Weiss, *Proc. Roy. Soc. A*, 1934, **147**, 332.

9. W.G. Barb, J.H. Baxendale, P. George and K.R. Hargrave, *Trans. Faraday Soc.*, 1957, **47**, 462.

10. F. Haber and R. Willstäter, *Chem. Ber.*, 1931, **64**, 2844.

11. W.C. Bray and M.H. Gorin, *J. Am. Chem. Soc.*, 1932, **54**, 2124.

12. D.T. Sawyer, A. Sobkowiak and T. Matsushita, *Acc. Chem. Res.*, 1996, **29**, 409.

13. S. Goldstein and D. Meyerstein, *Acc. Chem. Res.*, 1999, **32**, 547.

14. C. Walling, *Acc. Chem. Res.*, 1998, **31**, 157.

15. J.H. Baxendale, M.G. Evans and G.S. Park, *Trans. Faraday. Soc.*, 1946, **42**, 155.

16. M.K. Eberhardt, G. Ramirez and E. Ayala, *J. Org. Chem.*, 1989, **54**, 5922.

17. J.E. Repine, R.B. Fox and E.M. Berger, *J. Biol. Chem.*, 1981, **256**, 7094.

18. E. Linley, S.P. Denyer, G. McDonnell, C. Simons and J.-Y. Maillard, *J. Antimicrob. Chemother.*, 2012, **67**,1.

19. B. Halliwell and J.M.C. Gutteridge, *Biochem. J.*, 1984, **219**, 1.

20. J.P. Kehrer, *Toxicol.*, 2000, **149**, 43.

21. A.D. Bokare and W. Choi, *J. Hazard. Mater.*, 2014, **275**, 121.

22. D.A. Nichela, A.M. Berkovic, M.R. Costante, M.P. Juliarena and F.S. García Einschlag, *Chem. Eng. J.*, 2013, **228**, 1148.

23. J.F. Perez-Benito, *J. Inorg. Biochem.*, 2004, **98**, 430.

24. J. Kim and I.S. Metcalfe, *Chemosphere*, 2007, **69**, 689.

25. C.L. Lim, N. Morad, T. T. Teng and N. Ismail, *J. Hazard. Mater.*, 2009, **168**, 383.

26. I.A. Salem, *App. Catal. B: Environ.*, 2000, **28**, 153.

27. V. Shah, P. Verma, P. Stopka, J. Gabriel, P. Baldrian and F. Nerud, *App. Catal. B: Environ.*, 2003, **46**, 287.

28. J. Gabriel, V. Shah, P. Baldrian and F. Nerud, *Folia. Microbiol.*, 2000, **45**, 573.

29. H.R. Dittmar, I.L.Baldwin and S.B. Miller, *J. Bacteriol.*, 1930, **19**, 203.

30. C.E. Bayliss and W.M. Waites, *J. Gen. Microbiol.*, 1976, **96**, 401.

31. O.I. Aruoma, B. Halliwell, E. Gajewski and M. Dizdaroglu, *Biochem. J.*, 1991, **273**, 601.

32. D. Schutte, F.-T. Schmitz and H. Brünner, *Predominantly aqueous compositions in a fluffy powder form approximating powdered solids behaviour and process for forming same*, 1968, US 3393155 A.

33. B.P. Binks and R. Murakami, *Nat. Mater.*, 2006, **5**, 865.

34. I. Yamazaki and L.H. Piette, *J. Am. Chem. Soc.*, 1990, **113**, 7588.

35. K. Yagi, N. Ishida, S. Komura, N. Ohishi, M. Kusai and M. Kohno, *Biochem. Biophys. Res. Commun.*, 1992, **183**, 945.

36. B. Halliwell and J.M.C. Gutteridge, *FEBS. Lett.*, 1981, **128**, 347.

37. D.C. Harris, *Quantitative Chemical Analysis*, 8th Ed., 2010, W. H. Freeman and Company, New York.

38. B. Tadolini and L. Cabrini, *Mol. Cell. Biochem.*, 1990, **94**, 97.

39. K. Nam, W. Rodriguez and J.J. Kukor, *Chemosphere*, 2001, **45**, 11.

40. F. Nerud, P. Baldrian, J. Gabriel and D. Ogbeifun, *Chemosphere*, 2001, **44**, 957.

41. H. Lee, H.-J. Lee, D.L. Sedlak and C.Lee, *Chemosphere*, 2013, **92**, 652.

42. D.A. Nichela, A.M. Berkovic, M.R. Costante, M.P. Juliarena and F.S. Garcia Einschlag, *Chem. Eng. J.*, 2013, **228**, 1148.

43. G.J. Tortora, B.R. Funke and C.L. Case, *Microbiology An Introduction*, 10th Ed., 2010, Pearson Benjamin Cummins, San Francisco.

44. M. Bartoszek and W.W. Sułkowski, *Polish J. Of Environ. Stud.*, 2006, **15**, 41.

45. B.P. Binks, A.J. Johnson and J.A. Rodrigues, *Soft Matter*, 2009, **6**, 126.

46. E. Bormashenko, R. Balter and D. Aurbach, *J. Colloid Interface Sci.*, 2012, **384**, 157.

47. R.Y. Stainer, J.L. Ingraham, M.L. Wheelis and P.R. Painter, *General Microbiology*, 5th Ed., 1987, Macmillan Press Ltd., Hampshire.

CHAPTER 6

SUMMARY OF CONCLUSIONS AND FUTURE WORK

6.1 Summary of conclusions

This thesis presented an investigation into the encapsulation of fluids by solid particles. The aim of the research was to generate a novel hand sanitiser based on the Fenton reaction. As the two components of the reaction, namely copper sulfate and hydrogen peroxide, were required to be kept separate until the point of use; novel technologies for encapsulation of liquids were explored. For this research project dry water was of particular interest. As it is known that the surface tension of the liquid can be a limiting factor in the successful encapsulation of liquids, it was necessary to generate an understanding of how particles behave at air-liquid interfaces of varying surface tension. To do this, an investigation into the behaviour of aqueous foams stabilised with surfactants, fumed silica particles and a mixture of surfactants and particles was carried out. The effect of introducing ethanol into the aqueous phase was explored. A separate study looked at the fluorination and measurement of monodisperse silica particles at air-water interfaces. Again, the effect of ethanol introduction to the aqueous phase was explored. Finally, a study into the encapsulation of then Fenton reagents and their anti-microbial efficacy was carried out.

Chapter 3 comprised a study on the foaming of two commercial nonionic surfactants in pure water and in mixtures of water and ethanol. It was found that in both pure water and ethanol/water mixtures, that with increasing surfactant concentration, there was an increase in foamability and foam stability. Maxima in the foamability was observed for both surfactants, at 30 wt. % and 70 wt. % for Lamesoft PO65 and Silsurf DI-2510 respectively. Adding ethanol to the aqueous phase also effected an increase in the CMCs for both surfactants due to enhanced solubilisation of the surfactant tails reducing the hydrophobic effect. The behaviour of fumed silica particles in pure water and mixtures of ethanol and water was observed. The most hydrophobic silica formed climbing films in pure water but foams stable to collapse for over 1 year in 20 wt. % EtOH, particles of intermediate hydrophobicity formed stable foams in pure water and very unstable foams in 20 wt. % EtOH.

Mixtures of particles and surfactants were investigated by varying the surfactant concentration, particle concentration and particle hydrophobicity. Addition of particles to the surfactant solutions demonstrated an enhancement in the stability and foamability of the foams generated. There was an exception in the samples of 1 wt. % 100% SiOH in 1 wt. % Silsurf DI-2510, which formed a viscous gel that was difficult to aerate. The effect of particle hydrophobicity was investigated by aerating with 20% SiOH and 47% SiOH fumed silica particles to solutions of the surfactants. Addition of hydrophobic particles to Lamesoft PO65 was detrimental to the foamability, potentially due to the hydrophobic particles acting as anti-foams and rupturing the thin foam films between bubbles. Conversely, addition of hydrophobic particles to Silsurf DI-2510 demonstrated an enhancement in the foamability and stability. This was potentially be due to the particles stabilising the bubble surfaces alone. Alternatively some surfactant adsorption to the particle surfaces could have surface modified them, allowing for adsorption to the interface. As no adsorption isotherms of the surfactant molecules to the particle surfaces were carried out, it was impossible to determine whether the enhancement in stability was due to particle adsorption to the bubble surfaces, or particle blocking the plateau borders and reducing liquid drainage from the foam films.

Chapter 4 investigated the development of a protocol for fluorination of monodisperse silica particles. Monodisperse, micron-sized particles were selected as it allowed for direct measurement of the particle contact angle, an important parameter for understanding the particle behaviour at the interface. A range of silica particles were hydrophobised to varying extents with 1H, 1H, 2H, 2H-perfluorooctylmethyldichlorsilane. The particle contact angles were measured at an air-water interface using the film calliper method. It was observed that as the concentration of silane increased, the contact angle also increased and the contact angles were seen to range from 50.7° to >90°. The two most hydrophobic sets of particle broke thin films and so were assumed to be above 90°. When ethanol was introduced into the aqueous phase, a continual decrease in the contact angle was observed. Planar monolayers of the particles were spread at air-water and aqueous ethanol-air interfaces. In pure water, all particles were seen to aggregate at the interface, except the two most hydrophobic particles, which formed repulsive arrays.

The introduction of ethanol caused heavy aggregation. In the cases where repulsive arrays had formed in pure water, the addition of ethanol caused most of the monolayer to aggregate. However, there were localised areas of the monolayer where repulsive arrays were still observed.

Suspensions of the particles in water and 15 wt. % ethanol were aerated by homogenisation. Foams in pure water showed poor stability which is uncharacteristic of particle stabilised foams, and all foams collapsed within 10 days. Above concentrations of 1.6×10^{-4} M the systems were seen to phase-invert and form stable dry powders of liquid drops in air coated with a layer of particles. With addition of 15 wt. % to the aqueous phase, a significant improvement to the foamability and stability was seen, but dry powder systems were seen for only the most hydrophobic particles. This system was seen to be an intermediate between a dry powder and a foam, termed in the literature a "soufflé".

In Chapter 5, the kinetics of the Fenton reaction were studied by means of UV-visible spectrophotometry. The degradation of an azo-dye molecule was measured (by the hydroxyl radicals produced from the Fenton reaction) as a function of time. The variation in concentration of the dye molecule was then calculated from plots of absorbance against time, and converted to an initial reaction rate. It was seen that as both the concentrations of H_2O_2 and $CuSO_4$ were varied independently, the initial reaction rate passed through a maximum at 60 mM and 8 mM for H_2O_2 and $CuSO_4$, respectively. The effect of pH on the initial reaction rate was observed as it has been observed throughout the literature that the pH can have a significant effect on the progress of the reaction. From measurements of the rate of dye degradation over a pH range of 1-4.2 , the pH was seen to have a significant effect on the rate of the reaction. This has very important implications for the current application as it is necessary to acidify the reaction to denature the bacterial catalase, active catalase could potentially consume all hydrogen peroxide present. Additionally acidification aids in stabilising against degradation of the hydrogen peroxide.

In vitro anti-microbial testing was carried out on aqueous solutions of the Fenton reagents by exposing *Escherichia coli* bacteria to the reagents for 60 seconds and counting the log reduction in the quantity of bacteria. In accordance with the studies of the initial reaction rate at various pH values, at pH 4 the highest efficacy was observed, with an 8 log reduction for all concentrations of Fenton reagents used. This implies that all bacteria were killed. The efficacy was reduced as the solutions were acidified. Interestingly, it can be concluded from this that the effect of bacterial catalase is not significant. An explanation for this may be that the rate of production of hydroxyl radicals is many orders of magnitude faster than the consumption of hydrogen peroxide by catalase molecules. The *in vivo* study involved participants contaminating the skin surface with a culture of *E.coli*, the product was then applied to the skin and applied using a specified technique for 60 seconds. A pre- and post- application bacterial count was carried out and from this the log reduction in bacteria was calculated. Surprisingly, the *in vivo* studies do not show the same pH dependence as the *in vitro* and dye degradation studies and the efficacy is relatively independent of the pH. Unfortunately the *in vivo* testing with the current formulation does not show great promise as there was little difference in the log reduction between the Fenton reagents alone and the Fenton reagents mixed. None of the test solutions tested demonstrated an efficacy close to that observed for the reference samples (60% IPA). Further to this, there is a loss in efficacy when the formulations are applied in the powdered dry water format.

6.2 Future work

The following ideas are suggested from the work presented in the thesis.

For the foams generated with a mixture of particles and nonionic surfactants, presented in Chapter 3, it is suggested that a method for carrying out adsorption isotherms of the surfactant molecules to the particle surfaces is undertaken in addition to analysing the surfactant structures. Significantly long times are required to sediment the fumed silica nanoparticles from suspension which poses a challenge. Further to this, methods for analysing the surfactants could be investigated and carried out. As Lamesoft PO65 is a mixture of two different surfactants, this would require a separation step, so HPLC or GC-MS are potential options for analysis. As Silsurf DI-2510 is a polymer with a weight range (20-28 siloxane groups end capped with 10-12 PEG groups) a method to differenciate between polymers of varying size will be necessary. However, this work would provide useful in determining the adsorption characteristics of these surfactants to the fumed silica particle surfaces, if there is any adsorption. This may allow for some explanation of the foaming behaviour of these mixtures, as this was less clear and the trends were unclear in comparison to what is presented in the literature.

Further work regarding the fluorinated silica particles could further explore the unusual foaming behaviour in water, particularly the poor stability to disproportionation and coalescence observed. Some modelling of the interfaces between the close packed particles could be carried out, such as in the work of Akbarian *et al.* who used surface evolver calculations.[1] Additionally, it would be fruitful to quantify the amount of fluorine on the particle surfaces in order to relate this to the contact angles measured. The potential for fluorinated particles to act as encapsulating agents should be further explored; some brief laboratory experiments demonstrated that although dry water could be formed with the monodisperse hydrophobic silica particles, it was not possible to generate liquid marbles. Therefore the formation of liquid marbles is not solely dependent on the surface chemistry and must have some reliance on the physical structure. It may be interesting to fluorinate hydrophilic fumed silica particles and investigate their potential for encapsulating liquids of low surface tension.

In order to further investigate the potential of the encapsulated Fenton reaction as a hand sanitiser, it is clear from the anti-microbial studies that some significant work on the formulations should be carried out. As there was a loss of efficacy moving from an *in vitro* to an *in vivo* test, it may be necessary to increase the concentration of the Fenton reagents encapsulated in the dry water, to improve their performance on the skin surface. It was noted that there was difficulty in applying the powder to the skin surface during the test without losing a significant quantity of the powder. The dry water consistency was fluffy and light and there were some clear practicality issues of applying the product to the skin during the test. It could be possible to perhaps suspend the dry water in a gel, or perhaps suspend one encapsulated component in a gel formula containing the other component. Further to this, as it is shown that the reaction proceeds at a significantly faster rate at a higher pH this will pose issues for the long term stability of hydrogen peroxide at a non-acidic pH. For these studies, fresh solutions stored at low temperatures were used, which is clearly impractical. An investigation into other means of stabilising hydrogen peroxide in solution (so that a practical shelf life can be applied to the product) should be carried out. It would be necessary to investigate the potential toxicity of fumed silica particles for their use in this application, they do not cause irritation to the skin but issues may arise with exposure of the respiratory tract to these particles in use. Furthermore, future *in vivo* studies should be carried out on a larger sample size than five participants.
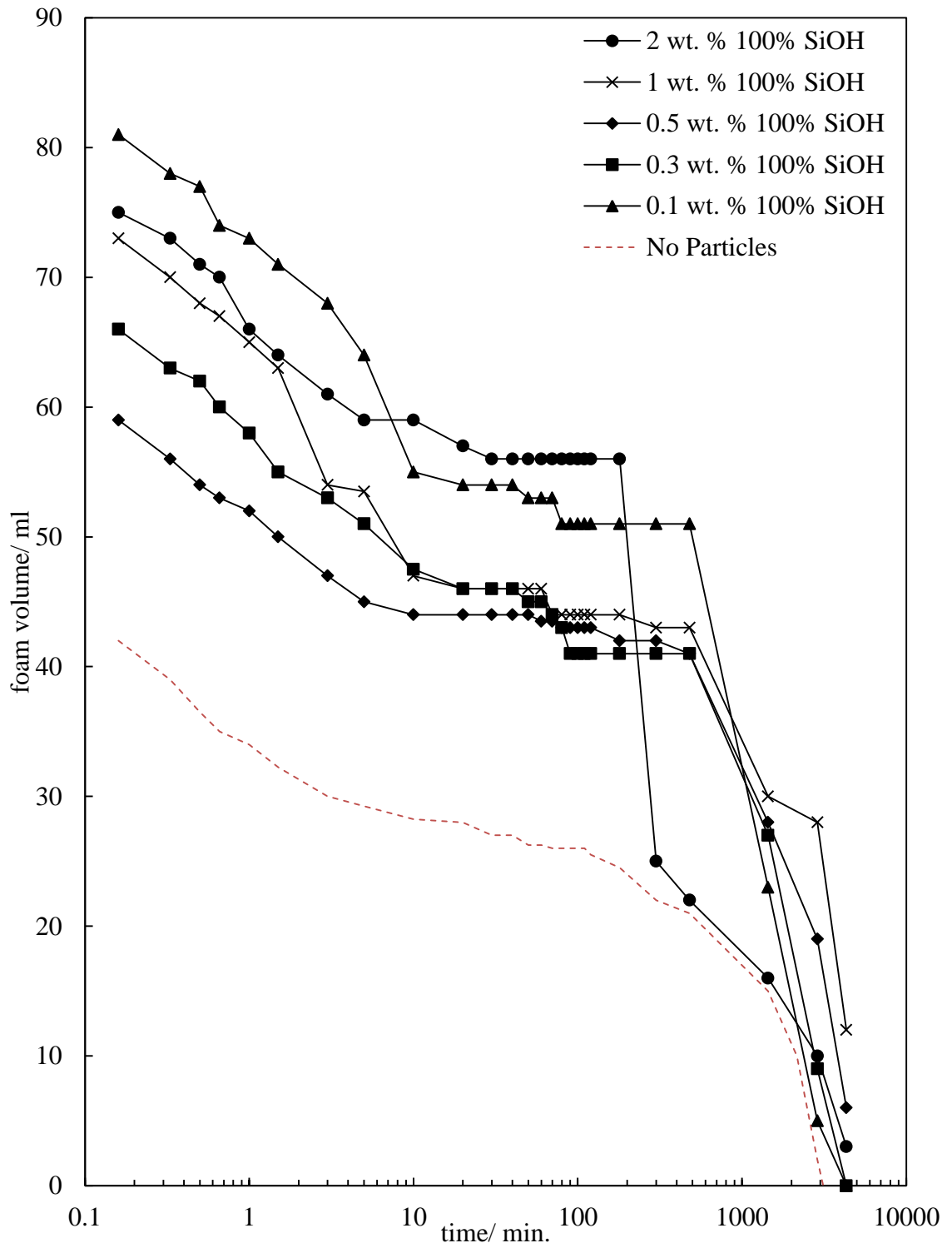
6.3   References

1. M. Abkarian, A.B. Subramaniam, S-H. Kim, R.J. Larsen, S-M. Yang and H.A. Stone, *Phys. Rev. Let.*, 2007, **99**, 188301.
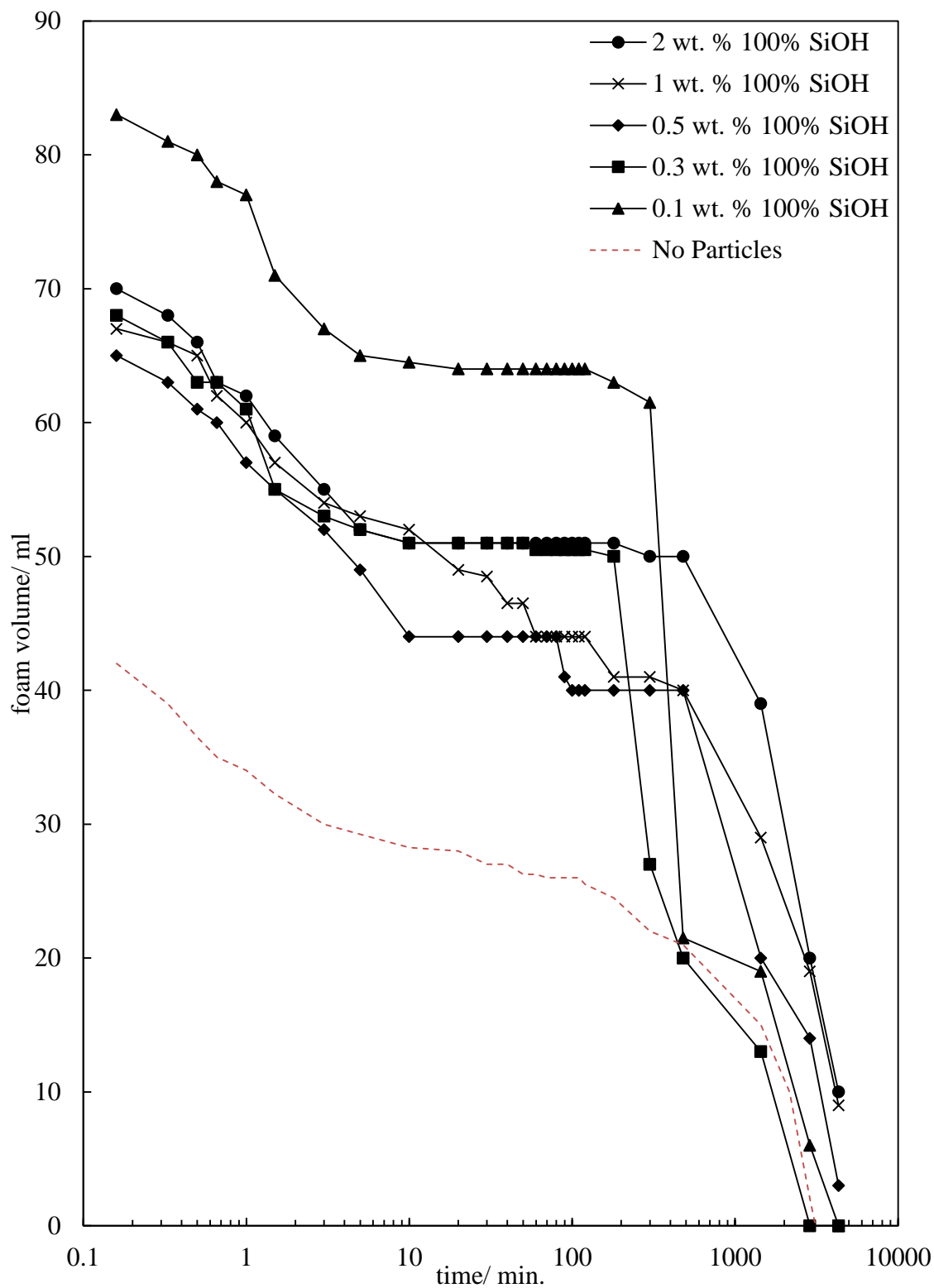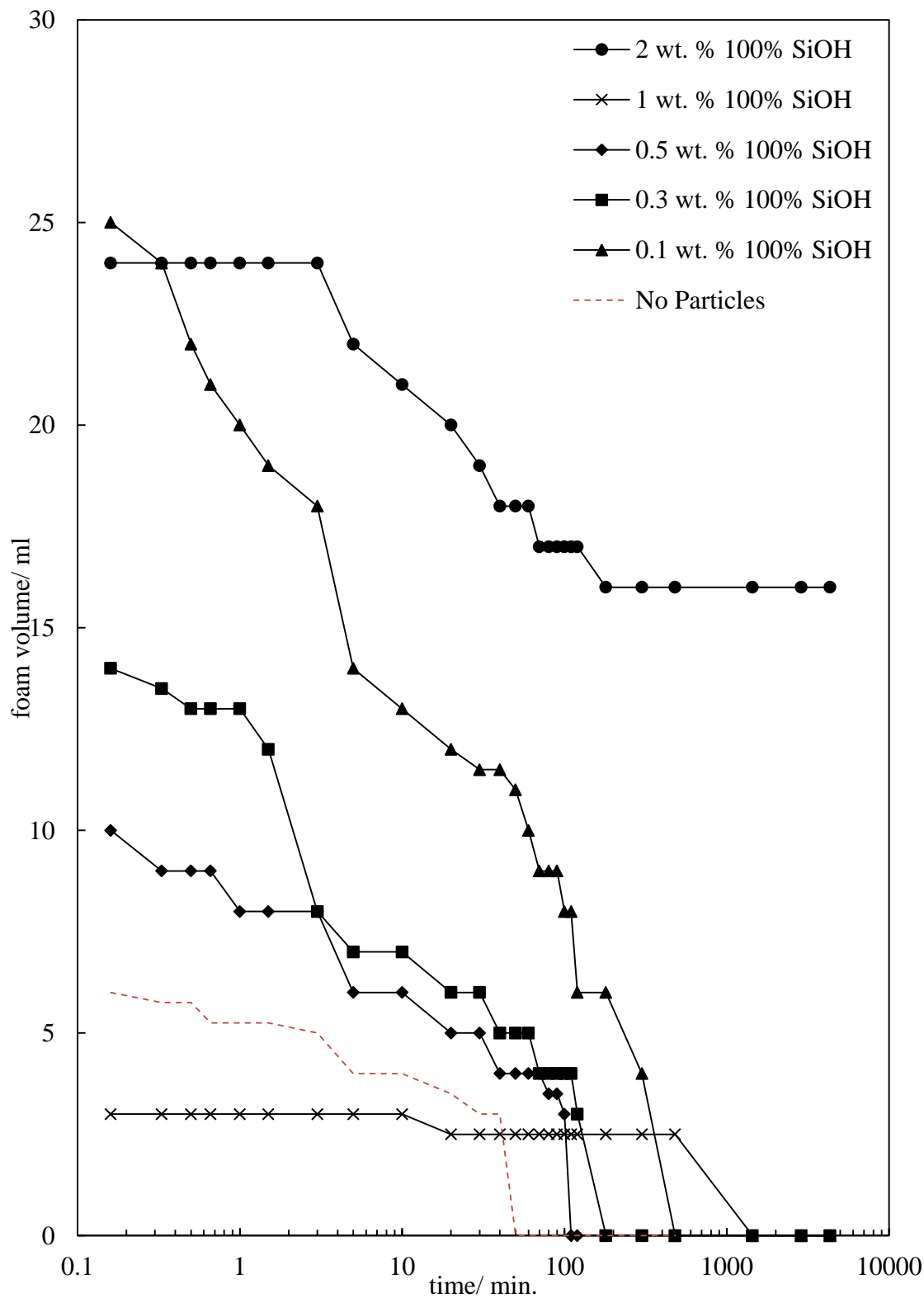
Figure 3.42(a). Foam volume as a function of time for foams generated by hand shaking (30 s) 20 ml of 1 wt. % Lamesoft PO65 containing 0-2 wt. % 100% SiOH fumed silica particles. Run 2 of 3 repeats.
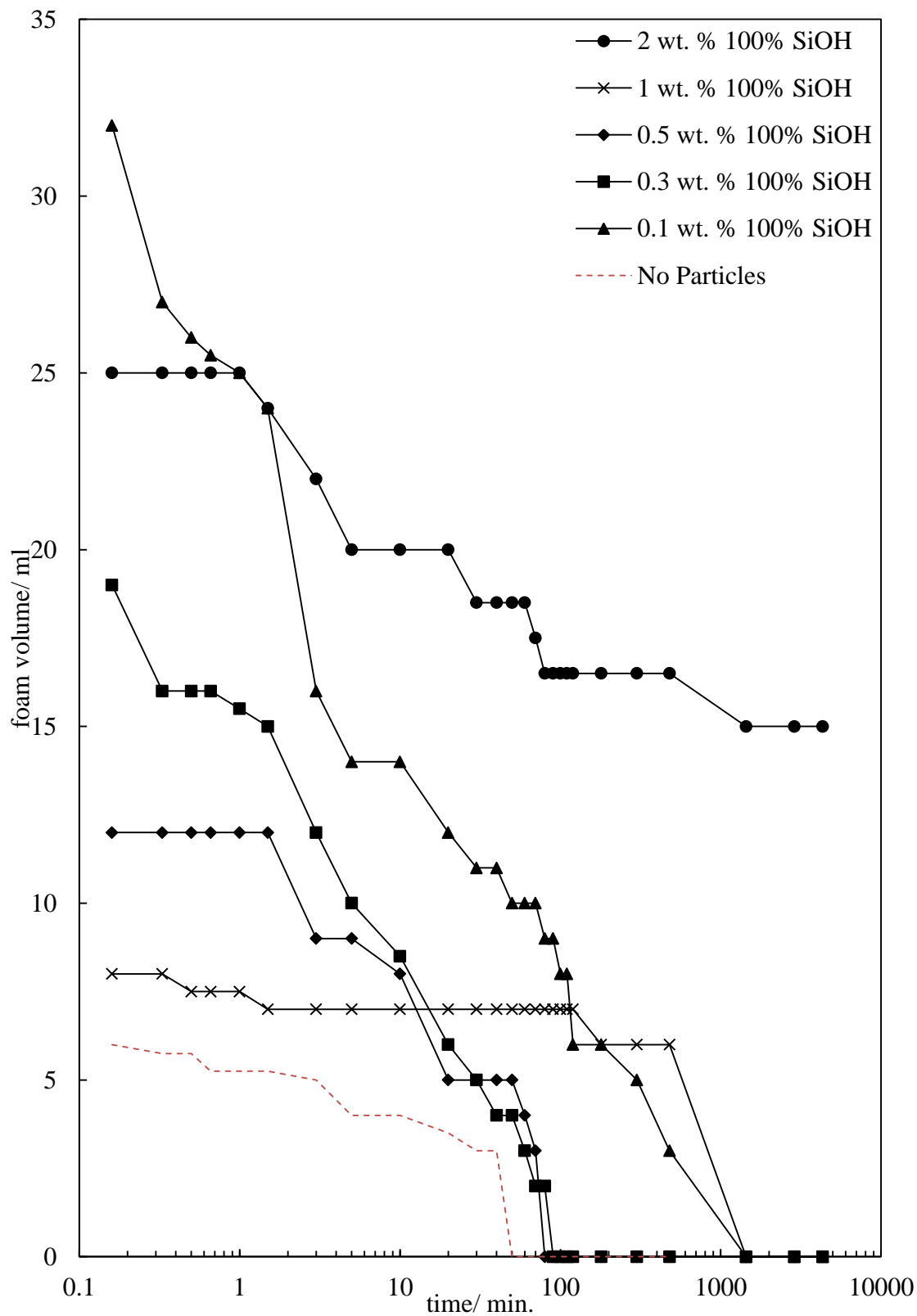
Figure 3.42(b). Foam volume as a function of time for foams generated by hand shaking (30 s) 20 ml of 1 wt. % Lamesoft PO65 containing 0-2 wt. % 100% SiOH fumed silica particles. Run 3 of 3 repeats.
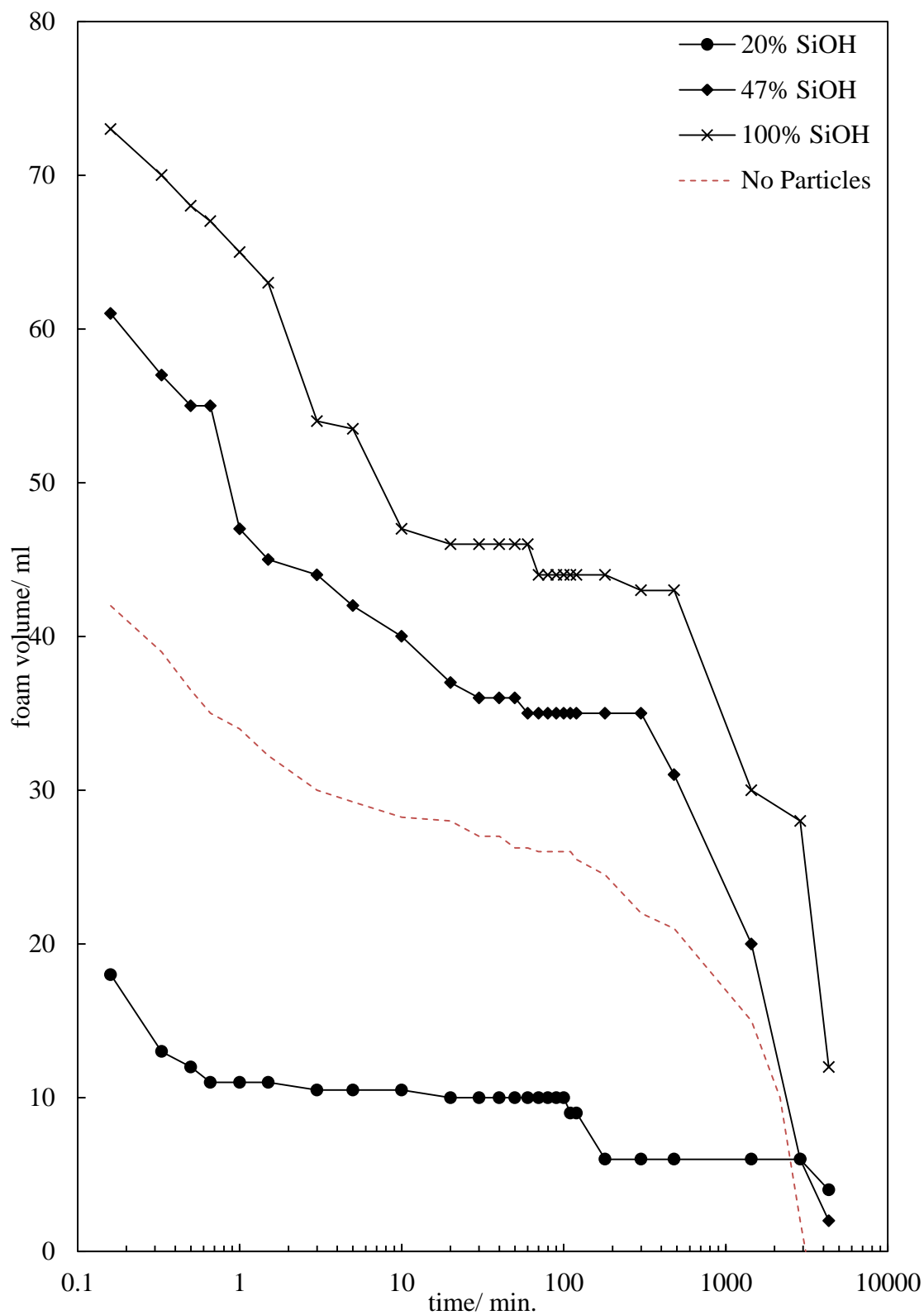
Figure 3.46(a). Foam volume as a function of time for foams generated by hand shaking (30 s) 20 ml of 1 wt. % Silsurf DI-2510 containing 0-2 wt. % 100% SiOH fumed silica particles. Run 2 of 3 repeats.
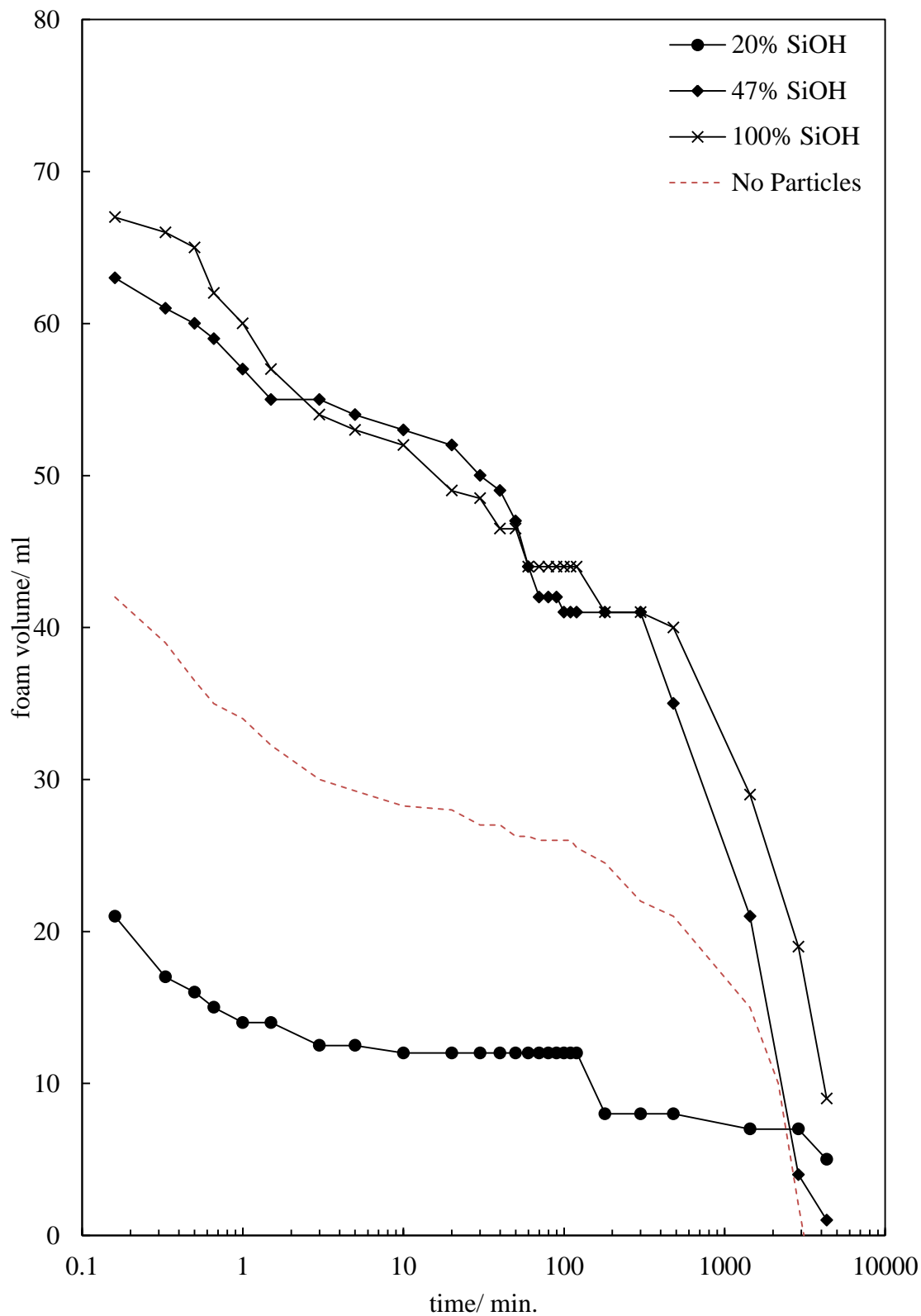
Figure 3.46(b). Foam volume as a function of time for foams generated by hand shaking (30 s) 20 ml of 1 wt. % Silsurf DI-2510 containing 0-2 wt. % 100% SiOH fumed silica particles. Run 3 of 3 repeats.
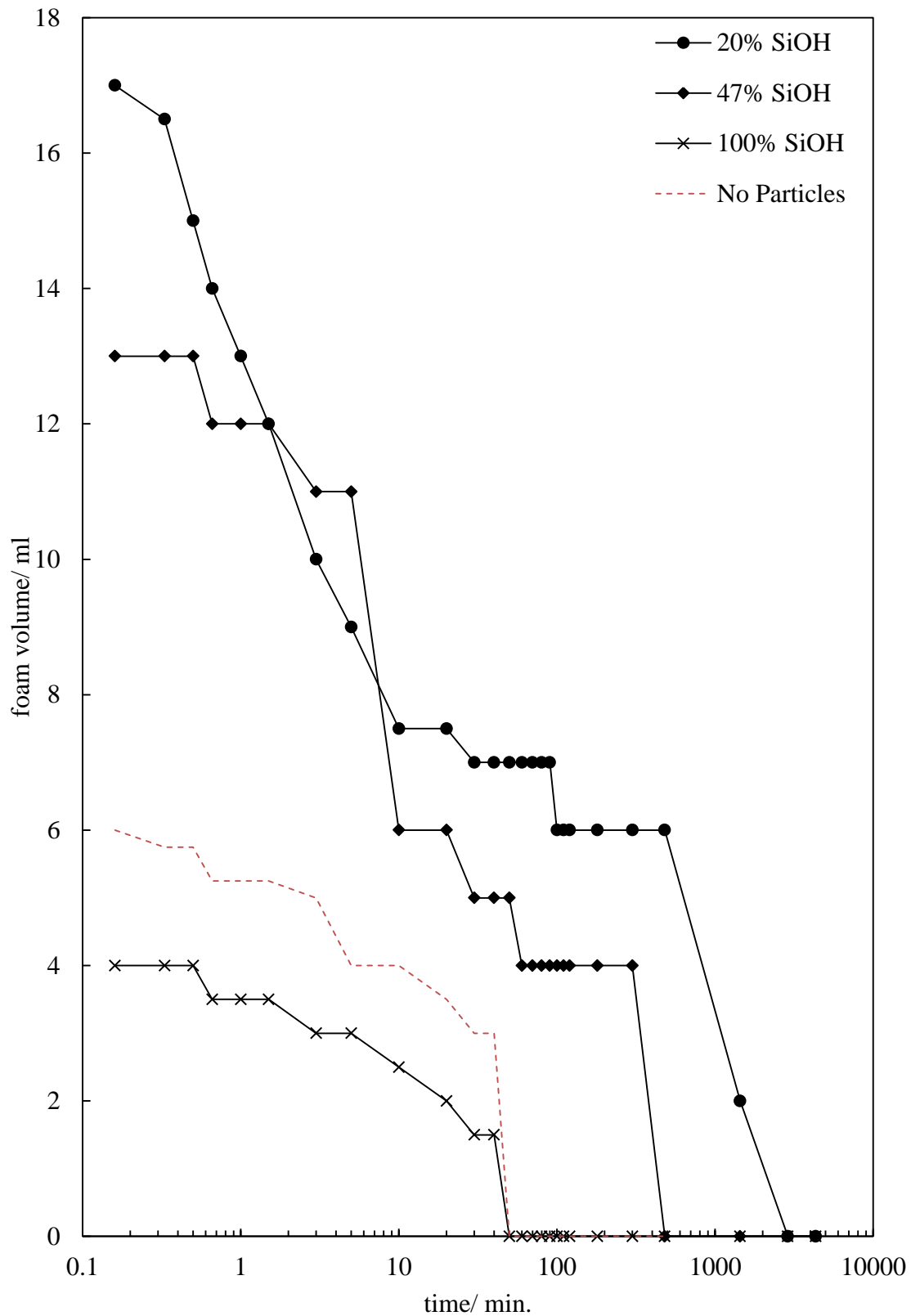
Figure 3.51(a). Foam volume as a function of time for foams generated by hand shaking (30s) 20 ml 1 wt. % Lamesoft PO65 containing 1wt. % fumed silica particles. Particle hydrophobicity is varied from 20-100% surface SiOH groups. Run 2 of 3 repeats.

Figure 3.51(b). Foam volume as a function of time for foams generated by hand shaking (30s) 20 ml 1 wt. % Lamesoft PO65 containing 1wt. % fumed silica particles. Particle hydrophobicity is varied from 20-100% surface SiOH groups. Run 3 of 3 repeats.

Figure 3.55(a). Foam volume as a function of time for foams generated by hand shaking (30 s) 20 ml of 1 wt. % Silsurf DI-2510 containing 1wt. % fumed silica particles. Particle hydrophobicity is varied from 20-100% surface SiOH groups. Run 2 of 3 repeats.

Figure 3.55(b). Foam volume as a function of time for foams generated by hand shaking (30s) 20 ml 1 wt. % Silsurf DI-2510 containing 1wt. % fumed silica particles. Particle hydrophobicity is varied from 20-100% surface SiOH groups. Run 3 of 3 repeats.